VINCRISTINE METABOLISM AND THE ROLE OF CYP3A5

Jennifer Bolin Dennison

Submitted to the faculty of the University Graduate School
in partial fulfillment of the requirements
for the degree
Doctor of Philosophy
in the Department of Pharmacology and Toxicology,
Indiana University

November 2007

Accepted by the Faculty of Indiana University, in partial
fulfillment of the requirements for the degree of Doctor of Philosophy.

_____

Stephen D. Hall, Ph.D., Chair

_____

Lisa M. Kamendulis, Ph.D.

_____

Sherry F. Queener, Ph.D.

Doctoral Committee

_____

Leonard C. Erickson, Ph.D.

_____

Steven A. Wrighton, Ph.D.

Date of
Oral Examination
November 1, 2007

ACKNOWLEDGEMENTS

The work presented herein would not have been possible without collaboration and the guidance of many individuals both at Indiana University and Eli Lilly and Company. I am especially grateful to Dr. Stephen Hall, my mentor, who consistently provided feedback while allowing me enough freedom to learn from my mistakes. I thank my committee members, Dr. Sherry Queener, Dr. Leonard Erickson, Dr. Steven Wrighton, and Dr. Lisa Kamendulis, who were supportive of my progress and gave valuable suggestions. I also thank Dr. David Jones and Ariel Topletz for their support.

The metabolite identification of vincristine was completed in collaboration with a team of chemists at Eli Lilly and Company including Dr. William Ehlhardt, Dr. Palaniappan Kulanthaivel, and Robert Barbuch. I am grateful for the opportunity to work with these world-class scientists who even after the project was completed, continued to support me and my research. Also at Eli Lilly, Dr. Michael Mohutsky performed the cryopreserved hepatocyte incubations with vincristine, a project funded by Eli Lilly. The study of vincristine in human subjects was enabled by Dr. Jamie Renbarger, a pediatric oncologist who is committed to the study of *Vinca* alkaloid individualized therapy.

I thank IUPUI and the PhRMA foundation for the financial support I received during my doctoral training.

Finally, I would like to thank my husband, David, for his support and encouragement. The pathway required to become a research scientist is long and arduous, and my family allows me to experience a balanced life.

ABSTRACT

Jennifer Bolin Dennison

VINCRISTINE METABOLISM AND THE ROLE OF CYP3A5

Vincristine is metabolized by the cytochrome P450 3A subfamily of enzymes possibly including CYP3A5, a genetically polymorphic enzyme. The contribution of CYP3A5 to the metabolism of vincristine was quantified by various *in vitro* models: cDNA-expressed enzymes, human liver microsomes, and human hepatocytes. With these models, the major CYP metabolite of vincristine, M1, was identified and extensively characterized. The rates of M1 formation in the cDNA-expressed enzyme models were at least 7-fold higher with CYP3A5 than CYP3A4; approximately 90% of the hepatic metabolism was predicted to be CYP3A5-mediated. For human liver microsomes with high CYP3A5 expression, the CYP3A5 contribution was substantial, approximately 80%. Human hepatocytes with at least one *CYP3A5*1* allele also metabolized vincristine, albeit at a slower rate (10-fold) than human liver microsomes. The CYP3A5 low-expressing hepatocytes did not metabolize vincristine. We conclude that for high CYP3A5 expressers, the majority of the CYP metabolism is mediated by CYP3A5. By *in vitro*/*in vivo* scaling with microsomes, the hepatic clearances of high CYP3A5 expressers are predicted to have a 5-fold higher hepatic clearance than low expressers. However, the role of metabolism in the systemic clearance of vincristine is unknown. To study the disposition of vincristine *in vivo*, a sensitive and selective LC/MS/MS assay was validated for the quantification of vincristine and M1 quantification in human

plasma. Vincristine and M1 were identified and quantified in select pediatric plasma and urine samples. For future large-scale clinical studies, the vincristine and M1 concentrations in plasma will be quantified to understand the role of *CYP3A5* genotype in vincristine pharmacokinetics. For patients that are CYP3A5 high expressers, the systemic clearance of vincristine may be higher than that of low CYP3A5 expressers. Thus, *CYP3A5* genotype may be an important determinant of inter-individual variability in clinical outcomes.

Stephen D. Hall, Ph.D., Chair

TABLE OF CONTENTS

LIST OF TABLES

LIST OF FIGURES

I. Introduction

A. Vincristine

1. Chemistry

Vincristine, a monoterpenoide indole alkaloid, was originally discovered as a natural product produced by the Madagascar periwinkle plant, *Catharanthus roseus*, but only in trace quantities.[1,2] For the commercial manufacture of vincristine today, vinblastine and N-desformylvinblastine are extracted from *Catharanthus roseus* leaves and chemically modified.[3] Vincristine has been synthesized using biomolecular engineering strategies from less complex intermediates, such as vindoline and catharanthine.[4] However, total biosynthesis from smaller molecules is not yet possible; to synthesize vinblastine in the periwinkle, at least 30 different enzymes and 35 chemical intermediates are required.[4] In fact, a chemical procedure for the *de novo* synthesis of vincristine was only recently discovered because the molecular structure of vincristine is unusually complex, even for a natural product.[5]

Vincristine is a highly functionalized alkaloid with a molecular weight of 825 and nine chiral centers (Fig. 1). All *Vinca* alkaloids, including vinblastine and vinorelbine, are comprised of two distinct parts—the catharanthine and vindoline moieties.[6] While the catharanthine moieties are the same as vincristine, vinblastine has a methyl substitution on the vindoline nitrogen in place of a formyl group (C-22'). Vinorelbine has the same structure as vinblastine without a hydroxyl group (C-14) on the catharanthine moiety but with a C14-C15 double bond on the piperidine ring.

Vinblastine and vinorelbine, commonly used as internal standards for vincristine assays, are structurally similar to vincristine with desirable chromatography properties.

For all three *Vinca* alkaloids, the molecular conjugation characteristics are identical—the catharanthine indole and the vindoline phenyl ring. As a result, as compared to vincristine, vinblastine and vinorelbine have similar ultraviolet absorption properties. In addition, the alkaloids have two nitrogens that are easily protonated: the allylic nitrogen on the vindoline side and the tertiary nitrogen on the catharanthine side. The corresponding pK_a values are approximately 5.4 and 7.4 for all the *Vincas*.[6] Thus, by HPLC, the relative retention times of the compounds are similar regardless of eluent pH. Finally, the compounds separate by HPLC without difficulty because vinblastine and vinorelbine are more lipophilic than vincristine (12-fold higher partition coefficient for vinblastine).[7]

Vincristine, as it is found in the vacuoles of plants, is present in multiple chemical forms including the free base, N-oxide, and salt.[3] Only a few degradation and metabolism products of vincristine have been described by *in vitro* studies. Vincristine was degraded after 72 h in glycine buffer to desacetylvincristine and N-formylleurosine (M4/M5 epoxide diastereomers in our studies).[8] Vincristine was oxidized by peroxidase and ceruloplasmin, a human serum enzyme, to yield a N-formylcatharanthine product (M2 in our studies).[9] Finally, in one hepatic metabolism study, vincristine was extensively metabolized by human liver hepatocytes to multiple compounds.[10] However, the chemical identities of these compounds were not determined.

As described for human hepatocytes, vincristine sulfate is rapidly metabolized and/or degraded to multiple compounds when administered intravenously to humans. For radiolabeled vincristine studies, the recovery of the parent drug by HPLC was 50 to 60%.[11,12] However, the actual vincristine recovery was possibly lower because the

vincristine and the metabolite/degradation products may have co-eluted under the HPLC conditions employed. Surprisingly, no compounds have been identified *in vivo* to account for the 40 to 50% loss of vincristine. The only reported *Vinca*-related compounds isolated from urine or bile were small amounts of degradation products (desacetylated, epoxide, and N-oxide derivatives).[13-15] These compounds are unlikely to have clinical significance because they accounted for less than 1% of the administered dose.[13,14]

2. Mechanisms of Action

Vincristine and other *Vinca* alkaloids bind to tubulin and as a result inhibit microtubule assembly.[16] The *Vinca* binding site on tubulin is distinct from the taxane or colchicine binding site.[17] X-ray structures of vinblastine and tubulin heterodimers revealed that vinblastine was equally bound to α and β-tubulin from adjacent heterodimers close to the GDP/GTP binding site on β-tubulin.[17] Vinblastine (VLB) at the inter-dimer interface (i.e. α1β1-VLB-α2β2) caused curvature in the protofilaments leading to spiral formation. As a result, vinblastine interfered with the dynamic instability at the (+) end of protofilaments and ultimately inhibited microtubule assembly.[17]

Although all *Vinca* alkaloids bind to the same site on tubulin, the individual compounds have different potencies. The overall binding affinity of vincristine to tubulin was 5-fold and 10-fold higher than the binding affinities of vinblastine and vinorelbine, respectively.[18] The *in vitro* potencies of the *Vinca* alkaloids with tubulin are the same rank order as the clinical doses from lowest to highest dose (vincristine > vinblastine > vinorelbine). This correlation may be expected if the dose-limiting toxicities of the drugs are caused by tubulin binding at the same site. However, in

addition to tubulin affinity, the maximum dose administered *in vivo* is a function of distribution to the site of toxicity (neurons for vincristine, bone marrow for vinblastine and vinorelbine) and the systemic clearance of the drug.

Therapeutic concentrations of *Vinca* alkaloids (less than 0.1 μM for vincristine) cause changes in microtubule dynamics and can block mitosis leading to cell-cycle arrest and apoptosis.[18] Recent evidence suggests that the actin cytoskeleton and microtubule function are intimately connected; disruption of the actin cytoskeleton caused by antimicrotubule drugs may be part of a critical pathway leading to apoptosis in cancer cells. For example, in multiple cell lines with resistance to antimicrotubule drugs, the actin cytoskeletal proteins such as γ-actin were mutated or had altered expression.[19,20] In response to antimicrotubule drugs addition, cancer cells also underwent anoikis, apoptosis caused by detachment to the extracellular matrix.[21]

The tubulin-binding characteristics of vincristine that destroy cancer cells are also likely responsible for the dose-limiting peripheral neuropathy in vincristine therapy. The binding of drug to microtubules in axons causes disarray characterized by a decrease in density and tangential orientation of the microtubules.[22] Of the *Vinca* alkaloids, neurotoxicity is unique to vincristine; the dose-limiting toxicity of all other approved *Vinca* alkaloids is myelosuppresion. Some investigators have hypothesized that compared to the other *Vinca* alkaloids, vincristine causes neurotoxicity because it has a higher affinity to tubulin isoforms primarily expressed in neurons (βII and βIII). However, with purified βII and βIII isoforms of tubulin, the *in vitro* data with vincristine showed only minor differences in affinity.[23] At this time, it is unclear whether these small differences are responsible for the neurotoxicity observed *in vivo*

during vincristine therapy but not observed with the other *Vinca* alkaloids. Other drug-specific factors to consider include the penetration of the drug to the site of toxicity and the ability of the cells to transport the drug.

3. Clinical Applications

Vincristine is currently used to treat a variety of malignancies in both pediatric and adult patients. In the United States every year, approximately 12,400 children less than 20 years old are diagnosed with cancer (0.3% rate of incidence), and 2500 children die from their disease.[24] The most common cancer in children is acute lymphoblastic leukemia (ALL, 19%) followed by lymphomas and reticuloendothelial neoplasms (16%).[24] Vincristine is used as part of standard therapy for these cancers and a variety of other cancers including neuroblastoma, non-Hodgkins' Lymphoma, Hodgkins' disease, Wilms' tumor, hepatic tumors, retinoblastoma, and rhabdomyosarcoma.[25] In adults, vincristine is commonly used in combination chemotherapy in the United States to treat ALL (1420 deaths/year), non-Hodgkins' Lymphoma (18,700 deaths/year), Hodgkins' disease (1070 deaths/year), and multiple myeloma (10,800 deaths/year).[25]

4. Dose-limiting Toxicity

For vincristine, the dose-limiting toxicity is a distinctive type of peripheral neuropathy with the following symptoms: limb weakness, abdominal pain, numbness in extremities, and constipation.[26] Severe toxic effects associated with vincristine treatment and overdose include seizures, paralytic ileus, bowel obstruction, urinary retention, hypertension, and severe musculoskeletal pain.[27] However, once therapy is discontinued, even for patients with severe neurotoxicity, the neuropathy for almost all patients is fully reversible.[27] No additional treatment during vincristine therapy is

known to alleviate neurotoxic symptoms. The Pediatric Oncology Group in a phase III clinical trial is currently investigating glutamic acid as a neuroprotective agent.[25]

Vincristine neurotoxicity can be a severe clinical problem with coadministration of certain antifungal and immunosuppressant drugs. The most commonly reported drugs that interact with vincristine are itraconazole and cyclosporin A.[28-31] Although the exact mechanism is unknown, these drug/drug interactions are most likely caused by inhibition of CYP3A enzymes and/or P-gp.[32-34] According to a few clinical case studies, other drugs may also potentiate vincristine neurotoxocity including verapamil, nifedipine, and isoniazid.[35] These drugs also inhibit CYP3A4 and, at least for verapamil, P-gp.[36,37]

The maximum dose recommendation for vincristine is 1.5 mg/m^2 per week with a maximum single dose of 2 mg and cumulative dose of 20 mg. The dosing of vincristine was decided more than 30 years ago based on clinical observations of more frequent and a faster onset of neurotoxic events at higher doses (3 mg/m^2).[38] However, in this study, the recommended dose of vincristine may not be appropriate for pediatric patients because only 5 of the 78 patients were children. The dosing recommendations for pediatric and adult patients were recently challenged by scientists and physicians because the maximum tolerated dose is not used for the majority of patients, especially for patients with a capped dose of 2 mg.[27] An increase in the maximum recommended dose for vincristine may be possible as shown by a pediatric Dutch ALL study; the maximum dose was increased to 2.5 mg without causing severe neurotoxic events.[39] At this time, it is unknown whether dose escalation of vincristine will result in clinically significant efficacy improvements. Phase III clinical trials are currently underway to

evaluate the clinical outcome differences between high and low dose vincristine in relapsed pediatric ALL patients.[25]

5. Effect of Ethnicity on Clinical Outcomes

Unlike for other types of pediatric cancers such as AML, the prevalence and the rates of survival for pediatric ALL differ by race.[24] Caucasian children have a 2-fold higher prevalence of ALL compared to African-American children (31 per million versus 15 per million).[24] On the other hand, African-American children have a lower survival rate relative to Caucasian children. According to the NCI, the 5-year survival rate of African-American children was 64% versus 78% for Caucasian children (treatment period 1985–1994).[24] The authors hypothesized that the lower survival rate of African-American children possibly reflected differences in the pharmacokinetics and/or the pharmacokinetics of the chemotherapeutic agents; differences in access to health care; or a lower incidence of readily curable ALL subtypes.[24] However, in an ALL study conducted by the Pediatric Oncology Group (treatment period 1981–1994), the survival rates were calculated after correcting for known prognostic factors such as compliance, clinical presentation, and tumor characteristics; African-American and Spanish surname children with vincristine combination chemotherapy had a 42% greater mortality rate when compared to Caucasian children.[40] The Children's Cancer Group also reported interracial differences in outcome for intermediate-risk ALL (treatment period 1990–1993); event-free-survival (EFS) was only 54% for African-American children compared to a Caucasian EFS of 82%.[41] In a larger retrospective study, the Children's Cancer Group evaluated the outcomes of Asian, Caucasian, Hispanic, and African-American children with standard and high-risk ALL (treatment period 1983–1995).[42]

After adjusting for risk factors, the 5-year survival rates of Hispanic and African-American children were significantly lower than those of Asian and Caucasian children ($p < 0.001$): Asian, 75%; Caucasian, 73%; Hispanic, 66%; and African-American, 62%.[42]

As suggested by many investigators, the interracial differences in clinical outcomes for ALL may be caused by pharmacokinetic and/or pharmacodynamic differences. However, to test such a hypothesis can be challenging because the individual effects of each drug given in combination often cannot be differentiated from each other. In this context, vincristine is an exceptional drug because its dose-limiting neurotoxic effects are unique and thus attributed to vincristine therapy alone. Interestingly, in a retrospective study at Riley Hospital (Indianapolis, IN), vincristine-related neurotoxicity was more commonly observed in Caucasian children compared to African-American children (35% versus 4.5%, $p = 0.004$).[43] As a logical extension of this observation, African-American children may be more likely to have a reduced exposure to vincristine resulting in less neurotoxicity but reduced overall survival rates. This hypothesis is the basis for our study of vincristine disposition and the role of the genetically polymorphic enzyme CYP3A5, an enzyme more commonly expressed in African-Americans.

6. Pharmacokinetics

a) Distribution

Vincristine diffuses into cells, binds to tubulin, and as a result, has a large steady-state volume of distribution (approximately 168 L/m^2).[44] Although many compounds with large volumes of distribution are highly lipophilic and concentrate in fat stores and cell

membranes, vincristine targets tubulin-rich tissues including muscle, intestines, platelets, and blood cells.[45] Vincristine also accumulates in red blood cells, white blood cells, and platelets resulting in an overall blood-to-plasma ratio of 1.2.[11] Interestingly, for specific cancer applications, vincristine-loaded platelets (incubated in vincristine and rinsed to remove excess drug) have been used for targeted drug delivery.[46] Vincristine does bind to plasma proteins, specifically α-glycoproteins, albeit with low affinity.[47] Thus, the fraction of drug unbound in human plasma is approximately 0.5 and not dependent on vincristine concentration (40 to 256,000 ng/mL).[48]

Tissue distribution of vincristine is also influenced by expression of multi-drug resistance proteins: P-gp, MRP1, and MRP2. These transporters can actively efflux vincristine from the cytoplasm of many cell types. Vincristine and/or its metabolic products are actively transported by hepatocytes into the bile most likely by P-gp and MRP2 in the cannalicular membrane.[12,49] For one patient treated with radiolabeled vincristine, at any time point up to 72 h, the concentration of vincristine-related compounds was 40-fold higher in the bile than the plasma.[12] As demonstrated in a mouse knockout model, expression of MRP1 reduced the accumulation of vincristine in several organs (kidney, lungs, and heart).[50] In addition, the expression of both P-gp and MRP1 protected the bone marrow from myelosuppression.[50] Vincristine penetration to the central nervous system is likely reduced by expression of P-gp and MRP1 at the blood-brain barrier. In one pediatric study, no vincristine was detected in the cerebral spinal fluid.[51] However, the peripheral nerve cells are apparently not as well protected; distribution and accumulation of vincristine are likely responsible for the cumulative peripheral neurotoxicity of vincristine.[38]

b) Clearance

Vincristine pharmacokinetics are typically characterized by one or two distribution phases followed by a log-linear decline in plasma concentrations with a terminal half life in adults of 23 to 84 h.[44,52] Some pharmacokinetic studies reported shorter terminal half lives (3 to 8 h) because the terminal elimination phase of vincristine was not adequately characterized by late time point samples.[11,53] To accurately fit the distribution phases, two or three-compartment pharmacokinetic models are typically used with elimination occurring from the central compartment.

The clearance of vincristine is primarily hepatobiliary with only 8 to 15% of the dose excreted in the urine.[11] These radiolabel studies estimated the percentage excreted unchanged in the feces and urine to be 50 to 60%.[11,12] However, the radiochromatograms from these studies are difficult to interpret for two reasons. First, the degradation products and/or metabolites of vincristine may have been artifacts of the *in vitro* assay because the vincristine degraded in the control samples. Also, as discussed earlier, the parent drug may have co-eluted by HPLC with other vincristine-related compounds.

Vincristine pharmacokinetic parameters, in particular clearance values, are highly variable between individuals and between studies. Early vincristine clinical studies estimate an 11-fold variability in drug exposure (dose-corrected area-under-the-curve, AUC) between adult patients.[53] More recent pediatric clinical pharmacokinetic studies report an 19-fold variability in the dose-corrected AUC.[54] Although the data are scattered, vincristine is generally reported to be a low to medium hepatic extraction ratio drug. Thus, hepatic metabolic clearance should be a primarily a function of intrinsic

clearance, the maximum metabolic clearance independent of binding and hepatic blood flow.

When evaluating vincristine pharmacokinetics in published studies, several issues need to be considered. First, for early pharmacokinetic studies, only adult patients were recruited; later in 1994, the studies shifted almost exclusively to pediatric patients.[11,12,44,52-61] This population change prohibits the direct comparison of pharmacokinetic data between the two eras. Another major concern with all studies is the uncertainty of the fit with the selected model (two or three compartment). Using a standard guideline for pharmacokinetic studies, the plasma should be sampled for at least three terminal half lives to account for the vast majority (~90%) of the drug exposure as determined by AUC, area under the curve. However, few studies have reported vincristine concentrations past one half life (24 h).[12,44,52,55] In fact, the pediatric studies routinely used limited sampling strategies and Bayesian approaches to estimate clearance.[54,56-61] As a result, the variability in clearance reported between patients may in part be attributed to high uncertainty in the model estimated parameters. Finally, over the last three decades, the analytical methods changed for vincristine quantification in plasma. For studies prior to 1994, the vincristine concentration was quantified by several different radioimmunoassay assays.[44,52,53,55] The specificities of these assays for vincristine are unknown. Early radiolabel studies quantified the vincristine-related compounds by direct liquid scintillation counting.[11,12] This method of detection was also non-specific for vincristine; by HPLC, only 40 to 50% of the parent drug was recovered.[11,12] In the 1990's, an HPLC assay was developed to quantify vincristine in plasma by electrochemical detection.[62] This particular method was utilized in all

pediatric pharmacokinetic studies of vincristine 1994–2005.[54,56-61] However, in common with the early radioimmunoassays, the specificity of this electrochemical detection method was unknown because vincristine-related compounds by HPLC could co-elute with the parent drug. In addition, the method could not be used to assay plasma samples collected more than 24 h after treatment because the assay limit of quantification for vincristine was 0.5 ng/mL.[62] For plasma samples collected more than 24 h post treatment, all the assays utilized in previous pharmacokinetic studies lacked the selectivity and/or the sensitivity to quantify vincristine. More sensitive and discriminating methods of detection, such as MS/MS, are required to effectively measure vincristine exposure over more than one terminal half life.

B. Cytochrome P450 3A Subfamily

1. Protein Function and Structure

The cytochrome P450s (CYPs) are heme-thiolate enzymes expressed by almost all types of organisms including bacteria, plants, and mammals.[63] For humans, at the time of this publication in GenBank®, the sequences of 54 functional CYPs are documented. The CYP enzymes within cells are localized to the mitochondria or the smooth endoplasmic reticulum (microsomal CYPs). Microsomal human CYP enzymes are expressed in the cells of multiple organs including the small intestines, lungs, kidney, and liver.[63] Hepatic CYPs and some intestinal CYPs are of particular importance because their activities are responsible for the systemic clearance of many drugs. As a result, CYP expression can be a major source of variability in drug exposure. Although at least 10 hepatic CYPs are clinically important in drug disposition, for drugs metabolized by CYPs, the CYP3A enzymes (CYP3A4 and CYP3A5) metabolize more than 50% of

marketed drugs including macrolide antibiotics, immunosuppresants, and anticonvulsants.[63] CYP3A substrates vary in chemical structure but compared to substrates of other CYPs, are typically high in molecular weight, approximately 200 to 800. CYP3A enzymes can metabolize even higher molecular weight substrates such as cyclosporin A with a molecular weight of 1203.[63]

Microsomal CYP enzymes as holoenzymes (heme-bound) catalyze the oxidization of substrates and the reduction of molecular oxygen.[63,64] Two molecules of NADPH provide the 2 e^- and 2 H^+ in the reaction; the redox partners are NADPH-cytochrome P450 reductase and cytochrome b_5. First, the substrate binds to the enzyme at the substrate recognition sequences (SRS) and displaces water from the heme. Upon substrate binding, the Fe^{3+} spin state changes from low to high spin. The substrate binding facilitates the reduction of the heme Fe^{3+} to the ferrous state (Fe^{2+}) by an electron transfer from NADPH-cytochrome P450 reductase. The Fe^{2+} enzyme complex binds molecular oxygen to form an oxy-P450 complex. Subsequently, the complex is reduced by a second electron transfer from NADPH-cytochrome P450 reductase or cytochrome b_5. After two protons are transferred, the O-O bond is cleaved to release water. The oxyferryl intermediate (Fe^{IV}=O) then oxides the substrate prior to its release.

For the CYP cycle, the change from the oxy-P450 complex to the oxyferryl intermediate is the rate-limiting step.[65] The electron transfer of this step is mediated by NADPH-cytochrome P450 reductase and/or cytochrome b_5. However, the exact role of cytochrome b_5 in this process is unknown. As described in several reviews, cytochrome b_5 in CYP reactions may transfer the second electron faster than with the reductase

alone, reduce P450 cycle uncoupling (increase the efficiency), or modulate activity of the complex as an allosteric effector.[65,66]

In a reconstituted system, the *in vitro* reaction kinetics can change profoundly with the addition of cytochrome b_5. For example, in the presence of cytochrome b_5, the 6β-hydroxylation of testosterone by CYP3A4 was stimulated 10-fold.[67] In a study with laurate and CYP4A7, not only was the activity 5-fold higher with cytochrome b_5, the K_m value increased 7-fold.[68] In this case, the change in K_m may have caused a conformation change in the enzyme complex. Cytochrome b_5 effects with the same substrate are also enzyme dependent. In a study with ifosfamide at concentrations at least 5-fold less than the K_m, the addition or co-expression of cytochrome b_5 differentially stimulated the rates of N-dechloroethylation with CYP3A4 and CYP3A5.[69] Using Supersomes with and without co-expressed cytochrome b_5, the N-dechloroethylation activity increased 3-fold for CYP3A5 with cytochrome b_5 but increased 16-fold for CYP3A4 with cytochrome b_5.[69] Finally, with the addition of cytochrome b_5, the metabolic profile of a substrate can be altered. For example, cytochrome b_5 was required for CYP3A5 to metabolize 17α-ethynlestradiol to 17α-oxirene metabolites; these metabolites were responsible for CYP3A5 mechanism-based inactivation.[70]

The *in vitro* enzyme preparations commonly used to evaluate the drug metabolism of substrates contain different amounts of NADPH-cytochrome P450 reductase and cytochrome b_5. cDNA-expressed enzymes, for example CYP3A4 and CYP3A5, can be commercially purchased with co-expressed NADPH-cytochrome P450 reductase (1 pmol/pmol CYP) and/or co-expressed cytochrome b_5 (7 pmol/pmol CYP3A4 or 18 pmol/pmol CYP3A5). These concentrations of redox proteins are much

higher than those in human liver microsomes: NADPH-cytochrome P450 reductase (~0.1 pmol/pmol CYP) and cytochrome b_5 (~1 pmol/pmol CYP).[71,72] Even though the kinetic effects of various concentrations of redox factors have been studied using reconstituted enzyme preparations, the full implications are unknown for individual substrates.[73] Also, given that the effects of cytochrome b_5 are concentration and enzyme dependent,[73] it seems unlikely that the cDNA-expressed enzymes (with or without cytochrome b_5 expression) will accurately predict drug metabolism *in vivo* for every substrate. Thus, models with physiological concentrations of proteins (human liver microsomes, hepatocytes) are necessary to validate the results of the reconstituted systems.

2. Pharmacogenetics

Only low frequency genetic mutations of the *CYP3A4* gene are known to affect CYP3A4 activity.[74] In contrast, *CYP3A5* genetic variants (*CYP3A5*3*, **6*, and **7* versus the wild type *CYP3A5*1*) are common. For individuals with at least one active *CYP3A5*1* allele, significant quantities of CYP3A5 are expressed (CYP3A5 high expressers); approximately 75% of African-Americans, 47% of East Asians, and 19% of Caucasians express high levels of CYP3A5.[75] For the *CYP3A5*3* genotype, a single nucleotide polymorphism (SNP, 6986A>G) in intron 3 creates a consensus splice site. If the mRNA is incorrectly spliced, the mature mRNA contains a premature termination codon. The resulting mRNA produces a truncated, non-functional protein of 101 amino acids; the full-length CYP3A5 protein contains 502 amino acids. Although the vast majority of the mRNA is spliced incorrectly, a small fraction of the mRNA is properly spliced. Consequently, functional CYP3A5 is produced by individuals with the

*CYP3A5*3/*3* genotype, albeit in much lower quantities than that produced by *CYP3A5*1* individuals.[76] The less common *CYP3A5*6* and *CYP3A5*7* coding region variants also produce reduced amounts (*CYP3A5*6*) or no CYP3A5 (*CYP3A5*7*).[76,77] These allelic variants are primarily found in African-American (*CYP3A5*6* and *CYP3A5*7)* and Hispanic (*CYP3A5*6*) populations.[75] Because such a small amount of active CYP3A5 is produced in individuals without the *CYP3A5*1* allele, the other genotypes described are effectively devoid of active CYP3A5 (CYP3A5 low expressers).

3. Expression

In the majority of Caucasian livers, CYP3A enzymes are the most abundantly expressed CYP enzymes in the liver, representing approximately 30% of the total microsomal CYP content.[78] The expression of hepatic CYP3A4 is variable between individuals (i.e. 1.1 to 40.8 pmol 3A4/mg for a liver biopsy study).[79] However, the high inter-individual CYP3A4 variability as reported for human liver microsomal banks (up to 75-fold variation) may be a reflection of variation in the sample preparation methods and/or the diseased and medicated donor population.[80,81] For healthy, unmedicated populations, the *in vivo* CYP3A activities between individuals are less variable; for example, the reported inter-individual variability was approximately 8-fold for midazolam intravenous clearance.[82]

To understand the variability in CYP3A4 expression and the potential for drug-drug interactions, the transcriptional regulation of *CYP3A4* has been studied extensively using cultured human hepatocytes and cell-based reporter assays.[83] Specifically, the following nuclear hormone receptors are known to modulate the transcription of

CYP3A4: the pregnane X receptor (PXR), the constitutive andostane receptor (CAR), the vitamin D receptor (VDR), and the glucocorticoid receptor (GR).[84] GR activation by endogenous concentrations of glucocorticoids (up to modest therapeutic concentrations) most likely indirectly induces CYP3A4 by increasing the transcription rates of *PXR* and *CAR* while PXR, CAR, and VDR activation directly induce CYP3A4 expression by increasing the transcription rates of *CYP3A4* mRNA. The induction of CYP3A4 by PXR, CAR, and VDR occurs at two binding sites on the *CYP3A4* promoter: the ER6 motif (position -160) and the DR3 site (position -7700).[83] Commonly studied ligands that directly induce CYP3A4 expression *in vivo* include phenobarbitol, phenytoin, and rifampin.

In addition to CYP3A4, PXR ligands induce transporters (P-gp, MRP2, and BSEP) and other CYP proteins (CYP2C8, CYP2C9, and CYP3A5).[83] The fold induction of CYP3A5 is generally reported to be less than that of CYP3A4 *in vitro*. For example, in human hepatocytes cultures, 1 mM phenobarbital induced CYP3A4 mRNA 200-fold but CYP3A5 mRNA only 10-fold.[84] Although the *CYP3A5* promoter contains an identical ER6 motif to the *CYP3A4* promoter, the DR3 site is not present.[84] As a result, even though CYP3A5 can be induced by PXR ligands, in a population potentially exposed to PXR ligands, the CYP3A5 protein content may vary less between individuals than that of CYP3A4 because CYP3A5 is less inducible. In support of this hypothesis, the CYP3A5 protein content in human liver microsome banks is typically less variable than the CYP3A4 protein content (22 to 164 pmol 3A5/mg vs. 5 to 187 pmol 3A4/mg).[81]

In some instances, the induction of CYP3A5 by nuclear receptor ligands may be equivalent or higher than the induction of CYP3A4. For example, *CYP3A5* transcriptional regulation by PXR in hepatocytes may be different from the regulation of *CYP3A5* in the intestines. *In vivo* studies before and after rifampin treatment quantified the fold changes in intestinal *CYP3A4* and *CYP3A5* mRNA; for each subject, the fold increase in *CYP3A5* mRNA was equivalent or higher than that of *CYP3A4* mRNA.[84] Also, unlike the *CYP3A4* promoter, the *CYP3A5* promoter contains two glucocorticoid response elements and directly responds to GR activation.[84] Therefore, as compared to an indirect induction of CYP3A4 by glucocorticoids, the expression of CYP3A5 may be more responsive. Finally, the regulation of CYP3A4 is not significant for many extra-hepatic tissues, such as the prostate and kidneys, because CYP3A5 is the primary CYP3A enzyme expressed.[85]

For individuals with the *CYP3A5*1* allele, CYP3A5 can represent more than 50% of the total CYP3A content in human liver microsomes.[71] The CYP3A5 protein contents for individuals with at least one *CYP3A5*1* allele are not consistent between microsomal liver banks; Westlind-Johnsson, et al. (2003)[80] estimated that CYP3A5 was 13 to 27% of the total CYP3A, whereas Lin, et al. (2002)[81] estimated a 40 to 80% contribution. A meta-analysis was recently published of all reported CYP3A4 and CYP3A5 contents for human liver microsomal banks (n = 45 for CYP3A5 high expressers, Caucasian livers).[86] In this report, regardless of the type of CYP3A standard used for immunoquantification, the mean contribution of CYP3A5 was approximately 40% of the total CYP3A protein. Thus, for CYP3A5 high expressers, the CYP3A5 protein is a substantial fraction of the total CYP3A protein.

4. Inhibition

CYP3A4 and CYP3A5 enzyme activities can be inhibited by a variety of clinically important drugs including macrolide antibiotics, HIV protease inhibitors, and antifungals. Many clinically relevant drug-drug interactions occur by mechanism-based inactivation of the CYP3A protein; this inhibition is persistent because the protein is irreversibly modified.[87] Alternatively, competitive inhibitors such as itraconazole continue to inhibit CYP3A enzymes for many days after the parent drug is eliminated from the plasma; the inhibition is likely caused by metabolites with long terminal half-lives. Interestingly, for most CYP3A inhibitors, regardless of the type of inhibition, CYP3A4 is more susceptible to inhibition than CYP3A5.[88-91] As a consequence, for individuals with high CYP3A5 expression, drug/drug interactions with CYP3A substrates can be less pronounced. For one clinical study with coadministration of itraconazole and clopidogrel, a protective effect on platelet aggregation was described for individuals with high CYP3A5 expression.[92] Likewise, after itraconazole administration, the midazolam clearance was less inhibited for individuals with high CYP3A5 expression (60 vs. 70% reduction in clearance with low CYP3A5 expression).[93] Similar clinical results were reported for verapamil, a calcium channel blocker that inhibits its own metabolism by CYP3A4 mechanism-based inactivation.[89] In this case, the verapamil oral clearances of patients with high CYP3A5 expression were on average 2-fold higher than the clearances of patients with low CYP3A5 expression.[94]

5. Roles of CYP3A4 and CYP3A5 in Drug Disposition

cDNA-expressed enzymes are routinely utilized to evaluate the selectivity of a substrate for CYP3A4 and CYP3A5. Because CYP3A4 and CYP3A5 have overlapping but not identical specificities for CYP3A substrates, the CYP3A5 contribution to metabolism is highly substrate dependent. For most tested substrates, the CYP3A5 intrinsic clearances are similar to or less than those of CYP3A4.[71,88,95,96] For example, the intrinsic clearances of tacrolimus with recombinant CYP3A4 and CYP3A5 were similar with less than a 2-fold selectivity for CYP3A5.[97] Some studies with midazolam showed a modest selectivity (3-fold) for CYP3A5;[71] in other studies with midazolam, the CYP3A5 activity was equivalent or less than that of CYP3A4.[95,96,98]

Because most CYP3A substrates are metabolized by both CYP3A4 and CYP3A5, the exact contribution of CYP3A5 to the metabolism of a CYP3A substrate is difficult to determine when both enzymes are present, as with HLMs. The role of CYP3A5 in the metabolism of CYP3A substrates can be evaluated using pairs of HLMs with similar CYP3A4 protein content but different CYP3A5 expression.[71] The pairing of liver samples by CYP3A4 content assumes that the CYP3A4 protein measured by Western blot is enzymatically equal for all HLMs. A highly selective CYP3A4 activity probe, such as itraconazole, can also be used to normalize the activities of CYP3A test substrates.[71] For this type of analysis, statistical differences of the normalized activities between high and low CYP3A5-expressing groups can be calculated. However, this technique cannot quantify the contribution of CYP3A5 of individual livers at different expression levels of CYP3A4. Nevertheless, for studies that utilized these approaches with various CYP3A substrates, up to 30 to 40% of the CYP3A metabolism was

attributed to CYP3A5 activity in high expressers.[71,99] If most substrates are equally selective for CYP3A4 and CYP3A5, this percent contribution is consistent with the CYP3A5 protein expression in the liver (~40% of the CYP3A).[86]

Because CYP3A5 intrinsic clearances are typically lower than or equal to those of CYP3A4, some investigators have proposed that CYP3A5 is not clinically significant in drug disposition.[80] The clinical studies that evaluate the impact of *CYP3A5* genotype on drug disposition are confounded by the variability in CYP3A4 expression and often show substrate dependence. The best studied CYP3A substrates *in vivo* are midazolam and tacrolimus. For clinical studies with midazolam, a common CYP3A *in vivo* probe, the clearance was increased for *CYP3A5*1* carriers[93,100] while other studies did not find a statistical difference between the *CYP3A5* genotypes.[82,101] In contrast, as reported by more than 20 clinical studies, the oral clearances (a function of systemic clearance and bioavailability) of the immunosuppressant tacrolimus were consistently a function of *CYP3A5* genotype.[102] To maintain therapeutic concentrations, the dosage requirements of CYP3A5 high expressers were approximately 25 to 45% higher than those of low expressers.[102] Because tacrolimus is an orally administered drug, CYP3A5 expression in the gut wall may have reduced the bioavailability and thus contributed to the increased dose requirements for CYP3A5 high expressers. However, as shown by two clinical studies of liver transplant patients, hepatic CYP3A5 at least in part contributes to the tacrolimus systemic clearance. For these studies, the majority of the variability in tacrolimus dosing one month post-transplantation was accounted for by the *CYP3A5* genotype of the donor liver, not the recipient *CYP3A5* genotype; the tacrolimus blood concentration/dose ratios were 30 to 60% higher for recipients of *CYP3A5*3/*3* donor

livers.[103,104] Thus, the reduced bioavailability caused by CYP3A5 expression in the gut wall may be less important to tacrolimus disposition than the effect of CYP3A5 expression in the liver.

6. CYP3A-mediated Metabolism of Vincristine

The CYP-mediated metabolism of vincristine has not been evaluated thoroughly using *in vitro* models.[16] Based on data from clinical and *in vitro* studies, CYP3A enzymes are hypothesized to metabolize vincristine. Consistent with CYP3A metabolism, numerous clinical drug-drug interactions were reported between vincristine and CYP3A inhibitors or inducers including itraconazole, nifedipine, and carbamazepine.[28,29,55,105] In addition, the role of CYP3A in the metabolism of vincristine is consistent with other *Vinca* alkaloids: vindesine and vinblastine. In studies with these *Vinca* alkaloids and human liver microsomes, CYP3A was the major CYP enzyme responsible for the formation of one major metabolite.[106,107] The rates of metabolite formation from vindesine and vinblastine were selectively inhibited by CYP3A chemical inhibitors: ketoconazole, troeandomycin, and erythromycin.[106,107] Vincristine was also a chemical inhibitor of metabolite formation; thus vincristine, like vinblastine and vindesine, may be a substrate of CYP3A enzymes.[106,107] Using fresh human hepatocytes, vincristine, vindesine, and vinblastine were transformed to four unknown compounds, presumably metabolites.[10] Unfortunately, experiments were not performed to conclusively determine the mechanisms of formation; for example, incubations without cells or with a chemical CYP inhibitor were not presented. In a different *in vitro* study, using Chinese hamster ovary cell lines, vincristine and vinblastine were less toxic for cells with CYP3A4 overexpression.[108] These results support the hypothesis that vincristine is a substrate of

CYP3A4. However, the complete biotransformation pathways and enzyme kinetics of vincristine are not reported in the literature.[109] The relative roles of CYP3A4, CYP3A5, or any other currently unidentified enzyme in the metabolism of vincristine are unknown.

Based on evidence of interracial differences in clinical outcomes with vincristine therapy, we hypothesized that expression of the genetically polymorphic enzyme CYP3A5 increases the rate of metabolism and ultimately systemic clearance. Thus, for individuals with high CYP3A5 expression, CYP3A5 is a major drug metabolizing enzyme. To understand the roles of CYP3A4 and CYP3A5 in the metabolism of vincristine, we studied the biotransformation of vincristine using various *in vitro* metabolism models: cDNA-expressed CYPs, human liver microsomes, and human cryopreserved hepatocytes. In addition, to understand the role of *CYP3A5* genotype in clearance, we developed a sensitive assay to quantify therapeutic concentrations of vincristine and the major CYP3A metabolite of vincristine in human plasma.

II. Materials

Amersham Biosciences (Buckinghamshire, UK)	[G-^{3}H] vincristine sulfate (3.30 Ci/mmol)
Baxter (Deerfield, IL)	cyclophosphamide
Bedford Labs (Bedford, OH)	methotrexate
Bio-Rad Laboratories (Hercules, CA)	acrylamide ammonium persulfate (APS) bisacrylamide 2-mercaptoethanol nitrocellulose (0.5 μm) SDS TEMED
BioWhittaker (Walkersville, MD)	hepatocyte maintenance media, cat CC3197
BD Gentest Corporation (Woburn, MA)	"Supersomes" cDNA-expressed CYPs co-expressed with or without CYP-reductase and cytochrome b_5 (CYPs 1A1, 1A2, 2A6, 2B6, 2C8, 2C9, 2C19, 2D6, 2E1, 2J2, 3A1, 3A2, 3A4, 3A5, 3A7, and 4A11) insect cell control microsomes WB-3A4 WB-3A5 WB-MAB-3A

CellzDirect (Pittsboro, NC)	cryopreserved hepatocytes (Lot numbers: SD012, SD017, Hu418, Hu4008)
Celsis In Vitro Technologies (Baltimore, MD)	cryopreserved hepatocytes (Lot numbers: AIT, CHD, EHI, FKM, MRS, REL, RML, SCA, ZIJ, ZYZ) hepatocyte thawing media, cat Z990006
Eli Lilly and Co. (Indianapolis, IN)	LSN335984
Enzon Pharmaceuticals (Bridgewater, NJ)	PEG-L-asparaginase
Janssen Pharmaceuticals (Beerse, Belgium)	hydroxyitraconazole (OH-ITZ) methoxyitraconazole (MeO-ITZ)
MetaChem Technologies Inc. (Torrance, CA)	C18 column Inertsil ODS3, 3.0 x 150 mm, 5-µm particle size
Millipore (Bedford, MA)	Centrifree YM-30
Ovation Pharmaceuticals (Deerfield, IL)	dactinomycin
PanVera Corporation (Madison, WI)	cytochrome b_5
Phenomenex (Torrance, CA)	C18 column, Luna, 4.6 x 150 mm, 5-µm particle size

Sigma Chemical Co.	5-bromo-4-chloro-3-indoylphosphate
(St. Louis, MO)	coumarin
	diethyldithiocarbamic acid (DDC)
	DMSO
	furafylline
	glycine
	6β-hydroxytestosterone
	itraconazole (ITZ)
	ketoconazole (KCZ)
	N-desmethyl diazepam (DMDZ)
	NADPH
	nitrotetrazolium blue chloride
	omeprazole
	orphenadrine citrate
	peroxidase, type VI
	pyronin Y
	quinidine
	ScintiVerse
	sulfaphenazole
	testosterone (TST)
	tris base
	tween-20
	vinblastine sulfate (VLB)
	vincristine sulfate (VCR)
	vinorelbine ditartrate (VRL)
XenoTech	cryopreserved hepatocytes
(Lenexa, KS)	(Lot number 652)

All other reagents were of HPLC grade and were purchased from Fisher Scientific (Pittsburgh, PA).

III. Methods

A. Vincristine Incubations with cDNA-expressed CYP Enzymes

1. Human Enzyme Panel

VCR (5 μM) was pre-incubated with CYPs 1A1, 1A2, 2A6, 2B6, 2C8, 2C9, 2C19, 2D6, 2E1, 2J2, 3A4, 3A5, 3A7, and 4A11 (50 pmol of CYP for CYPs 2A6, 2C8, and 2E1; 25 pmol for remaining CYPs) and insect cell microsomes (control; matched protein content to highest CYP) in a suitable buffer (final volume 250 μL) at 37°C. The insect cell microsomes were utilized to account for any endogenous CYP activity. P450 reductase was co-expressed with all CYPs, and cytochrome b_5 was co-expressed with CYPs 2J2, 2E1, and 3A7. Although CYPs 3A4 and 3A5 were also available with co-expressed cytochrome b_5, the enzymes without cytochrome b_5 were utilized to determine the relative CYP activity as a worst case. In accord with the recommendation of the manufacturer, CYPs 2A6, 2C9, and 4A11 incubations were performed in 100 mM Tris buffer with 5 mM $MgCl_2$, pH 7.4 at 37°C and the remaining incubations in buffer (100 mM Na_2HPO_4 with 5 mM $MgCl_2$, pH 7.4). The reactions were initiated with the addition of NADPH (0.5 mM). After 1 h, the incubations were quenched with an equal volume of acetonitrile, chilled, and centrifuged. All incubations with the CYP enzymes were performed in duplicate with the duplicates split by at least three other incubations. The first and last incubations were controls, and the remaining two controls were inserted evenly between CYP incubations. The supernatants were directly assayed by HPLC with UV detection. Statistical significance ($p < 0.05$) was determined using one-way ANOVA for multiple comparisons.

2. Rat CYP3A1 and CYP3A2

cDNA-expressed rat CYP3A1 or CYP3A2 with co-expressed P450 reductase and cytochrome b_5 (100 pmol/mL) was pre-incubated with VCR (40 μM) and buffer (100 mM Na_2HPO_4 with 5 mM $MgCl_2$, pH 7.4). NADPH (0.5 mM) was added to start the reaction. After 30 min, the incubation was quenched with an equal volume of acetonitrile and frozen at -80°C until analysis by HPLC.

3. Inhibition of CYP3A4 Activity with Vincristine and Vinblastine

VCR (0, 10, 20, or 40 μM) and VLB (0, 2.5, 5, or 10 μM) were coincubated in buffer (100 mM Na_2HPO_4 with 5 mM $MgCl_2$, pH 7.4) with cDNA-expressed CYP3A4 with co-expressed cytochrome b_5 (50 pmol/mL). NADPH (0.5 mM) was added to start the reaction. The incubations were quenched after 15 min with an equal volume of acetonitrile and frozen at -80°C until analysis by HPLC. All possible combinations of VCR and VLB concentrations were used, except the zero/zero, for a total of 15 incubations. For each drug combination, the rates of formation were quantified for M1 from VCR and for the equivalent M1 compound from VLB. The identical experiments were also performed using cDNA-expressed CYP3A5 with co-expressed cytochrome b_5 (50 pmol/mL) and an incubation time of 3 min.

4. Inhibition of CYP3A4 and CYP3A5 Activity with Cyclosporin A

VCR (10 μM) in buffer (100 mM Na_2HPO_4 with 5 mM $MgCl_2$, pH 7.4) was co-incubated at 37°C with cyclosporin A (CsA, 10 μM) and enzyme (CYP3A4 or CYP3A5 with co-expressed cytochrome b_5, 48 pmol/mL). The final concentration of methanol was approximately 2.4% (v/v). This concentration was initially chosen because organic concentrations up to 4% (v/v) with cyclosporin A were previously reported.[110] The

vehicle controls without CsA contained an equivalent amount of methanol. The incubations were quenched with an equal volume of acetonitrile after 15 min for CYP3A4 reactions and 3 min for CYP3A5 reactions. The rates of M1 formation were quantified by HPLC.

For other incubations, VCR was co-incubated with multiple concentrations of CsA (0.4 to 25 μM) at a reduced methanol concentration (0% or 0.3%, v/v). For incubations without methanol, the CsA in methanol was evaporated to dryness. The residue was dissolved in buffer (100 mM Na_2HPO_4 with 5 mM $MgCl_2$, pH 7.4) with VCR (20 μM) prior to addition of the enzyme (CYP3A4 or CYP3A5 without cytochrome b_5, 50 pmol/mL). The quench times were 15 min for CYP3A4 reactions and 3 min for CYP3A5 reactions. For incubations at 0.3% methanol, CsA in methanol was added directly to the buffer (100 mM Na_2HPO_4 with 5 mM $MgCl_2$, pH 7.4) and VCR at 37°C. The enzyme (30 pmol/mL) and finally NADPH (0.5 mM) were added for a total volume of 667 μL, and the incubations were quenched with an equal volume of acetonitrile after 15 min. VRL was used as an internal standard. The vehicle controls contained 0.3% methanol but no CsA, and the negative controls lacked NADPH. The fraction of activity not inhibited by CsA (f) and the inhibition dissociation constant (K_i) were estimated using a modified competitive inhibition Michaelis-Menten equation:

Eqn. 1

$$V = (1-f)\left(\frac{V_{\max} \cdot S}{K_m(1+I/K_i)+S}\right) + f\left(\frac{V_{\max} \cdot S}{K_m + S}\right)$$

The maximum rates of M1 formation (V_{max}) were determined from the positive control, and the K_m values were determined from incubations without inhibitors. The substrate

concentration (*S*) was a constant, 20 μM, and the inhibitor concentration (*I*) was the concentration of CsA.

5. Radiolabeled Vincristine

^{3}H-vincristine sulfate combined with unlabeled vincristine sulfate was purified by HPLC. The fractions containing purified VCR as determined by retention time were evaporated to dryness at room temperature. VCR at approximately 10 μM (2 x 10^{6} dpm per incubation) was incubated with CYP3A4 with co-expressed cytochrome b_5 (12.5 pmol), CYP3A5 with co-expressed cytochrome b_5 (25 pmol), and control insect microsomes (matched by CYP3A5 protein content) at a final volume of 250 μL for 15 min. The incubations were quenched with an equal volume of acetonitrile and frozen at -80°C until analysis by HPLC and scintillation counting.

6. Kinetics of M1 Formation using CYP3A4 and CYP3A5

To reduce the VCR-related impurities in the commercially available drug, vincristine sulfate was purified prior to use by HPLC. For the HPLC fractions, a standard curve was used with VRL as an internal standard to quantify the concentration of VCR. Just prior to use, the fractions containing purified VCR were evaporated to dryness at room temperature.

To determine the Michaelis-Menten parameters for CYP3A4 and CYP3A5, VCR (1 to 45 μM) in buffer (100 mM Na_2HPO_4 with 5 mM $MgCl_2$, pH 7.4) was pre-incubated for 3 min with the appropriate CYP enzyme. The reaction was initiated with the addition of NADPH (0.5 mM). After a set incubation time, the incubation was quenched with an equal volume of acetonitrile, chilled, and centrifuged. (For preliminary experiments, the quench and HPLC conditions are described in Methods,

pg. 31). The supernatant (25 or 50 µL) diluted with an equal volume of 0.2% formic acid was directly assayed by HPLC. The Michaelis-Menten parameters of CYP3A4 and CYP3A5 were estimated with enzyme preparations containing cDNA-expressed enzyme alone, with co-expressed cytochrome b_5, and with supplemented cytochrome b_5 (PanVera Corp., Madison, WI) at a molar ratio of 3:1 immediately preceding the incubations. For CYP3A4 and CYP3A5, the enzyme alone and the enzyme supplemented with cytochrome b_5 were tested during the same experiment. This design minimized the variability potentially caused by enzyme lot number or thaw cycle. The incubation conditions for CYP3A4 (25 or 50 pmol, 15 min, 500 µL incubation) and CYP3A5 (25 pmol, 3 min, 500 µL incubation) reactions were optimized based on the HPLC assay limits of quantification and linear conditions. To determine linearity, CYP concentrations and incubation times were varied, and the conditions were selected in which less than 15% of the parent drug was metabolized. Microsomes without cDNA-expressed CYPs (insect cell control Supersomes) were utilized as negative controls.

The Michaelis-Menten constants (K_m) and maximal rates of metabolism (V_{max}) were estimated by fitting the data to a one-enzyme model using non-linear least square regression analysis (WinNonlin 4.0, Pharsight, Mountain View, CA).

B. Quantification of Metabolite Formation and Vincristine Depletion by HPLC

1. Base Extraction and Neutral pH Eluent

The VCR incubation was quenched with ethyl acetate (3 volumes) and 5 N sodium hydroxide (10% by volume). The organic layer was removed and evaporated at room temperature using a rotary evaporator, and the residue was dissolved in mobile phase A (defined below). Separation of VCR and other compounds including M3 was achieved

using a Waters 600E HPLC system (Milford, MA) and a C18 column (Luna, 4.6 x 150 mm, 5-µm particle size; Phenomenex, Torrance, CA) at a flow rate of 1 mL/min with UV detection at 254 nm. The mobile phase consisted of 11 mM sodium phosphate, pH 7.4: methanol (80:20, v/v, mobile phase A) and 11 mM sodium phosphate, pH 7.4: methanol (20:80, v/v, mobile phase B). Starting at 0% B, the gradient conditions were as follows: 0–1 min 0% B, 1–5 min linear increase to 70% B, 5–30 min linear increase to 100% B, 30–35 min 100% B, 35–36 min linear decrease to 0% B, and 36–40 min 0% B. For experiments designed to identify unknown peaks that were collected using the formic acid chromatography (below), the gradient conditions were optimized for separation of M3 from VCR: 0–3 min 66% B, 3–23 min linear increase to 80% B, 23–28 min linear increase to 100% B, 28–42 min 100% B, and 42–50 min 66% B.

2. Acidic pH Eluent

Unless otherwise stated, the following procedure was routinely used to quantify and purify VCR and M1 by HPLC. The VCR incubations with cDNA-expressed enzymes or human liver microsomes were quenched with an equal volume of acetonitrile and stored at -80°C. The thawed samples were vortexed and centrifuged at 1800 *g* to remove any precipitate. A 60 µL aliquot of the supernatant was diluted with an equal volume of 0.2% formic acid, and 100 µL of the solution was injected on the column. Chromatographic separation of M1, M2, VCR, and VRL (internal standard) was achieved with a C18 column (Inertsil ODS3, 3.0 x 150 mm, 5-µm particle size; MetaChem Technologies Inc., Torrance, CA) at a flow rate of 0.4 mL/min. The HPLC system was an Agilent 1100 Series (Wilmington, DE) with a Hewlett Packard 1050 Series UV detector (Wilmington, DE). The mobile phase consisted of 0.2% formic acid

(mobile phase A) and methanol (mobile phase B). The analytes were eluted using the following gradient conditions: 0–7 min 20% B, 7–42 min linear increase to 56% B, and 42–52 min 80% B. The parent drug and metabolites were detected by ultraviolet absorbance at a wavelength of 254 nm.

For quantification of the radiolabeled compounds, fractions of the eluent were collected in 20-second aliquots. The radioactivity of each fraction was determined by liquid scintillation counting (LS3801 scintillation counter; Beckman, Fullerton, CA) with 5 mL of scintillation cocktail (ScintiVerse; Fisher Scientific Co., Fair Lawn, NJ). Prior to counting, the counting efficiency of scintillation counter was calibrated to the quench level using eight tritiated solutions with various degrees of quench. For product samples, the counting efficiencies were interpolated from the quench curve with typical values between 40 and 60%. The target total radioactivity of triated compounds separated by HPLC was typically 500,000 dpm. The unknown eluent aliquots were counted for 30 min or less to achieve final counts with 0.5 to 20% coefficients of variation.

To allow quantification of M1 by UV detection using a VCR standard curve, the extinction coefficients of M1 and VCR were determined by synthesizing M1 from radiolabeled VCR. The radiolabeled M1 and VCR were injected simultaneously on the HPLC column. The eluent fractions for both compounds were collected for scintillation counting. The ratios of the UV area and the radioactive counts (converted to dpm) of each peak were used to calculate the relative extinction coefficients of the compounds. Injections were performed in triplicate. The relative extinction coefficients of M1 and VCR were not significantly different ($p = 0.78$).

C. Preparation of Metabolites and Derivatives for Structural Identification

1. M1 and M1-acetate

VCR (30 μM) was pre-incubated with cDNA-expressed CYP3A5 (100 pmol) and buffer (100 mM Na_2HPO_4 with 5 mM $MgCl_2$, pH 7.4, total volume 1 mL). The reaction was started with the addition of NADPH (0.5 mM). After 40 min, the incubation was extracted with methylene chloride (1 mL). The organic extract was evaporated at room temperature, and M1 was isolated by HPLC. The M1 eluent fractions were extracted with methylene chloride (6 mL), and the solvent was evaporated at room temperature to yield M1. M1-acetate was prepared by mixing M1 and 100 μL of acetic anhydride at room temperature. After 30 min, the reaction was quenched with 200 μL of water and extracted with methylene chloride (3 x 1 mL). The organic extract was dried and reconstituted in the HPLC mobile phase prior to LC/MS/MS analysis.

2. M2 with Peroxidase

Large quantities of M2 were prepared by the oxidation of VCR by horseradish peroxidase (HRP) and hydrogen peroxide, a procedure previously described[9] with slight modifications. Briefly, vincristine sulfate (1.5 mg) was dissolved in 7 mL of buffer (100 mM Na_2HPO_4, pH 7.4) at 37°C. A solution of HRP (1.2 mg), 100 mM Na_2HPO_4 buffer at pH 7.4 (350 μL), and hydrogen peroxide (125 μL, final reaction concentration 0.4 mM) was added to the VCR solution and incubated at 37°C in a shaking water bath for 2 h. The final mixture was extracted with methylene chloride (6 mL), and the organic extract was dried at room temperature. The residue was purified by HPLC, and the eluent fractions were dried to yield M2 (0.5 mg).

3. M3

VCR (30 μM) was pre-incubated with cDNA-expressed CYP3A5 (100 pmol) and buffer (100 mM Na_2HPO_4 with 5 mM $MgCl_2$, pH 7.4, total volume 1 mL). The reaction was initiated with the addition of NADPH (0.5 mM). After 40 min, the incubation was quenched with ethyl acetate (0.5 mL) and 5 N NaOH (100 μL) to promote the base rearrangement of M1. Additional ethyl acetate (3 mL) was added, and the organic layer was evaporated. The resulting residue was purified by HPLC to yield M3.

The product M3 was also prepared directly from HPLC eluent fractions containing purified M1. The fractions (50% of the available volume) were evaporated at room temperature, and the residue was dissolved in water (1 mL) and 5 N NaOH (20 μL). The solution was extracted with ethyl acetate (1 mL), and the organic layer was evaporated at room temperature to yield M3. The residue was dissolved in mobile phase for direct HPLC injection. For the control experiment, the purified HPLC fractions with M1 (the remaining 50%) were evaporated, and the residue was dissolved in mobile phase for HPLC analysis.

D. Structural Determination of Vincristine Metabolites

1. LC/MS Analysis

LC/MS analysis for all non-radiolabeled compounds was performed on a Shimadzu VP Series HPLC (Shimadzu Scientific Instruments Inc., Columbia, MD) interfaced with either a triple quadrupole or ion trap mass spectrometer (TSQ Quantum or LTQ mass spectrometer, Thermo Electron Corporation, Waltham, MA). The analytes were separated on a C18 column (Inertsil ODS-3, 2.1 x 150 mm, 5-μm particle size; MetaChem Technologies, Inc.) at a flow rate of 0.2 mL/min. The mobile phase

consisted of 0.2% formic acid (mobile phase A) and methanol (mobile phase B). The analytes were eluted using the following gradient conditions: 0–3 min 20% B, 3–28 min linear increase to 50% B, 28–45 min linear increase to 80% B, and 45–50 min 80% B. Full scan mass spectra were obtained between 150 to 1050 Da. Positive ion MS/MS was conducted for the ions of interest using argon as the collision gas at 1.5 mTorr and the collision energy of -40 volts. Accurate mass measurements were performed using a Waters Micromass Q-TOF II quadrupole/orthogonal time-of-flight mass spectrometer (Waters Corporation, Milford, MA). The protonated ion (m/z 311.0814) of sulfadimethoxine (Sigma-Aldrich, St. Louis, MO) was used as the lock mass in all accurate mass determinations.

2. NMR Analysis

NMR spectra were acquired on an Inova 500 MHz NMR system equipped with either a 5 mm cold triple-resonance probe or a 3 mm IFC indirect detection probe (Varian Inc., Palo Alto, CA). Compounds were dissolved in either CD_3OD or DMSO-d_6, transferred to a 3 mm NMR tube, and sealed prior to NMR analysis. Proton and carbon chemical shifts were referenced to the residual solvent signals at 3.3 and 49 ppm, respectively, in CD_3OD and at 2.49 and 39.5 ppm, respectively, in DMSO-d_6. Two-dimensional NMR experiments were performed using Varian standard pulse sequences.[111]

E. Preparation of Human Liver Microsomes

Human liver microsomes (HLMs, $n = 56$) were prepared from human liver tissues from the Clinical Pharmacology Liver Bank at Indiana University as described previously.[112] Protein concentrations of the HLMs were determined using the Lowry method.[113]

F. CYP3A4 and CYP3A5 Characterization for Human Liver Microsomes

1. Testosterone 6β-Hydroxylation

Testosterone in methanol was added to incubation buffer (100 mM Na_2HPO_4 with 5 mM $MgCl_2$, pH 7.4) for a final concentration of 200 μM (0.3% methanol, v/v). Microsomal enzyme (0.1 mg/mL) was pre-incubated at 37°C for 3 min, and the reaction was initiated with NADPH (1 mM) for a total volume of 1 mL. Incubations without NADPH were utilized as negative controls. After 10 minutes, the reactions were quenched with an equal volume of chilled ethyl acetate and extracted with an additional 4 mL of ethyl acetate. DMDZ was used as an internal standard. The solvent was evaporated at room temperature, and the residue was reconstituted in the HPLC mobile phase, 20 mM ammonium acetate (pH 6.4)/methanol (40:60, v/v). Chromatographic separation of 6β-hydroxytestosterone from testosterone and other related metabolites was performed on a C18 column (Luna, 4.6 x 150 mm, 5-μm particle size; Phenomenex, Torrance, CA) at a flow rate of 1 mL/min with UV detection at 254 nm. The limit of quantification for 6β-hydroxytestosterone was 330 pmol/mL. Each HLM from the liver bank (n = 56) was incubated with testosterone in triplicate; the coefficients of variation for the replicates were on average <5 % with a maximum of 14%.

2. Itraconazole Hydroxylation

Itraconazole (ITZ) is hydroxylated by CYP3A4 on the methylene carbon of the secondary butyl side chain to form hydroxyitraconazole (OH-ITZ).[34] ITZ was chosen as a substrate because its hydroxylation was reported to be CYP3A4 specific.[34] To confirm these results, the hydroxylase activity at 200 nM ITZ was quantified for cDNA-expressed CYP3A4 (10 pmol/mL, 2 min incubation) and CYP3A5 (100 pmol/mL, 15

min incubation) with co-expressed cytochrome b_5; the results were compared to NADPH negative controls. A higher protein concentration and longer incubation time were required for CYP3A5 because of its lower catalytic activity compared to CYP3A4.

For HLM incubations, an ITZ stock solution was formulated; ITZ in methanol was added to incubation buffer (100 mM Na_2HPO_4 with 5 mM $MgCl_2$, pH 7.4) for a final concentration of 1 μM (0.2% methanol, v/v). The entire ITZ stock solution was aliquoted to 9 tubes, the number of tubes required for one set of incubations. The experiments were also performed at 500 nM ITZ using one ITZ stock solution for multiple sets of incubations (more than 30 tubes). The microsomal enzymes (0.04 to 0.10 mg/mL) were pre-incubated at 37°C with the ITZ stock solution for 3 min, and the reactions were initiated with NADPH (1 mM) for a total volume of 1 mL. After 3 min, the reactions were quenched with an equal volume of ethyl acetate:hexane (50:50, v/v) and 5 N NaOH (40 μL). A time of 3 min was chosen to ensure linear conditions because extended incubations cause the formation of secondary metabolites from ITZ as described previously.[34] To estimate the V_{max}, the ITZ concentrations were chosen higher than the reported apparent K_m, 44 nM.[34] The apparent K_m for one representative HLM with CYP3A5 expression (IUL-49) was estimated in a separate experiment; IUL-49 (0.074 mg/mL) was incubated with a range of ITZ concentrations (1000, 500, 250, 125, 63, 31, and 16 nM) and NADPH (1 mM) in buffer (100 mM Na_2HPO_4 with 5 mM $MgCl_2$, pH 7.4) at 37°C for 3 min. For all experiments, incubations without NADPH were utilized as negative controls. MeO-ITZ was added as an internal standard, and each incubation was extracted with an additional 3 mL of ethyl acetate:hexane (50:50, v/v). After the organic layer was evaporated at room temperature, the residue was

reconstituted in the HPLC mobile phase, 5 mM ammonium acetate/acetonitrile (20:80, v/v). Chromatographic separations of OH-ITZ were performed on a C18 column (Luna, 4.6 x 150 mm, 5-µm particle size; Phenomenex, Torrance, CA) at a flow rate of 1 mL/min. Atmospheric pressure chemical ionization mass spectrometry (LC/APCI-MS, Finnigan Navigator; Thermo Electron Corporation, Waltham, MA) was used to monitor the following ions: *m/z* 721 (OH-ITZ), 705 (ITZ), and 733 (MeO-ITZ). The limit of quantification for hydroxyitraconazole was 1.6 pmol/mL. Select HLMs (n = 22) were incubated with ITZ in triplicate, and the coefficients of variation were on average <10% with a maximum of 18%.

3. Quantification of CYP3A4 and CYP3A5 by Western Blot

Immunodetectable CYP3A4 was quantified in select HLMs (n = 22) from the Clinical Pharmacology Liver Bank. Purified CYP3A4 (14 nmol/mg protein; Invitrogen Corporation, Carlsbad, CA) was used as a standard. CYP3A4 standards at 3 concentrations (0.3 to 1.2 pmol or 0.75 to 3.0 pmol) and protein from typically 4 unknown HLMs were loaded on the same 15-lane gel (Trans-Blot cell, 16 x 20 cm, Bio-Rad Laboratories, Hercules, CA). All duplicate samples were separated by at least 3 lanes, and lanes 1 and 15 were used for two of the six standards. To account for matrix effects, IUL-39, a HLM preparation in which CYP3A4 could not be detected, was added to the standards to give approximately the same total protein content as the unknown samples. Microsomal protein (20 to 50 µg) and the reference standards were diluted with an SDS and β-mercaptoethanol denaturing solution containing a dye (pyronin Y) to a final volume of 20 µl. The diluted samples were heated for 5 min at 95 to 100°C and then loaded on a 0.1% SDS–9.6% polyacrylamide gel. The proteins were separated by

electrophoresis at 44 mV for approximately 3 h until the dye migrated to the bottom of the gel. The proteins were transferred to nitrocellulose over 5 h at 4°C using a constant current of 40 mA. The membrane was soaked in blocking buffer (5% nonfat dry milk in phosphate buffered saline) for 1 h at room temperature and then incubated with a rabbit anti-CYP3A4 primary antibody (1:500, WB-3A4, Gentest, Woburn, MA) for 2 h. After rinsing with phosphate buffered saline with 0.1% tween, the blot was incubated with a goat anti-rabbit secondary antibody (1:500, Gentest, Woburn, MA) for 1 h. The membrane was rinsed with phosphate buffered saline with 0.1% tween and then developed using a 2% solution (m/v) of 5-bromo-4-chloro-3-indolyl phosphate in DMSO (125 µl) and a 0.002% solution (m/v) of nitro blue tetrazolium in 10 mM Tris/HCl, pH 9.5 (13 mL). For all standard curves, the nitrocellulose was developed long enough to quantify the lowest standard concentrations but not too long to prevent saturation at the highest standard concentrations (typically 5 to 15 min). For each gel, standards and unknown samples were assayed at least in duplicate and quantified by densitometry (Kodak 1D, Eastman Kodak, Rochester, NY). The standard curve for each blot was fit by linear regression using the band intensities of the 6 standards; the linearity was maintained at the highest CYP3A4 concentrations. The band intensities of the unknown HLMs were within the values of the high and low standards on the blot. The percent differences between unknown duplicates were less than or equal to 15%; for more than two values, the coefficient of variation was no more than 15%. Similarly, the CYP3A5 content was determined for all high expressers of CYP3A5 (n = 10) in duplicate using a rabbit anti-CYP3A5 primary antibody (WB-3A5, Gentest, Woburn, MA) with 20 µg of loaded protein. In an initial screening experiment, the CYP3A5

reference standard was chosen from three lots of CYP3A5 Supersomes without cytochrome b_5 co-expression. For each lot, equal amounts of CYP3A5 holoprotein per the manufacturer certificate of analysis were loaded on a gel, and the Supersomes lot with the weakest signal or the lowest concentration of apoprotein was chosen. cDNA-expressed CYP3A5 (lot 22), loaded with protein from IUL-52 (a HLM with no detectable CYP3A5), was used for the standard curves (0.23 to 1.2 pmol; 0.5 to 2.0 pmol; or 1.0 to 3.0 pmol). In addition, the CYP3A5 content at 150 µg of loaded protein was estimated for each of the *CYP3A5*3/*3* HLMs. For HLMs that did not express CYP3A5 contrary to their genotype, the HLMs (150 µg loaded protein) were assayed on at least two Western blots with other *CYP3A5*3/*3* HLMs and at least one HLM with high CYP3A5 expression. The purity of CYP3A5, lot 22, was directly compared to purified CYP3A4 utilizing a non-specific, monoclonal CYP3A antibody (WB-MAB-3A, Gentest, Woburn, MA). To generate a standard curve, multiple concentrations of CYP3A4 and CYP3A5 were loaded on the same gel (0.48 to 3.8 pmol CYP3A4 and 0.5 to 8 pmol CYP3A5). The slopes of the signal intensities for each CYP, excluding any signals that were saturated, were utilized to estimate the purity of CYP3A5.

G. Vincristine Incubations with Human Liver Microsomes

1. Kinetics of M1 Formation

All HLMs with at least one *CYP3A5*1* allele (n = 12) and select HLMs with *CYP3A5*3/*3* genotype (n = 10) were used to determine the Michaelis-Menten parameters associated with M1 formation from VCR. The HLMs with *CYP3A5*3/*3* genotype were chosen to include a range of CYP3A activities as determined by testosterone 6β-hydroxylation (700 to 11900 pmol/mg/min). VCR (5, 10, 15, 25, 50,

and 100 μM) was dissolved in buffer (100 mM Na_2HPO_4 with 5 mM $MgCl_2$, pH 7.4) and pre-incubated with select HLMs (0.7 to 3.0 mg/mL) at 37°C. The reaction was initiated with the addition of NADPH (0.5 mM) for a final incubation volume of 250 μL. Incubations without NADPH were utilized as negative controls. The incubations were quenched with an equal volume of acetonitrile, chilled, and centrifuged. The supernatant (50 μL) diluted with an equal volume of 0.2% formic acid was directly assayed by HPLC. For the chosen incubation times (4 to 20 min), the initial substrate concentrations were not reduced by more than 20%. In addition, the incubation conditions for the HLMs were within the linear range for protein concentration and incubation time. Prior to use, the vincristine sulfate starting material was not purified to remove an epoxide impurity (M5) that co-elutes with M1. Even though M5 was included in the M1 integrated area, this impurity did not increase during incubations with or without NADPH (LC/MS/MS data not shown). Thus, the epoxide content in the starting material was subtracted from the M1 area to calculate the final M1concentration. The Michaelis-Menten constants, K_m and V_{max}, were determined by fitting the data to a one-enzyme model (WinNonlin 4.0, Pharsight, Mountain View, CA). The 95% prediction intervals for CYP3A5 low expressers were calculated using SigmaPlot 8.0 (Systat Software, San Jose, CA). The V_{max} and K_m values were estimated for each HLM with average coefficients of variation of 4.2% and 11.1%, respectively.

2. Selective CYP Chemical Inhibition of M1 Formation

Selective chemical inhibitors were used to quantify the contribution of human drug metabolizing CYPs to the formation of M1 from VCR using HLMs.[114] *Vinca* alkaloids that are known CYP3A substrates, VLB and VRL, were used as additional positive

controls at concentrations demonstrated to inhibit VCR metabolism with cDNA-expressed enzymes.[16] HLMs (n = 3, low CYP3A5 expressers; n = 2, high CYP3A5 expressers) were pooled by combining equal amounts of protein. VCR, 15 μM, was incubated with furafylline (CYP1A2, 20 μM), coumarin (CYP2A6, 20 μM), orphenadrine (CYP2B6, 100 μM), sulfaphenazole (CYP2C9, 10 μM), omeprazole (CYP2C19, 10 μM), quinidine (CYP2D6, 5 μM), DDC (CYP2E1, 50 μM), ketoconazole (CYP3A, 1 μM), VLB (10 μM), and VRL (10 μM). All chemical inhibitors were dissolved in methanol and evaporated to dryness. For incubations with competitive inhibitors, pooled HLMs (2 mg/mL), VCR dissolved in buffer (100 mM Na_2HPO_4 with 5 mM $MgCl_2$, pH 7.4), and NADPH (0.5 mM) were added at 37°C for a final volume of 250 μL. The incubations were quenched with acetonitrile after 15 minutes, and VRL (or VLB if an inhibitor co-eluted with VRL) was used as an internal standard. VCR without inhibitor was used to determine the non-inhibited rate of M1 formation. For mechanism-based inhibitors (DDC, furafylline, and orphenadrine), the inhibitors were pre-incubated with the HLM pool (2 mg/mL) and NADPH (0.5 mM) for 15 minutes prior to adding VCR (9.2 μL) in water for a total volume of 250 μL. The reactions were then quenched after 15 min. The HLM pool incubated without inhibitor was used as the control. Sample preparation and HPLC/UV analysis of M1 were the same as described above for VCR metabolism. No interfering peaks from the inhibitors were detected for M1.

3. Cyclosporin A Inhibition of M1 Formation

The rates of M1 formation were quantified for select HLMs (n = 12, CYP3A5 low expressers; n = 10, CYP3A5 high expressers) at one concentration of CsA. VCR (10

μM) was incubated in buffer (100 mM Na_2HPO_4 with 5 mM $MgCl_2$, pH 7.4) at 37°C with CsA (25 μM; 4.8% methanol, v/v). Vehicle controls with 4.8% methanol were used without CsA. The incubation time (4 to 20 min) and protein concentration (1.0 or 2.0 mg/mL) were selected for each HLM; for these conditions, the initial VCR concentration was not reduced by more than 15%. The incubations (250 μL) were initiated with NADPH (0.5 mM) and quenched with acetonitrile. VRL was added as the internal standard. The samples were frozen at -80°C until analysis by HPLC.

Using two HLMs (IUL-59 and IUL-86), the rates of M1 formation were quantified with CsA at various concentrations (0, 0.5, 1, 2, 5, 10, 20, and 40 μM). Prior to the incubations, the methanol from the CsA stock solution was evaporated in the incubations tubes. To facilitate CsA dissolution, the microsomal protein (1.0 mg/mL) was added to the incubation tubes first. All incubations were quenched with acetonitrile after 10 min. The other incubation and quench conditions were identical to the screening experiments at 4.8% methanol (above).

The rates of M1 formation were quantified at 20 μM VCR with HLMs (n = 3, CYP3A5 low expressers; n = 3, CYP3A5 high expressers) at different concentrations of CsA (0.4 to 25 μM, 0.3% methanol). VCR in buffer (100 mM Na_2HPO_4 with 5 mM $MgCl_2$, pH 7.4) was co-incubated at 37°C with CsA and microsomal enzyme (1.0 or 2.0 mg/mL). The incubations were initiated with NADPH (0.5 mM) in a total volume of 667 μL and quenched with an equal volume of acetonitrile after 20 min. The vehicle controls contained 0.3% methanol but no CsA; the negative controls lacked NADPH. The fraction of activity not inhibited by CsA (f) and the inhibition dissociation constant (K_i) was estimated using Eqn. 1. The maximum rates of M1 formation (V_{max}) were

determined from the positive control, and the K_m values were determined from incubations without inhibitors. The substrate concentration (*S*) was a constant, 20 μM, and the inhibitor concentration (*I*) was the concentration of CsA. For IUL-79, because the model did not fit the data, the highest concentration of CsA was used to estimate the uninhibited fraction.

4. Inhibition of M1 Formation by Methanol and Acetonitrile

VCR (20 μM) and IUL-42 (1.2 mg/mL) were co-incubated in buffer (100 mM Na_2HPO_4 with 5 mM $MgCl_2$, pH 7.4 at 37°C) in the presence of methanol or acetonitrile (0, 0.25, 0.5, 1, and 2%). The incubations were initiated with NADPH (0.5 mM) in a total volume of 200 μL and quenched after 4 min. VRL was added as an internal standard. The rates of M1 formation were quantified by HPLC.

H. Binding of Vincristine

1. Microsomal

The fraction unbound of VCR with HLMs was quantified using ultrafiltration (Centrifree YM-30, Millipore, Bedford, MA). Pooled HLMs (described by Methods, pg. 42) were assayed at 5 μM VCR in buffer (100 mM Na_2HPO_4 with 5 mM $MgCl_2$, pH 7.4) at 0.7, 1.2, 2.0, and 3.0 mg/mL of protein. After the VCR solution was incubated at 37°C for 30 minutes, 800 μL aliquots were added in triplicate to the filtration devices and the control tubes to determine initial concentrations. For the chosen centrifugation conditions (37°C, 4 minutes, 1400 *g*), less than 15% of the total volume was filtered. VRL was the internal standard, and an equal volume of acetonitrile was used to precipitate protein. VCR concentrations were quantified by HPLC. The apparent fraction unbound ($f_{u,app}$) was defined as the ratio of the unbound concentration in the

filtrate to the total concentration. A partition approach assuming non-saturable binding of VCR to protein and the ultrafiltration apparatus[115] was used to calculate the fraction unbound caused by non-specific binding to the ultrafiltration device ($f_{u,nsb}$) and the fraction unbound (f_u) at any protein concentration (C_p) using $f_{u,app}$. The binding parameter (K) and $f_{u,nsb}$ were estimated by non-linear regression (WinNonlin 4.0, Pharsight, Mountain View, CA) for the pooled HLMs using the following relationship:

Eqn. 2

$$f_{u,app} = f_{u,nsb} \cdot f_u = f_{u,nsb}\left(\frac{1}{1+(C_p \cdot K)}\right)$$

2. Plasma

The fraction unbound of VCR was quantified using human plasma from three donors. The plasma samples with VCR (1 μM) were incubated at 37°C for 30 minutes. For one donor, the plasma was diluted (1:1, 1:4, and 1:9) with phosphate buffered saline (0.14 M NaCl, 0.01 M Na_2HPO_4, pH 7.4). As described previously with microsomes, the apparent fractions unbound ($f_{u,app}$) were used to estimate the binding parameter (K) and the fraction unbound caused by the non-specific binding to the ultrafiltration apparatus ($f_{u,nsb}$) by Eqn. 2. For the plasma dilutions, the protein concentration (C_p) was expressed as a percentage of the plasma. For all samples, VRL was used as an internal standard, and an equal volume of acetonitrile was used to precipitate protein.

3. Whole Blood

Freshly collected, heparinized whole blood (250 μL) was incubated at 37°C for 15 minutes with HPLC purified ^{3}H-VCR (100 nM final concentration, 1.0 x 10^4 dpm). After the samples were centrifuged for 5 min at 1800 *g*, aliquots of the supernatant (2 x

50 µL) were collected for scintillation counting (LS3801 scintillation counter; Beckman, Fullerton, CA). For the control experiments, human plasma was used in place of whole blood. The blood-to-plasma ratio (BPR) was calculated by dividing the dpm values from the controls by the dpm values from the whole blood. All incubations were performed in duplicate.

The partitioning of VCR and M1 in whole blood and plasma was also determined at high and low concentrations of drug at room temperature. Freshly collected, heparinized blood (1.3 mL) was spiked with different volumes of VCR/M1 stock solution (4.6/2.3 and 0.2/0.1 ng/mL final concentrations). The samples were rocked at room temperature for 15 min and then held stationary for 15 min. The whole blood samples were centrifuged for 10 min at 1800 *g*, and the plasma (0.5 mL) was aliquoted into polypropylene extraction tubes. The plasma was stored at -80°C until extraction and quantification of VCR and M1 by LC/MS/MS.

I. Incubations with Cryopreserved Human Hepatocytes

1. Cell Preparation

Cryopreserved human hepatocytes (Celcius In Vitro Techonologies, CellzDirect, or Xenotech) were rapidly thawed in a water bath at 37°C for 75 to 90 s. The vials were emptied into pre-warmed hepatocyte thawing media and suspended by gentle inversion. To isolate the cells, the suspension was centrifuged at 50 g for 5 min at room temperature. After the supernatant was removed, 2 mL of hepatocyte maintenance media (37°C, perfused with oxygen:CO_2, 95:5) was added. The cells were suspended by gently inverting the tube. The viability of the cells was quantified using an automated viability analyzer (Vi-Cell, Beckman-Coulter, Fullerton, CA); the post-thaw

viability was more than 50%. The cell suspension was diluted with hepatocyte maintenance media to target a concentration of 3.0 x 10^6 cells/mL.

2. Vincristine and Testosterone Incubations

For intact cell incubations with VCR, 50 µL of the cell suspension (150,000 cells/well) was added to an individual well of a 96-well flat bottom plate with 50 µL of VCR (4 µM final concentration) in hepatocyte maintenance media. In some wells, chemical inhibitors (ketoconazole, 10 µM; CsA, 20 µM; and LSN335984, 5 or 50 µM) were coincubated with VCR. The plates were incubated in a humidified CO_2 incubator with shaking for up to 4 h at 37°C. Each well was quenched with 100 µL of 20 µM VRL (internal standard) in acetonitrile. For certain wells, the cells were separated from the media by centrifugation at 50 *g* for 5 min prior to the quench. In this case, an aliquot of the media after centrifugation was added to an equal volume of quench solution. After the excess media was removed, the cell pellet was dissolved in 100 µL of quench solution. Two additional negative control experiments were performed at each time point using the same 96-well flat bottom plates; VCR was incubated in media without cells, and the cell suspension was sonicated prior to mixing with VCR. All solutions were stored at -80°C until analysis by LC/MS (Methods, pg. 51).

Additional experiments were performed with sonicated cryopreserved hepatocytes supplemented with NADPH. After the hepatocytes were counted and diluted to the target concentration as described in the previous section, the cells were centrifuged at 50 *g* for 5 min. The media was removed and replaced with incubation buffer (100 mM Na_2HPO_4 with 5 mM $MgCl_2$, pH 7.4). The hepatocyte suspension was sonicated to create the "cell lysate." This cell preparation (50 µL) was added to 50 µL

of a VCR (4 μM final concentration) and NADPH (0.5 mM final concentration) solution in incubation buffer. The solution was incubated for up to 2 h at 37°C in a shaking water bath and then quenched with 100 μL of 20 μM VRL (internal standard) in acetonitrile. The samples were stored at -80°C prior to analysis by LC/MS.

To quantify the CYP3A4 activity, testosterone (final concentration 200 μM, 0.75% methanol) was added in methanol to the incubation buffer. An appropriate volume of cell lysate was added to the testosterone solution (200 μL) with NADPH (1 mM) for a pre-sonicated cell density of 0.3 x 10^6 cells/mL. The suspension was incubated in a shaking water bath for 10 min, quenched with 200 μL of ethyl acetate, and stored at -80°C prior to analysis by HPLC as described in Methods, pg. 37, with slight modifications. Because the incubation volume was only 200 μl, the chromatographic separation of the metabolites was achieved on a smaller diameter C18 column (Inertsil ODS-3, 2.0 x 150 mm, 5-μm particle size; MetaChem Technologies, Inc) at an eluent flow rate of 0.2 mL/min.

3. Michaelis-Menten Kinetics of M1 Formation

For one lot of cryopreserved hepatocytes (EHI), the Michaelis-Menten kinetic parameters were estimated for intact cells and cell lysate (NADPH supplemented). VCR at approximately 100, 50, 25, 12.5, 6.3, and 3.1 μM was incubated with the appropriate cell preparation (1.5 x 10^6 cells/mL). The incubations were quenched with 20 μM VRL in acetonitrile after 90 min (intact cells) or 13 min (cell lysate). The no cell controls or NADPH negative incubations were also performed at each concentration of VCR and quenched after 90 or 13 min, respectively. The samples were stored at -80°C prior to HPLC analysis.

4. Radiolabeled Vincristine

The HPLC eluent fractions of purified ^{3}H-VCR (10 μCi) were divided between microcentrifuge tubes and evaporated to dryness at room temperature. Except when noted, the conditions for the incubations with cryopreserved hepatocytes (Celcius In Vitro Technologies, lot EHI) were the same as described previously in Methods, pg. 48. ^{3}H-VCR (8 μM, approximately 1 x 10^{7} dpm/tube, 50 μL final volume) was dissolved in media, transferred to individual wells in a 96-well plate, and incubated with intact cells or intact cells with ketoconazole (10 μM) for 4 h. The ^{3}H-VCR at the same concentration was also incubated with a cell lysate preparation in microsomal incubation buffer with and without NADPH for 30 min. For the intact cell incubation without ketoconazole, the media and cells were separated by centrifugation, and radiochromatograms were generated from both fractions. All incubations were quenched with an equal volume of acetonitrile and stored at -80°C prior to analysis.

To generate radiochromatograms, the samples were thawed and centrifuged at 1800 *g* for 10 min. The supernatant was diluted with an equal volume of 0.2% formic acid and directly injected on a C18 column (Inertsil ODS-3, 3 x 150 mm, 5-μm particle size; MetaChem Technologies, Inc.). Separation of analytes was achieved using gradient conditions previously described (Methods, pg. 35) at an eluent flow rate of 0.4 mL/min. The samples were fractionated into 96-well Scintiplate-96 plates at 15 sec/well using a Gilson 215 Liquid Handler. The plates were dried using a GenerVac Personal Evaporator and counted using a Perkin Elmer 1450 LCS and Luminescence Counter (MicroBeta TriLux).

5. Quantification of M1 and Vincristine by LC/MS

All hepatocyte samples containing VCR were thawed, vortexed, and centrifuged at 1800 *g* for 10 min. The supernatant was diluted with an equal volume of 0.2% formic acid. For the experiments described in Methods, pg. 48, the M1 and VCR concentrations were quantified by LC/MS analysis (ThermoQuest; ThermoFinnigan, San Jose, CA) in positive electrospray ionization (ESI^+) mode using selected ion monitoring of VCR (*m/z* 413), M1 (*m/z* 397), and VRL (*m/z* 390*)*. Xcalibur software (version 1.0, ThermoFinnigan, San Jose, CA) was utilized for data acquisition and processing. The VCR/M1 standard and the chromatography conditions were identical to those used during LC/MS/MS analysis of plasma (below).

J. *CYP3A5* Genotyping

DNA samples isolated from the Indiana University human liver bank samples and cryopreserved hepatocytes were genotyped for the *CYP3A5*3* and *CYP3A5*6* allelic variants using allele-specific PCR methods and primers described previously[116] with SYBR-green detection.[117] A TaqMan allelic discrimination assay (Applied Biosystems, Germany) was used to determine the *CYP3A5*7* allelic variant.[118] The genotypes were determined by the Clinical Pharmacology Pharmacogenetics Core Laboratory.

K. Prediction of CYP3A5 Contribution to Vincristine Metabolism

The fraction of cytochrome P450 metabolism mediated by CYP3A5 (f_{3A5}) was estimated using the following relationship:

Eqn. 3

$$f_{3A5} = \frac{(C_P \times CL_{\text{int}})_{3A5}}{(C_P \times CL_{\text{int}})_{3A5} + (C_P \times CL_{\text{int}})_{3A4}}$$

The intrinsic clearances (CL_{int}) of CYP3A4 and CYP3A5 were calculated using the estimated Michaelis-Menten parameters of M1 formation with cDNA-expressed enzymes (V_{max}/K_m). The intrinsic clearances were used to estimate contribution because the therapeutic concentrations of VCR are well below the K_m. The protein contents (C_P) of CYP3A4 and CYP3A5 were estimated by the median immunoquantified values as determined by Western blot in HLMs with high CYP3A5 expression (n = 10) described in Methods, pg. 39.

The contribution of CYP3A5 to the formation of M1 was estimated for individual HLMs with high CYP3A5 expression (n = 10). Using only CYP3A5 low expressing HLMs (n = 12), the relationship was defined by linear regression (without weighting) between the CYP3A4 selective activities (or protein contents) and the maximum rates of M1 formation. With this correlation, using the CYP3A4 selective activity (or protein content), the maximum rate of M1 formation mediated by CYP3A4 ($V_{max,3A4}$) was calculated for each high CYP3A5 expresser; the remaining M1 activity ($V_{max,3A5}$) was assumed to be mediated by CYP3A5. Thus, the fraction of metabolism mediated by CYP3A5 $(f_{3A5})_{HLM}$ was calculated using the following equation:

Eqn. 4

$$(f_{3A5})_{HLM} = \frac{V_{\max} - V_{\max,3A4}}{V_{\max}}$$

L. Prediction of Vincristine Hepatic Clearance

For individual livers, a corresponding hepatic blood clearance of VCR (CL_H) was estimated using the well-stirred model:[119]

Eqn. 5

$$CL_H = Q_H \left(\frac{f_{u,p}/\rho \cdot CL_{\text{int}}}{Q_H + f_{u,p}/\rho \cdot CL_{\text{int}}} \right)$$

The well-stirred model assumes that the unbound drug concentration in the plasma is in rapid equilibrium and equal to the unbound intracellular hepatocyte concentration; this concentration is directly related to the rate of drug elimination.[119] Also, the liver is a well-stirred compartment such that the concentration of drug in the liver is equal to the concentration in the venous blood.[119] For VCR, a plasma fraction unbound ($f_{u,p}$) of 0.51[48] and a blood-to-plasma ratio (ρ) of 1.2[11] were used. Hepatic blood flow (Q_H) of 1500 mL/min for a 70 kg man was assumed. Intrinsic clearance (CL_{int}) was calculated using the estimated Michaelis-Menten parameters, V_{max}/K_m, from the *in vitro* model. The *in vitro*/*in vivo* scaling assumed a liver mass of 1.5 kg, a microsomal mass of 45 mg per 1 g of liver, and a microsomal mass of 1 mg per 3 x 10^6 hepatocytes.[120]

M. Quantification of Vincristine in Human Plasma and Urine

1. Synthesis of M1 from Vincristine

The major metabolite of VCR, M1, was not commercially available as a reference standard. To quantify M1 in plasma, a stock solution containing M1 and VCR was prepared by incubating VCR with cDNA-expressed CYP3A5. Vincristine sulfate in methanol (100 µl, 0.2 mg/mL) was evaporated at room temperature and dissolved in buffer (100 mM Na_2HPO_4 with 5 mM $MgCl_2$, pH 7.4). VCR (20 µg/mL), cDNA-

expressed CYP3A5 (50 pmol/mL), and NADPH (0.5 μM) were incubated for 30 minutes at 37°C (1 mL total volume). The incubation was quenched with methylene chloride (8 mL) and 200 μl of 10% trichloroacetic acid (TCAA). After the organic extract was dried at room temperature, the residue was reconstituted in 0.2% formic acid in water/methanol (80:20, v/v). The resulting VCR and M1 stock solution was stored at 4°C. Just prior to each use, the concentrations of VCR and M1 in the stock solution were quantified by HPLC. Analyte separation was achieved on an analytical C18 column (Inertsil ODS-3, 3.0 x 150 mm, 5-μm particle size; MetaChem Technologies Inc., Torrance, CA). The mobile phase consisted of 0.2% formic acid (mobile phase A) and methanol (mobile phase B). The analytes were eluted using the following gradient conditions: 0–7 min 20% B, 7–42 min linear increase to 56% B, 42–52 min 80% B, and 52–60 min 20% B. Standard curves were generated from two independent stock solutions of vincristine sulfate in methanol (0.2 mg/mL), and the average values were used to calculate the unknown concentration of VCR in the stock solution. M1 was previously shown to have the same extinction coefficient as VCR.[121] Therefore, the M1 concentration was calculated as a fraction of the VCR concentration using area ratios. All samples were assayed in triplicate.

2. Purification of Internal Standard

To optimize the sensitivity of the assay by LC/MS/MS, VLB was purified by HPLC prior to use because trace amounts of VCR were present in the raw material. The HPLC conditions were the same used to quantify M1 and VCR (Methods, pg. 53). The purified VLB, approximately 10 μg, was collected in mobile phase, diluted with water to a final volume of 10 mL, and stored at 4°C.

3. Standards, Quality Controls, and Sample Preparation for Urine

For quantification of VCR and M1 in urine, calibration standards were prepared using a stock solution of VCR and M1 (Methods, pg. 53). The stock solution was serially diluted (1:4) with 0.2% formic acid in water and methanol (80:20, v/v) to prepare 6 working solutions daily. The calibration standards were prepared by adding the following solutions to 100 µL of blank urine: 10 µL of the appropriate working solution; 80 µL of 0.2% formic acid in water and methanol (50:50, v/v); and 10 µL of purified VLB in 5% methanol. Two QC working solutions were prepared daily by independent serial dilutions of the stock solution (1:1 and 1:99). With these working solutions, the QC standards were prepared using the identical procedure as described for the calibration standards. For the clinical samples, the urine was centrifuged to remove any precipitates. The preparation was identical to the calibration standards with one exception; 10 µL of 0.2% formic acid in water and methanol (80:20, v/v) was added to 100 µL of urine instead of 10 µL of working solution. For all samples, 50 µL of each solution was directly injected and analyzed by LC/MS/MS.

4. Plasma Assay Development

a) Extraction Solvent and pH

A protein precipitation method was first evaluated without an extraction step. VCR (0.1 µM) and VRL (0.1 µM) were quantified in plasma (150 µL) after precipitation with 10% TCAA (30 µL). The sample was centrifuged at 1800 *g* for 10 min, and the supernatant (20 µL) was diluted with an equal volume of 0.2% formic acid and analyzed by LC/MS. After this method was unsuccessful, extraction procedures were pursued.

Screening experiments were performed to determine the optimum solvent choice and pH for the extraction of VCR and M1 from buffer. VCR (1 μM) was incubated in buffer (100 mM Na_2HPO_4 with 5 mM $MgCl_2$, pH 7.4) with cDNA-expressed CYP3A5 (50 pmol/mL) and NADPH (0.5 mM) at 37°C for 9 min. The incubations (300 μL) were quenched with an equal volume of solvent, either acetonitrile or an immiscible organic solvent (ethyl acetate, hexanes, t-methylbutylether, or methylene chloride). To reduce the pH of extraction for certain incubations, 10% trichloroacetic acid (70 μL) was added. Extraction at a high pH was not tested because M1 was known to degrade to M3 readily in the presence of NaOH. In all cases, VRL was used as an internal standard. For the incubations that were quenched with acetonitrile, the solids were removed by centrifugation; the supernatant was evaporated; and the residue was dissolved in mobile phase A for direct HPLC injection. For the other incubations quenched with immiscible solvents, the organic layer was evaporated, and the residue was dissolved in mobile phase A for HPLC analysis. To determine relative recoveries of VCR, M1, and VRL using the various immiscible solvents, the UV areas were compared to the acetonitrile control. In addition, to evaluate degradation of VCR, the VCR N-oxide was quantified.

VCR (1 μM) was spiked into blank human plasma (500 μL) and extracted with toluene (1 mL) or methylene chloride (1 mL). The organic phases were evaporated at room temperature, and the residues were reconstituted in mobile phase A (0.2% formic acid and methanol, 20:80, v/v) for analysis by HPLC and LC/MS. The recoveries of VCR were estimated by HPLC; the VCR-related impurities were compared between the samples using LC/MS in full scan mode. The experiment was repeated with increased

volumes of toluene and methylene chloride (4 mL each) and the addition of 100 µL of 10% TCAA.

b) Internal Standard

For the VCR plasma assay, two possible internal standards, vinblastine (VLB) and vinorelbine (VRL), were investigated. VCR (40 ng/mL) and each internal standard (40 ng/mL) were extracted from plasma (0.5 mL) with methylene chloride (3.5 mL) and in some cases 100 µL of 10% TCAA. Prior to separation of the methylene chloride, the two-phase solution in the phase separator apparatus was either agitated by manual shaking (10 sec) or by mechanical shaking (10 min). The extraction recoveries for all analytes were quantified by LC/MS.

c) Adsorption

VCR, VRL, and VLB solutions (0 to 50% methanol) were formulated using water stock solutions in different materials of construction (glass or polypropylene). The analyte concentrations were quantified by LC/MS. For another experiment, VCR in methanol (30, 10, 3, 1, 0.3, 0.1 ng) was evaporated in polypropylene tubes alone and in the presence of VLB (20 ng). The residue was dissolved in mobile phase A (0.2% formic acid: water, 80:20, v/v), and the recovery was quantified by LC/MS for VCR.

d) Dissolution of Concentrate

Because the residue after the methylene chloride extraction was not easily dissolved in mobile phase A, the recoveries of VCR (20 ng) and VLB (20 ng) were quantified by LC/MS using two different dissolution approaches. The pellet was first dissolved using methanol (25 µL), and the tube was vortexed for 10 sec. The final composition was adjusted with 100 µL of 0.2% formic acid. Alternatively, after mobile phase A (125

μL) was added, the pellet was scraped from the tube with a pipette tip, and the tube was vortexed for 10 sec.

e) Optimization of LC/MS Conditions

A solution containing VCR in mobile phase A was infused directly to the mass spectrometer (ThermoQuest; Thermo Electron Corporation, Waltham, MA) in positive ESI mode to optimize the detection settings for the maximum signal, the VCR dicharge ion at *m/z* 423.2. The signal to noise ratio was also evaluated for the VCR monocharge and dicharge ions by LC/MS for the neat stock solution and the extracted standards with VCR. Separation of analytes was achieved using a C18 column (Inertsil ODS-3, 2.1 x 150 mm, 5-μm particle size; MetaChem Technologies Inc., Torrance, CA) at a flow rate of 0.2 mL/min. The methanol concentration during the gradient elution was adjusted to allow baseline separation of M1, VCR, and internal standard without interference from peaks in the blank plasma. For LC/MS/MS analysis, a solution containing VCR and M1 and a separate solution with VLB were infused in mobile phase B to determine the optimal detection conditions.

5. Standards and Quality Control Samples for Plasma

A stock solution of VCR at 1.2 ng/μL and M1 at 0.62 ng/μL as described above (Methods, pg. 53) was used to prepare calibration and QC samples for plasma extraction. Working solutions were prepared the day of the experiment by diluting the stock solution with 0.2% formic acid in water and methanol (80:20, v/v). Calibration standards at nominal concentrations of 24, 8, 2.4, 0.8, 0.24, 0.08, 0.024, and 0.012 for VCR and 12, 4, 1.2, 0.4, 0.12, 0.04, and 0.012 ng/mL for M1 were prepared by spiking 20 μL of the appropriate working solution into 500 μL of pooled blank plasma.

Separate working solutions were used to prepare three concentrations of QC samples by adding appropriate amounts of working solution to pooled blank plasma, and 500 µL aliquots were frozen at -20°C until use. The nominal concentrations of the QC samples were 19, 0.92, and 0.047 ng/mL for VCR and 9.5, 0.47, and 0.024 ng/mL for M1. For routine analysis, QC samples were prepared daily from the same stock solution as the calibration standards but with independent dilutions of the stock solution.

6. Final Extraction Conditions for Plasma

To 500 µL of plasma, 10 µL of purified VLB in water (1 ng/µL), 100 µL of 10% trichloroacetic acid in water, 20 µL of 0.2% formic acid in water and methanol (80:20, v/v), and 8 mL of methylene chloride were added. The sample was vortexed for 30 sec, centrifuged at 1800 *g* for 10 min, and then transferred to a phase separator (Biotage, Uppsala, Sweden). The organic layer was collected and evaporated at room temperature using a Savant concentrator (Thermo Electron Corporation, Waltham, MA). The residue was reconstituted in 125 µL of 0.2% formic acid in water and methanol (80:20, v/v), and the solution (50 µL) was injected on the analytical column for LC/MS/MS analysis.

7. Instrumentation and Chromatographic Conditions

The analytes were detected using an API 4000 LC/MS/MS spectrometer (Applied Biosystems, Foster City, CA) in line with an 1100 HPLC system (Agilent Technologies, Palo Alto, CA) including a degasser, quaternary pump, and autosampler. The data were acquired and processed using Windows® 2000 platform-based Analyst software, version 1.4.1. Separation of analytes was achieved using a C18 column (Inertsil ODS-3, 2.1 x 150 mm, 5-µm particle size; MetaChem Technologies Inc., Torrance, CA) at a

flow rate of 0.2 ml/min. The mobile phase compositions were 0.2% formic acid in water/methanol (80:20, v/v, mobile phase A) and 0.2% formic acid in water/methanol (20:80, v/v, mobile phase B). Starting at 0% B, the gradient conditions were as follows: 0–0.5 min linear increase to 10% B, 0.5–6.5 min linear increase to 18% B, 6.5–10.5 min linear increase to 100% B, 10.5–14.5 min 100% B, and 14.5–20 min 0% B.

A flow injection analysis was performed on each analyte to maximize sensitivity (Table 1). The analytes were optimized at a source temperature of 650°C, under unit resolution for quadrupoles 1 and 3, and the optimal gas pressures were as follows: collision gas 12 psi, curtain gas 31 psi, ion source gas (1) 40 psi, ion source gas (2) 45 psi.

8. Method Validation for Plasma

Plasma calibration standards (n = 8 for VCR and n = 7 for M1) were used to generate standard curves on four separate occasions. The VCR to internal standard area ratios were fit using linear regression with a weighting factor of *1/x*. The M1 standard curve used a power fit without weighting. The fit was considered acceptable if the mean calculated values of the calibration standards over the four batches for each value were ≤ 15% of the nominal values or ≤ 20% for the low limit of quantification. Values for calibration standards were excluded from the standard curve if the calculated accuracies were < 55% or > 145% of the nominal concentration. At least six points were used to generate each standard curve.

Intra-day accuracy and precision were evaluated at three concentrations (0.012, 0.8, and 24 ng/mL for VCR and 0.012, 0.40, and 12 ng/mL for M1) by analyzing five replicates at each concentration independent of the standard curve samples. QC samples

were assayed on four separate days to calculate inter-day accuracy and precision. The intra-day and inter-day accuracies were accepted if the calculated values were ≤ 15% of the nominal concentration or ≤ 20% for the low limit of quantification. The precision of intra-day and inter-day samples was acceptable if the percent coefficient of variation (%CV) was ≤ 15% or ≤ 20% for the low limit of quantification.

The specificity was evaluated using blank plasma pooled from three human donors. The following drugs were tested for assay interference: cyclosphosphamide, methotrexate, dactinomycin, and asparaginase. For each compound, the maximum therapeutic plasma concentrations were used to calculate the appropriate amounts of drug formulation to dissolve in 0.2% formic acid in water/methanol (80:20, v/v). The maximum plasma concentrations used in this study follow: cyclophosphamide, 1000 μg/mL; methotrexate, 45 μg/mL; dactinomycin, 50 ng/mL; and asparaginase, 1 IU/mL. The solutions, one per drug, were assayed using the same conditions as the plasma samples.

The recoveries of VCR and M1 were determined by comparing the analyte to internal standard area ratios of unextracted samples to the ratios of the extracted samples. For the unextracted samples, the VCR and M1 in mobile phase were added directly to the extracted residue of a plasma sample with only internal standard.

The VCR and M1 concentrations of the stock solution were evaluated at the beginning and end of the validation experiments using HPLC analysis. The post-preparative stability studies used QC sample re-injections at the end of the run time (n = 6 for each QC concentration, ≥ 10 h storage at room temperature). The freeze-thaw and short-term stabilities of VCR and M1 in plasma were evaluated in triplicate using high

(19 ng/mL for VCR and 9.5 ng/mL for M1) and low concentrations (47 pg/mL for VCR and 24 pg/mL for M1). For the freeze-thaw stability studies, the plasma samples were thawed three times at room temperature and refrozen for at least 12 h between thaws. The short-term (pre-preparative) stability studies evaluated VCR and M1 in plasma after 15 h of room temperature storage. In all cases, the analytes were considered stable if the concentrations were within 20% of the untreated sample concentrations. The reported *p*-values between the treated and the QC control groups were determined using the Student's *t* test.

For routine analysis, the standard curve and six QC samples (three concentrations in duplicate) were assayed. The standard curve was accepted if at least four out of six of the calculated concentrations of the QC samples were within 20% of the nominal values, with at least one QC sample passing at each concentration.

9. Method Application

To determine the pharmacokinetic profiles of VCR and M1, a prospective study 2006–2007 was conducted in pediatric subjects undergoing treatment for rhabdomyosarcoma at Riley Hospital (Indianapolis, IN) and Children's Memorial Hospital/Northwestern University (Chicago, IL). The typical regimen included concurrent treatment with VCR (1.5 mg/m^2), dactinomycin, and cyclophosphamide. The study was approved by the Institutional Review Boards of Indiana University-Purdue University and Children's Memorial Hospital, and the patients were enrolled after written informed consent. Blood samples pre-dose and approximately 15 min, 1 h, 2 h, 4 h, 6 h, and 24 h post VCR dose were collected in heparinized tubes. The plasma was separated within 30 min and stored at -80°C until analysis. The plasma samples were extracted in duplicate,

and the VCR and M1 concentration data were fit by non-linear regression using a two-compartment model (WinNonlin 4.0, Pharsight, Mountain View, CA).

A different study was conducted at Riley Hospital (Indianapolis, IN; 2002–2004) for patients that were treated with VCR for a variety of malignancies including rhabdomyosarcoma and neuroblastoma. Urine and/or whole blood samples (pre-dose and various time points up to 24 h post-dose) were collected from the pediatric patients. The study was approved by the Institutional Review Board of Indiana University-Purdue University, and the patients were enrolled after written informed consent. VCR and M1 were quantified in the plasma and urine samples.

IV. Results

A. Metabolite Identification with cDNA-expressed Cytochrome P450s

For preliminary experiments with VCR and cDNA-expressed CYPs, the incubations were quenched with base and extracted with ethyl acetate. These conditions were chosen to potentially improve the extraction efficiency of *Vinca* alkaloids (pKa ~ 7.4). At the time, the chemical stability was unknown for the major metabolite M1. As we later discovered, the sodium hydroxide added during the extraction chemically transformed M1 to M3. In addition, the initial chromatography conditions at a neutral pH did not allow baseline separation of M1 and VCR. Once these issues were discovered, the post-incubation sample preparation and chromatography conditions were optimized to quantify M1 without degradation to M3. The next section describes the initial kinetic data with the base extraction method and explains the process used to discover the relationship between M1 and M3.

1. HPLC Analysis with Neutral pH Eluent and Base Extraction

After VCR was incubated with cDNA-expressed cytochrome P450 3A5 (rCYP3A5) as described in Methods (pg. 30), VCR and one major metabolite (M3) were detected by HPLC analysis (Fig. 2; Methods, pg. 31). The UV baseline noise may have masked the formation of other VCR minor metabolites because UV detection is not selective for VCR-related compounds. Thus, metabolite profiling was completed using radiolabeled VCR (Methods, pg. 30). The ^{3}H-VCR was first purified by HPLC because the radiochemical purity of VCR was poor (approximately 60%). VCR at multiple concentrations (0.1 to 100 μM, 10^{6} dpm) was incubated with rCYP3A5. The potential metabolites were identified by comparing the radiochromatograms of the incubation

extracts with and without NADPH (Fig. 3). As shown previously by UV detection (Fig. 2), M3 was the dominant metabolite (21 min). Another minor metabolite M2 was observed at 17 min. The M3 molar concentrations were estimated using the total radioactivity of the eluent fractions containing M3 by retention time. The rates of M3 formation with rCYP3A5 displayed saturable kinetics with a K_m value of approximately 10 μM (Fig. 3f).

The rates of M3 formation for rCYP3A5 and rCYP3A4 were quantified using the identical incubation conditions (5 μM VCR, 50 pmol CYP/mL, 15 min incubation time; Methods, pg. 31). As compared to the rate of M3 formation with rCYP3A5, the rate of M3 formation with rCYP3A4 was approximately 10-fold lower; M3 was 2.2% of the initial VCR UV area for rCYP3A4 versus 23% for rCYP3A5. Additional experiments were performed to identify initial velocity conditions for the kinetic analysis of rCYP3A4 and rCYP3A5 with VCR. However, the rates of M3 formation were not reproducible between experiments. For example, 15 min incubations with rCYP3A5 resulted in 13% M3 formation (% of initial VCR area by UV); for the identical experiment three weeks later, the M3 formation was 28%. A potential cause of these inconsistencies was discovered after the incubation extracts were assayed by LC/MS using an acidic mobile phase (Fig. 4; Methods, pg. 32). Using this assay, three metabolite peaks (M1, M2, and M3) were detected in the rCYP3A5 incubations. Only two peaks (M2 and M3) were previously discovered by HPLC with a neutral pH eluent (Fig. 3). The identities of the peaks were determined by collecting the individual metabolite peaks from the acidic chromatography system (Fig. 5a) and then assaying the purified metabolites on the neutral pH system (Fig. 5b–f; Methods, pg. 31). The

retention times of M2 and M3 increased approximately 18 min for the acidic chromatography system, compared to the neutral pH chromatography (Fig. 5a,d). Using the acidic chromatography system, another metabolite, M1, eluted 2 min before VCR (Fig. 7a). By neutral pH chromatography, the M1 eluted approximately one min after VCR and had an unusually broad peak shape (Fig. 7c). In addition, when purified M1 was injected, another smaller peak was detected with the same retention time as M3; a small amount of M3 was likely produced by M1 degradation during the purification process. The close retention time of M1 to VCR and the broad peak shape of M1 explain why M1 in the presence of VCR was not previously detected by neutral pH chromatography (Fig. 5b).

After M1 was discovered as a metabolite, a series of experiments were performed to understand the relationship between M1 and M3. First, the effects of the extraction and base addition on the incubations were evaluated. VCR incubations with cDNA-expressed enzymes were quenched with acetonitrile to precipitate the protein, and the supernatant was directly assayed by HPLC and LC/MS. Interestingly, M3 was not present; the only metabolites detected were M1, the major metabolite, and M2 (Fig. 6). Consistent with this result, M3 was not detected after the same solution was extracted with ethyl acetate but without sodium hydroxide. To demonstrate that M3 was a product of M1 base treatment, HPLC-purified M1 was treated with sodium hydroxide and then extracted with ethyl acetate. The extract and the untreated control solution were assayed by HPLC. As determined by UV detection and by radioactive counting in another experiment, the major compound in the extract was M3 (Fig. 7); the conversion of M1 to M3 was nearly quantitative. In contrast, the conversion of M1 to M3 was not

quantitative using the previously described extraction procedure (Fig. 5a; Methods, pg. 31). Thus, for VCR incubations previously extracted with ethyl acetate and base, the rates of M1 formation were underestimated by measurement of M3 alone. The formation of M3 may have been a function of a variety of post-incubation conditions including temperature, agitation, and storage time. Instead of studying these variables in detail, alternate sample preparation and analytical methods were developed to quantify M1.

2. HPLC Analysis with Acidic pH Eluent and Acetonitrile Quench

Using an acidic eluent and methanol gradient (Methods, pg. 32), baseline separation was achieved for the major products of VCR metabolism by rCYP3A5 (Fig. 6): M1 (21 min), VCR (23 min), and M2 (35 min). M3, a compound formed from M1 under basic conditions, had a retention time of 38 min (peak not shown). Radiochromatograms were also generated from incubations of ^{3}H-VCR (10 μM) with rCYP3A4 and rCYP3A5 (Fig. 8). The major metabolite for both rCYP3A4 and rCYP3A5-mediated metabolism of VCR was M1. This peak was not present in VCR incubations with the insect microsome controls. Other potential minor metabolites (M2, M4, and M5) were detected in all samples. For M2, only the rCYP3A5 reaction produced levels higher than the control, approximately 10% of M1 by UV area. Although another earlier eluting compound, M4 (19.3 to 19.7 min), was present in larger quantities than the control, the total amount was only 2% of the total radioactivity for both rCYP3A4 and rCYP3A5 incubations. M5 (21.0 to 21.3 min) was detected in the control but was not a discrete peak in the other incubations because the M1 peak retention time (20.5 to 20.7 min) was too close to M5 to allow resolution by radiochromatography. In contrast, with

the HPLC assay used to determine the kinetic parameters with UV detection, M5 could be distinguished from M1 by retention time. For all radiochromatograms (Fig. 8; Methods, pg. 30), the radioactivity counted from 10 to 45 min was at least 95% of the total radioactivity in the samples; no additional peaks with retention times before 10 min or after 45 min were identified.

B. Structural Determination of Vincristine Metabolites by LC/MS/MS and NMR

1. M2

The MS spectrum of the minor metabolite M2 revealed a primary protonated molecular ion peak at *m/z* 839, a mass 14 Da higher than that of the VCR ion peak (Methods, pg. 35). The N-formylvindoline (NFV) segment of the molecule was unchanged from VCR as determined by MS/MS fragmentation showing a product ion at *m/z* 471, the protonated NFV segment. Accurate mass measurement of M2 was used to determine the molecular formula, $C_{46}H_{54}N_4O_{11}$. These results indicated that M2 was likely the same molecule previously described from the oxidation of VCR with horseradish peroxidase or ceruloplasmin (Fig. 9).[9] To test this hypothesis, VCR was incubated with horseradish peroxidase and hydrogen peroxide using a similar procedure (Methods, pg. 34). Two compounds that displayed retentions times different from VCR were isolated by HPLC. The compound that eluted at an earlier retention time than VCR was not conclusively identified by ^{1}H NMR although the retention time was similar to the early eluting VCR epoxide (M4). The second compound eluted at the same retention time as the compound M2 generated by CYP3A5-mediated metabolism of VCR, and a direct comparison by LC/MS/MS and ^{1}H NMR confirmed that that the compounds were identical. In the proposed mechanism for the formation of M2, the carbon α to the

piperidine nitrogen of VCR is oxidized followed by the fission of the C-13 and C-14 bond (Fig. 9).[9] Similar biotransformation pathways catalyzed by horseradish peroxidase have been described previously with other *Vinca* alkaloids including leurosine and vinblastine.[122,123] The MS/MS product ions and the complete NMR characterization of M2 are reported elsewhere.[9,121]

2. M1 and M3

The primary metabolite generated by the metabolism of VCR with rCYP3A5 and rCYP3A4 is M1, a compound with a primary protonated molecular ion peak at *m/z* 793. MS/MS analysis revealed a structural change to the DHC segment of the molecule (Fig. 1). However, with a VCR mass loss of 32 Da, the possible chemical structures of M1 were not obvious. The structural identification of this compound by ^{1}H NMR was challenging because M1 was not stable during standard sample preparation methods. Specifically, evaporation in methanol to remove residual water for ^{1}H NMR degraded M1 so that direct analysis in methanol was not possible. To determine whether alternate sample preparations would be suitable, VCR was incubated with rCYP3A5 to generate M1, and the resulting incubation solution was extracted with various solvents including hexanes, ethyl acetate, and methylene chloride (Methods, pg. 55). The effect of acid on recovery and degradation was evaluated using trichloroacetic acid, and methylene chloride extraction with acid treatment most effectively concentrated M1 and VCR without degradation (Fig. 10). This extraction procedure was used to purify larger quantities of M1 (Methods, pg. 34), and the concentrated extract was analyzed by LC/MS/MS (Methods, pg. 35). In addition to an ion at *m/z* 793, an ion at *m/z* 811 was observed with a molecular formula of $C_{45}H_{55}N_4O_{10}$ as determined by accurate mass

measurements (Fig. 11). Based on this observation, the ion at *m/z* 793 was hypothesized to be a source-induced fragment ion caused by dehydration of the primary compound at *m/z* 811, a compound with a mass 14 Da less than VCR. The M1 extract was also dissolved in deuterated methanol for structural analysis by ^{1}H NMR. This approach was unsuccessful because, as before, the M1 degraded in methanol.

Because direct structural analysis was not possible, a chemical modification approach was utilized to define the structure of M1. As reported earlier, base treatment of M1 results in the chemical transformation to a stable derivative M3. The mass of the primary protonated molecular ion for M3 was *m/z* 779 with a molecular formula of $C_{44}H_{50}N_4O_9$ by accurate mass measurements. MS/MS analysis with a product ion of 469 revealed that the NFV segment of VCR was chemically intact (Fig. 1). Extensive analyses by NMR as described elsewhere[121] indisputably verified the structure of M3 (Fig. 9). Based on the structure of M3 and the proposed mechanism for the formation of M2, the biotransformation pathway and structure of M1 were deduced (Fig. 9). To form M1 and M2, VCR is initially oxidized at the position α to the piperidine nitrogen. However, instead of cleavage at the C-13 to C-14 bond to form M2, fission of the N-12 to C-13 bond initiates the formation of M1. As a secondary amine, the compound M1 is likely reactive under basic conditions causing an intramolecular amidation to form M3, a mass loss of 32 Da.

To further confirm the structure of M1, additional chemical modifications of M1 were attempted by chemically targeting the reactive secondary amine (Methods, pg. 34). Attempts to directly formylate the M1 secondary amine with formic acid were unsuccessful. However, using acetic anhydride, the secondary amine on M1 was readily

acetylated. M1-acetate was detected by LC/MS as a major product with a DHC segment modification and a molecular ion peak at *m/z* 853, a mass gain of 42 from M1. In addition, the retention time of M1-acetate was approximately 17 min later than M1, a dramatic shift likely caused by modification to a protonatable amine group. Altogether, these results confirm the proposed molecular weight (*m/z* 811) and structure of M1 (Fig. 9).

3. M4 and M5

The compounds M4 and M5 are present as impurities in commercially available vincristine sulfate. M4 may also be a minor metabolite produced during the rCYP3A5-mediated metabolism of VCR (Fig. 6). M5 as an impurity can interfere with the quantification of M1 by UV detection because the retention times are similar. The MS/MS data support a chemical modification to the DHC segment compared to VCR. The structures of M4 and M5 are likely isomeric epoxides because the protonated molecular ion peaks of M4 and M5 are identical at *m/z* 823, 2 Da less than the VCR ion peak. The vinblastine equivalent compound for one of the diasteromers has been previously identified as leurosine, a natural product isolated from the plant, *Catharanthus roseus*.[122] ^{1}H NMR analysis was not used to characterize M4 and M5 because they were not identified as major metabolites (Fig. 6).

C. Enzyme Kinetics of Vincristine Metabolism with cDNA-expressed CYPs

1. CYP Human and Rat CYP Panel

VCR was incubated with a panel of cDNA-expressed human CYPs (Methods, pg. 27). As determined by parent drug disappearance and M1 formation, the metabolism of VCR was primarily mediated by rCYP3A4 and rCYP3A5 (Fig. 12). The VCR disappearance

was normalized to insect microsome controls ($n = 4$). The M1 values were not corrected because M1 was not detected in the control. Using one-way ANOVA analysis, the VCR disappearance was different from the control for the following CYP enzymes: rCYP3A4 ($p < 0.001$), rCYP3A5 ($p < 0.001$), rCYP3A7 ($p < 0.01$), and rCYP2E1 ($p < 0.05$). However, only rCYP3A4 and rCYP3A5 depleted the substrate by more than 10%. M1 formation accounted for 70% and 50% of parent drug loss in the rCYP3A5 and rCYP3A4 incubations, respectively. The formation of M2, a minor metabolite, accounted for 7% parent loss with rCYP3A5 and 2% loss with rCYP3A4. The formation of M4, another minor metabolite, accounted for 1% parent loss with rCYP3A5 and 4% loss with rCYP3A4.

For rCYP3A1 and rCYP3A2 incubations (Methods, pg. 28), the rates of M1 formation and vincristine depletion were not detectably different from the insect cell control incubations. Thus, rat CYP enzymes do not readily metabolize VCR.

2. Competitive Inhibition of CYP3A4 with Vincristine and Vinblastine

The rates of formation of M1 from VCR and the formation of the M1-equivalent for vinblastine (identification by LC/MS/MS, data not shown) were used to estimate the competitive inhibition dissociation constants for VCR and vinblastine with rCYP3A4 and rCYP3A5 (Methods, pg. 28). A competitive inhibition model was used to simultaneously fit all concentrations of VCR and vinblastine by non-linear regression. Vinblastine was a much more potent inhibitor of rCYP3A4 activity than VCR; the estimated K_i values for rCYP3A4 were 2 μM and 38 μM with vinblastine and VCR, respectively (Fig. 13). VCR did not selectively inhibit rCYP3A5 compared to rCYP3A4; the estimated K_i values were 39 μM and 38 μM for inhibition of rCYP3A5

and rCYP3A4, respectively. However, the K_i value for rCYP3A5 had a high degree of uncertainty (CV = 54%).

3. Competitive Inhibition of M1 Formation with Cyclosporin A

To determine whether CsA was a selective chemical inhibitor of CYP3A4 activity, VCR was incubated with rCYP3A4 (or rCYP3A5) and CsA (Methods, pg. 28). The rates of M1 formation with VCR (10 μM) were quantified using a range of inhibitor concentrations at different methanol concentrations. For the initial experiments with 2.4% methanol and 10 μM CsA, rCYP3A4 activity was completely inhibited while at the same concentration of inhibitor, only 15% of the rCYP3A5 activity was inhibited. Although CsA was a selective inhibitor of rCYP3A4 using these conditions, the high methanol concentration inhibited the formation of M1 in the vehicle controls. Thus, alternative conditions were investigated at lower methanol concentrations. For incubations without methanol (Fig. 14a), complete inhibition of rCYP3A4 activity was not possible. The residual activities of rCYP3A4 at high apparent concentrations of CsA were likely a result of the CsA not dissolving completely in the incubation buffer. Consistent with this hypothesis, when the methanol concentrations were increased to 0.3%, CsA again completely inhibited the rCYP3A4 activity whereas the rCYP3A5 activity was only reduced 15% (Fig. 14b).

4. Kinetics of M1 and M2 formation with rCYP3A4 and rCYP3A5

VCR at various concentrations was incubated with rCYP3A4 (or rCYP3A5) and supplemented cytochrome b_5 (Methods, pg. 30). The rates of M1 and M2 formation were quantified in duplicate over two sets of experiments approximately 30 min apart (Fig. 15). The rates of M1 formation (major metabolite) and M2 formation (minor

metabolite) demonstrated saturable kinetics with rCYP3A4 and rCYP3A5. While the K_m values for M1 and M2 formation were similar with rCYP3A4 and rCYP3A5, the V_{max} values were 6 to 10-fold higher with rCYP3A5. For this experiment, some scatter was noticed between the duplicate values, especially for the M1 values. The rates of M1 formation determined from the second set of experiments were consistently lower than the first indicating that the enzyme preparation with supplemented cytochrome b_5 was probably not stable.

The role of enzyme preparation on the kinetics of M1 formation was determined for rCYP3A4 and rCYP3A5 (Fig. 16). The K_m and V_{max} values were estimated for rCYP3A4 and rCYP3A5 with and without cytochrome b_5 (Table 1). For both rCYP3A4 and rCYP3A5 incubations, the presence of cytochrome b_5 consistently increased the V_{max} values; the highest V_{max} values were estimated with co-expressed cytochrome b_5. The intrinsic clearance values (V_{max}/K_m) with rCYP3A5 were consistently higher than those with rCYP3A4 for all preparations (9 to 14-fold higher for rCYP3A5). The K_m values were not statistically different for preparations without cytochrome b_5 and co-expressed cytochrome b_5. The kinetic parameters were not estimated for M2 or M4 because at the lowest concentrations of VCR, the compounds could not be consistently quantified by HPLC. However, for the rCYP3A4 and rCYP3A5 reactions, the M2 and M4 concentrations were higher than the control concentrations at the highest VCR concentration (48 μM). Correcting for the amounts in the controls, M2 was less than 10% of the M1 values for both rCYP3A5 and rCYP3A4 reactions. M4 was approximately 5% of M1 for rCYP3A5 incubations and 15% of M1 for rCYP3A4

reactions. The concentrations of M5 for both rCYP3A4 and rCYP3A5 reactions were not measurably higher than the concentrations in the controls.

5. Prediction of CYP3A5 Contribution to Vincristine Metabolism

The kinetic data from the cDNA-expressed CYPs can be used to estimate the CYP3A5 contribution to the metabolism of VCR with a few assumptions (Eqn. 3). First, to use the intrinsic clearance values (V_{max}/K_m), the therapeutic unbound concentration of VCR (< 0.1 μM) must be lower than the measured K_m (approximately 20 μM). The rates of M1 formation should account for all the VCR metabolism by CYP3A4 and CYP3A5. For the protein concentrations of CYP3A4 and CYP3A5 as determined by Western blot (Methods, pg. 39), all the CYPs need to have the same percentage of active holoprotein. Finally, only CYP3A4 and CYP3A5 are assumed to metabolize VCR.

The CYP3A5 contribution for CYP3A5 high expressers was calculated as a fraction of the total activity using the selectivity data from each enzyme preparation: 0.91 (no cytochrome b_5); 0.92 (supplemented cytochrome b_5); and 0.88 (co-expressed cytochrome b_5). Regardless of the preparation method, the CYP3A5 contribution to VCR metabolism was substantial, approximately 90%.

D. Characterization of CYP3A4 and CYP3A5 in Human Liver Microsomes

1. *CYP3A5* Genotype

The bank of HLMs (n = 56) was genotyped for *CYP3A5*3*, **6*, and **7*; these alleles were previously associated with low or null expression of CYP3A5. Without these defective alleles, the HLMs by elimination were assumed to have active *CYP3A5*1* alleles. One liver, IUL-40, was homozygous and 11 livers were heterozygous for *CYP3A5*1* (Table 2).

2. Protein Expression

CYP3A4 and CYP3A5 concentrations in select livers (n = 12 for *CYP3A5*1* livers, n = 10 for *CYP3A5*3/*3* livers) were quantified by Western blot (Fig. 17; Methods, pg. 39). To effectively quantify the CYP content in the HLMs, the CYP standards were co-loaded with an equal amount of protein from an HLM without detectable expression of the CYP. When the standards were loaded without this HLM, the CYP intensity of the standard alone was much higher than the standard with the co-loaded HLM (Fig. 17a). The CYP standard alone also ran slower on the gel than the standard with a co-loaded HLM. As a result, all the standards were loaded with an appropriate amount of "blank" microsomal protein. For the CYP3A5 standard curves, IUL-52 (*CYP3A5*3/*3*) was the HLM typically loaded with the standards (Fig. 17b). The standards and unknowns were separated by at least 4 lanes with standards on lanes 1 and 15. These conditions were chosen to account for errors that can naturally occur during a Western blot procedure including uneven transfers and uneven development of the nitrocellulose. To estimate the concentrations of the CYPs in the unknown samples, the intensities of all 6 standards were fit by linear regression (Fig. 17c), and the unknown values were estimated by interpolation. The duplicate values for all unknown HLMs were within 15% of each other on the same blot. The HLMs were assayed for both CYP3A4 and CYP3A5 content (Table 2). For CYP3A5 high expressers with only one *CYP3A5*1* allele, the CYP3A4 and CYP3A5 protein contents (Table 2) were not correlated (r^2 = 0.07).

Because CYP3A5 was not available for purchase as a purified enzyme, two different types of CYP reference standards were used—purified CYP3A4 enzyme and

CYP3A5 Supersomes. To determine the percentage of CYP3A5 as holoprotein, the relative intensities of the purified CYP3A4 and the CYP3A5 Supersomes were compared by Western blot using a CYP3A non-specific antibody (Fig. 18; Methods, pg. 39). This type of comparison assumed that the antibody was equally immunoreactive with both CYPs. For this particular lot of Supersomes (lot 22), the CYP3A5 values were similar to the CYP3A4 values. As a result, the CYP3A5 Supersomes standard was used to quantify the CYP3A5 content in the HLMs without a purity correction (Table 2).

Compared to the *CYP3A5*3/*3* livers, the CYP3A5 protein concentrations were higher for 10 livers with at least one *CYP3A5*1* allele ($p < 0.001$). However, for two livers (IUL-57 and IUL-71), the CYP3A5 protein concentrations were comparable to other HLMs with the *CYP3A5*3/*3* genotype (Fig. 19). As a result, IUL-57 and IUL-71 were classified as CYP3A5 low expressers contrary to genotype (Table 2). Although low CYP3A5 expression could be explained by general enzyme degradation, for these two livers, the CYP3A4 protein concentrations and the CYP3A4 activities were typical of the *CYP3A5*3/*3* HLMs. At this time, the exact cause for the discrepancy between *CYP3A5* genotype and expression is unknown.

3. CYP3A4 Activity Assays

The itraconazole hydroxylase activity, testosterone 6β-hydroxylase activity, and CYP3A4 content by Western blot were quantified for select HLMs with low and high CYP3A5 expression (Table 2). To estimate the maximum velocities for the itraconazole hydroxylase activities, the HLMs were incubated with itraconazole at target concentrations of 0.5 or 1 μM, concentrations much higher than the K_m (54 nM, Fig. 20; Methods, pg. 37). Although the target concentration of ITZ was higher than the K_m, the

actual concentrations as measured by LC/MS were initially variable; the concentrations declined over time until the ITZ stock solution was reformulated (Fig. 21a). Given that ITZ is a highly lipophilic drug, the initial decline in ITZ concentration was likely caused by adsorption of ITZ to the polypropylene container. For later incubations, to maintain a high ITZ concentration, the ITZ stock solution was freshly formulated for each set of reactions (Fig. 21b). These later reactions were used to quantify the CYP3A4 activities of the HLMs (Table 2).

As another measure of CYP3A activity, the testosterone 6β-hydroxylase activities for the HLMs were also quantified (Table 2; Methods, pg. 37). The testosterone 6β-hydroxylase activity was correlated to CYP3A4 content and itraconazole activity (r^2 = 0.77 and 0.98, respectively) but did not differ between CYP3A5 high and low expressers (Fig. 22). Thus, CYP3A5 did not significantly contribute to testosterone 6β-hydroxylation.

E. Vincristine Metabolism with Human Liver Microsomes

1. Metabolite Profiles by HPLC

The formation rates of VCR metabolites, including compounds previously described from recombinant enzyme incubations (M1, M2, M3, and M4), were quantified for select HLMs (n = 22; Methods, pg. 41). By comparing the chromatograms to controls lacking NADPH, M1 was identified as the major metabolite. M4 was a minor metabolite with rates of formation 10% or less than those of M1. Representative chromatograms for incubations with IUL-73 (a CYP3A5 high expresser) and the corresponding negative control are shown in Fig. 23. The chemical structures of M1 and M4 were confirmed by LC/MS/MS (data not shown).

2. Kinetics of M1 Formation

For all HLMs, VCR metabolism as determined by M1 formation displayed Michaelis-Menten kinetics (Fig. 24). The V_{max} and K_m values were estimated by non-linear regression (Table 2). The K_m values were corrected for microsomal protein (Methods, pg. 45). The V_{max} values for the CYP3A5 high and low expresser groups were not directly compared because the CYP3A5 low expressers were not selected randomly and therefore did not represent the population. An alternative approach was used to compare V_{max} values between the groups (Methods, pg. 53). The K_m values between the groups were directly compared because the K_m values of the CYP3A5 low expresser group were not correlated to V_{max} values ($r^2 = 0.26$). The K_m values for CYP3A5 high and low expressers (18.4 ± 5.2 μM and 20.5 ± 5.2 μM, respectively) were not statistically different ($p = 0.49$). The K_m values of M1 formation using HLMs (average 19.6 μM) and rCYP3A5 and rCYP3A4 with co-expressed cytochrome b_5 (16.7 and 19.9 μM, respectively) were in good agreement. The K_m values of the recombinant CYPs were not corrected for non-specific binding because the incubations had low protein concentrations ($C_p \leq 0.55$ mg/ml) corresponding to a $f_u \geq 0.92$ using Eqn. 2 and the estimated values of K from HLMs.

3. Selective Chemical Inhibition of M1 Formation

To quantify the contribution of hepatic drug metabolizing CYPs in VCR metabolism, the rates of M1 formation were determined with selective chemical inhibitors in pooled HLMs at 15 μM VCR (Fig. 25; Methods, pg. 42). The rates of M1 formation in incubations with omeprazole, quinidine, ketoconazole, VLB, and VRL were significantly lower than the control incubations ($p < 0.05$). Only known CYP3A

substrates, VLB and VRL, and the CYP3A inhibitor, ketoconazole, inhibited the M1 formation rate by more than 25%. The rate of VCR disappearance was significantly reduced by ketoconazole, VLB, and VRL ($p < 0.05$, data not shown).

As shown previously (Fig. 14), CsA is a potent, selective inhibitor of rCYP3A4 and was therefore used to selectively inhibit CYP3A4 in HLMs (Methods, pg. 43). For the initial screening experiment with a select number of HLMs, CsA more effectively inhibited the formation of M1 with CYP3A5 low expressers; the degree of inhibition was dependent on the CYP3A4 activity of the HLM (Fig. 26b). However, the vehicle controls with 4.8% methanol were also inhibited (Fig. 26a). Interestingly, methanol also selectively inhibited CYP3A4; the CYP3A5 low expressers were selectively inhibited by methanol alone (approximately 20% more inhibition with low expressers). In addition, the inhibition response of the HLMs to 4.8% methanol was highly variable.

One methanol-sensitive HLM (IUL-42, 70% inhibition) was selected to determine the maximum concentration of solvent without loss of activity (Methods, pg. 45). At various acetonitrile and methanol concentrations, the activity of IUL-42 was quantified; 7% of the activity was inhibited at an organic concentration of 0.5% (Fig. 27). The inhibition was independent of solvent choice.

As a result of this study, the concentration of methanol chosen for the next CsA inhibition experiments was 0.3%. The inhibition of M1 formation by CsA was determined for HLMs with low (Fig. 28a) and high expression of CYP3A5 (Fig. 28b). The M1 rates of formation for CYP3A5 low expressers were not completely inhibited by CsA; the remaining activities as estimated by the modified Michaelis-Menten equation (Eqn. 1) were 27% for IUL-6 and less than 10% for IUL-78 and IUL-55. The

percents of activity remaining after CsA inhibition for the CYP3A5 high expressers (IUL-79, -59, and -73, Table 3) were in the same rank order as would be predicted by their CYP3A4 protein content and activity (Table 2). As determined by CsA inhibition, the percent contributions of CYP3A5 to M1 formation were likely underestimated because rCYP3A5 was somewhat inhibited (15%) by CsA (Fig. 14).

4. Prediction of CYP3A5 Contribution to Vincristine Metabolism

The V_{max} values of M1 formation from VCR for CYP3A5 low expressers were correlated with CYP3A4 activity and protein content: testosterone 6β-hydroxylase activity (r^2 = 0.89, Fig. 29a); itraconazole hydroxylase activity (r^2 = 0.91, Fig. 29b); and CYP3A4 protein content (r^2 = 0.75, Fig. 29c). The CYP3A5 low expressers were assumed to have an insignificant amount of CYP3A5 activity as compared to CYP3A4 activity. For the HLMs with CYP3A5 low expression, regression lines and corresponding 95% prediction intervals for the M1 V_{max} values were calculated using each measure of CYP3A4 (activity or protein content). Using these prediction intervals, the V_{max} values from the CYP3A5 high expressers were compared to the CYP3A5 low expressers. Regardless of CYP3A4 measure, the V_{max} values of all the CYP3A5 high expressers were above the 95% prediction intervals established by the CYP3A5 low expressers. To determine the specific contribution of CYP3A5 to M1 formation at V_{max} for CYP3A5 high expressers, the CYP3A4 contributions were subtracted from the V_{max} values. For each CYP3A5 high expresser, the CYP3A4 contribution was the corresponding best-fit V_{max} value of the CYP3A5 low expressers at a specific CYP3A4 measurement (activity or protein content). The resulting CYP3A5 contributions (% of total activity, Table 3) for the CYP3A5 high expressers were in good agreement with

each other, regardless of the CYP3A4 value (activity or protein content) used to determine the CYP3A4 contribution to M1 formation. The average contribution of CYP3A5 to the formation of M1 for CYP3A5 high expressers at V_{max} was 81% of the total activity (Eqn. 4). Thus, with CYP3A5 high expressers at V_{max}, VCR metabolism to M1 was primarily mediated by CYP3A5. This result was similar to the CYP3A5 contribution predicted using cDNA-expressed enzymes, approximately 90%.

The CYP3A5 contributions to the rate of M1 formation using intrinsic clearances, rather than V_{max} values, were also quantified because therapeutic concentrations of VCR are less than 1 μM, well below the K_m. However, as indicated earlier, the K_m values of M1 formation for CYP3A5 high and low expressers were not statistically different ($p = 0.49$). As a result, the calculated CYP3A5 contributions for CYP3A5 high expressers using V_{max} values were similar to the CYP3A5 contributions using intrinsic clearances (data not shown).

The CYP3A5 activities of M1 formation for the high CYP3A5 expressers, calculated by subtraction of the CYP3A4 contribution using ITZ hydroxylase activities, were correlated to the CYP3A5 protein content ($r^2 = 0.95$, Fig. 30). The correlation was highly influenced by IUL-40 because its CYP3A5 protein content was much higher than those of the other HLMs (Table 2), yet even without including IUL-40 in the analysis, the CYP3A5 activities were correlated to the CYP3A5 protein content ($r^2 = 0.63$). The CYP3A5 M1 activities using testosterone 6β-hydroxylation to calculate the CYP3A4 contribution were almost identical to the CYP3A5 activities calculated using itraconazole hydroxylation as a CYP3A4 standard (Table 3). Thus, the CYP3A5

activities derived using testosterone 6β-hydroxylation were also correlated to CYP3A5 protein content ($r^2 = 0.96$).

The specific activities of M1 formation for CYP3A4 and CYP3A5 in HLMs were calculated using the protein contents as quantified by Western blot and the maximum rates of M1 formation. For the CYP3A5 high expressers, the ITZ hydroxylase activity was used to calculate the CYP3A4 contribution to the rate of M1 formation as described earlier. The specific activities were 7-fold higher for CYP3A5 (Fig. 31) and consistent with the values obtained using cDNA-expressed CYP3A4 and CYP3A5 (Table 1).

5. Prediction of Vincristine Hepatic Clearance for CYP3A5 High and Low Expressers

The hepatic clearance of VCR was estimated for each HLM using the well-stirred model (Eqn. 5). An alternate more complex physiological model, the parallel-tube model, does not assume that the concentration of drug is the same throughout the liver.[124] However, the well-stirred model was appropriate because VCR is a low to medium extraction ratio drug and not highly bound to blood cells and plasma proteins. Thus, with these conditions, the well-stirred model would predict similar hepatic clearances to the parallel-tube model.[124] M1 was assumed to be the only metabolite formed from VCR, and the rate of M1 formation was assumed to be equal to the rate of VCR disappearance. The testosterone 6β-hydroxylase activities of CYP3A5 low expressers were correlated to the rate of M1 formation (Fig. 29a). Thus, for the HLMs that were not initially selected for incubation with VCR (all CYP3A5 low expressers not listed in Table 2), the M1 maximum rates of formation from VCR were estimated by linear interpolation using

the testosterone 6β-hydroxylase activities. The average K_m (20.5 μM) of the CYP3A5 low expressers was used for each HLM not incubated with VCR. The intrinsic and hepatic clearances of the HLM bank classified by CYP3A5 expression are presented in Fig. 32. For the two groups, the intrinsic and hepatic clearances were statistically different ($p < 0.001$) with the median of CYP3A5 high expressers 7- and 5-fold higher than low expressers, respectively. Median values were used to compare the CYP3A5 low and high expressers because the data from both groups were not normally distributed.

F. Binding

1. Microsomal

Using pooled HLMs, the fraction unbound of VCR was estimated by ultrafiltration (Methods, pg. 45). The binding was quantified for the lowest concentration of VCR used during the HLM kinetic experiments (5 μM). For the binding experiments, buffer controls without protein were intended to correct for non-specific binding to the apparatus. However, for these negative controls, the VCR fraction unbound was consistently lower than the fraction unbound with protein (values plotted on y-axis, Fig. 33a). Thus, the negative controls in buffer could not be used to correct for non-specific binding. Pre-treatment of the device with 1% BSA, as described previously,[48] improved the recovery of the buffer control to 77% versus 66% but did not completely remove the non-specific binding of VCR to the apparatus. An alternate approach (Eqn. 2) was used to estimate the fraction unbound caused by non-specific binding ($f_{u,nsb} = 0.76 \pm 0.05$) and the parameter K (0.161 ± 0.05 ml/mg) with non-linear regression. These values

were used to calculate the fraction unbound (f_u) at any protein concentration (C_p) and then to correct the K_m values for the HLMs (f_u = 0.67 to 0.90, Fig. 33).

2. Plasma

The fraction unbound of VCR in plasma was estimated at 1 μM, a concentration approximately 10-fold higher than the maximum therapeutic concentration (Methods, pg. 46).[56] Like the buffer controls for the microsomal binding experiments, the PBS controls were unable to correct for non-specific binding to the apparatus (values plotted on y-axis, Fig. 33b). Thus, a dilution approach with PBS was used to estimate the fraction unbound in human plasma from one donor (Eqn. 2). The parameters $f_{u,nsb}$ and K were determined from the apparent binding measured with undiluted plasma (100%) and with diluted plasma at three concentrations (50, 20, and 10%). The estimated fraction unbound caused by non-specific binding ($f_{u,nsb}$) was 0.64 ± 0.02, and the parameter K was 0.0064 ± 0.0008 (% of undiluted plasma)$^{-1}$. The $f_{u,nsb}$ value was used to estimate the fraction unbound (f_u) for two other plasma donors. The final fraction unbound of VCR for the three donors (f_u = 0.595 ± 0.007) was similar to other reported values of 0.41 and 0.51.[47,48] Using the median value of 0.51 in the well-stirred model (Eqn. 5), the hepatic clearances were estimated for each HLM (Table 2).

3. Whole Blood

Freshly heparinized whole blood at 37°C was used to estimate the blood-to-plasma ratio of VCR at 100 nM, a concentration close to the maximum therapeutic concentration (Methods, pg. 46). At this concentration, radiolabeled VCR was utilized because the VCR was below the HPLC limit of quantification. For this experiment, the estimated blood-to-plasma ratio was 1.14 to 1.20.

An additional experiment also estimated the blood-to-plasma ratio of VCR and M1 at typical to low therapeutic concentrations (0.2 and 4.6 ng/mL for VCR, 0.1 and 2.3 ng/mL for M1). However, because the primary purpose of the experiment was evaluate the effect of ascorbic acid on VCR and M1 stability in whole blood, the experiment was performed at room temperature. The VCR and M1 concentrations in the plasma were quantified by LC/MS/MS (Methods, pg. 59). The blood-to-plasma ratios were similar at both VCR concentrations (1.08 and 1.10). Likewise, the blood-to-plasma ratios of M1 were similar at both M1 concentrations (0.72 and 0.80).

G. Human Hepatocytes

1. Vincristine Degradation in Media

Initial incubations with cryopreserved hepatocyte (lots SD012 and SD017) and VCR resulted in the formation of VCR degradation products with no evidence of metabolism (Fig. 34; Methods, pg. 48). For both the no cell controls and the hepatocyte inbubations, the fractions of ions as the epoxide 1 or epoxide 2 (typical degradation products) increased as the concentration of VCR was reduced (Fig. 34a,b). The binding of VCR to the hepatocytes may have protected the VCR somewhat from degradation because the degradation was the highest in the no cell controls. The M1 concentrations with hepatocytes were similar to the M1 concentrations of the no cell controls (Fig. 34c). This observation was consistent for screening incubations with other lots of hepatocytes (lots 652, Hu418; data not shown). The formation of M1 in the no cell controls was unexpected because M1 was not previously observed in buffer or plasma standards. To verify that M1 was formed in the media standards, the degradation of 15 μM VCR at 37°C was quantified by LC/MS in plasma, buffer, and media after 0 and 4 h (Fig. 35a).

Consistent with the previous incubation results, the media formed substantial amounts of M1, unlike the plasma and buffer standards. Although the M1 concentration in media was the highest at the 4 h time point, M1 formation was also apparent at the 0 time point. The effects of other incubation variables (oxygen purging and shaking) on the degradation of 10 μM VCR were evaluated (Fig. 35a; Methods, pg. 47). Although the shaking during the 4 h incubation had little effect, oxygen purging increased the concentration of VCR degradation products, in particular epoxide 1.

2. Selection of Cryopreserved Hepatocytes

To potentially differentiate the rates of M1 formation caused by degradation from the rates caused by metabolism, high CYP3A activity hepatocytes were chosen and incubated at high cell concentrations (1.5×10^6 cells/mL; Methods, pg. 47). Based on data from previous microsomal studies, livers with high CYP3A5 expression were expected to have the highest rates of M1 formation. Unfortunately *CYP3A5* pre-genotyped hepatocytes were not available commercially. As an alternative, African-American hepatocytes were purchased ($n = 9$, 70% probability of CYP3A5 expression).[75] The hepatocytes were genotyped for *CYP3A5* polymorphisms using DNA extracted from the residual cells. By *CYP3A5* genotype, the CYP3A5 expression for three lots (REL, CHD, and MRS) could not be predicted because the livers had multiple *CYP3A5* SNPs which could prevent expression on one or both chromosomes. These livers were later categorized by phenotype using VCR activity (Table 4). Of the 9 African-American livers, 7 were categorized as CYP3A5 high expressers, and 2 livers (with inconclusive genotypes) were CYP3A5 low expressers. For this study, one additional Caucasian liver (AIT, *CYP3A5*1/*3*) was purchased from the same vendor.

3. Testosterone 6β-hydroxylase Activity

For all lots, the testosterone 6β-hydroxylase (CYP3A) activity was reported for the intact cells by the vendor. To provide additional information on the CYP3A activity, we quantified the testosterone 6β-hydroxylase activity for the cell lysates (sonicated hepatocytes) supplemented with NADPH (Methods, pg. 48). The activities of the cell lysates were highly variable between lots with a 100-fold range in values (Table 4). The CYP3A cell lysate activities were not correlated to the reported intact cell activities.

4. Vincristine Depletion and M1 Formation for CYP3A5 High Expressers

The metabolism of VCR was investigated using both intact hepatocytes and cell lysates (Table 4; Methods, pg. 48). For livers with a conclusive *CYP3A5*1* genotype, for example EHI, VCR was almost exclusively metabolized to M1 as determined by HPLC (Fig. 36). Using radiolabeled VCR with both cell preparations, M1 was also identified as the major metabolite (Fig. 37; Methods, pg. 50). With the cell lysate, M1 formation by retention time accounted for approximately 50% of the total radioactivity not VCR (Fig. 37a). For the intact cells, the rate of M1 formation in the media was inhibited approximately 70% by ketoconazole, a CYP3A inhibitor (Fig. 37c). The VCR/M1 concentration ratios were approximately the same in the media and cell fractions (Fig. 37b).

To estimate the rates of metabolism, M1 and VCR concentrations were quantified by LC/MS at multiple time points up to 4 h. The rate constants for VCR depletion (k) were estimated by non-linear regression assuming a first-order reaction (Fig. 38b). Similarly, the rate constants for M1 formation were also estimated assuming that M1 was the terminal product and the only metabolite of VCR. For these two

methods, the rate constant estimated from VCR depletion was typically higher than the rate constant estimated from M1 formation. However, in all cases, the M1 formation accounted for at least 42% of the VCR depletion (range = 42 to 131%) as shown by the differences in intrinsic clearances calculated using the rates of M1 formation and VCR depletion (Table 4).

When the M1 formation rate constants were estimated for the lysates, the assumption of first-order kinetics was not valid for two lots of hepatocytes (FKM, SCA; Fig. 38a). Although the mechanism is currently unknown, for these two lots, M1 was rapidly formed from VCR and then degraded and/or metabolized at later time points. With hepatocyte lot SCA, the initial VCR concentration was reduced 90% by an apparent first-order reaction over 40 min. The M1 concentration correspondingly increased early in the reaction but later stabilized, even as the VCR concentration continued to decline. As a result, for lots FKM and SCA, the rate constants for M1 formation were estimated using the 10 min time point only. Interestingly, for lots FKM and SCA, the concentrations of VCR and M1 were effectively modeled by non-linear regression using a kinetic model with two rate constants: k_1 (the first-order constant for VCR depletion and M1 formation) and k_2 (first-order constant for M1 depletion) (Fig. 38a).

5. Prediction of Intrinsic Clearance for CYP3A5 High Expressers

Using the estimated rate constants for CYP3A5 high expressers, the intrinsic clearances of VCR were predicted with the intact cells and the cell lysates (Table 4). For most lots, the intrinsic clearances for the two cell preparations were dramatically different from each other; the cell lysate predicted values at least 10-fold higher than those predicted

with intact cells. In addition, the values from the cell lysate were more variable than those from intact cells. As compared to the intrinsic clearances predicted with human liver microsomes (Table 2), the cell lysate values were similar for CYP3A5 high expressers. The cell lysate activities for M1 formation and TST 6β-hydroxylation were somewhat correlated (r^2 = 0.67). The cell lysate activities for TST 6β-hydroxylation did not predict the rate of M1 formation with intact cells (r^2 = 0.03). Interestingly, although the values were similar to each other, the highest activity hepatocytes for M1 formation with intact cells were lots with the *CYP3A5*1/*1* genotype (median value = 101 versus 59 mL/min for *CYP3A5*1/*0* livers, Table 2).

6. Effects of Inhibitors on M1 Formation

To determine whether M1 formation was mediated by CYP3A enzymes, ketoconazole was used as a selective CYP3A inhibitor (Fig. 39a). For each lot of hepatocytes, the cells were incubated with VCR for 4 h with and without ketoconazole. The M1 concentrations of the incubations with ketoconazole were 8 to 38% of the positive control incubations without inhibitor (Table 5). The concentrations of M1 were not 0% of the positive control because M1 was formed in the controls as discussed earlier. However, the CYP-mediated formation of M1 was completely inhibited by ketoconazole; the final concentrations of M1 with ketoconazole were comparable to those of the sonicated cell controls for lot EHI, a typical CYP3A5 high expresser (Fig. 39a). For hepatocyte incubations with radiolabeled VCR (lot EHI), the concentration of M1 by retention time was 30% of the positive control, a value approximately 2-fold higher than the remaining M1 concentration after ketoconazole inhibition for the same lot of hepatocytes (17%, Fig. 37c). However, the radiochromatogram value should be

somewhat higher than the value determined by LC/MS because M1 and EPOX1, a degradation product, co-elute by HPLC.

Two other chemical inhibitors were also co-incubated with VCR: CsA (a selective CYP3A4 inhibitor) and LSN335984 (a selective P-gp inhibitor). CsA at 25 μM was chosen because the drug at this concentration was previously used to inhibit the formation of M1 by CYP3A4 in HLMs. For all hepatocyte lots incubated with CsA, the rates of M1 formation were unaffected (Table 5). This result would be expected if CsA did not enter the cells or if CYP3A4 did not metabolize VCR. The Pgp inhibitor LSN335984 was initially chosen to reduce the rate of VCR efflux from the hepatocytes and thus potentially increase the intracellular, unbound concentration of VCR. For screening experiments with hepatocyte lot EHI, 5 μM LSN335984 (a typical concentration for cell culture transporter experiments) was metabolized faster than VCR and did not affect the rate of M1 formation (data not shown). To prevent the depletion of LSN335984 from the media, the concentration of LSN335984 was increased to 50 μM although the non-selective inhibition on CYP enzymes at this concentration was unknown. For the remaining hepatocyte incubations, the rates of M1 formation with 50 μM LSN335984 were partially inhibited, not increased as was predicted if the intracellular concentration of VCR was increased (Table 5). Although the mechanism is unknown, the reduced rates of M1 formation may have been caused by inhibition of CYP3A5 by LSN335984.

7. Michaelis-Menten Kinetics of M1 Formation

To better understand the differences in rates of M1 formation between intact cells and cell lysates, the Michaelis-Menten kinetic parameters were estimated for Lot EHI using

both cell preparations (Methods, pg. 49). The K_m of the cell lysate was 3-fold lower than the K_m of the intact cells; the V_{max} of the cell lysate was 3-fold higher than that of intact cells (Fig. 40). Altogether, the intrinsic clearance of the cell lysate (V_{max}/K_m) was 9-fold higher than that of the intact cells. For the intact cell system, the rate of VCR diffusion through the cell membrane may be relatively slow compared to the rate of metabolism. In this case, because the intra-cellular concentration of VCR would be less than the extracellular concentration, the apparent K_m would be higher than the value predicted using HLMs. However, a V_{max} change is not likely caused by transport effects, provided the transport is not saturable.

8. Prediction of Intrinsic Clearance for CYP3A5 Low Expressers

VCR depletion and M1 formation were not observed using specific lots of intact hepatocytes: 652, CHD, Hu418, MRS, SD012, and SD017 (Table 4). For these lots, categorized as CYP3A5 low expressers, the M1 concentration during the incubations surprisingly decreased (inset, Fig. 39b). Perhaps the decline was caused by M1 degradation and/or metabolism as described earlier with lysate incubations.

Although the intact cells of CYP3A5 low expressers did not metabolize VCR, the CYP3A4 activities were typical of other CYP3A5 high expressers as determined by the testosterone 6β-hydroxylase activities of the intact cells from the vendor (lots CHD and MRS) and of the cell lysate (lot MRS, Table 4). The CYP3A5 low expressing hepatocytes used during the screening experiments also effectively metabolized a probe CYP3A substrate, verapamil (data not shown). In direct contradiction with the intact cell results, the cell lysate of MRS effectively metabolized VCR to M1 (Table 4). At this time, we do not understand why the hepatocytes without CYP3A5 expression did

not metabolize VCR. Nevertheless, the predicted intrinsic clearance of VCR for CYP3A5 low expressers is essentially zero. This prediction contradicts the human liver microsome data and the hepatocyte lysate data.

H. Assay Development for the Quantification of M1 and Vincristine in Plasma

The methods for VCR quantification were chosen to optimize VCR stability and recovery. Direct precipitation methods were first used to quantify VCR in plasma. For one method, the plasma was quenched with an approximately equal volume of methanol and froze the sample to facilitate protein precipitation. Although this procedure effective isolated VCR from the protein, by the nature of the procedure, the method naturally diluted the plasma and did not enable a large percentage of the sample to be injected on column. Using an alternate procedure, 10% trichloroacetic acid (TCAA) was added to the plasma to precipitate the protein. This method effectively precipitated the protein while only adding a small volume of acid to the plasma. Unfortunately the chromatography that resulted from these samples was unacceptable because the peak shapes of VCR and VRL were broad.

At this point, conditions for an extraction procedure were explored including solvent choice, solvent volume, and pH. Previously, the extraction of VCR, M1, and VRL was evaluated in a screening experiment with various solvents (Fig. 10, Methods, pg.). For this experiment, methylene chloride with TCAA addition effectively extracted VCR, M1, and VRL from buffer without degradation. Based on this experiment, methylene chloride was a logical choice. Toluene was also considered as an extraction solvent for the plasma assay because aromatic solvents have historically been used in the extraction of *Vinca* alkaloids from the periwinkle plant.[1] In moving

forward with plasma extractions for VCR, toluene and methylene chloride were both tested. For toluene, although the extraction recovery was reasonable at a neutral pH (49% with 2 volumes of solvent), VCR degraded to the N-oxide. At a low pH, the extraction recovery was less than 2%. The methylene chloride extraction efficiencies for VCR were consistent with the previous experiment in buffer (46 to 59% with 4 volumes of solvent + TCAA). In addition, the VCR N-oxide was not detected by LC/MS. Therefore, for extraction of VCR in plasma, methylene chloride was chosen as the solvent.

The internal standard (VLB or VRL) was chosen based on recovery with methylene chloride. VCR with the internal standards was extracted with 2 volumes of methylene chloride. The effects of acid addition and mechanical shaking were determined by quantifying the relative recoveries of VCR and the internal standard (Table 6). For all the extraction condition, the recovery of VLB was significantly higher than VRL. Thus, for the VCR extraction procedure, VLB was chosen as the internal standard. Acid addition and mechanical shaking did increase the recoveries of VCR and VLB; these conditions were included in the final VCR extraction procedure.

Now that the conditions for the extraction were somewhat optimized for recovery, standard curves with VCR were generated for therapeutic concentrations of VCR (0.2 to 100 ng/mL). Unfortunately, the LC/MS responses of VCR were not linear because the VCR working solution adsorbed to the container. Specific experiments were designed to choose an appropriate material of construction (glass or polypropylene) and to choose the correct solution composition (0 to 50% methanol) for the serial dilutions (Fig. 41). For the most lipophilic compound, VRL, regardless of

tube material, the recoveries continued to increase even at the highest two concentrations, 30 and 40% methanol. The recoveries of VCR and VLB were the least sensitive to methanol concentration in polypropylene tubes. For VCR, recoveries in polypropylene tubes were similar at 20, 30, and 40% methanol. As a result, for later extractions with plasma, the VCR standard curves were generated from working solutions in 20% methanol, diluted in polypropylene tubes.

Polypropylene tubes were also chosen for the dissolution of the methylene chloride extract in 0.2% formic acid: methanol (80:20). The recoveries of VCR and VLB were 10 to 15% higher in polypropylene tubes compared to glass tubes (silanized or not). The most consistent recovery of the analytes (80% for VCR) was accomplished by scraping the pellet from the polypropylene wall. Other techniques (methanol dissolution) resulted in 5 to 10% less recovery. The internal standard VLB was also required for high recovery of VCR because VLB acted as a carrier for VCR at low concentrations (Fig. 42a).

Finally, using the initial gradient conditions (Fig. 41), the standard curves generated by LC/MS were unable to quantify concentrations of VCR below 0.4 ng/mL (Fig. 42b). An extended gradient method was chosen to eliminate the baseline noise from the blank plasma. Although the baseline noise was not present in the LC/MS/MS assay, the assay was developed to work using both LC/MS and LC/MS/MS detection.

I. Validation of M1 and Vincristine Quantification in Plasma

1. Liquid chromatography and mass spectrometry

ESI in positive mode was chosen for the analysis of VCR, M1, and vinblastine (internal standard). Previously for *Vinca* alkaloids, ESI was shown to have the greatest

sensitivity when compared to EI or APCI.[15,125] Q1 scans of VCR, M1, and vinblastine revealed that the dicharge ions were the most intense precursor ions. As expected from our previous work,[121] the dehydrated dicharge ion for M1 at a *m/z* of 397.2 was the dominant Q1 ion. The two Q3 product ions for each compound with the most intense signals were selected for automated MRM optimization (Fig. 43, Table 7). The Q3 ions for each compound with the highest signal-to-noise (S/N) ratio were used to quantify the analytes in standards and clinical samples (400 ms dwell times). The alternate Q3 ions for VCR and M1 (100 ms dwell times) were used to verify compound identities.

Representative chromatograms of a high QC standard are presented in Fig. 44. Baseline separation in the standard samples was achieved for all compounds using a series of linear gradients (Fig. 44). The M1 and VCR chromatograms of a representative blank plasma sample and the standards at the low limit of quantification are presented in Fig. 45a,b. No interference was detected in the blank plasma sample for any monitored ions. The chromatograms of an extracted patient plasma sample at the last time point (20 h post VCR dose) are also presented (Fig. 45c). For this sample, M1 and VCR concentrations were within the limits of quantification.

2. Validation data

The standard curves were generated using analyte/internal standard area ratios (Fig. 46). The VCR standard curve (0.012 to 24 ng/mL) was fit using a linear regression model with *1/x* weighting (slope = 0.154 ± 0.011, mean r^2 = 0.993). The M1 standard curve (0.012 to 12 ng/mL) required a power fit ($y = mx^{\gamma}$) to consistently fit the data (m = 0.045 ± 0.005, γ = 1.01 ± 0.01, mean r^2 = 0.994). The average calculated concentration values

(n = 4) for the calibration standards at each concentration met the accuracy requirements of the validation for the models chosen (90 to 115% for VCR and 93 to 110% for M1).

VCR and M1 were extracted from plasma using 10% trichloroacetic acid and methylene chloride. The recoveries of VCR and M1 averaged 62% and 58%, respectively, with no differences between low, medium, and high concentrations (Table 8). The limits of detection and quantification for VCR and M1 are summarized in Table 9. The concentration limit of detection (cLOD) in plasma was defined as the lowest plasma concentration tested with a S/N ratio of at least 3. The concentration limit of quantification (cLOQ) was the lowest plasma concentration tested for which the intra-day accuracy (80 to 120%) and precision (%CV $\leq$ 20) standards were met (n = 4) and for which the S/N ratio was at least 5. The mass limit of detection (mLOD) and the mass limit of quantification (mLOQ) were defined as the mass of drug on column at the cLOD and cLOQ, respectively. The intra-day and inter-day accuracy and precision data are presented in Table 10 with three concentrations of each compound tested. The acceptance criteria as described in the methods section were met for both VCR and M1.

The stability of VCR and M1 in the stock solution at 4°C was evaluated at the beginning and end of the validation experiments by HPLC with UV detection. The VCR and M1 concentrations after 14 days were 96% and 98%, respectively, of the original values. The post-preparative stability of VCR and M1 was also quantified by injecting the QC samples (high, medium, and low concentrations, n = 6 total) 10 to 26 h after the first injections. This process was repeated for three standard curves, and the average accuracies of the reinjected samples for each concentration were calculated. No

degradation was detected for VCR (90 to 97% accuracy) or M1 (93 to 98% accuracy) at any concentration.

The stability of VCR and M1 in plasma after 15 h at room temperature and after three freeze-thaw cycles was determined using QC samples of high (19 ng/mL VCR, 9.5 ng/mL M1, $n = 3$) and low (0.047 ng/mL VCR, 0.024 ng/mL M1, $n = 3$) concentrations. The VCR concentrations after 15 h at room temperature were on average 85.3% (high) and 81.8% (low) of the control group (untreated QC samples), but the differences were not statistically significant ($p = 0.08$, high and $p = 0.06$, low). The VCR concentrations were also unaffected by multiple freeze-thaw cycles at high (92.2% accuracy, $p = 0.35$) and low (89.5% accuracy, $p = 0.25$) concentrations. Unlike VCR, M1 was not stable in plasma after 15 h; the M1 concentrations at both high and low concentrations were only 20% of the untreated QC sample concentrations. However, the freeze-thaw stability studies showed no statistical differences in M1 concentrations between the previously thawed and untreated QC samples for high (84.2% accuracy, $p = 0.20$) and low (98.4% accuracy, $p = 0.88$) concentrations. To understand the processing stability of VCR and M1, stability studies at room temperature for VCR and M1 at therapeutic concentrations were conducted using freshly heparinized whole blood. The recovery of VCR and M1 after 3 h was within 15% of the control (15 min) value. Thus, although M1 degrades in plasma, standard processing times (< 3 h) should be acceptable for routine processing and freezing of the plasma samples. The selectivity of the assay was evaluated using blank plasma from healthy human donors ($n = 3$), and no interference was detected for M1, VCR, or vinblastine. The drugs potentially coadministered with VCR were also assayed individually to evaluate interference, and no interfering peaks were detected.

J. M1 and Vincristine Concentrations in Patient Samples

1. Urine

The urine samples from the 2002–2004 clinical studies were assayed for M1 and VCR concentration (Fig. 47). In addition, two samples of the VCR clinical formulation were directly assayed by LC/MS/MS to determine the administered VCR/M1 plasma concentration ratio. Compared to the VCR/M1 plasma concentration ratio of the clinical formulation, the patient sample metabolite ratios were similar but highly variable. For the urine samples from the two patients with high CYP3A5 expression, the VCR/M1 ratios were not different from those of other patients (200 vs. 10 to 1000 for all patients). For two urine samples collected at different time points (patient 14), the VCR/M1 ratios were drastically different (100-fold lower concentration after 3 h). A high VCR/M1 ratio would be expected during the initial distribution phases of VCR, while the VCR concentration is highest in the blood before it completely distributes to the tissues. To predict the exposure of patients to VCR or plasma VCR/M1 concentration ratios of a patient, the VCR/M1 concentration ratios in urine would be most useful if the samples were collected during the terminal elimination phase of VCR.

2. Plasma from 2002–2004 Clinical Studies

Over 100 plasma samples were collected from pediatric patients receiving VCR 2002–2004. These samples were assayed for VCR and M1 content after the assay was validated in 2007. Compared to the standard curve samples, the VCR chromatograms of the patient samples included three additional peaks (Fig. 48); by retention time, these compounds were tentatively identified as epoxide 1 (M4), epoxide 2 (M5), and VCR-NO. For one representative sample, the VCR-NO signal intensity as quantified by

LC/MS was 10-fold higher than the VCR signal intensity (Fig. 49). Thus, the VCR in these clinical samples had degraded.

3. Plasma from Rhadomyosarcoma Patients, 2006–2007

Samples from patients (n = 4) treated for rhabdomyosarcoma were assayed in duplicate for VCR and M1 up to 24 h after treatment. The lowest VCR and M1 concentrations (0.47 ng/mL and 16 pg/mL, respectively) were above the LOQ for all plasma samples, and the concentration of M1 at any time point was 1.7 to 22.3% of the VCR concentration (Fig. 51). The plasma concentration versus time profiles of VCR and M1 are shown in Fig. 50. Using a two-compartment model with elimination from the central compartment, the fitted parameters of VCR for two patients and the average values of the parameters for all patients are listed in Table 11. The average terminal half life of 27 h and clearance of 491 mL/min/m^2 for VCR are consistent with previously published pharmacokinetic data in adults.[56,126] However, for almost all the model fitted parameters, the uncertainty was somewhat high, approximately 30% for plasma clearance, because the model was required to extrapolate past the last time point at 24 h. More importantly, the two-compartment model chosen to fit the data may not be correct at later time points. In fact, adult pharmacokinetic studies with VCR past 24 h routinely used a three-compartment model to describe the data.[44,52] For the patients in our study, the plasma time points described less than 50% of the AUC. A better estimation of exposure and clearance would be achieved if additional plasma samples were collected at later time points (48, 72 h).

V. Discussion

A. Key Pathways of Metabolism and Major Metabolites of Vincristine

The primary objective of this study was to understand the role of CYP3A5 in the metabolism of vincristine. This information could then be used to predict how *CYP3A5* genotype in patients may influence the systemic clearance of vincristine. To begin to understand the role of CYP3A5, some fundamental questions about the metabolism of vincristine needed to be answered. What cytochrome CYP enzymes metabolize vincristine? What are the primary metabolites of vincristine? Previously published evidence from multiple *in vivo* and *in vitro* studies suggested that vincristine is metabolized by CYP3A enzymes.[16] However, even though vincristine is one of the most studied chemotherapeutic agents, fundamental metabolism data was not available for vincristine with cytochrome CYP enzymes. To this point, other research scientists have commented on the "frustrating paucity" of information related to *Vinca* alkaloid metabolism.[127] This apparent void in the literature is likely caused by multiple factors including model selection for metabolism and analytical techniques.

For the first *in vitro* studies, we chose to use commercially available cDNA-expressed CYP enzymes produced from baculovirus-infected insect cells. In pre-clinical drug development, these enzymes are the industry standard because the activities between lots of enzyme are consistent. In addition, the substrate selectivity can be evaluated for individual CYP enzymes. For this study, cDNA-expressed CYP3A4 and CYP3A5 were incubated with vincristine. In the incubated mixtures, one primary metabolite (M3) was first observed at a later retention time than vincristine by HPLC (Fig. 5d). However, when LC/MS detection was used, the metabolic profiles of

these same incubates were different. Two metabolites were detected, one at an earlier retention time than vincristine (M1) and one at a much later time (M3) (Fig. 4). After a series of experiments, a relationship between M1 and M3 was realized; M1 degraded to M3 in the presence of base (Fig. 7). Thus, M1 was the only major metabolite of vincristine because M3 formation was an artifact of post-incubation base treatment (Fig. 6). To quantify M1 by UV detection, the initial HPLC conditions had to be optimized to enable baseline separation of M1 and vincristine (Fig. 5a). In addition, to prevent the formation of M3, base was no longer added to the incubations. In retrospect, UV analysis was a poor choice for the initial metabolic profiling of vincristine. Alternatively, LC/MS ion monitoring would have detected M1 from the beginning. In fact, we were fortunate that sodium hydroxide was added to the initial vincristine incubations; without the base-catalyzed conversion of M1 to M3, vincristine depletion and metabolite formation would not have been observed by HPLC at all. Perhaps other investigators who previously studied the CYP metabolism of vincristine were misled, as we were initially, by non-selective methods of detection (electrochemical or UV).[127]

Isolation and identification of the primary metabolite M1 was particularly challenging because it is chemically unstable. Direct mass measurement of M1 by LC/MS was not straightforward because the compound readily lost water in the source (*m/z* 811 → 793). The actual mass was not apparent until high concentrations of M1 were infused (Fig. 11). In addition, M1 degraded during normal procedures for metabolite isolation, including evaporation with water or methanol. Thus, to chemically identify M1, stable derivatives of M1 were synthesized and characterized: M3, the base-catalyzed product, and M1-acetate. The structure of M3 was conclusively determined

by LC/MS/MS and NMR analysis. For the acetylated product (M1-acetate), the Q1 mass by LC/MS/MS (*m/z* 853) was consistent with acetylation of the proposed M1 compound (*m/z* 811).

Using the information from the M1 derivatives and the exact mass of M1, the chemical structure of M1 was deduced (Fig. 9); the compound is a unique secondary amine with modifications on the vincristine Catharanthine moiety. The proposed mechanism of formation begins with the CYP-mediated hydroxylation of the carbon α to the piperidine ring nitrogen. The piperidine ring reversibly opens between the nitrogen and the hydroxyl group. The resulting aldehyde is then oxidized to a carboxylic acid; the acid is eliminated to yield M1. These oxidations (best categorized as N-dealkylation and oxidative deformylation) are typical CYP-mediated reactions.[63] Although it was previously recognized that the two heterocyclic amines of vincristine were vulnerable to oxidation by cytochrome CYP enzymes, the structure of M1 is radically different from any previously proposed metabolites of vincristine.[127] These structures were predicted without consideration of sequential oxidation possibilities. Other CYP3A substrates are reported to undergo sequential metabolism including itraconazole and docetaxel.[34,128] In fact, the major metabolite of vincristine with horseradish peroxidase is M2, a compound formed by two sequential oxidations.[9]

M2 was detected as a minor metabolite of vincristine using cDNA-expressed CYP3A5 (Fig. 6, approximately 10% of M1 by area); CYP3A4 and human liver microsomes did not produce M2. The chemical structure of M2 was confirmed by LC/MS/MS to be the same as a product from a different enzyme system, horseradish peroxidase.[9] We used this enzyme to more efficiently synthesize microgram quantities

of M2 for NMR analysis. Just like M1, the first step in M2 synthesis is the hydroxylation of the carbon α to piperidine nitrogen (Fig. 9). However, unlike M1, the carbon-carbon bond of the diol is cleaved leaving a formyl group on the piperidine nitrogen. This type of oxidation is rarely observed with CYP enzymes. Specifically, during the last step, mitochondrial $P450_{scc}$ oxidizes cholesterol to pregnenolone by cleaving the C-C bond of the diol.[129] When selecting sites of oxidation on the vincristine-intermediate diol, CYP3A4 and CYP3A5 preferentially oxidize the aldehyde to produce M1. Interestingly, for other non-CYP enzymes such as peroxidases and copper oxidases, M2 is the only vincristine metabolite reported.[9,127]

Based on the CYP metabolism of vincristine, other *Vinca* analogues are also likely metabolized by CYP3A enzymes. In particular, *Vinca* alkaloids with identical Catharanthine moieties to vincristine, such as vinblastine and vindesine, may be metabolized to an M1-equivalent molecule. In fact, the CYP3A-mediated M1 equivalent for vinblastine has been discovered by our laboratory (data not shown, manuscript in progress). Other investigators have observed one primary metabolite (M) of unknown chemical identity from the incubation of radiolabeled vinblastine and vindesine with human liver microsomes.[106,107] Using sodium perchlorate/perchloric acid (acidic pH) and an extended methanol gradient, these compounds by HPLC eluted later than their parent drug (+ 4 min). Based on our HPLC data with vincristine at an acidic pH (Fig. 5a), the metabolites by retention time appear most like M2 or M3-equivalent compounds. However, the incubations were not pretreated with a strong base, a requirement for the production of vincristine M3 from M1. Without LC/MS data, we cannot know with certainty what compounds were observed in these studies.

Other *Vinca* alkaloids such as vinorelbine are likely to have a different metabolic pathway from vincristine because the hydroxyl group β to the piperidine nitrogen is not present (Fig. 1). After the initial hydroxylation, this hydroxyl group is required for the subsequent oxidation reactions to produce M1 and M2. Published data is consistent with this assessment; vinorelbine is metabolized to multiple compounds primarily by CYP3A4.[109] Unlike with vincristine, one dominant metabolite has not been identified for vinorelbine. The results from our laboratory (not shown) are in agreement with this finding.

Once M1 was identified as a primary metabolite of CYP3A4 and CYP3A5, the relative roles of other hepatic (and a few non-hepatic) CYP enzymes were assessed. After each enzyme was incubated with vincristine, the vincristine depletion and M1 formation were quantified (Fig. 12). CYP3A4 and CYP3A5 were the only two enzymes with more than 20% depletion of vincristine. Interestingly, with 90% vincristine depletion, CYP3A5 was the most active enzyme. Vincristine was a statistically significant but poor substrate of other enzymes: CYP3A7 (a fetally expressed CYP3A enzyme) and CYP2E1. Consistent with previous experiments, the depletion of vincristine corresponded to an increase in M1 concentration; 50 to 70% of the vincristine depletion was accounted for as M1.

We demonstrated that cDNA-expressed CYP3A4 and CYP3A5 enzymes are the primary drug metabolizing enzymes for vincristine. However, the results from cDNA-expressed enzymes need to be carefully interpreted in combination with data from other *in vitro* models. The cDNA-expressed enzymes lack all the cofactors and proteins found in a human hepatocyte. In addition, compared to human liver microsomes,

recombinant enzymes contain higher concentrations of co-expressed redox coenzymes (NADPH-cytochrome P450 reductase and cytochrome b_5). The concentration of cytochrome b_5 can significantly alter the kinetics of a reconstituted system; in some cases, even the metabolic profile of a substance can change.[70]

As an alternative to cDNA-expressed enzymes, human liver microsomes are often used to evaluate CYP metabolism of drugs. In this study, a select number of human liver microsomes from the Indiana University Liver Bank were incubated with vincristine and NADPH. These human livers were phenotyped for CYP3A5 content. A liver of each type (one high and one low CYP3A5 expresser) was used to identify any vincristine metabolites. As with the cDNA-expressed enzyme system, the only major metabolite formed with human liver microsomes was M1 (Fig 23).

M1 formation was confirmed to be primarily mediated by CYP3A4 and/or CYP3A5 using selective chemical inhibitors of CYP enzymes (Fig. 25). The activity was reduced 80% with the addition of ketoconazole, a typical CYP3A selective inhibitor. Other CYP3A substrates, vinblastine and vinorelbine, also competitively inhibited M1 formation. The inhibition by the *Vinca* alkaloids was not surprising because in a different study, vincristine inhibited the metabolism of vinblastine.[107] The rates of formation for M1 were somewhat reduced, approximately 20%, when CYP2D6 and CYP2C19 were chemically inhibited. This reduction in activity by quinidine and omeprazole may have been caused by non-selective effects of the chemical inhibitors on CYP3A4 or CYP3A5. For example, the K_m of omeprazole hydroxylation with CYP3A4 is equal to the concentration used in this experiment.[130] In addition, the selectivity of chemical inhibitors is unknown for CYP3A5. Thus, the reduction in activity by

quinidine and omeprazole may be an artifact of the method. In any case, the CYP3A enzymes were the primary drug metabolizing enzymes of vincristine.

To understand the relative roles of CYP3A4 and CYP3A5 in human liver microsomes, the activity of CYP3A4 was selectively inhibited by cyclosporin A (Fig. 26b). As predicted by the cDNA-expressed enzyme system (Fig. 14), the rates of M1 formation for CYP3A5 low expressers were more inhibited by cyclosporin A than those for high expressers (Fig. 26b, Fig. 28). The degree of inhibition for both high and low expressers was predicted by 6β-testosterone hydroxylase activity, a CYP3A4 activity probe (Fig. 22b). This correlation was expected for CYP3A5 high expressers because the residual activity after CYP3A4 inhibition should be CYP3A5-mediated. However, for human liver microsomes without CYP3A5 activity, this relationship is less obvious. Perhaps for the microsomes with lowest CYP3A4 activity, the other less active CYP enzymes (or even the small amount of CYP3A5, Table 2) are primarily responsible for the metabolism of vincristine, albeit at an extremely slow rate.

Although some useful data were obtained from the initial cyclosporin A inhibition experiments (Fig. 26b), the organic solvent concentration was high (4.8% methanol). As a result, the basal activities of high and low CYP3A5 expressers were unequally inhibited in the vehicle controls (Fig. 26a). While all the microsomes showed variable response to the methanol, the CYP3A5 low expressers were the most sensitive to methanol inhibition. This data imply that the CYP3A4 activity with vincristine is more sensitive to methanol concentration than the CYP3A5 activity. As previously reported, hepatic CYP enzymes in microsomes are not equally inhibited by organic solvents.[131] Our data for CYP3A4 and CYP3A5 are consistent with this observation.

Later cyclosporin A inhibition experiments used lower concentrations of methanol (0.3%, Fig. 28); this concentration did not significantly affect the basal activity the microsomes (Fig. 27).

To provide additional evidence of CYP3A4-mediated metabolism for vincristine, the CYP3A4 activities of the human liver microsomes were characterized with selective probe substrates, itraconazole and testosterone (Table 2, Fig. 29). For CYP3A5 low expressers, a strong correlation was observed between CYP3A4 activities (ITZ and TST) and the rates of M1 formation (r^2 = 0.89 and 0.91). Although the protein content of CYP3A4 also correlated to the rates of M1 formation (r^2 = 0.75), less of the relationship was explained by CYP3A4 protein expression as compared to CYP3A4 activity. As previously reported, CYP3A4 activity is commonly correlated to but not completely explained by CYP3A4 protein content; typical r^2 values for CYP3A4 are 0.74 to 0.78.[80,132] In our study, the testosterone 6β-hydroxylase activity was also correlated to CYP3A4 protein content with an r^2 value of 0.77. Other than protein content, several factors likely influence the activity of CYP3A4 including variable heme coupling, assay uncertainty, and variable expression of coenzymes. In any case, the majority of the variability in the rates of M1 formation was accounted for by CYP3A4 activity and protein content. Thus, CYP3A4 is a major drug metabolizing enzyme of vincristine for CYP3A5 low expressers.

The roles of CYP3A4 and CYP3A5 were also evaluated for CYP3A5 high expressers. Compared to CYP3A5 low expressers with equivalent CYP3A4 activities, the high expressers more rapidly metabolized vincristine to M1 (Fig. 29). All values for CYP3A5 high expressers were outside of the 95% confidence interval established by

CYP3A5 low expressers. Hence, CYP3A5 expression is a significant factor in the metabolism of vincristine. In addition, the CYP3A5 protein content was correlated to the predicted CYP3A5 activity with vincristine (Fig. 30, $r^2 = 0.95$). This analysis and the data from the selective chemical inhibition experiment (Fig. 28b) provide strong evidence of CYP3A4 and CYP3A5 involvement in vincristine metabolism for CYP3A5 high expressers.

For the last *in vitro* model, cryopreserved hepatocytes were used to evaluate the metabolic profile of vincristine. Unlike the two other *in vitro* models, hepatocytes contain physiological concentrations of enzymes, coenzymes, and NADPH. Of particular importance, the previous models were unable to evaluate the potential roles of phase II enzymes. In previously published studies, investigators hypothesized that secondary metabolism (possible phase II) of vincristine may be responsible for the formation of three metabolites.[10] From our previous work with cDNA-expressed enzymes and microsomes, we anticipated that vincristine would be metabolized by hepatocytes to at least one compound, M1, by CYP3A4 and CYP3A5 (if present).

We first incubated vincristine with hepatocytes of unknown *CYP3A5* genotype. To our surprise, the hepatocytes produced no apparent metabolites of vincristine (Fig. 39b). In fact, for these incubations, the concentrations of M1 were high at time zero (2 to 3% of vincristine) and then decreased with time; an increase in concentration was not detected for any vincristine-related compounds. This observation was true using multiple concentrations of vincristine (0.1 to 50 μM) and cells concentrations up to 1.5 x 10^6 cells/mL.

Initially, the high concentration of M1 at time zero was a concern, particularly at low concentrations of vincristine (Fig. 34). As shown in Fig. 35, unlike plasma or buffer solutions, a small percentage of vincristine in media readily degraded to M1 at time zero (2 to 3%). Thus, the high concentrations of M1 and other degradation products (especially epoxide 1) at time zero were artifacts of the model. Although we do not have an explanation for the degradation, we were able to account for the formation of M1 at time zero; the initial concentrations of M1 were quantified by LC/MS and subtracted from the values at later time points. This correction was possible because the concentrations of M1 were high at time zero but did not detectably change over 4 h for the sonicated cell controls (Fig. 39). In addition, for the remaining incubations, the vincristine concentrations were always 4 μM or higher to minimize degradation.

Vincristine metabolism was not detected using the following cryopreserved hepatocyte lots: 652, Hu418, MRS, SD012, and SD017. Various control experiments were performed to ensure that the activity of CYP3A4 and the viability of the cells were normal. In addition, to verifying that vincristine was not adsorbed to the wells or cells, the free concentrations of vincristine were quantified in the media. In the absence of an alternate explanation, we hypothesized one of two possibilities; either CYP3A4 was not able to metabolize vincristine, or vincristine was not entering the cells.

The latter explanation was partially discounted after hepatocytes with high CYP3A5 expression were incubated with vincristine. Multiple lots of African-American hepatocytes were tested until a CYP3A5 high expresser (*CYP3A5*1/*1*) was discovered. The hepatocytes from this donor (EHI) were able to metabolize vincristine

to M1 (Fig. 36a). Yet, the rates of M1 formation were much lower than those predicted using the IU human liver microsomes (Table 2). To further understand this observation, in paired experiments with intact cells, hepatocytes were sonicated to release their intracellular contents. For the same lot of hepatocytes, vincristine was then incubated with both intact cells in media and sonicated cells in buffer supplemented with NADPH (Table 4). For the sonicated cell preparation, the activity was 4 to 69-fold higher than the intact cells. Thus, although vincristine is able to enter the cells, the concentration of vincristine inside the cells may be lower than that in the media. Alternatively, the CYP enzymes inside the intact cells may be less efficient in metabolizing vincristine. In any case, for all experiments for intact and sonicated cells, the formation of M1 almost completely accounted for the depletion of vincristine (> 80% recovery by UV, Fig. 36a). The formation of M1 in the intact cells was substantially reduced with the addition of ketoconazole, confirming the role of CYP3A4 and/or CYP3A5 in the metabolism of vincristine (Fig. 37c). However, taking into consideration the lack of detectable activity with CYP3A5 low expressers, the CYP3A4-mediated metabolism of vincristine may be insignificant in hepatocytes. In support of this hypothesis, the rates of M1 formation for CYP3A5 high expressers were not inhibited by cyclosporin A, a selective CYP3A4 inhibitor.

In a previously published study with vincristine and hepatocytes, vincristine was readily metabolized to at least three compounds.[10] In our studies, using CYP3A5 high expressing hepatocytes, vincristine was metabolized relatively slowly to only one major metabolite (Fig. 36). It is unknown why the previously published hepatocyte data conflict with our results. However, based on our experience with hepatocytes, the

metabolism described previously may have been vincristine degradation. First, we do not know the stabililty of the radiolabeled vincristine using their incubation conditions because the authors did not present an appropriate "no cell" or "sonicated cell" control. The N-oxide, two diasteramеric epoxides, and M2 are common vincristine impurities and degradation products. In addition, the concentrations of vincristine (0.5 μM) were much lower than in our experiments (4 μM). As indicated earlier, vincristine is highly susceptible to degradation by epoxidation at low concentrations in media (Fig. 34a). The investigators also did not present evidence to specifically implicate CYP metabolism, such as inhibition with ketoconazole. As for the *CYP3A5* genotype of the hepatocytes, the study was conducted in France, a primarily Caucasian population with a low frequency (< 20%) of CYP3A5 high expressers. Based on our experience with cryopreserved hepatocytes, the metabolism of vincristine is not detectable using a typical CYP3A5 low expresser (Table 4). Although the investigators may have only published the positive results from numerous donors, the probability is low that these French investigators tested a high CYP3A5 expresser the first time. Finally, although the authors indicated that they were pursuing the chemical identification of the metabolites, no publications on the topic followed. Presumably, either the results were not reproducible (because of CYP3A5 expression), or the compounds were difficult to isolate and identify as described previously.

After evaluating vincristine with three *in vitro* metabolism models, we opted not to thoroughly pursue other types of models. In a screening experiment, we did incubate rat liver microsomes and rat cDNA-expressed CYP3A enzymes (CYP3A1 and CYP3A2) with vincristine. The formation rates of M1 and the rates of depletion for

vincristine were extremely slow or not detectable. Based on this data, the rat model is not representative of vincristine metabolism in humans. Other investigators have utilized *in vivo* rat and mice models to study vincristine disposition.[127,133] One group discovered three potential metabolites in the bile of rats. However, these compounds may have been degradation products (see above hepatocytes discussion).[1] Consistent with our results, another group was unable to find any vincristine metabolism with rat liver microsomes.[14] These investigators also did not observe metabolism with mouse liver microsomes. However, we do not have any *in vitro* data to support this observation.

The human *in vitro* models of metabolism all confirmed that vincristine was metabolized by CYP3A4 and/or CYP3A5 to one primary metabolite M1. The next approach was to identify and quantify metabolites in human plasma or urine samples. Unfortunately, because of the low therapeutic dose (2 mg maximum) and high volume of distribution, the plasma vincristine concentrations are extremely low, less than 0.2 ng/mL after 24 h. As a result, we were unable to detect any *Vinca*-related metabolites with a mass spectrometer in scan mode. Perhaps this approach would have been more successful for vinblastine, a compound administered at a higher clinical dose.

To quantify vincristine and M1 in plasma, we developed and validated a more sensitive LC/MS/MS assay using selected reaction monitoring. Previously developed assays were either not selective or not sensitive enough to detect vincristine (or M1) in plasma. Of the previously published methods, the most discriminating methods utilized LC/MS or LC/MS/MS technology and could detect vincristine concentrations as low as 0.2 ng/mL with a lowest mLOQ of 15 pg.[126,134-136] The LC/MS/MS method by Skolnik

et al.[135] is modestly better (2-fold) than an alternative LC/MS method by Schmidt *et al.*[126] (Table 8). Compared to these assays, our LC/MS/MS assay is 10-fold more sensitive than the lowest reported mLOQ. The sensitivity of our assay using LC/MS detection (data not shown) is consistent with the reported mLOQ by Schmidt *et al.*[126] Comparing our LC/MS/MS assay to the method by Skolnik *et al.,*[135] the apparent sensitivity differences can be explained by two possibilities. First, in our assay, we purified the vinblastine internal standard by HPLC prior to use. In our experience, all commercially available vinblastine contains trace amounts of vincristine. Without purification, the cLOQ of vincristine in the current assay would not have been better than 0.1 ng/mL. Second, the current assay monitored the dicharge ions of vincristine and vinblastine which resulted in greater sensitivity than the monocharge ions by LC/MS or LC/MS/MS. Although we did not test the ionization of vincristine with exactly the same mobile phase, monitoring of dicharge ions may improve the sensitivity of the assay by Skolnik *et al.*[135]

This same group recently published an updated LC/MS/MS method for vincristine quantification.[137] The improved method has a cLOQ of 50 pg/mL, a major improvement over the previous method (500 pg/mL). To achieve this sensitivity, the investigators changed the internal standard to vinorelbine because the vinblastine standard degraded to an interfering compound. In our hands, vinblastine did not degrade but contained vincristine as a trace impurity. In addition, for their new method, the eluent composition was optimized to improve ionization by LC/MS/MS. Their method continued to monitor the monocharged Q1 ion of vincristine, unlike our method. Even so, the overall sensitivity of the method is similar to ours with a mLOD of 0.8 pg

(Table 8). Based on this value, their assay could achieve a mLOQ value of less than 2 pg but was only validated to a mLOQ of 4 pg, a value almost 4-fold higher than our assay.

Although the method by Lee *et al.*[137] can quantify low vincristine concentrations in plasma, our method also quantifies M1, the major *in vitro* metabolite of vincristine. M1 is more sensitive to degradation than vincristine in plasma and during sample preparation.[121] The previously published assays isolated vincristine by solid-phase extraction and then evaporated the methanol and/or methanol eluent.[126,135,137] Using this procedure based on our experience, M1 would likely degrade. The inverse is also true; M1 could be generated by this method. Vincristine dissolved in methanol will degrade to low levels of M1 by evaporation alone (data not shown). Methylene chloride evaporation or processing steps with other solvents that do not require evaporation minimize M1 degradation and formation in our experience.

After the method for vincristine quantification was validated for plasma, a modified procedure without an extraction step was used to assay urine samples by LC/MS/MS. Other detection methods, for example LC/MS in scan mode, were unable to detect M1, even using concentrated samples. By selected ion monitoring, the concentrations of M1 were quantified in the urine. Low concentrations of *Vinca* compounds in the urine were expected because most of the *Vinca*-related compounds are excreted in the bile. Other researchers have encountered similar difficulties; only one type of *Vinca*-related compound, a deacetylated derivative, has been isolated and conclusively identified from the urine.[13,14] These compounds represented less than 1% of the parent drug by radioactivity. Although the investigators call the deacetylated

Vinca alkaloids "metabolites," these compounds may actually be metabolites, degradation products, or impurities in the formulation. In our experience, multiple impurities are present in the clinical formulation and the analytical grade vincristine, including desacetylvincristine, M2, and M1.

The vincristine and M1 concentrations were quantified for the clinical formulation of vincristine and for several patient urine samples. Compared to the ratios of VCR/M1 in the clinical formulation, the concentration ratios in most patient urine samples were similar (Fig. 47). Like the deacetylated *Vinca* alkaloids isolated in previous studies, it is unclear using the urine data alone whether M1 is a metabolite of vincristine or an impurity in the formulation. However, the data from patient 14 are consistent with the hypothesis that M1 is a metabolite; the VCR/M1 ratio in urine was substantially lower in a later time point sample. The data are nevertheless inconclusive because the VCR/M1 ratio of the clinical formulation is unknown for this particular patient. Also, more importantly, the disposition properties of M1 as compared to vincristine are unknown. The volumes of distribution for M1 and vincristine are likely different as indicated by the blood-to-plasma ratios at room temperature (0.8 for M1, 1.1 for vincristine).

The concentrations of vincristine and M1 were quantified in human plasma samples from two clinical studies. For samples from the first study, the vincristine was obviously degraded to epoxides and an N-oxide derivative (Fig. 48, Fig. 49). Although the exact cause is unknown, samples from these studies prior to analysis were stored for more than 2 years at -20°C. This type of degradation was not observed for samples from the second clinical study stored for 8 months or less at -80°C.

For the second study of patients, the M1 concentration paralleled that of vincristine for the terminal elimination phase (Fig. 50). These data are strong evidence that M1 formation from vincristine is rate limiting *in vivo*. However, the data presented do not prove that M1 is a major metabolite *in vivo*. We were unable to search for other vincristine-related compounds by LC/MS because the plasma concentrations were too low. Previous radiolabeled vincristine clinical studies determined that the majority of vincristine-related compounds are eliminated in the bile. Fecal samples could be used to scan for unknown metabolites although previous investigators had trouble with vincristine stability in the feces control samples.[11]

Even if M1 is a major metabolite of vincristine *in vivo*, the M1 contents in urine and feces will not likely account for a large percentage of the administered vincristine because M1 is not chemically stable in plasma. In the stability studies performed for the method validation, 80% of M1 degraded after 15 h at room temperature. In addition, during hepatocyte lysate incubations in sodium phosphate buffer, M1 was also rapidly metabolized and/or degraded. Multiple degradation products of M1 were observed after radiolabeled vincristine was incubated with hepatocyte lysate (Fig. 37a). M1 was a definite precursor to one of these compounds (retention time = 22 min). This compound by LC/MS/MS (data not shown) was identical to M1 but without a methyl ester group on the Catharanthine moiety. Admittedly, these experimental results could be artifacts of the *in vitro* experimental conditions. However, in past radiolabeled vincristine studies, vincristine was metabolized or degraded to multiple compounds in the feces and bile with ~50% of the parent drug remaining. A modern radiolabeled study with vincristine using LC/MS technology would provide the data necessary to complete a

material balance with vincristine and perhaps identify additional metabolites or degradation products.

B. Contribution of CYP3A5 to Vincristine Metabolism

Once M1 was conclusively identified as the major metabolite formed by CYP3A4 and CYP3A5-mediated metabolism of vincristine, the contribution of CYP3A5 to the formation of M1 could be estimated. CYP3A5 contribution was quantified using data from the *in vitro* models with cDNA-expressed enzymes and human liver microsomes.

The first approach to quantifying the contribution of CYP3A5 to M1 formation with vincristine was using cDNA-expressed enzymes, both CYP3A4 and CYP3A5. The other CYP enzymes were not examined because in an experiment with a panel of enzymes, CYP3A4 and CYP3A5 were the only enzymes with substantial substrate depletion and M1 formation (Fig. 12). The CYP3A4 and CYP3A5 enzymes were available commercially with and without co-expressed cytochrome b_5, a coenzyme present *in vivo* that typically increases the reaction rate but may also alter the affinity of the enzyme for the substrate. Each enzyme was examined using three preparations: without cytochrome b_5, with supplemented cytochrome b_5, and with co-expressed cytochrome b_5. For CYP3A4 and CYP3A5, the rates of M1 formation at different concentrations of vincristine were used to estimate the Michaelis-Menten kinetic parameters (Fig. 16). Regardless of preparation with or without cytochrome b_5, the maximum rates of M1 formation were 6 to 9-fold higher for CYP3A5 compared to CYP3A4; the K_m values were not statistically different between the enzymes (Table 1). Overall, the intrinsic clearances (V_{max} /K_m) were 9 to 14-fold higher for CYP3A5 than CYP3A4. This high degree of selectivity for CYP3A5 was unexpected because almost

all reported substrates of CYP3A are equally or preferentially metabolized by CYP3A4.[71,88,95,96] One clinically relevant CYP3A5-selective substrate is tacrolimus which has a modest 2-fold selectivity for CYP3A5.[97] As a consequence, individuals with at least one *CYP3A5*1* allele (high CYP3A5 expression) require a higher dose to maintain therapeutic trough concentrations.[102] For other substrates, for example midazolam, CYP3A4 and CYP3A5 have equal intrinsic clearances *in vitro*.[95,96,98] However, high expression of CYP3A5 does not result in clinically significant differences (even if statistically different) in clearance of midazolam.[82,93,100,101]

The relative role of CYP3A5 in the metabolism of vincristine can be estimated as a fraction of the total CYP3A activity using cDNA-expressed enzyme kinetic data (Eqn. 3). For this calculation to be correct, the Western blot assay must be able to accurately quantify the relative amounts of active CYP enzymes, specifically CYP3A4 and CYP3A5. The literature values of CYP3A4 and CYP3A5 contents are highly variable between liver banks.[86] These discrepancies are probably caused by differences in Western blot methods including enzyme standards. Purified CYP3A4 (Invitrogen) was chosen as our standard; the CYP3A5 standard was one lot of Supersomes (no cytochrome b_5, Gentest). To account for any incomplete heme incorporation in the CYP3A5 standard, the CYP protein concentrations of each CYP3A4 and CYP3A5 standard were compared by Western blot with a non-specific CYP3A antibody (Fig. 18). The CYP3A5 lot we chose to use as a standard (lot 22) had no measurable apoprotein by Western blot. However, in our experience, the apoprotein content in Supersomes is highly variable between lots (data not shown). To account for the apoprotein in most lots, the CYP protein concentration as compared to the manufacturer value needs to be

increased. Without correction, the CYP contents may be underestimated for unknown human liver microsome samples. Consistent with this assessment, a recent meta-analysis reported that the absolute concentrations of the CYP3A4 and CYP3A5 enzymes are lower in human liver microsomes when Supersomes are used for standards.[86]

To calculate the CYP3A5 contribution by Eqn. 3, the average CYP3A5 protein content was determined by Western blot assay of human liver microsome samples from the Indiana University Liver Bank. For individuals heterozygous for *CYP3A5*1* and classified as CYP3A5 high expressers (Table 1), approximately 40% of the CYP3A protein content was CYP3A5. Completing the calculation (Eqn. 3) using the estimated intrinsic clearances for CYP3A4 and CYP3A5 (Table 1), the average CYP3A5 contribution to vincristine metabolism is 88 to 92 %, the vast majority of the metabolism for CYP3A5 high expressers.

However, the contribution of CYP3A5 varies between individuals (50 to 93%) based on CYP3A4 and CYP3A5 content. Consistent with other human liver microsome banks, the CYP3A4 content (10-fold) is more variable than the CYP3A5 content (3-fold).[81] The differential variability between CYP3A4 and CYP3A5 expression is likely caused by several factors. First, CYP3A4 expression is more easily induced by PXR substrates than CYP3A5.[84] Although the patient histories are unknown for the IU liver bank, PXR ligands such as phenytoin are frequently administered to patients.[79] In addition, as compared to CYP3A5, CYP3A4 is generally more susceptible to mechanism-based inhibition. For example, using cDNA-expressed enzyme models, mechanism-based inhibitors erythromycin and saquinavir only inactivate CYP3A4.[88,138] *In vivo*, selective competitive inhibition of CYP3A4 with drugs such as itraconazole

may also reduce the CYP3A4 contribution to metabolism. For vincristine, severe neurotoxicity caused by vincristine overdose was observed with concurrent administration of intraconazole.[28] If the itraconazole toxicity was caused by inhibition of metabolism, individuals with high CYP3A5 expression may be protected from this type of drug-drug interaction.

The CYP3A5 contribution to vincristine metabolism was also calculated using a bank of human liver microsomes. By genotype, twelve livers in the Indiana University liver bank were predicted to be expressers of CYP3A5. The actual number of CYP3A5 high expressers was ten as determined by Western blot phenotyping. Although the cause of this discrepancy is unknown, the two livers with low CYP3A5 expression may have a rare genetic polymorphism. Our laboratory plans to sequence the *CYP3A5* genes of the individuals to determine if any additional functionally relevant SNPs are present. An additional ten livers were chosen with low CYP3A5 expression and a range of CYP3A4 activities as determined by testosterone 6β-hydroxylase activity. The Michaelis-Menten parameters of M1 formation from vincristine were estimated for each human liver microsomal sample (n = 22, Fig. 24, Table 2). The K_m values (corrected for binding) were not correlated to the CYP3A4 activities of the microsomes. Thus, even though the CYP3A5 low expressers were not selected randomly, the K_m parameters were directly compared between the groups. No statistical differences in K_m values were detected between the CYP3A5 high and low expressers. This result was expected because the K_m values for cDNA-expressed CYP3A4 and CYP3A5 were not statistically different (Table 1).

For CYP3A5 low expressers, the maximum rates of M1 formation were highly correlated with the testosterone 6β-hydroxylase activities (r^2 = 0.91). This relationship was used to estimate the V_{max} values of M1 formation for the remaining untested human liver microsomes in the bank (n = 34). With all the V_{max} values, the two groups of microsomes with high and low CYP3A5 expression were compared; the CL_{int} median value was 7-fold higher for the CYP3A5 high expressers versus low expressers with some overlap between the groups (Fig. 32). The intrinsic clearances of a few CYP3A5 low expressers were phenotypically similar to those of CYP3A5 high expressers. These CYP3A5 low expressers were predicted to have relatively high CYP3A4 activities. To test this hypothesis, the CYP3A4 activity was selectively inhibited with cyclosporin A. For cDNA-expressed enzymes, CYP3A4 activity for M1 formation is completely inhibited with 25 μM of cyclosporin A. However, using the same conditions, only 15% of the CYP3A5 activity is inhibited. As predicted by the recombinant system, the CYP3A5 high expressers were less inhibited by cyclosporin A than the low expressers (Fig. 26b). This experiment needs to be interpreted with caution because the methanol alone inhibited M1 formation in the vehicle controls (Fig. 26a). Nevertheless, from Fig 26b, the CYP3A5 high expressers retained at least 60% of their original activity after cyclosporin A inhibition. The CYP3A5 contribution to M1 formation was likely higher than 60% because cyclosporin A non-selectively inhibited cDNA-expressed CYP3A5.

The calculation of CYP3A5 contribution to M1 formation by human liver microsomes is not as straightforward as with the cDNA-expressed enzymes. With human liver microsomes, the contribution of CYP3A5 cannot be determined directly because the CYP3A4 and CYP3A5 are co-expressed. Previous investigators have

looked for statistical differences in microsomal activities between the groups of CYP3A5 high and low expressers.[71] In contrast, we chose to use three different normalization approaches to calculate the contribution of CYP3A5 for each CYP3A5 high-expressing microsomal sample. First, for CYP3A5 low expressers, the itraconazole hydroxylase activities (highly selective for CYP3A4) of the microsomes were correlated with the V_{max} of M1 formation. This correlation was used to predict the CYP3A4-mediated V_{max} of M1 formation for CYP3A5 high expressers. The CYP3A5 contribution for each CYP3A5 high expresser was the difference of the actual V_{max} and the calculated CYP3A4-mediated V_{max}. A similar normalization approach was used to calculate the CYP3A4-mediated V_{max} of M1 formation using testosterone 6β-hydroxylase activities. Testosterone 6β-hydroxylase is thought to be mediated primarily by CYP3A4 with some contribution (10%) by CYP3A5.[95] At least for the incubation conditions used in this study, the testosterone 6β-hydroxylase activities were highly correlated with the itraconazole hydroxylase activities and CYP3A4 protein content (Fig. 22); these relationships were independent of CYP3A5 expression. Thus, the testosterone 6β-hydroxylase activities were only dependent on CYP3A4 activity. For the last normalization, the CYP3A4 protein content was used to estimate the CYP3A4 activity of CYP3A5 high expressers. Interestingly, regardless of the normalization approach, the average estimated CYP3A5-mediated metabolism of vincristine for CYP3A5 high expressers was consistently 80% (Table 3). The CYP3A5 contribution to metabolism for an individual liver (43 to 93%) was dependent on the CYP3A4 activity. As predicted by these two *in vitro* models, the contributions of CYP3A5 to vincristine metabolism are on average between 80 to 90% for CYP3A5 high expressers. For other

published human liver microsome studies with CYP3A substrates, the estimated CYP3A5 contribution to metabolism was 30 to 40%.[71] Thus, vincristine is a unique, CYP3A5-selective substrate.

To provide additional evidence of CYP3A5 selectivity, the specific activities of CYP3A4 and CYP3A5 in M1 formation were calculated for human liver microsomes and compared to the cDNA-expressed enzyme activities (Fig. 31). The selectivity was similar for all the models regardless of cytochrome b_5 expression. The enzyme specific activities for the microsomes were somewhere between V_{max} values for the cDNA-expressed enzymes with supplemented cytochrome b_5 and co-expressed cytochrome b_5 (Table 1). However, the specific activities for the microsomes were calculated based on both holoprotein and apoprotein as determined by Western blot. Thus, the variability in heme incorporation lowered the specific activities of the enzymes. Correcting for the CYP3A heme incorporation (69%),[86] the CYP3A4 and CYP3A5 specific activities for the human liver microsomes are almost identical to the values of cDNA-expressed CYP3A4 and CYP3A5 with co-expressed cytochrome b_5 (3 and 19 pmol M1/min/pmol CYP versus and 3 and 22 pmol M1/min/pmol CYP). We conclude that the high contribution of CYP3A5 to the metabolism of vincristine (80 to 90%) *in vitro* is a result of a relatively high CYP3A5 specific activity.

C. Effect of CYP3A5 Expression on the Clearance of Vincristine

The role of CYP3A5 in the clearance of most CYP3A substrates is not well understood. To estimate the role of CYP3A5 expression in the clearance of vincristine, we used kinetic data from multiple *in vitro* models to complete *in vitro*/*in vivo* scaling. The predicted hepatic clearances were compared for CYP3A5 high and low expressers.

These values were then compared to published clearance values of adult patients treated with vincristine.

To estimate intrinsic clearances with human liver microsomes and hepatocytes, the *in vitro* V_{max}/K_m ratio was scaled by microsomal protein content and cell concentration as appropriate. For hepatocytes, the intrinsic clearance was estimated by M1 formation rates at one vincristine concentration below the K_m. The liver donors were categorized into high and low CYP3A5 expressers. For this study, CYP3A5 phenotype by Western blot was used to characterize the human liver microsomes; for the hepatocytes, *CYP3A5* genotype was used exclusively. CYP3A5 phenotyping is preferred to *CYP3A5* genotyping because the *CYP3A5*1* genotype-phenotype relationship is not absolute. The *CYP3A5* genotype was determined by elimination of three common gene SNPs; other less common SNPs may alter the expression of CYP3A5. In fact, *CYP3A5* genotype did not accurately predict CYP3A5 expression in 2 out of 12 human liver microsomes in this study. In addition, if more than one type of SNP is identified for one individual, the CYP3A5 expression cannot be predicted because the chromosomal locations of the two SNPs are unknown. Three African-American livers in our hepatocyte study fell in this category (Table 4).

To complete the *in vitro*/*in vivo* scaling for all *in vitro* models, the well-stirred model for hepatic clearance was utilized (Eqn. 5). This model was chosen because vincristine is a low to intermediate extraction ratio drug with unbound therapeutic concentrations well below the K_m. The model requires an estimation of the fraction unbound of drug in the plasma, whole blood, and microsomes. The fraction unbound in plasma (0.6) and the blood-to-plasma ratio (1.2) estimated in this study were in good

agreement with the previously published results (0.5 and 1.2 respectively).[11,47] Rapid equilibrium between plasma proteins and erythrocytes was assumed although it was reported that the binding of vincristine to platelets and blood cells is not quickly reversible.[139] The calculated clearance may be overestimated in this case because regardless of the intrinsic clearance, the hepatic clearance can never equal hepatic blood flow. However, this effect is likely minor because vincristine is a low to medium extraction ratio drug.

Based on previously published *in vitro/in vivo* scaling data, the intrinsic clearances estimated using human liver microsomes typically underpredict *in vivo* intrinsic clearances by 9-fold.[140] To compensate for the under-prediction, an empirical scaling factor is often used. However, for vincristine, the human liver microsome data of CYP3A5 low expressers accurately predicted the clearance from the pharmacokinetic studies in Caucasian populations. Using the human liver microsome model, the median hepatic clearances of CYP3A5 high expressers were 5-fold higher than low expressers with extraction ratios of 0.5 and 0.1 respectively (Fig. 32b). These values were in good agreement with the adult literature for hepatic clearance of vincristine (50 to 300 mL/min, 0.03 to 0.2 equivalent extraction ratios).[44,52] However, the clearances estimated in the clinical studies may have been underestimated because the vincristine plasma assays were not selective for the parent drug.[52]

Compared to the human liver microsome kinetic data, the human hepatocyte data predicted a much lower *in vivo* clearance for vincristine. Based on the rates of M1 formation for the most active hepatocyte lot, the extraction ratio was only 0.04. Thus, after correcting for binding, the intrinsic clearances predicted by hepatocytes were well

below hepatic blood flow and effectively equal to the hepatic clearances. For the CYP3A5 low expressers, the predicted intrinsic clearances were zero because vincristine metabolism was not observed. To verify the cells from CYP3A5 low expressers were capable of M1 formation, the rates of M1 formation for one lot (MRS) were estimated using a hepatocyte lysate preparation supplemented with NADPH. The rates of M1 metabolism were typical of CYP3A5 low expressing human liver microsomes.

The estimated hepatic clearances using human hepatocytes are inconsistent with the reported clearance of vincristine for adults and approximately 10-fold lower than the predicted values from human liver microsomes. Like with human liver microsomes, other investigators have reported a 5-fold systemic underprediction of *in vivo* intrinsic clearance using cryopreserved hepatocytes.[141] Although an underprediction of *in vivo* clearances was expected using human hepatocytes, the hepatocyte kinetic data were expected to more closely match the human liver microsome data. In particular, the CYP3A5 low expressers with high CYP3A4 activity (lot MRS) were predicted to have intrinsic clearances similar to those of typical CYP3A5 high expressers. The published studies that have compared the predicted clearances of hepatocytes and microsomes are conflicting and confounded by the variability of the preparations. For example, one study reported that the midazolam intrinsic clearance estimated with human liver microsomes was 5-fold higher compared to the hepatocyte estimated value. However, like all these type of studies, the lots of cryopreserved hepatocytes and the microsomes were not from the same liver, and the numbers of different lots tested were small (n = 3 to 7). In another study, when compared to human liver microsomes, the cryopreserved hepatocytes predicted at least a 3-fold higher intrinsic clearance for midazolam. Again

the variability between lots may in part explain the discrepancy between the reports. We designed our experiments to remove this variable by preparing cell lysates from the same lots of hepatocytes. For the various lots of cryopreserved hepatocytes, the intrinsic clearances of CYP3A5 high expressers were 4 to 69-fold lower than those predicted using paired cell lysate preparations (Table 4). From this data, we concluded that hepatic clearance with cryopreserved hepatocytes may be a function of intrinsic clearance and hepatic transport.

The uptake of vincristine by hepatocytes is primarily diffusion rate limited while the export is mediated by active transporters in the canalicular membrane, specifically P-pg and MRP2.[10,12,49] To understand the potential role of active transport in our hepatocyte study, we coincubated vincristine with transporter inhibitors: cyclosporin A (P-gp and MRP2) and LSN335984 (P-gp). The rates of M1 formation were unaffected or slightly reduced by the inhibitors, perhaps as a result of CYP3A inhibition (Table 5). Thus, assuming the transporter function of hepatocytes is representative of *in vivo* transport, active transport in hepatocytes may not be an important determinant of the vincristine intracellular concentration.

To demonstrate the rates of M1 formation were influenced by vincristine transport, the Michaelis-Menten kinetic parameters of M1 formation were estimated for one lot of hepatocytes (EHI); both intact cells and cell lysate preparations with NADPH were incubated with vincristine (Fig. 40). The K_m value for the intact cells was 3-fold higher than that of the cell lysate. Therefore, at least for this lot of hepatocytes, membrane transport was possibly responsible for approximately 50% of the reduced intrinsic clearance. The 3-fold change in V_{max} values accounted for the remaining 50%

reduction. This result was unexpected because the V_{max} values can only change if the CYP activity is reduced. At this time, we have no explanation for why the CYP activity with vincristine would be lower for intact hepatocytes versus the cell lysate preparation from the same lot. Additional studies will be required to understand this effect.

Assuming the hepatocyte model is representative of the *in vivo* cells, one possibility is that drug metabolism and consequently *CYP3A5* genotype play a minor role in the overall clearance of vincristine. Case reports of drug/drug interactions with vincristine and itraconazole are consistent with CYP3A and/or P-gp inhibition.[35] Perhaps almost all the vincristine is concentrated in the bile by active transport and eliminated unchanged. For example, the clearance of fexofenadine is primarily biliary and controlled by OATP drug uptake transporters and P-gp. Reported drug/drug interactions with fexofenadine and ketoconazole can be only be explained by inhibition of transport, not CYP3A inhibition, because 95% of fexofenadine is eliminated unchanged in the bile or urine. Vincristine and/or vincristine-related compounds are also concentrated in the bile (at least 20-fold higher than the plasma) presumbly by P-pg and MRP2. However, the percentage of vincristine unchanged in the feces was reported to be less than 60%, not 95% like fexofenadine.[11] As discussed earlier, the actual percentage of the vincristine dose excreted unchanged may be higher (because of parent degradation during the *in vitro* assay) or lower than 60% (because the parent drug and metabolites may have co-eluted by HPLC). Also, for any value not close to 100% like fexofenadine, more information about the product composition would be required to separate the roles of degradation, biliary excretion, and metabolism. Because the therapeutic concentration is low for vincristine, the biological samples, particularly fecal

material, would be difficult to analyze and complete a material balance without a radiolabel. Even with a radiolabel, the degradation products of vincristine and M1 would be difficult to distinguish from one another because M1 degrades in plasma to multiple compounds of unknown composition.

Although transport may play a role in the clearance of vincristine, hepatic metabolism by CYP3A enzymes may also be clinically significant. The clearances of certain drugs, such as midazolam, are almost entirely mediated by CYP3A enzymes.[96] The role of CYP3A enzymes is evident *in vivo* by clearance changes with co-administration of chemical inhibitors (itraconazole) and inducers (rifampin).[93] The clearance changes of midazolam can be attributed to CYP3A inhibition or induction because midazolam is not a ligand of any known transporters.[36] In contrast, because vincristine and other CYP3A substrates such as docetaxel are substrates of P-gp, *in vivo* chemical inhibition and inducer studies are more difficult to interpret. For example, the docetaxel clearance *in vivo* was reduced only 1.7-fold versus 6-fold for midazolam with the same dose of ketoconazole.[142] This result may possibly indicate that CYP3A enzymes are not clinically important in the disposition of docetaxel. However, in clinical study using the selective P-pg inhibitor R101933, the docetaxel clearance was also not significantly affected.[143] As an added complication, the inter-individual variability in CYP expression may change the relative contribution of biliary excretion and metabolism. For example, the clearance of vincristine for individuals with high CYP3A5 expression may be primarily CYP3A5-mediated while the clearance for individuals with low CYP3A5 expression may be primarily biliary.

The most direct way to understand the role of CYP3A5 metabolism in vincristine clearance is to compare vincristine exposure of high and low CYP3A5 expressers *in vivo*. A clinical study with pharmacokinetic vincristine data can also be used to recommend dose adjustments for individualized therapy. Historically, estimation of exposure in vincristine patients has been technically challenging because the concentrations in plasma are low. In addition, because the terminal half life of vincristine is approximately 24 h, plasma samples over several days are required to accurately assess the exposure by AUC. In our study, a vincristine assay using LC/MS/MS was developed that could accurately quantify vincristine in plasma at concentrations at least 3 terminal half lives past the initial dose. At the time of this report, estimations of vincristine exposure by this method were limited to four patients with low CYP3A5 expression over 24 h (Fig. 50). Additional patients with high CYP3A5 expression and longer sampling time points are required to determine whether high CYP3A5 expression reduces exposure to vincristine. Patient recruitment for these prospective studies is in progress. The results of these studies will hopefully provide a definitive answer to whether *CYP3A5* genotype is clinically significant in vincristine therapy.

D. Conclusions

Using cDNA-expressed enzymes and human liver microsomes, vincristine is metabolized by cytochrome P450 enzymes CYP3A4 and CYP3A5 to one primary metabolite, M1; this secondary amine readily degrades in basic solutions and in plasma. *In vitro*, cDNA-expressed CYP3A5 selectively metabolizes vincristine to M1. The rates of M1 formation are at least 7-fold higher with CYP3A5 than CYP3A4. For CYP3A5

high expressing microsomes, the CYP3A5 contribution to M1 formation is substantial, approximately 81% of the total CYP activity. With cryopreserved hepatocytes, the rates of M1 formation are much lower than those of human liver microsomes. The M1 rates of formation may be limited by vincristine transport. Further studies are required to understand why CYP3A5 low expressing hepatocytes do not metabolize vincristine. *In vivo*, M1 is likely a product of vincristine because the plasma concentration of M1 parallels that of vincristine during the terminal elimination phase. Although the role of metabolism in the systemic clearance of vincristine is presently unknown, CYP3A5 expression is predicted to increase metabolic hepatic clearance at least 5-fold. Thus, for vincristine chemotherapy, CYP3A5 expression as predicted by *CYP3A5* genotype may be an important determinant of inter-individual variability in clinical outcomes. Further *in vivo* studies are required to understand the impact of CYP3A5 expression on vincristine pharmacokinetics.

Table 1. Michaelis-Menten parameters for M1 formation with CYP3A4 and CYP3A5

V_{max} units = pmol M1/pmol CYP/min, K_m units = μM, fitted values ± 1 standard deviation, CL_{int} = V_{max} /K_m

	No cytochrome b_5			Supplemented cytochrome b_5 (3:1 ratio)			Co-expressed cytochrome b_5		
	CYP3A4	CYP3A5	*p*-value	CYP3A4	CYP3A5	*p*-value	CYP3A4	CYP3A5	*p*-value
V_{max}	0.90 ± 0.06	8.1 ± 0.4	<0.0001	1.49 ± 0.07	11.0 ± 1.0	<0.0001	2.97 ± 0.17	21.5 ± 0.9	<0.0001
K_m	19.7 ± 3.0	14.3 ± 1.7	0.14	25.7 ± 2.6	13.3 ± 3.2	0.009	19.9 ± 2.5	16.7 ± 1.6	0.30
CL_{int}	0.046 ± 0.004	0.57 ± 0.04	<0.0001	0.058 ± 0.003	0.83 ± 0.13	<0.0001	0.15 ± 0.01	1.29 ± 0.08	<0.0001

Table 2. Characterization of human liver microsomes by CYP3A5 genotype, CYP3A4 and CYP3A5 protein content, and V_{max} with vincristine (VCR), testosterone (TST), and itraconazole (ITZ) as substrates. Metabolites for V_{max} are in parentheses.

		Protein Content (pmol/mg)		V_{max} (pmol/min/mg)			VCR *in vitro*/*in vivo* scaling		
Liver	*CYP3A5* genotype	3A4	3A5	ITZ (OH-ITZ)	TST (6β-OH)	VCR (M1)	K_m [a] (μM)	CL_{int} [b] (mL/min)	CL_H [c] (mL/min)
CYP3A5 high expressers									
IUL-40	** 1 / * 1*	103.8	89.4	121.3	7244	1262	14.0	6070	823
IUL-32	** 1 / * 3*	20.9	18.2	18.1	1021	172	18.2	636	169
IUL-41	** 1 / * 3*	14.7	20.5	52.5	2886	467	26.2	1200	291
IUL-42	** 1 / * 3*	23.7	16.1	26.4	1518	302	25.1	813	210
IUL-59	** 1 / * 3*	36.3	14.7	51.6	3274	302	14.6	1400	328
IUL-66	** 1 / * 3*	24.4	20.6	32.7	2223	327	17.0	1300	310
IUL-73	** 1 / * 3*	96.1	20.1	147.0	6564	521	15.9	2220	461
IUL-74	** 1 / * 6*	10.7	26.2	13.5	1958	470	16.1	1970	424
IUL-79	** 1 / * 3*	11.2	13.6	15.4	1291	201	17.0	803	208
IUL-85	** 1 / * 3*	85.5	24.8	39.4	4013	393	20.7	1280	305
CYP3A5 low expressers[d]									
IUL-6	** 3 / * 3*	19.0	0.8	33.8	3082	80.3	22.2	244	69.7
IUL-49	** 3 / * 3*	48.8	0.8	52.3	2511	68.3	23.8	193	55.9
IUL-52	** 3 / * 3*	14.8	0.0	8.4	1337	8.8	11.4	52.0	15.5
IUL-55	** 3 / * 3*	130.4	0.8	136.2	7260	245	29.8	555	150
IUL-57	** 1 / * 3*	40.6	0.8	41.1	3947	104	31.2	225	64.5
IUL-65	** 3 / * 3*	15.6	0.6	14.7	1139	18.3	10.7	115	33.8
IUL-71	** 1 / * 7*	10.9	1.1	41.9	2950	49.9	15.8	213	61.3
IUL-72	** 3 / * 3*	25.3	0.9	27.1	2100	40.1	20.6	132	38.4
IUL-75	** 3 / * 3*	78.2	2.3	108.2	4938	140	15.6	609	163
IUL-78	** 3 / * 3*	109.5	3.1	148.7	6993	198	19.2	695	183
IUL-81	** 3 / * 3*	71.7	2.0	65.2	3424	132	22.5	395	110
IUL-86	** 3 / * 3*	77.8	2.1	160.0	8851	288	23.0	844	217

[a] Corrected for microsomal binding to vincristine.
[b] Intrinsic clearance = $CL_{int} = V_{max} \cdot 1500$ g liver $\cdot$ 45 mg microsomal protein/ g liver/ K_m for a 70 kg man
[c] Hepatic clearance = $CL_H = Q \cdot f_{u,p} / \rho \cdot CL_{int} / (Q + f_{u,p} / \rho \cdot CL_{int})$ where $f_{u,p} = 0.51$, $\rho = 1.2$, and $Q = 1500$ ml/min for a 70 kg man
[d] HLMs not selected randomly.

Table 3. Percent contribution of CYP3A5 to vincristine metabolism for CYP3A5 high expressers. Using values from the CYP3A5 low expressers as standards, the CYP3A4 contribution for each CYP3A5 high expresser was calculated from the CYP3A4 content, testosterone 6β-hydroxylase activity, and itraconazole hydroxylase activity. Metabolites are in parentheses. The remaining CYP3A5 activity was quantified after selective inhibition of CYP3A4 with cyclosporin A.

	% contribution by CYP3A5 to M1 formation			
Liver	Protein content	TST (6β-OH)	ITZ (OH-ITZ)	CsA[a]
IUL-40	83	86	84	ND
IUL-32	75	87	83	ND
IUL-41	93	80	82	ND
IUL-42	84	84	86	ND
IUL-59	75	75	72	71
IUL-66	85	84	84	ND
IUL-73	62	57	54	46
IUL-74	95	92	95	ND
IUL-79	88	83	88	79
IUL-85	55	81	84	ND
Avg ± SD	80 ± 13	81 ± 11	81 ± 10	NA

[a] ND = not determined, NA = not applicable

Table 4. Characterization of cryopreserved hepatocytes by *CYP3A5* genotype and CYP3A activity. Multiple lots of hepatocytes were genotyped for CYP3A5 expression and assayed for CYP3A activity using testosterone and vincristine as probe substrates. For each lot of hepatocytes, the intrinsic clearances of vincristine were estimated with intact cells and NADPH-supplemented cell lysate; the rates of M1 formation or the rates of vincristine depletion were used to estimate the intrinsic clearances.

			Testosterone 6β-Hydroxylase Activity (pmol/min/mg)[a]		*VCR Intrinsic Clearance* (mL/min)[a]			
Lot	Ethnicity[b]	*CYP3A5* genotype	Cells[b]	Lysate	Cells[c]		Lysate	
CYP3A5 high expressers					Formation	Depletion	Formation	Depletion
AIT	C	** 1 / *3*	246	4300	59	140	1755	1755
EHI	AA	** 1 / * 1*	744	3300	173	270	1620	1913
FKM	AA	** 1 / *7*	522	8700	59	133	4050	4500
REL	AA	** 3 / *6*[d]	300	4700	41	97	563	1035
RML	AA	** 1 / *1*	456	10500	88	108	608	608
SCA	AA	** 1 / *3*[e]	564	25500	86	180	5625	6525
ZIJ	AA	** 1 / *1*	75	2200	95	72	968	1260
ZYZ	AA	** 1 / *1*[e]	297	260	106	108	405	473
CYP3A5 low expressers								
652	U	**3 / *3*	U	ND	0	0	ND	ND
CHD	AA	** 3 / * 7*[d]	84	ND	0	0	ND	ND
Hu418	U	**3 / *3*	U	ND	0	0	ND	ND
MRS	AA	** 3 / * 7*[d]	2025	4300	0	0	293	855
SD012	U	ND	U	ND	0	0	ND	ND
SD017	U	ND	U	ND	0	0	ND	ND

ND = not determined, U = unknown

[a] CL_{int} = Initial rate of reaction / substrate concentration x (45 mg protein / g liver) x (3 x 10^6 cells/ mg protein) x 1500 g liver for a 70 kg man

[b] Reported by vendor, In Vitro Technologies. AA = African-American, C = Caucasian. Other vendors (Xenotech for 652, Cellzdirect for others) did not provide ethnicity information.

[c] Values reported as zero are not different from the sonicated cell controls.

[d] Genotype data alone cannot predict the CYP3A5 phenotype.

[e] Not genotyped for *CYP3A5*6*.

Table 5. Effects of chemical inhibition on M1 formation with cryopreserved hepatocytes.
VCR and multiple lots of cryopreserved hepatocytes were incubated with and without chemical inhibitors (cyclosporine A, LSN335984, and ketoconazole) for 4 h. The final concentration of M1 with inhibitor was expressed as a percentage of the control without inhibitor.

	% of positive control at 4 h		
Lot	CsA	LSN	KTZ
CYP3A5 high expressers			
AIT	127	72	18
EHI	95	66	17
FKM	125	48	18
REL	105	42	17
RML	106	38	12
SCA	148	77	38
ZIJ	99	49	11
ZYZ	68	45	8
CYP3A5 low expressers			
CHD	108	81	93
MRS	99	92	71

CsA = 25 μM cyclosporin A; LSN = 50 μM LSN335984; KTZ = 10 μM ketoconazole

Table 6. Relative recoveries of vincristine, vinblastine, and vinorelbine from plasma.
VCR, VLB, and VRL were extracted with methylene chloride (4 vol). The signal intensities of the analytes were quantified by LC/MS. The effects on recoveries were determined for acid addition (TCAA) and mechanical agitation. The controls were not extracted.

	VCR and VLB Extraction		VCR and VRL Extraction	
	VCR Intensity	VLB Intensity	VCR Intensity	VRL Intensity
Control	3.5×10^6	12×10^6	3.0×10^6	17×10^6
+ shake	0.75×10^6	0.5×10^6	1.1×10^6	$< 0.1 \times 10^6$
+ acid	1.5×10^6	5.5×10^6	2.4×10^6	0.5×10^6
+ shake, + acid	2.2×10^6	8.0×10^6	3.0×10^6	2.2×10^6

Table 7. MS parameters for multiple-reaction monitoring of M1, vincristine (VCR), and vinblastine (VLB) dicharge ions.

	M1		VCR		VLB
Q1 → Q3 (*m/z*)	397.3 → 337.3	397.3 → 376.2	413.2 → 362.2	413.2 → 392.1	406.3 → 271.7
Declustering potential (V)	65	65	65	65	60
Entrance potential (V)	10	10	10	10	8
Collision energy (V)	30	20	30	20	40
Exit potential (V)	12	12	10	10	10
Dwell time (ms)	100	400	400	100	100

Table 8. Extraction efficiency for vincristine and M1 in human plasma.

	Low	Medium	High
Vincristine			
Nominal concentration (ng/mL)	0.120	0.792	24.0
VCR/IS area ratio not extracted[a] (*a*)	0.017 (0.002)	0.11 (0.00)	3.07 (0.10)
VCR/IS area ratio extracted (*b*)	0.010 (0.001)	0.069 (0.001)	1.92 (0.05)
Recovery (%)[b]	61	64	62
M1			
Nominal concentration (ng/mL)	0.0610	0.402	12.2
VCR/IS area ratio not extracted[a] (*a*)	0.0039 (0.0004)	0.022 (0.001)	0.70 (0.02)
VCR/IS area ratio extracted (*b*)	0.0022 (0.0008)	0.013 (0.001)	0.40 (0.03)
Recovery (%)[b]	56	61	57

[a] Vincristine and M1 in mobile phase A added after extraction and evaporation of methylene chloride. $n = 3$ except for the low extracted samples where $n = 2$; numbers in parentheses are standard deviations or the range for the low extracted samples.
[b] Recovery is defined as (b/a) x 100%.

Table 9. Limits of detection and quantification for vincristine and M1 for the current method and a comparison of vincristine limits from previously published methods.

	Current method		Schmidt *et al.*[126]	Skolnik *et al.*[135]
Method	LC/ESI-MS/MS		LC/ESI-MS	LC/ESI-MS/MS
Analyte	M1	VCR	VCR	VCR
mLOD (pg)	0.7	0.8	17	6
mLOQ (pg)	1.4	1.5	33	15
cLOD (pg/mL)	6	6	90	200
cLOQ (pg/mL)	12	12	180	500

mLOD; mass limit of detection, mLOQ; mass limit of quantification, cLOD; concentration limit of detection, cLOQ; concentration limit of quantification

Table 10. Intra-day (n = 5) and inter-day (n = 4) precision and accuracy for vincristine and M1 in human plasma.

	Intra-day			Inter-day		
	Low	Medium	High	Low	Medium	High
Vincristine						
Nominal concentration (ng/mL)	0.0120	0.792	24.0	0.0468	0.924	18.6
CV (%)	16.8	4.9	5.0	13.8	8.8	11.9
Accuracy (%)	105.6	105.0	103.2	96.8	95.6	87.4
M1						
Nominal concentration (ng/mL)	0.0122	0.402	12.2	0.0234	0.462	9.30
CV (%)	12.9	12.3	2.2	16.3	6.5	14.8
Accuracy (%)	109.1	106.0	111.9	92.7	87.5	85.3

Table 11. Pharmacokinetic parameter estimates for patients (n = 4) treated with vincristine (1.5 mg/m^2). The vincristine kinetic parameters were estimated for all 4 patients. The data from two patients (patient 1 and patient 2) are presented with the percent coefficient of variation values (% CV) for the model fit. The mean for all patients is presented with the standard deviation (SD), the interpatient variability. The data were modeled using a two-compartment model with $1/y^2$ weighting.

Parameter	Patient 1 (% CV)	Patient 2 (% CV)	Mean (SD) n = 4	Minimum	Maximum
Cl_p (ml/min/m^2)	778 (23)	389 (35)	490.8 (195.0)	354	778
$t_{1/2\alpha}$ (min)	25.2 (17)	24.0 (14)	18.6 (7.0)	11.3	25.2
$t_{1/2\beta}$ (min)	1368 (36)	2719 (46)	1643 (733)	1070	2719
V_C (L/m^2)	170 (20)	138 (17)	114 (49)	65	170
V_2 (L/m^2)	1142 (20)	1249 (17)	891 (376)	439	1249

Cl_p; plasma clearance, $t_{1/2\alpha}$; first compartment half life, $t_{1/2\beta}$; second compartment half life, V_C; central volume of distribution, V_2; second compartment volume of distributio

Dihydro-hydroxycatharanthine

(DHC)

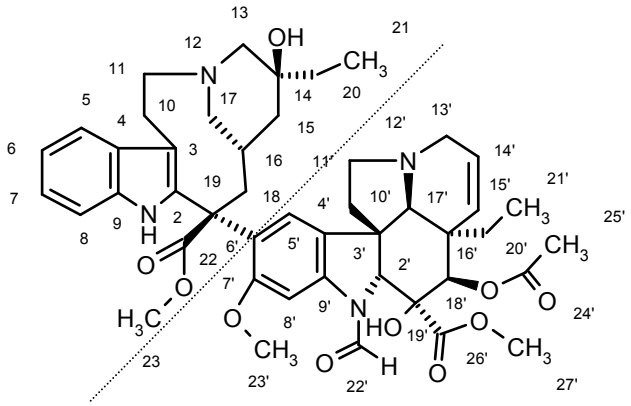

Vincristine

***N*-Formylvindoline**

(NFV)

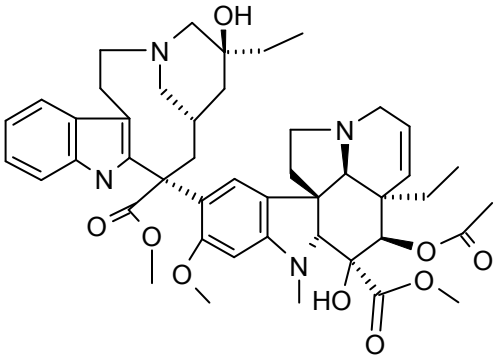

Vinblastine

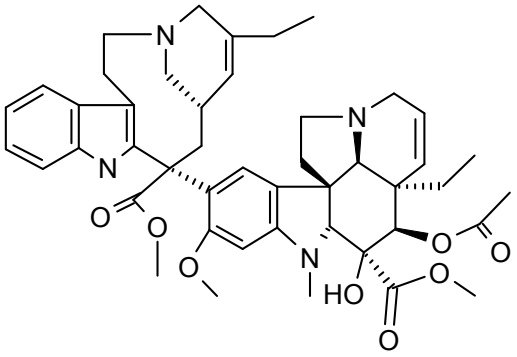

Vinorelbine

Fig. 1. Chemical structures of vincristine, vinblastine, and vinorelbine. The two segments of vincristine (DHC and NFV) are separated by a dotted line.

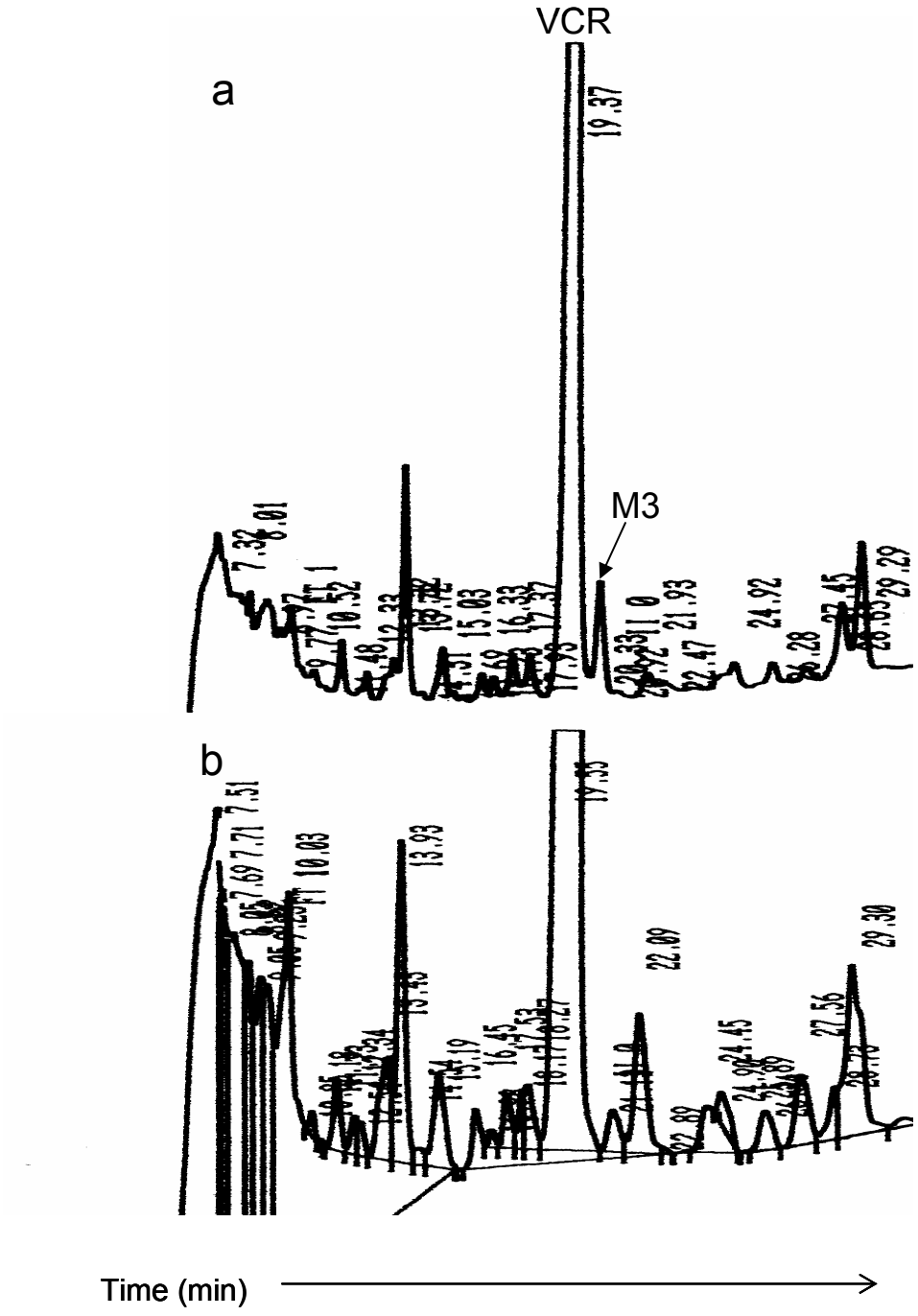

Fig. 2. Representative UV chromatograms of vincristine and its metabolites using a basic extraction and neutral pH chromatography. Vincristine (5 μM) was incubated for 5 min with rCYP3A5 (50 pmol/mL) and NADPH (1 mM) at 37°C (a) or without enzyme and NADPH (b). The solution was quenched with ethyl acetate and extracted using NaOH and additional ethyl acetate. Internal standard was not added. A putative metabolite M3, not in the control sample, was detected by UV absorbance approximately 1 min after the parent drug (VCR). Note that the attenuation of plot (b) is 2-fold less than that of (a).

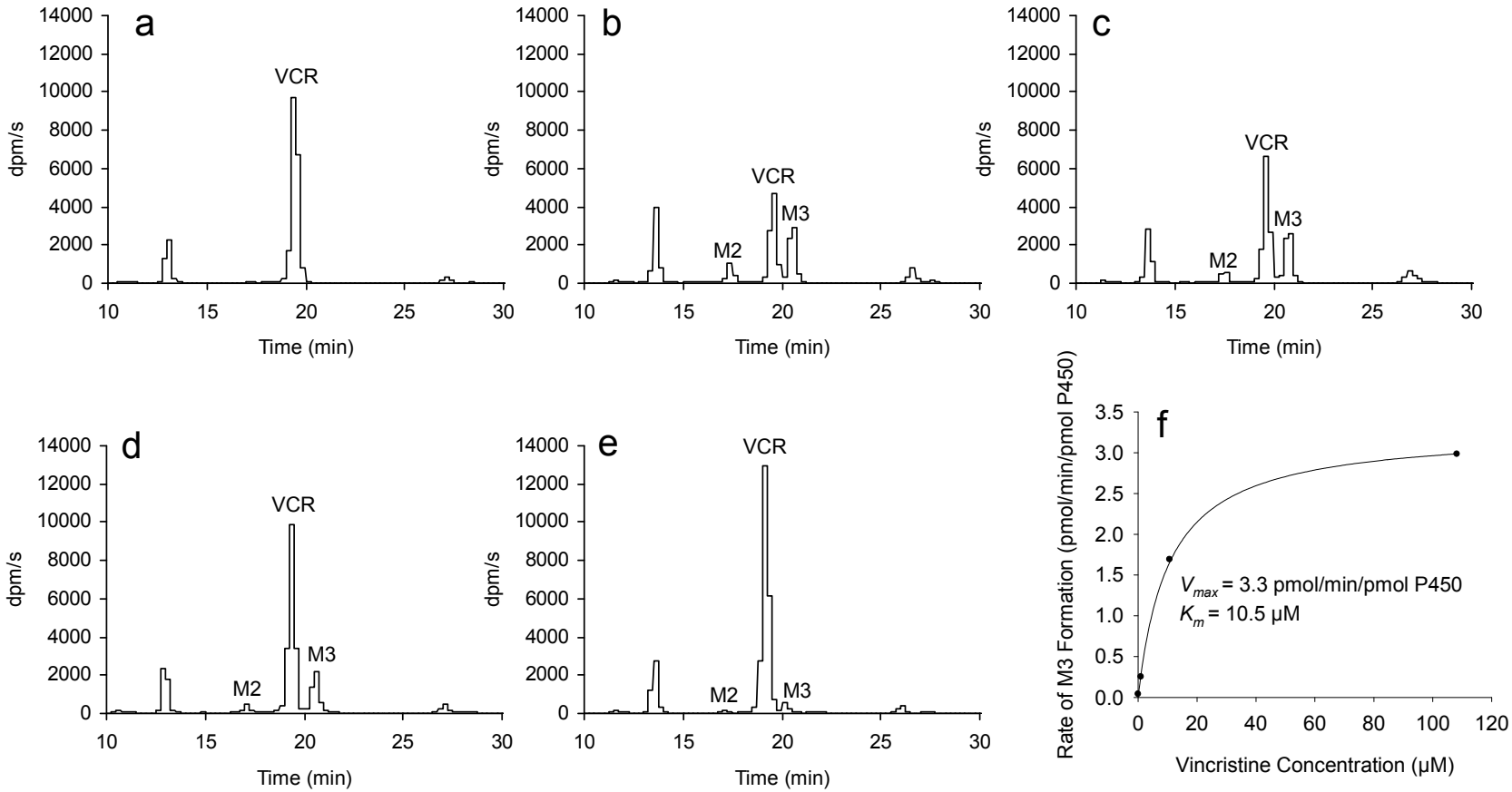

Fig. 3. Radiochromatograms of M2 and M3 formation from vincristine with rCYP3A5. The vincristine control without addition of NADPH is shown in panel (a). Different concentrations of 3H-vincristine at 0.1 (b), 1.0 (c), 10 (d), and 100 μM (e) were incubated with rCYP3A5 (50 pmol/mL) for 30 min with NADPH (1 μM). From the areas of the radiochromatograms, the rates of M3 formation at initial velocity conditions were estimated assuming non-saturable first-order kinetics for the two lowest concentrations where the parent drug was depleted more than 20%. The Michaelis-Menten kinetic parameters of M3 formation were estimated using non-linear regression (f).

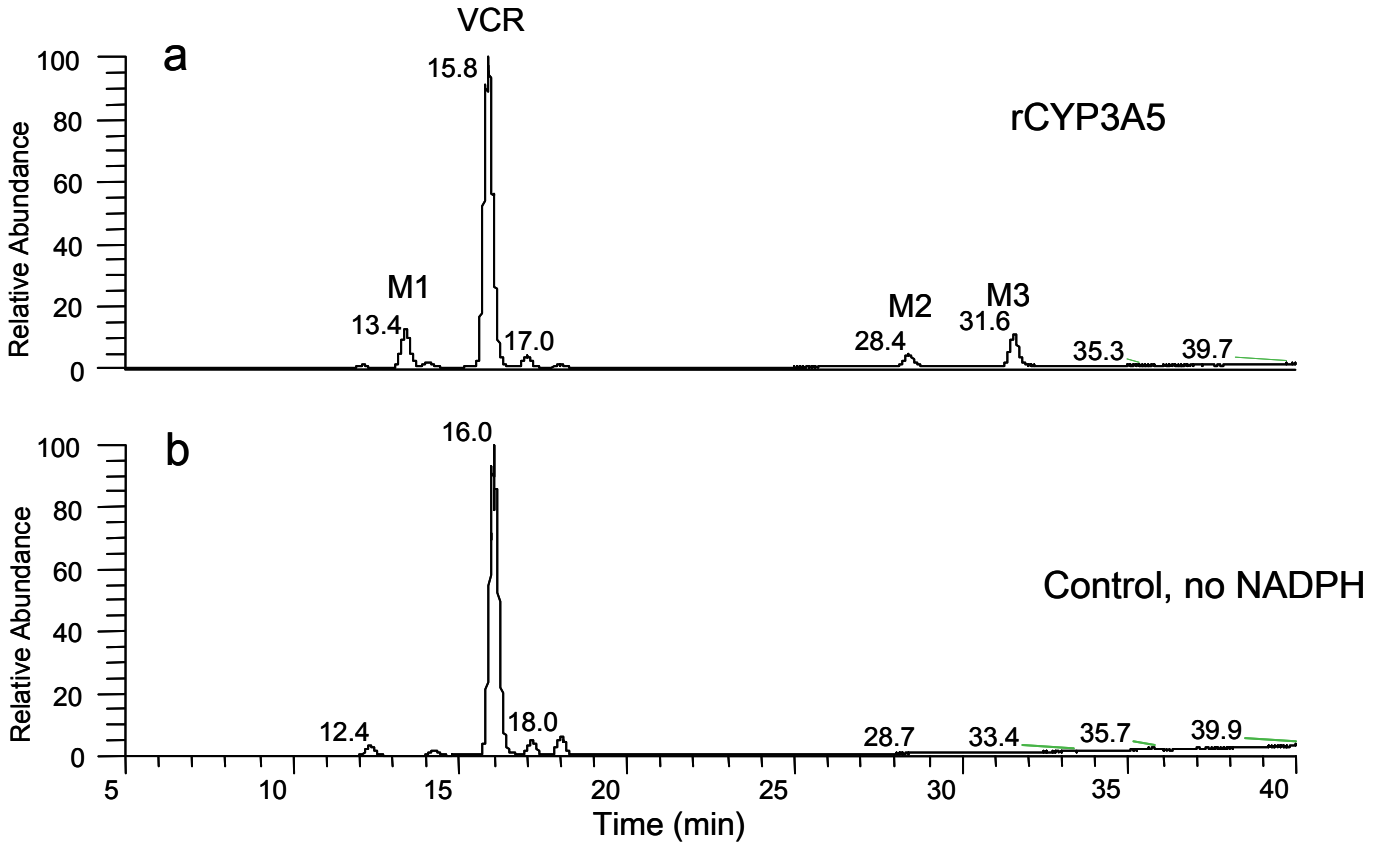

Fig. 4. Total ion chromatographs of vincristine incubated with rCYP3A5 with (a) and without NADPH (b). The sample preparation included NaOH treatment and ethyl acetate extraction. Three compounds (M1, M2, and M3) not present in the control were detected in the NADPH positive sample.

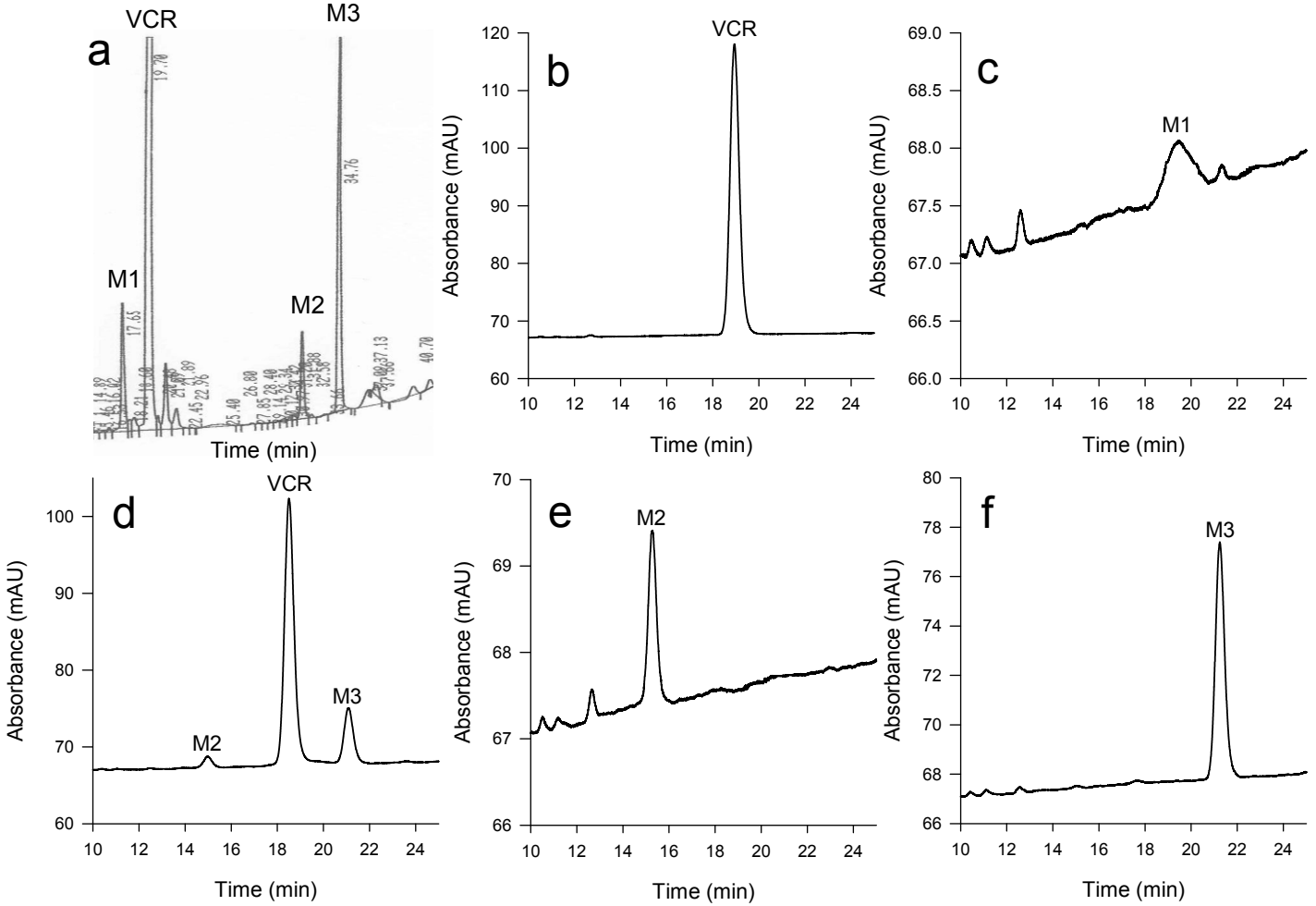

Fig. 5. Identification of metabolites using alternate chromatography systems. Vincristine (20 μM) was incubated with rCYP3A5 (50 pmol/mL) for 30 min and then extracted with ethyl acetate and NaOH. The sample was split in two and assayed by HPLC using an acidic pH eluent (a) and using a neutral pH eluent (d). The product peaks were collected from the acidic HPLC system (a) and reassayed by HPLC using the neutral pH system to determine the corresponding retention times of vincristine (b), M1 (c), M2 (e), and M3 (f).

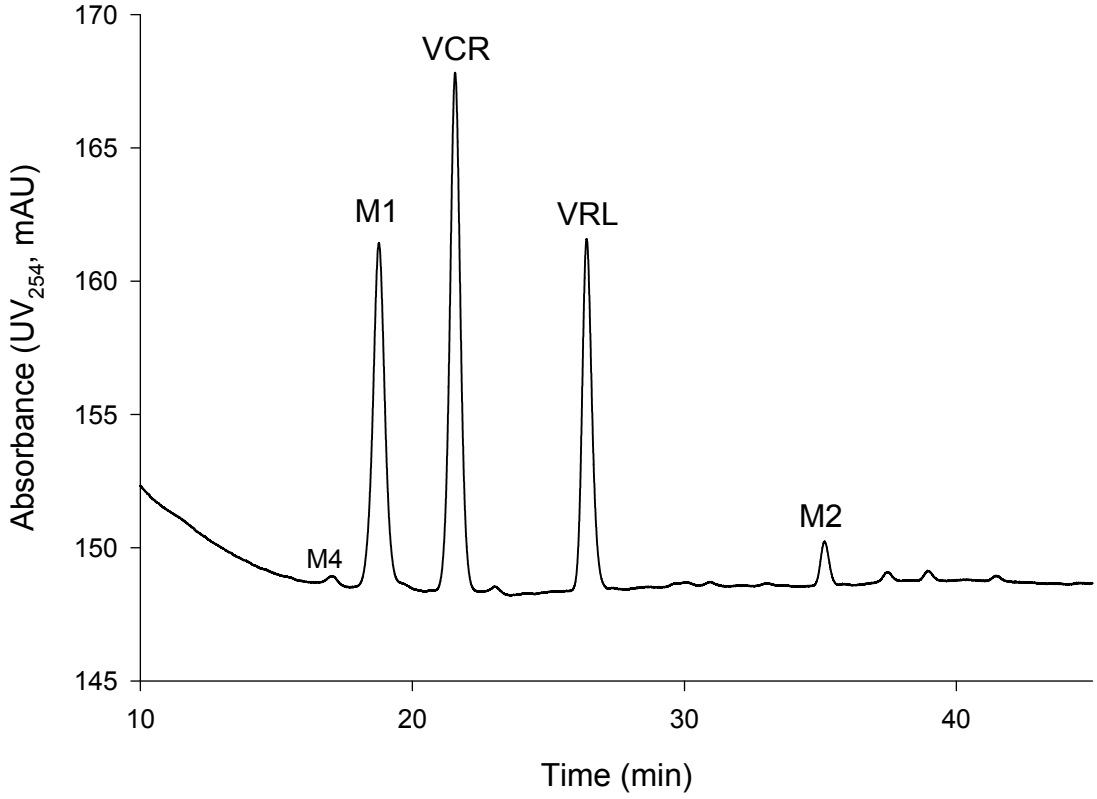

Fig. 6. Representative UV chromatogram of CYP3A5-mediated metabolism of vincristine using an acidic pH eluent. Vincristine (20 μM) was incubated for 30 min with rCYP3A5 (50 pmol/mL) and NADPH (0.5 μM) at 37°C. The solution was quenched with acetonitrile and diluted with an equal volume of 0.2% formic acid prior to analysis by HPLC. The vincristine metabolites are labeled as follows: M1 (major), M2 (minor), and M4 (minor). Vinorelbine (VRL) was used as an internal standard.

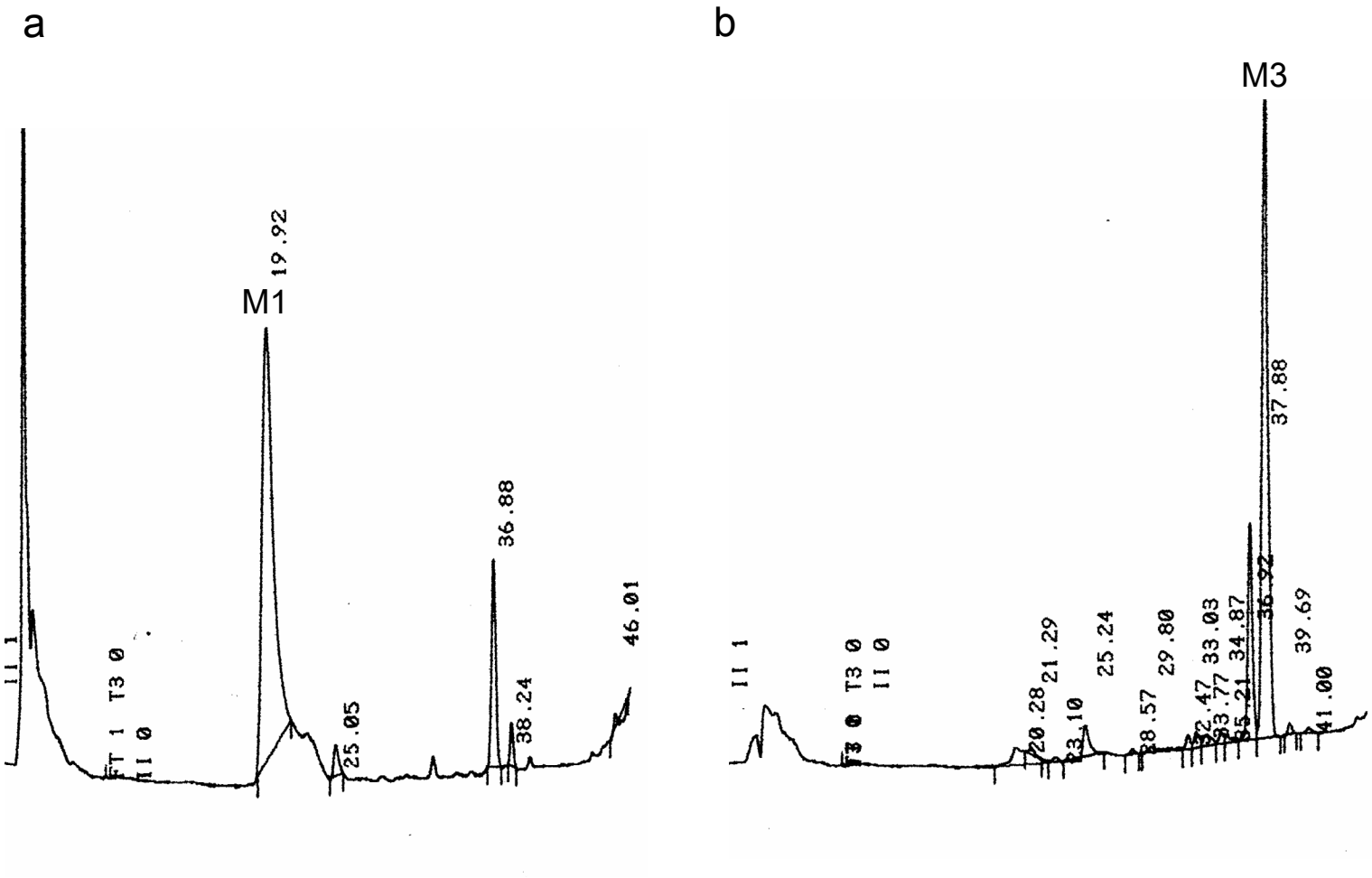

Fig. 7. Base-promoted conversion of M1 to M3. Eluent fractions containing HPLC purified M1 were split into two parts. One part was evaporated at room temperature and analyzed directly by HPLC, plot (a). For the second part, sodium hydroxide was added to complete the conversion of M1 to M3. The solution was extracted with ethyl acetate, and the organic extract was evaporated. The residue was assayed by HPLC, plot (b).

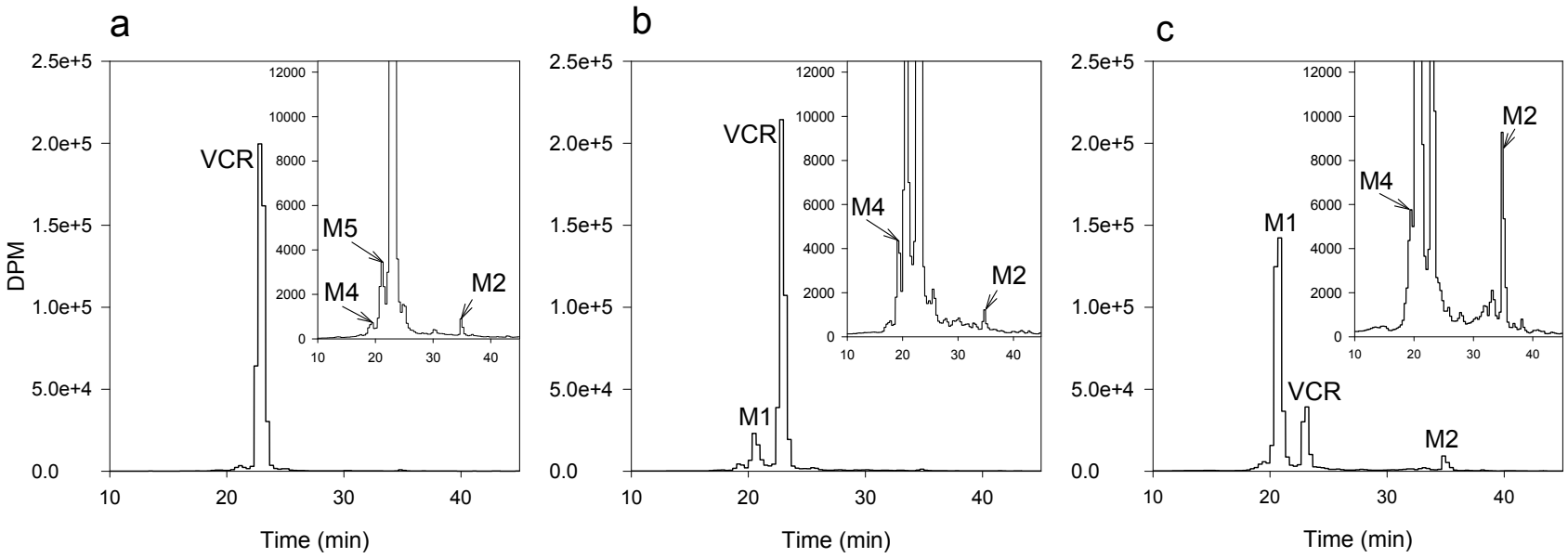

Fig. 8. Radiochromatograms of vincristine incubated with cDNA-expressed CYP3A4 and CYP3A5. ^{3}H-vincristine (10 µM) was incubated for 15 min with insect control microsomes, matched to CYP3A5 protein content (a), cDNA-expressed CYP3A4 with co-expressed b_5, 50 pmol/ml (b) and CYP3A5 with co-expressed b_5, 100 pmol/ml (c). At least 95% of the radioactivity is represented from 10 to 45 min, and no distinctive peaks different than the control are present outside of this time range. All dpm values are normalized to total radioactivity recovered.

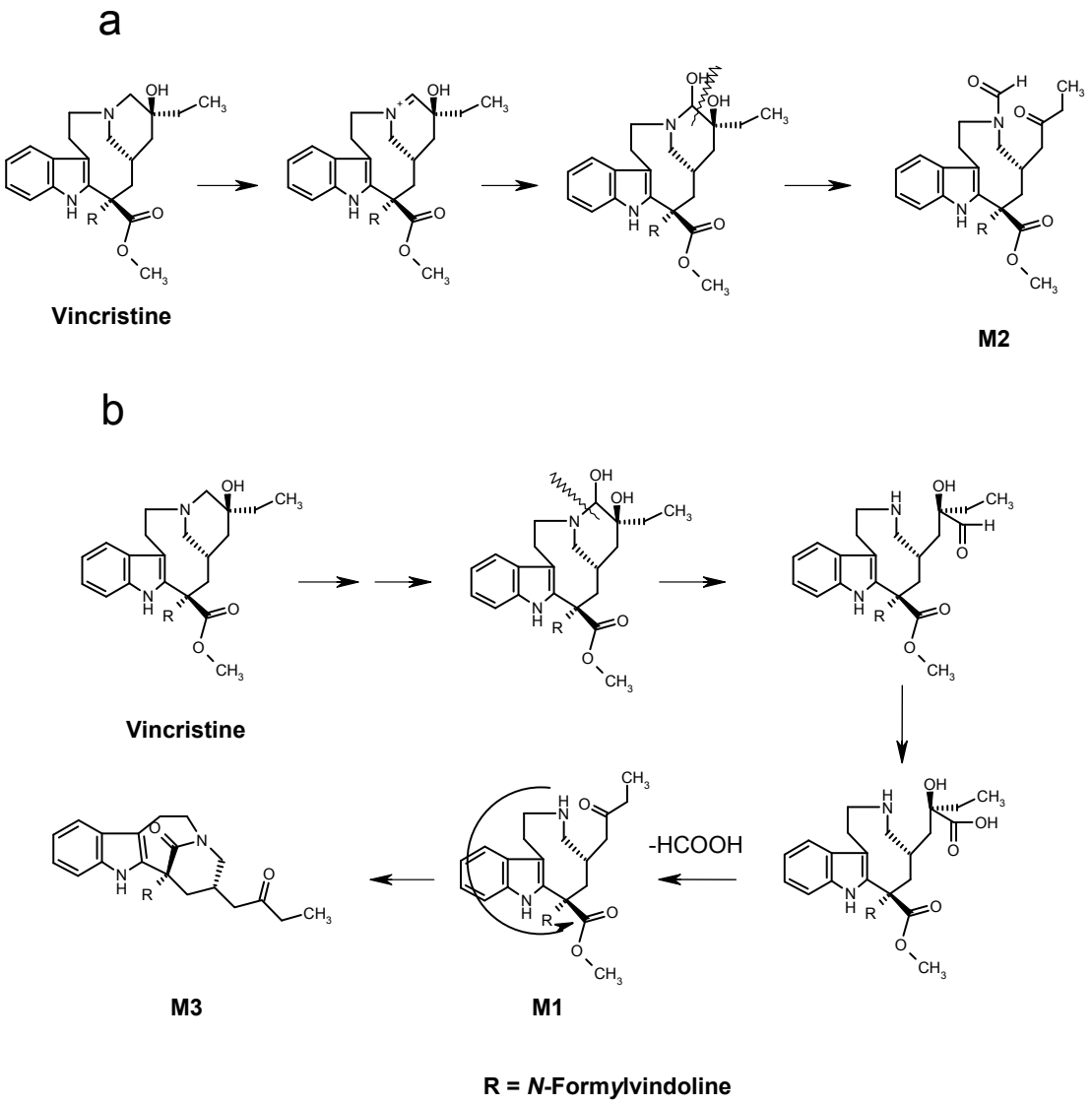

Fig. 9. Proposed biotransformation pathways of vincristine catalyzed by CYP3A4 and CYP3A5. (a) formation of M2; (b) formation of M1 and M3. Structures not labeled are putative intermediates.

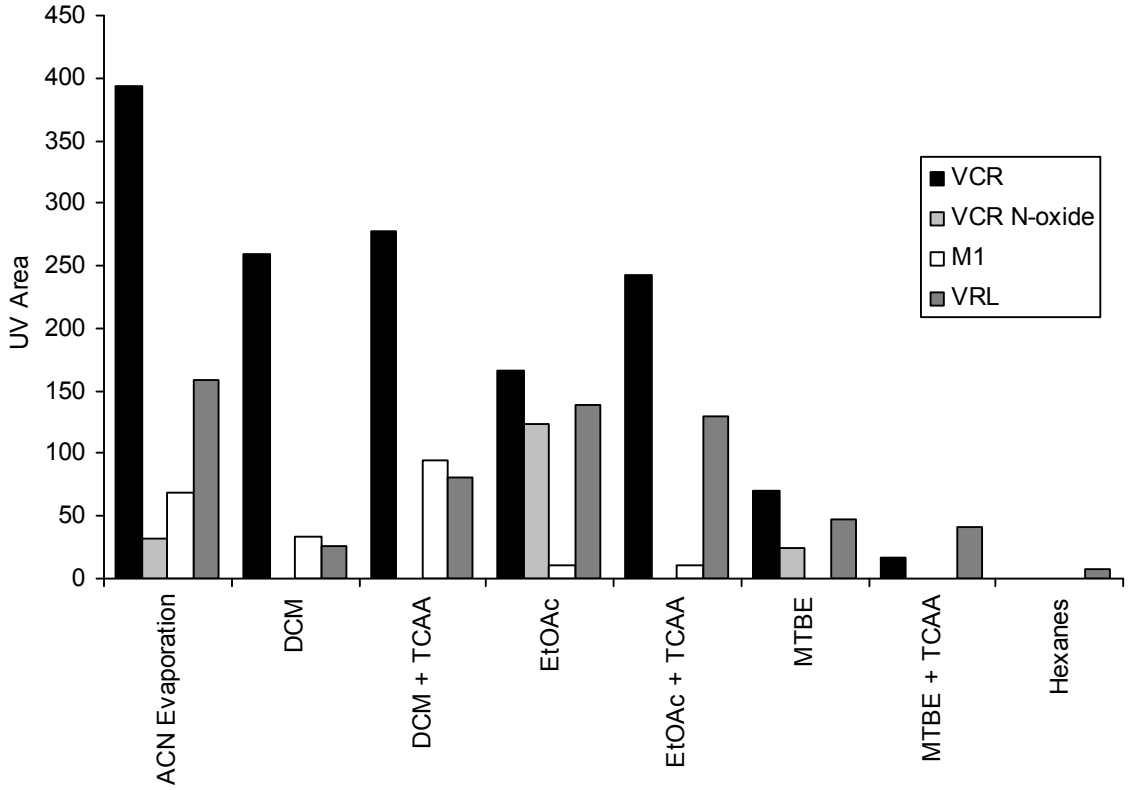

Fig. 10. Extraction recoveries of vincristine, M1, and vinorelbine. VCR (1 μM) in sodium phosphate buffer was incubated with cDNA-expressed CYP3A5 (50 pmol/mL) and NADPH (0.5 mM) for 9 min at 37°C. The solution was split between tubes and extracted with an equal volume of dichloromethane (DCM), ethyl acetate (EtOAc), methyl t-butyl ether (MTBE), or hexanes. For certain extractions, trichloroacetic acid (TCAA) was used to reduce the pH. The control was quenched with acetonitrile and evaporated without extraction. The dried residues for all samples were assayed by HPLC.

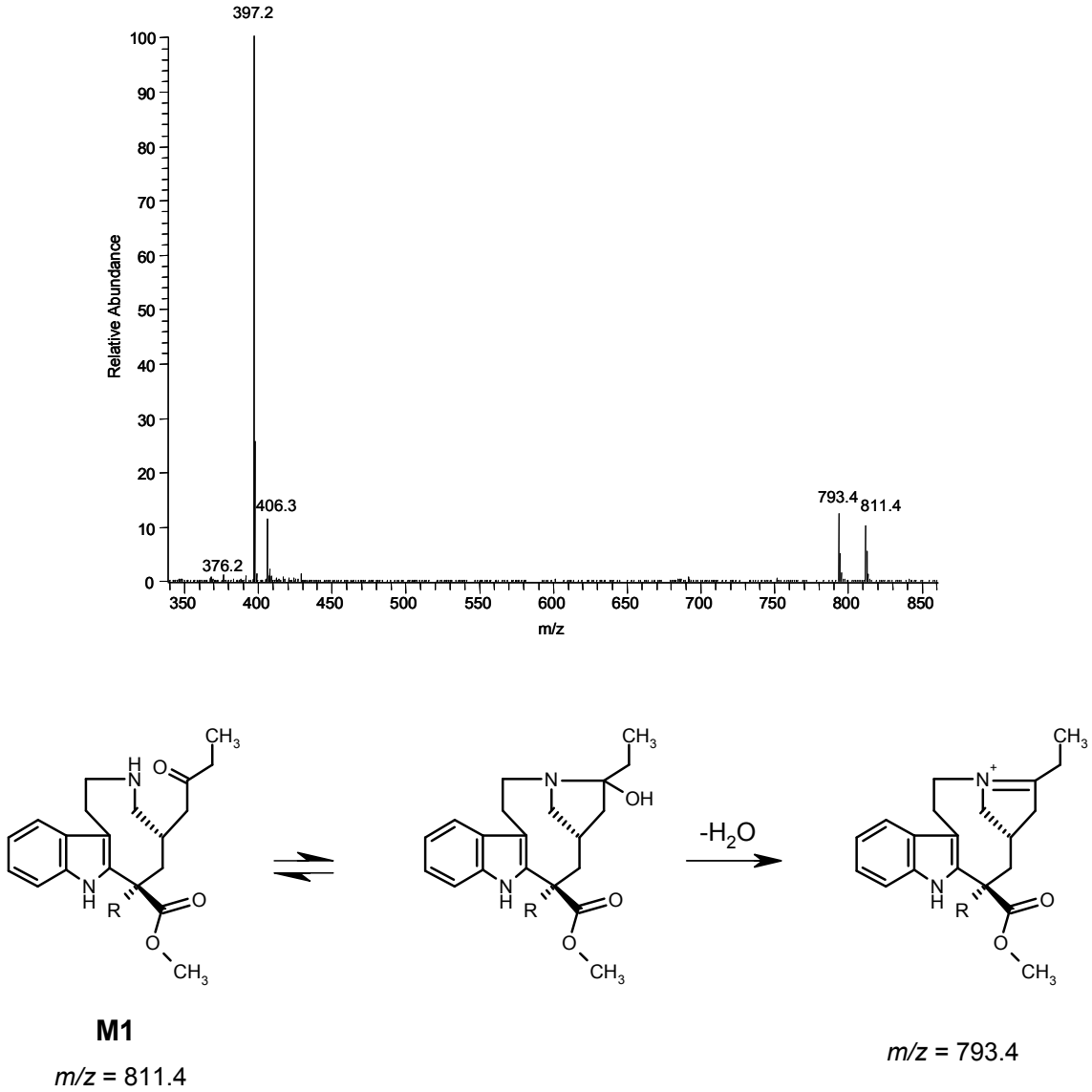

Fig. 11. Evidence of MS source-induced dehydration for M1 and the proposed mechanism. The full scan mass spectrum of M1 (top) has two primary ions at *m/z* 811 and 793. The ions at *m/z* 406 and 397 are the dicharged molecular ion and the dicharged source-induced dehydration ion, respectively. Based on the chemical structure of M1, a mechanism of dehydration was proposed (bottom).
R = *N*-formylvindoline

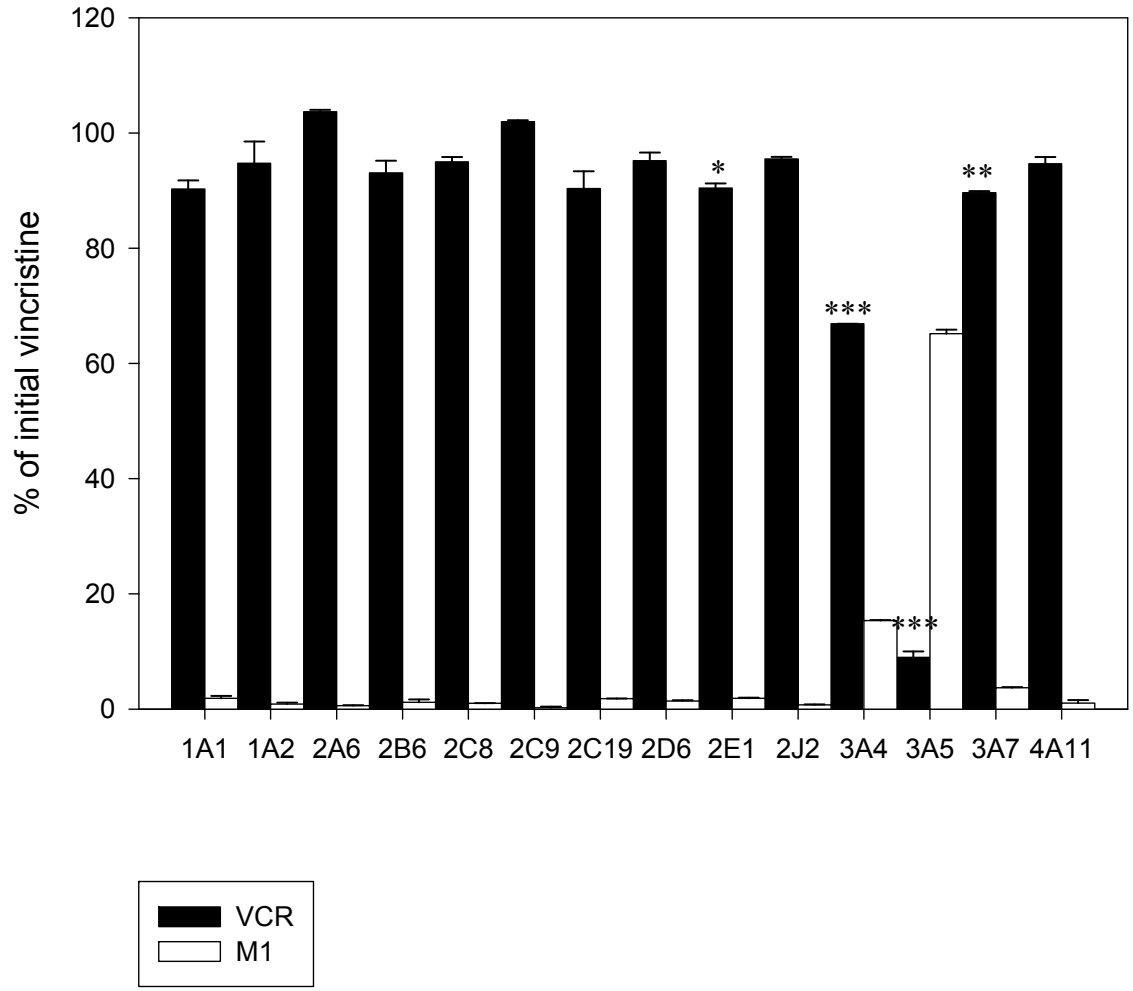

Fig. 12. Vincristine disappearance and M1 formation for various CYPs. All enzymes were tested in duplicate (25 or 50 pmol, 5 µM vincristine, 250 µl final volume). Vincristine and M1 concentrations were compared to an internal standard and normalized to the average of an insect microsome control. The enzymes were tested in the absence of cytochrome b_5 with the exception of coexpressed b_5 in CYPs 2J2, 2E1, and 3A7. Error bars represent data ranges ($n = 2$) for each P450. Statistical differences from the control incubations were calculated for vincristine disappearance using one-way ANOVA analysis, *$p <$ 0.05, **$p < 0.01$, ***$p < 0.001$.

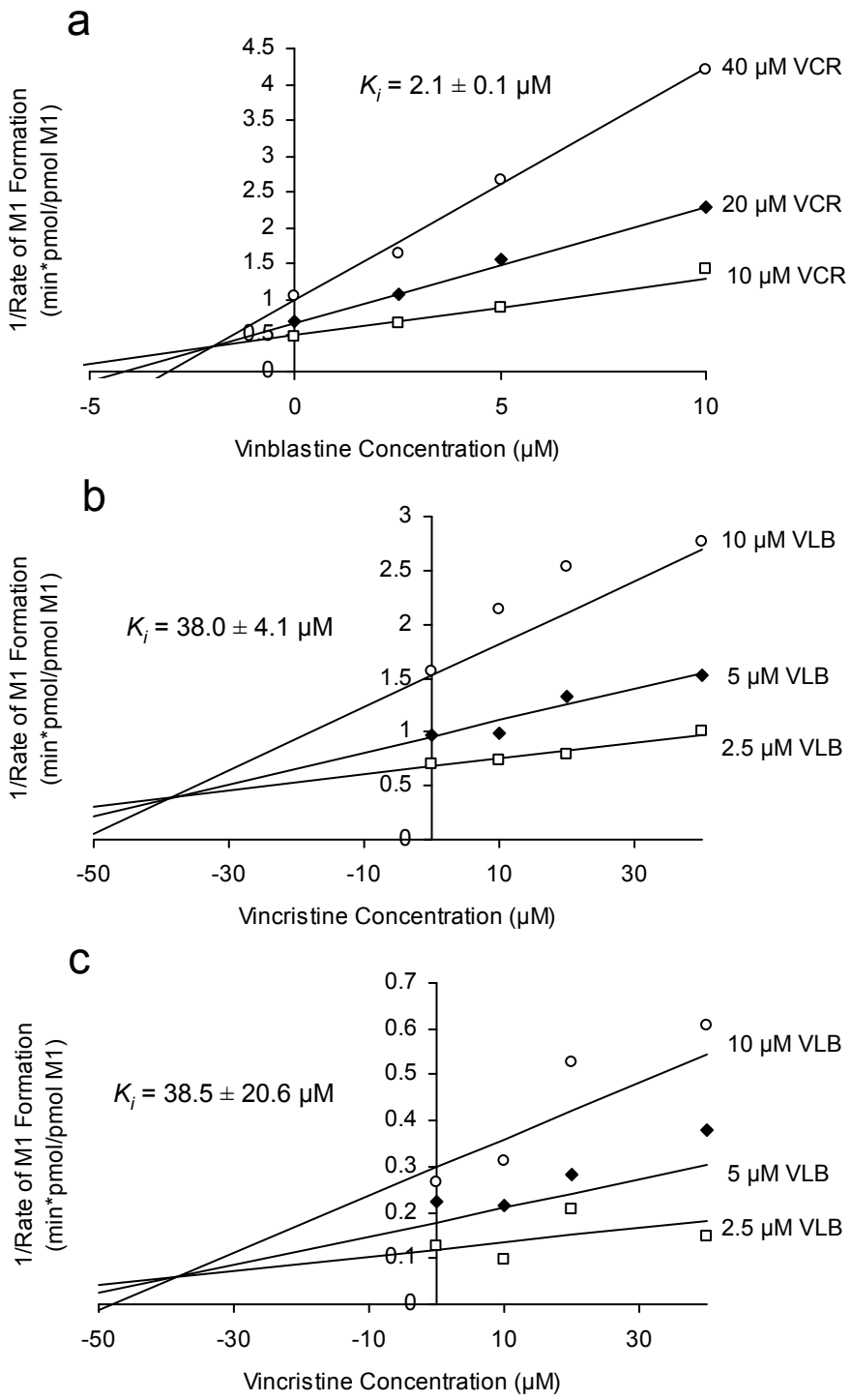

Fig. 13. Competitive inhibition of CYP3A4 and CYP3A5 with vincristine and vinblastine. Vincristine and vinblastine at various concentrations were coincubated with cDNA-expressed CYP3A4 (a,b) or CYP3A5 (c) at 50 pmol/mL. Vincristine inhibition with vinblastine for CYP3A5 is not presented because the data did not fit the model. The rates of M1 formation from vincristine and vinblastine were assayed simultaneously by HPLC. Using a competitive inhibition model, K_i (± SD) was estimated for each CYP and inhibitor by non-linear regression. The V_{max} and K_m values were estimated previously.

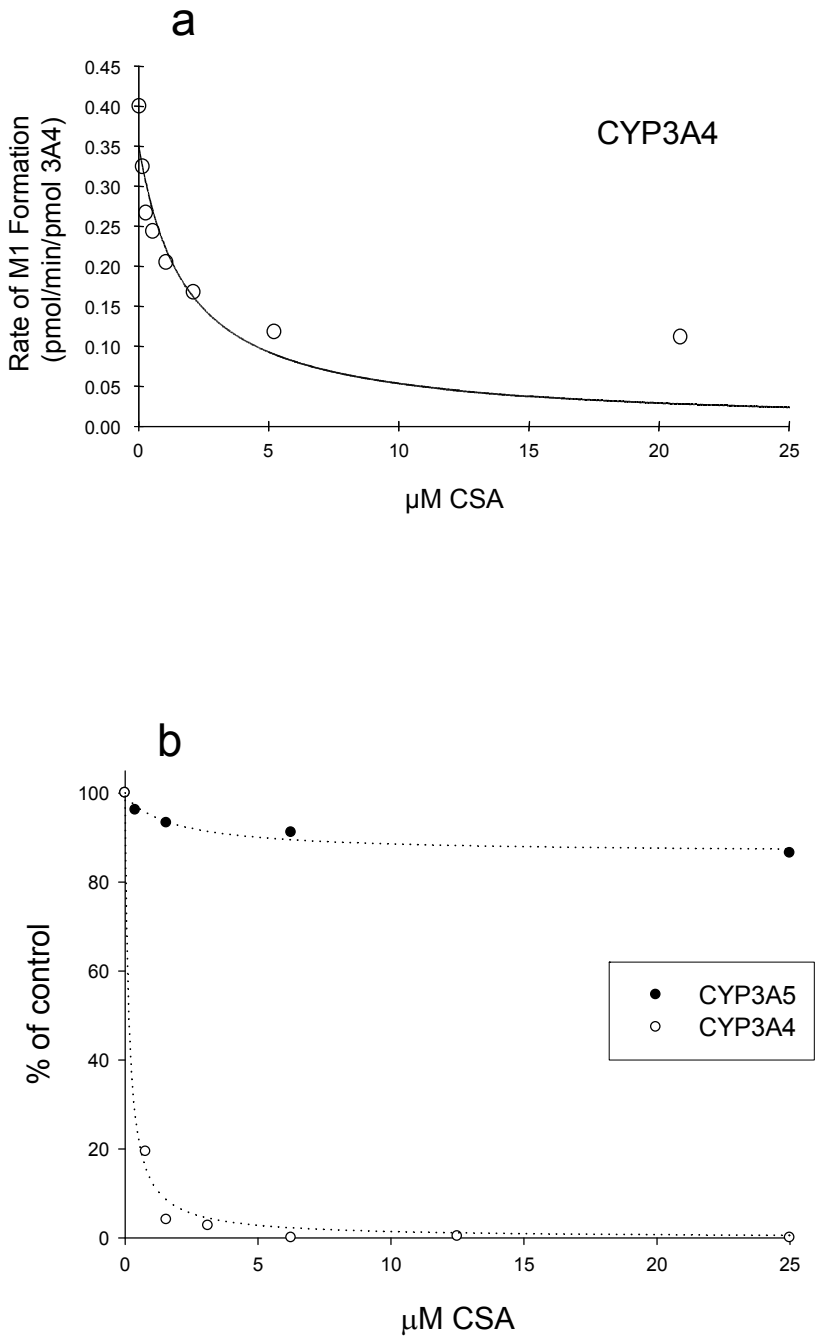

Fig. 14. Competitive inhibition of CYP3A4 and CYP3A5 activities with cyclosporin A. Vincristine (10 µM) was coincubated with cDNA-expressed CYP3A4 and/or CYP3A5 at various concentrations of CsA in 0% methanol (a) and 0.3% methanol (b). For plot (b), the control incubations were performed without CsA in 0.3% methanol. The fitted lines were estimated using Eqn. 1. For plot (a), the uninhibited fraction was set at zero.

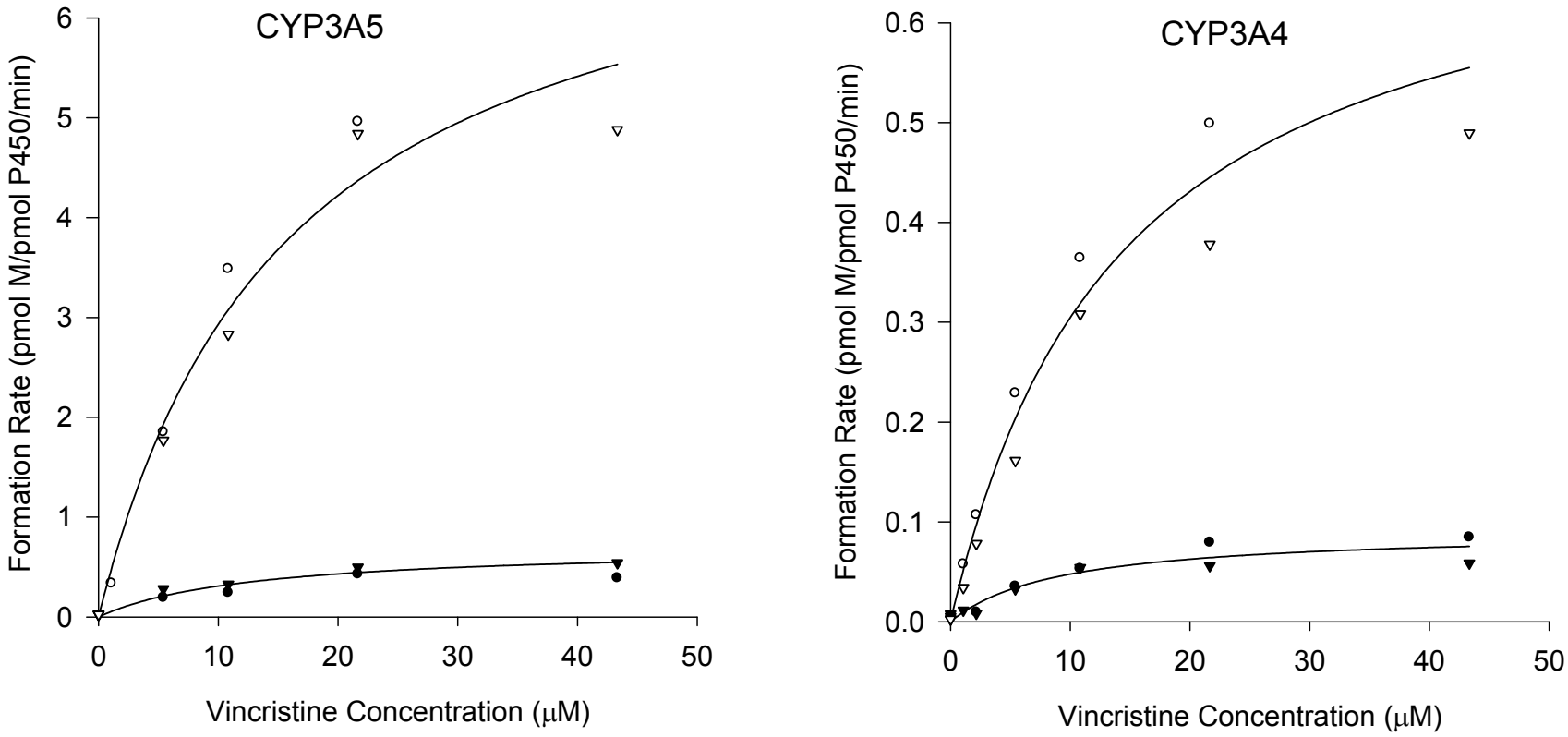

Fig. 15. Kinetics of M1 and M2 formation from vincristine with CYP3A4 and CYP3A5. VCR at various concentrations was incubated with CYP3A4 or CYP3A5 supplemented with b_5 (3:1). For one set of experiments, the incubations were performed using one CYP enzyme preparation and 6 concentrations of VCR (circles). The identical incubations were repeated approximately 30 min later with the same CYP enzyme preparation to provide duplicate values (triangles). The rates of M1 (open symbols) and M2 (closed symbols) formation were quantified by HPLC. Not all values were available because of poor chromatography. The Michaelis-Menten parameters were estimated with a one-enzyme model using non-linear regression.

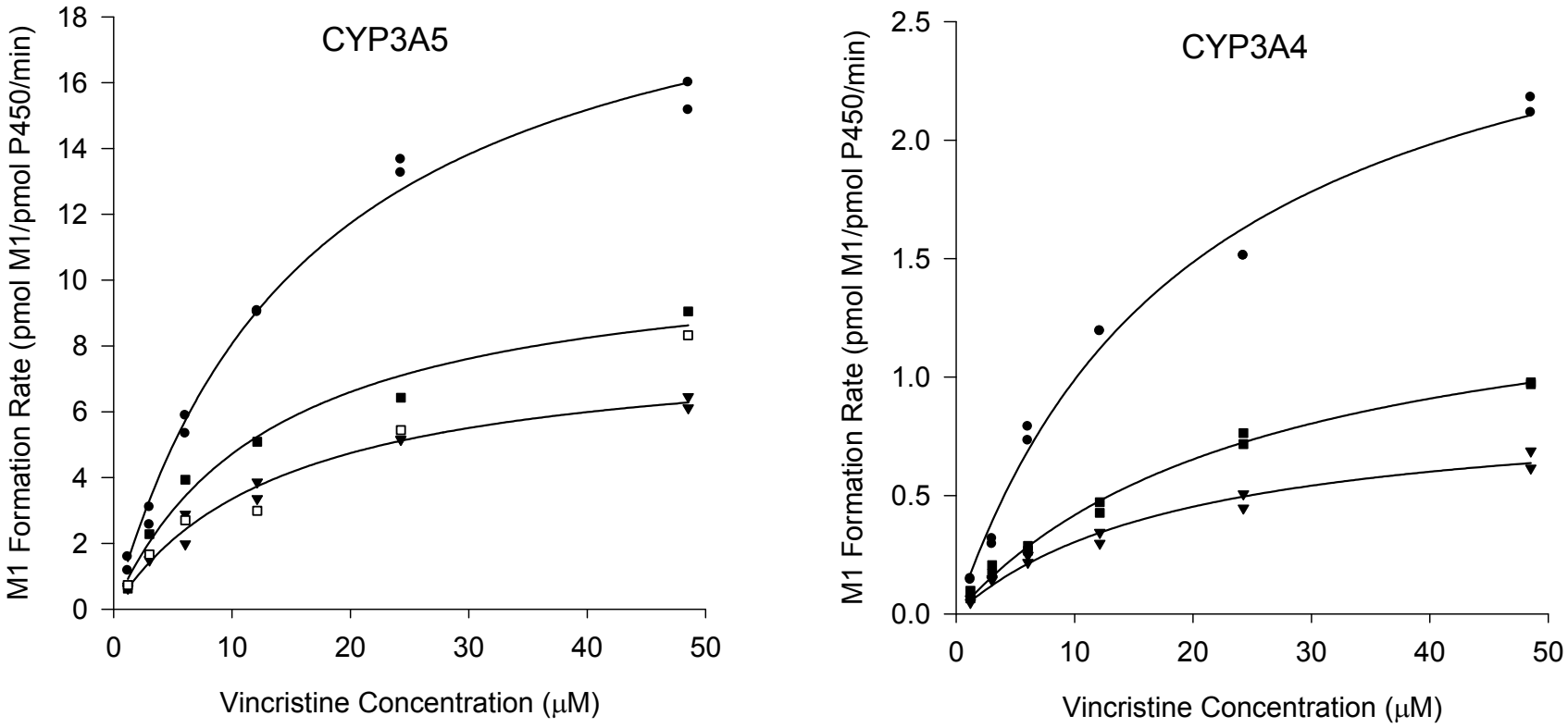

Fig. 16. Effect of enzyme preparation on the kinetics of M1 formation with CYP3A4 and CYP3A5. Vincristine was incubated with multiple enzyme preparations: enzyme with co-expressed cytochrome b_5 (•), enzyme with supplemented b_5 (3:1) (▼), and enzyme without b_5 (■ or □). For the enzyme preparation with CYP3A5 and supplemented b_5 , the duplicate incubations (□) used the enzyme preparation approximately 30 min after the first set of incubations; this data was excluded in the kinetic analysis. Data was fit to a one-enzyme model to determine Michaelis-Menten parameters.

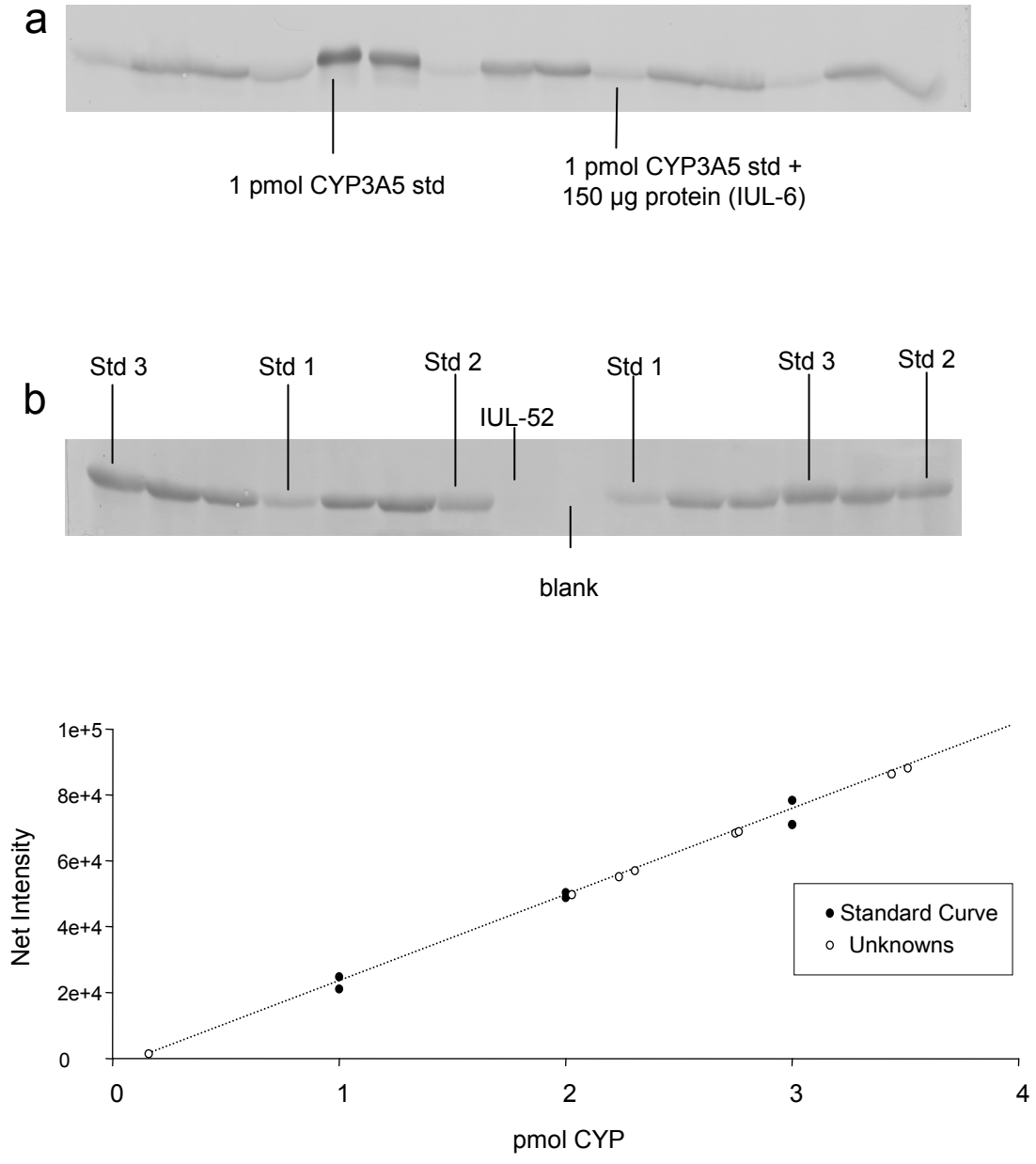

Fig. 17. Quantification of CYP3A4 and CYP3A5 in human liver microsomes by Western blot. The cDNA-expressed CYP3A5 standard (1 pmol) was assayed with and without a co-loaded standard, IUL-9 (a). IUL-9 and IUL-52 do not have immunodetectable CYP3A5. A typical Western blot (b) was loaded with 3 concentrations of standards in duplicate, a blank, and a protein loading control (IUL-52). The protein loading control was added to each of the P450 standards to match the protein content of the unknowns (20 µg in this case). A standard curve was generated using the 6 standard values, and the P450 concentrations of the unknown HLMs were calculated by linear interpolation.

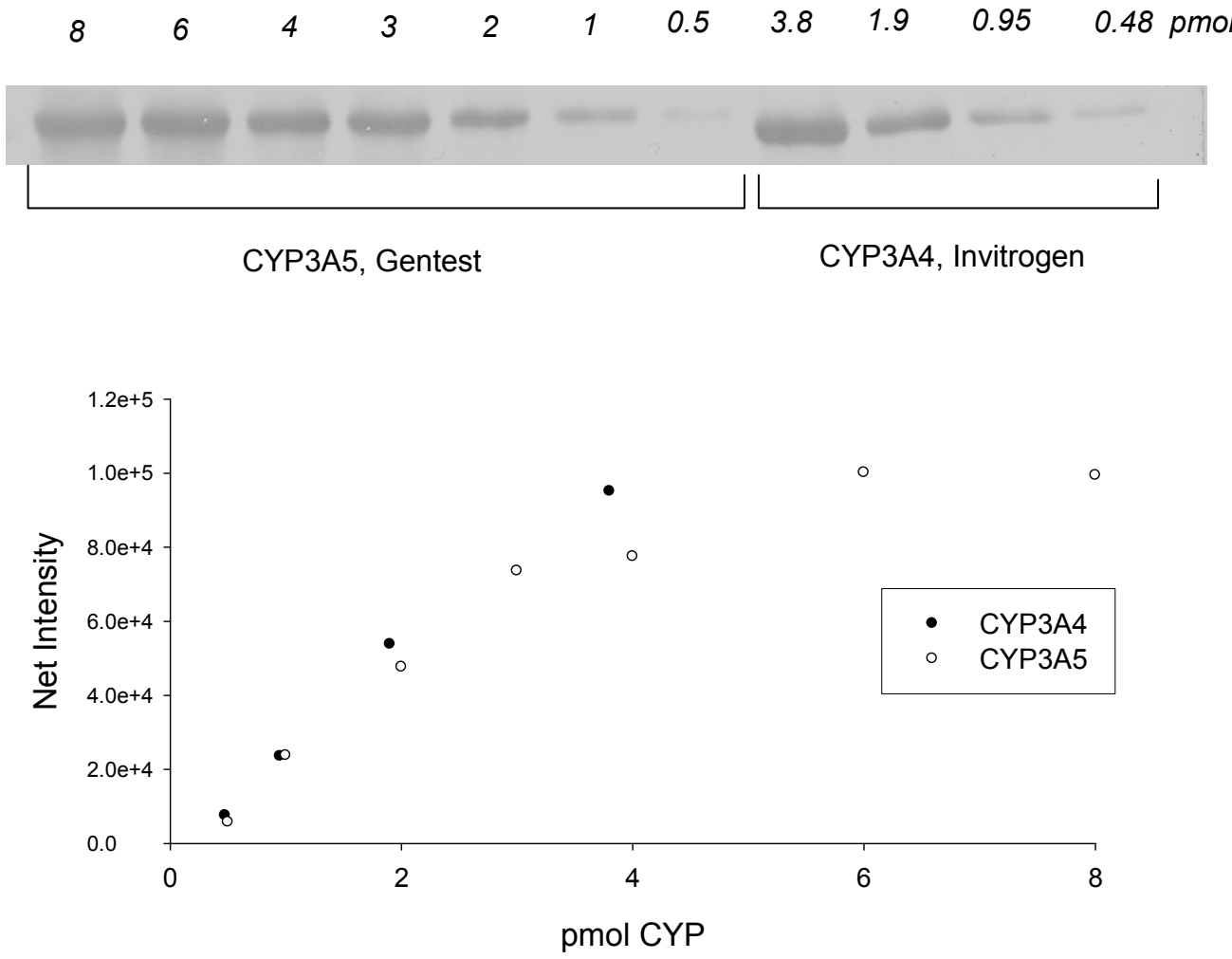

Fig. 18. Western blot comparison of CYP3A4 and CYP3A5 standards. By assuming equal immunoreactivities of the enzymes, the purity of the CYP3A4 and CYP3A5 standards were directly compared using a non-specific CYP3A antibody.

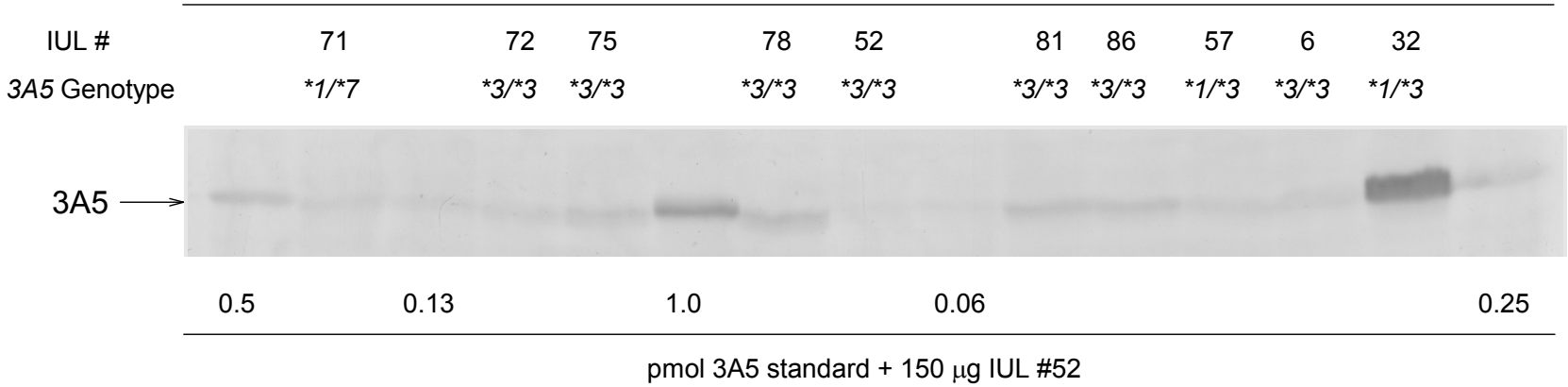

Fig. 19. Western blot of CYP3A5 for IUL-57 and IUL-71. The immunoreactive CYP3A5 protein contents of IUL-57 and IUL-71 were compared to those of *CYP3A5*3/*3* livers. IUL-52, an HLM with no detectable CYP3A5, was added to the CYP3A5 standards. IUL-32 (*CYP3A5*1/*3*) was used as a positive control for CYP3A5 expression. Each well was loaded with 150 μg of protein.

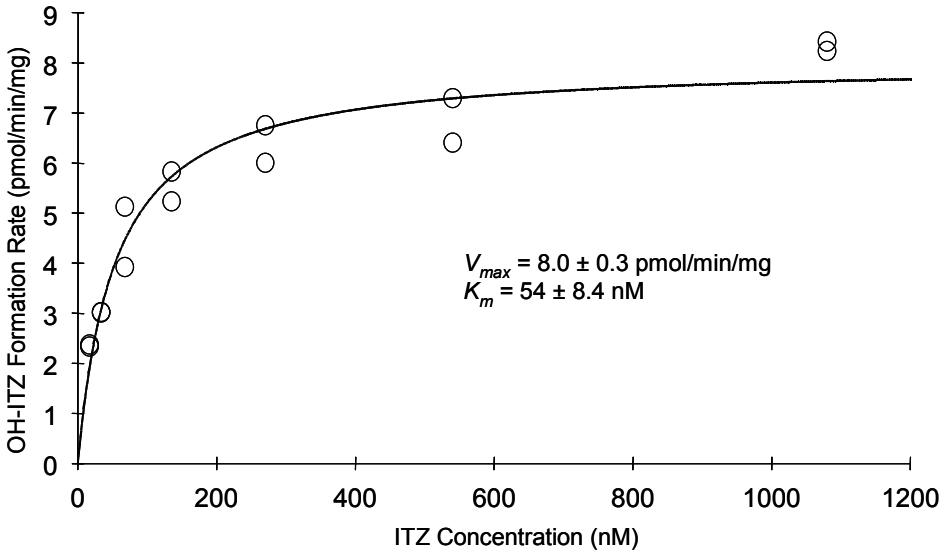

Fig. 20. Michaelis-Menten kinetics of itraconazole hydroxylation with IUL-49. ITZ at multiple concentrations (0.2% methanol) was incubated in duplicate for 3 min with IUL-49. The kinetic parameters were estimated by non-linear regression.

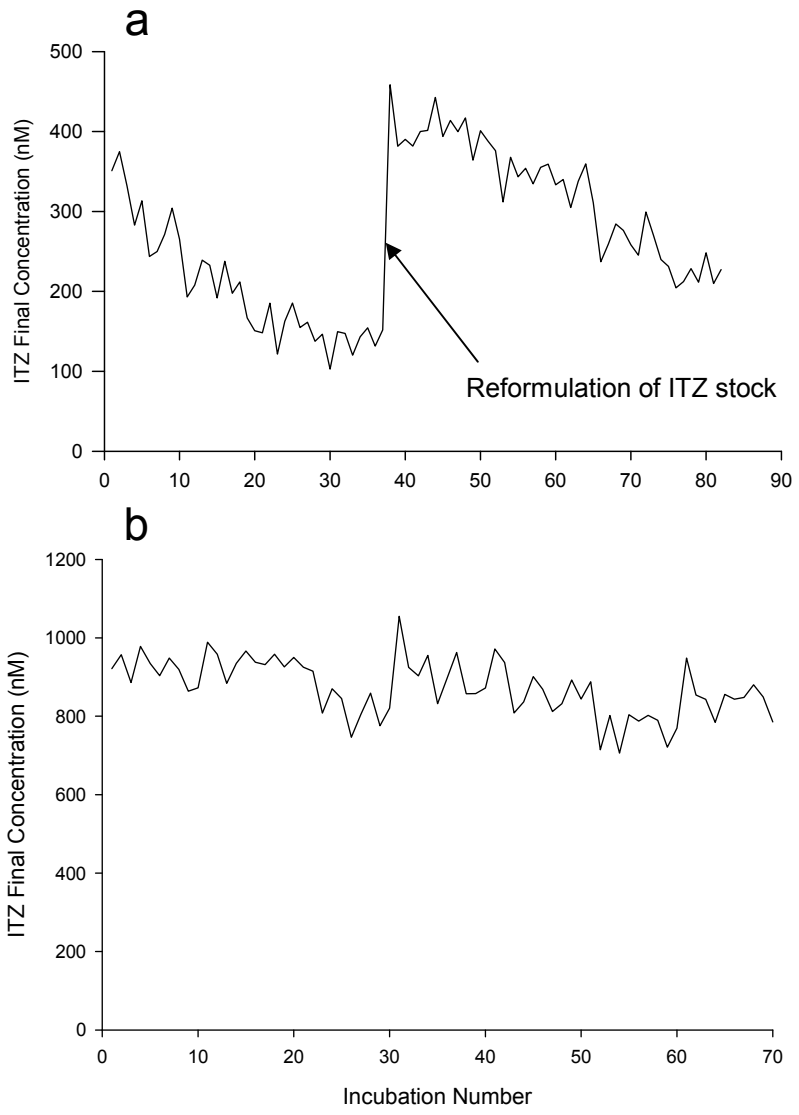

Fig. 21. Final itraconazole concentration as a function of stock solution preparation. ITZ incubations with HLMs were performed on two independent days. For the first day (a), the initial target concentration of ITZ was 500 nM (0.1% methanol). Two working stock solutions in 50 mL plastic tubes were formulated for the 90 incubations. For the second day (b), the initial target concentration of ITZ was 1000 nM (0.2% methanol). Working stock solutions were freshly formulated in glass for each batch of incubations (9 tubes per batch).

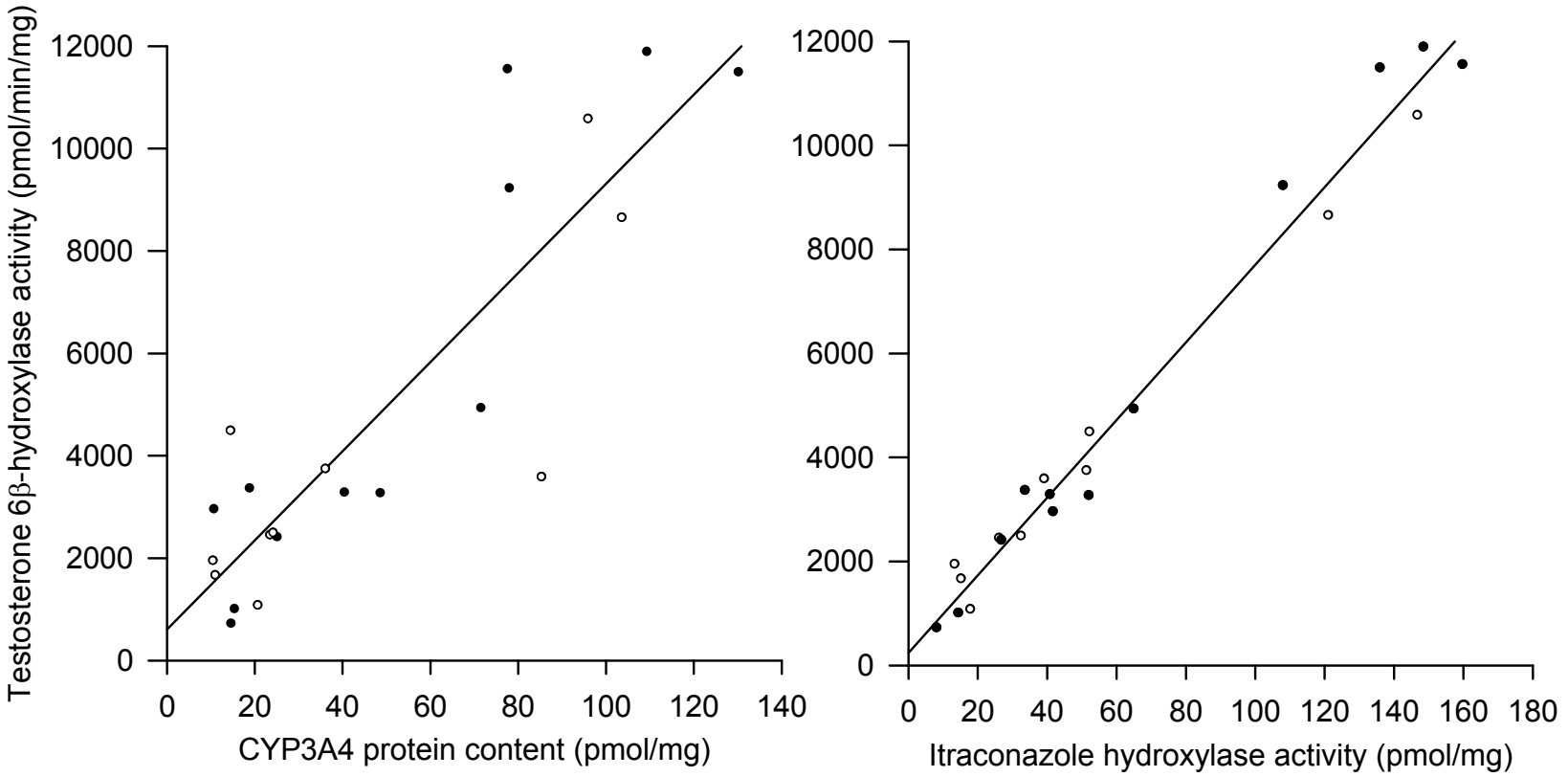

Fig. 22. Correlation between CYP3A activities and CYP3A4 protein content in human liver microsomes. A select number of HLMs (n = 22) were characterized by CYP3A4 content, testosterone 6β-hydroxylase activity, and itraconazole hydroxylase activity. The testosterone hydroxylase activity was correlated to CYP3A4 protein content (a) and to itraconazole hydroxylase activity (b). Microsomes are separated by CYP3A5 expression: ● low expression and ○ high expression, at least one *CYP3A5*1* allele. Two microsomes (IUL-57 and IUL-71) with a genotype of *CYP3A5*1/*0* are plotted as CYP3A5 low expressers.

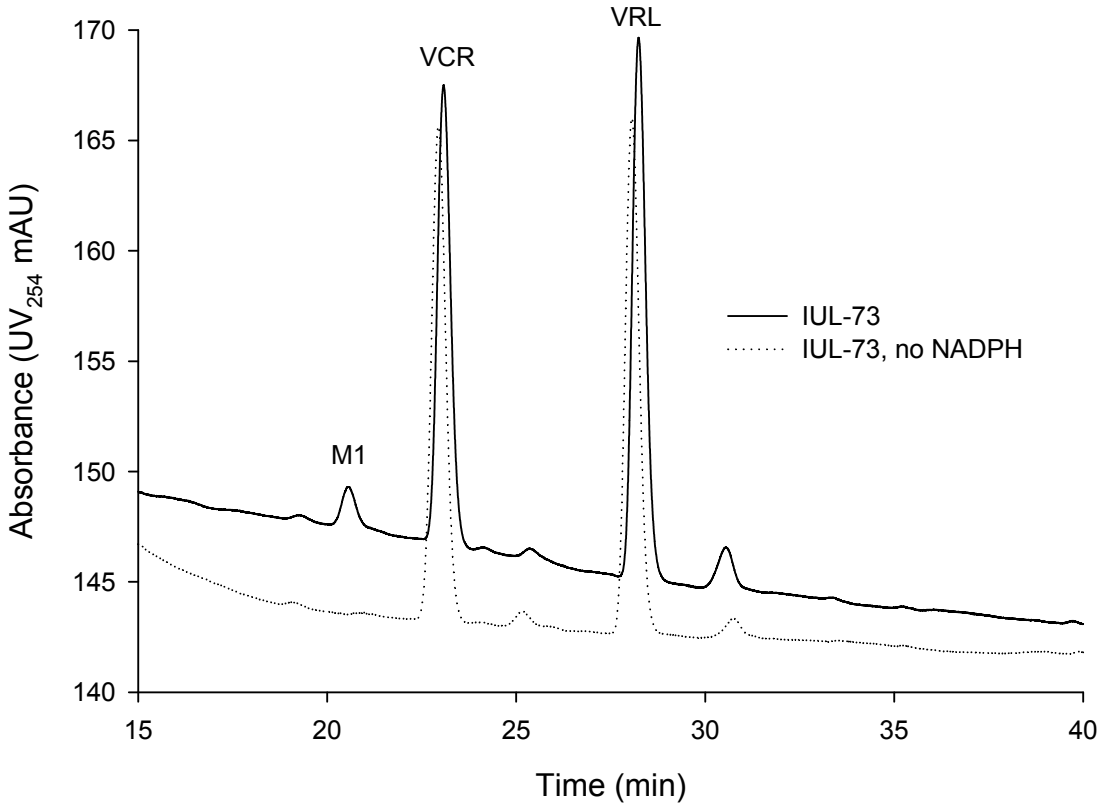

Fig. 23. Representative UV chromatogram of vincristine biotransformation with human liver microsomes. VCR was metabolized to one major metabolite (M1) after incubation with human liver microsomes, IUL-73, for 10 min with and without NADPH. Vinorelbine (VRL) was the internal standard. The peak at 31 min was not vincristine-related as determined by LC/MS/MS.

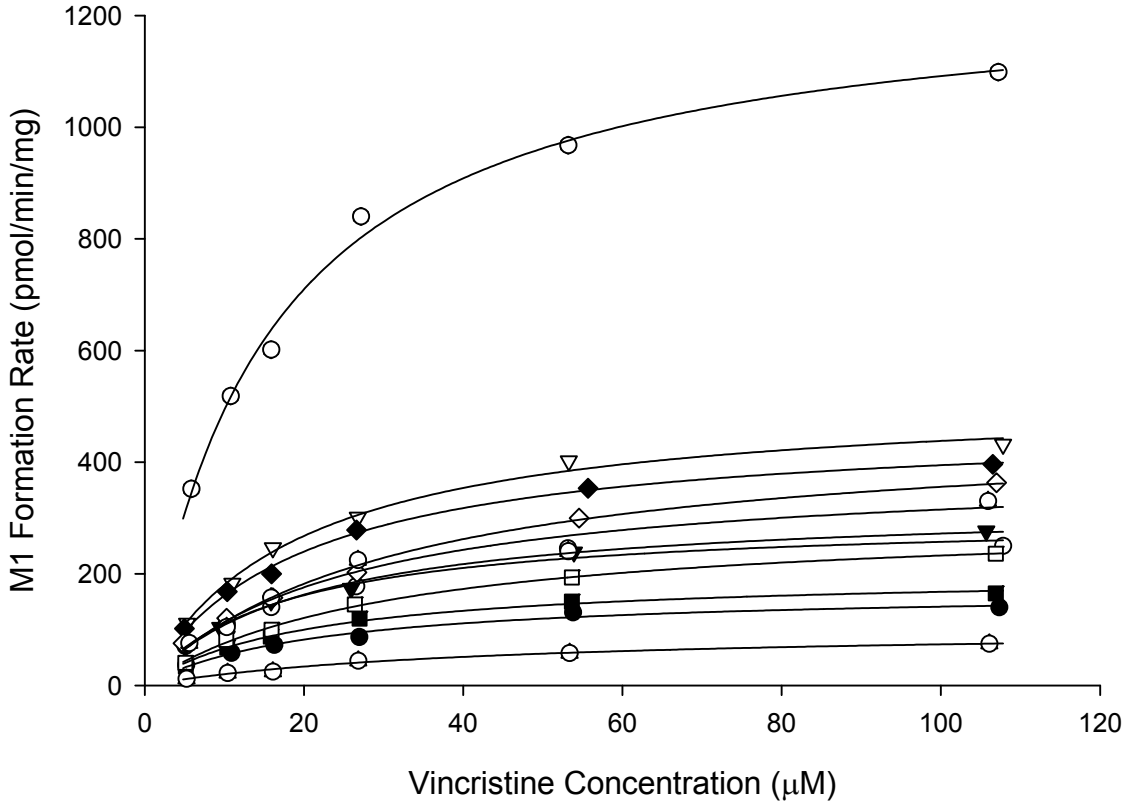

Fig. 24. Michaelis-Menten curves for rates of M1 formation with *CYP3A5*1* human liver microsomes. Vincristine (5 to 108 μM) was incubated with microsomal protein (0.5 to 1.2 mg/mL) from livers with at least one *CYP3A5*1* allele. The initial M1 rates of formation at each concentration of VCR were used to estimate the Michaelis-Menten kinetic parameters of each liver by non-linear regression.

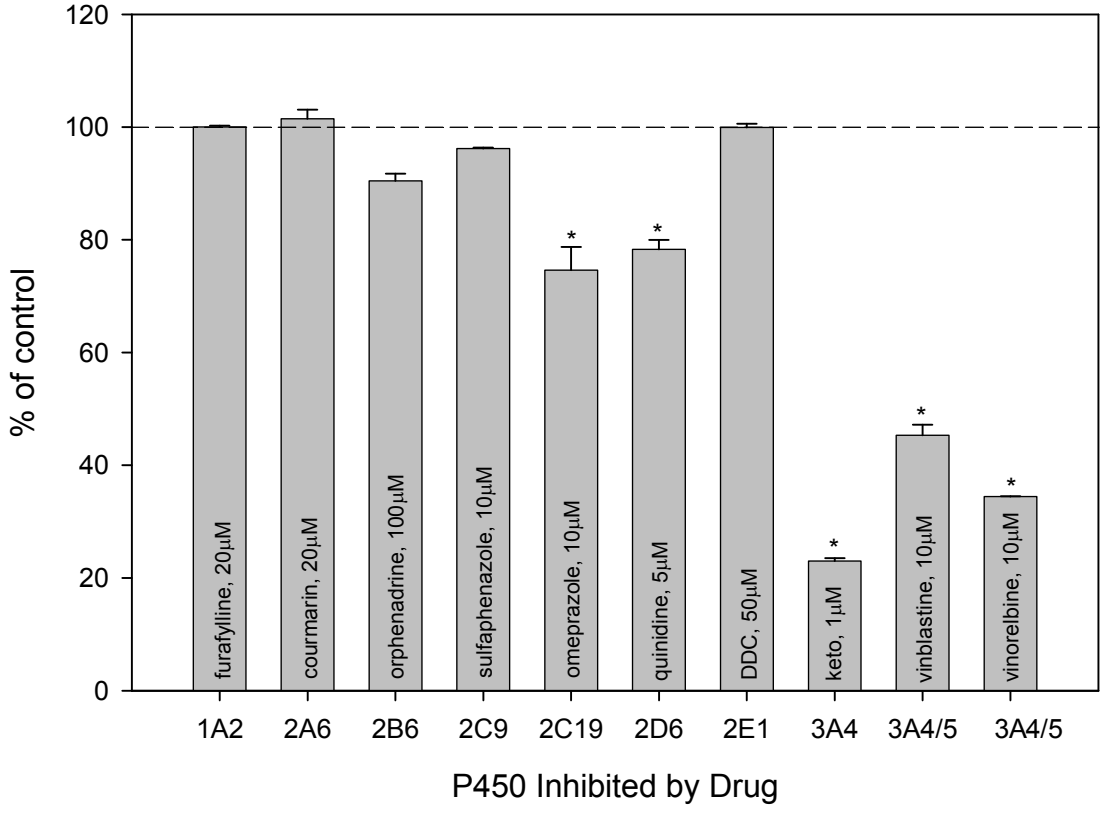

Fig. 25. Rates of M1 formation normalized to control activity after chemical inhibition of hepatic CYPs in human liver microsomes. Vincristine (15 μM) was incubated with pooled HLMs (2 mg/mL) in the presence of selective CYP chemical inhibitors for 15 min. The control experiments were completed without inhibitors. *$p < 0.01$

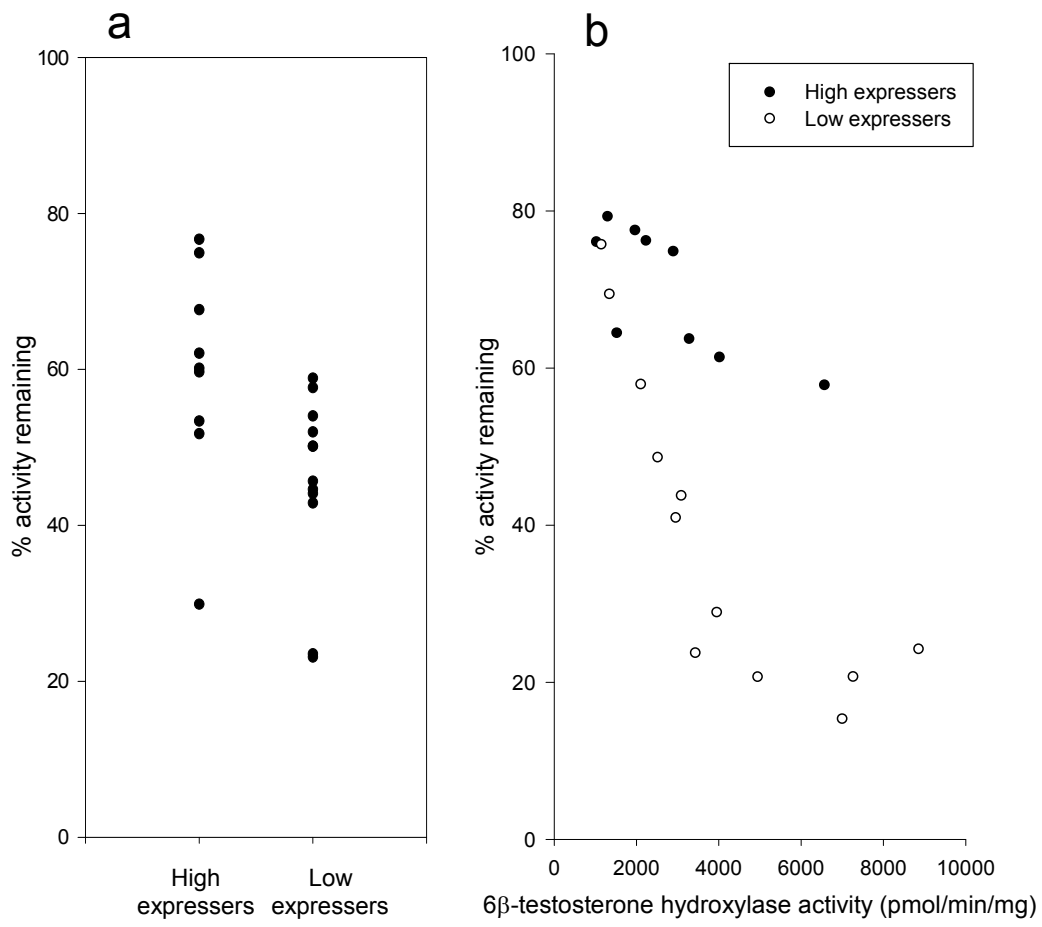

Fig. 26. Inhibition of vincristine metabolism by the addition of methanol (a) and cyclosporin A (b). Vincristine (10 μM) was incubated with a panel of CYPs and CsA (25 μM). For the CYPs, the vehicle controls contained 4.8% methanol and were compared to the previously estimated rate of M1 formation at 10 μM VCR in plot (a). The competitive inhibition of CsA was determined by comparing the rates of M1 formation from the vehicle control incubations to the CsA inhibited incubations (b). The degree of CsA inhibition was evaluated as a function of CYP3A4 activity by plotting the 6β-testosterone hydroxylase activities on the x-axis.

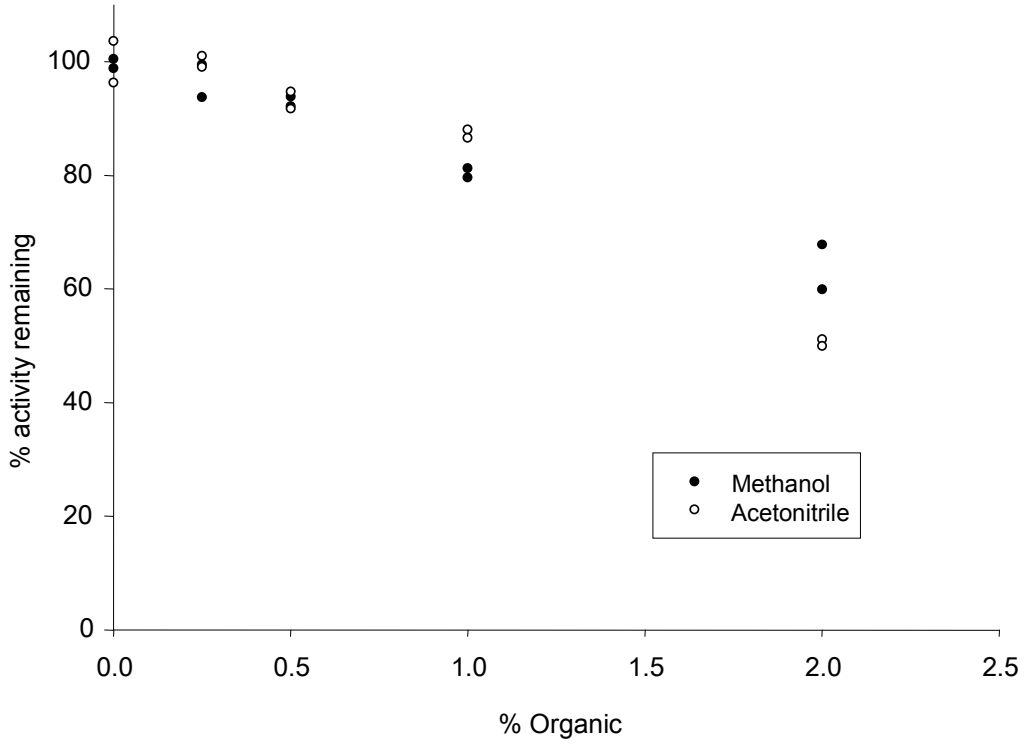

Fig. 27. Inhibition of M1 formation with methanol and acetonitrile for IUL-42. Vincristine (20 μM) and IUL-42 (1.2 mg/mL) were coincubated in duplicate with various concentrations of methanol and acetonitrile. The control incubations were performed without solvent (0% organic).

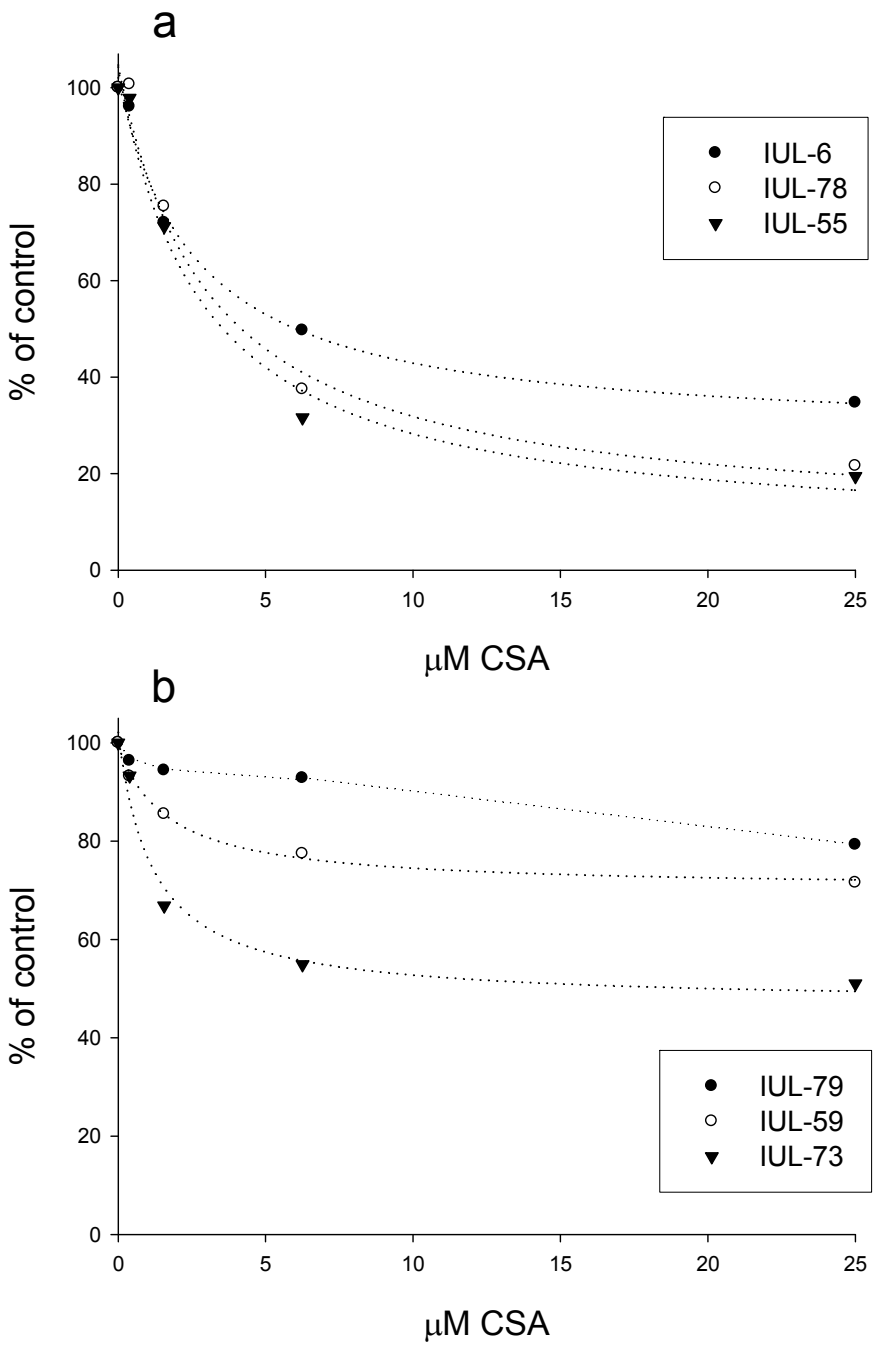

Fig. 28. Selective inhibition of CYP3A4 by cyclosporin A for CYP3A5 low expressers (a), and CYP3A5 high expressers (b). Points represent individual values (IUL-6, 59, and 73) or the average of replicates (CYP3A4, CYP3A5, IUL-55, 78, and 79). Non-linear regression was used to fit data points to Eqn. 1 (dotted lines), except for IUL-79 because the data did not fit model.

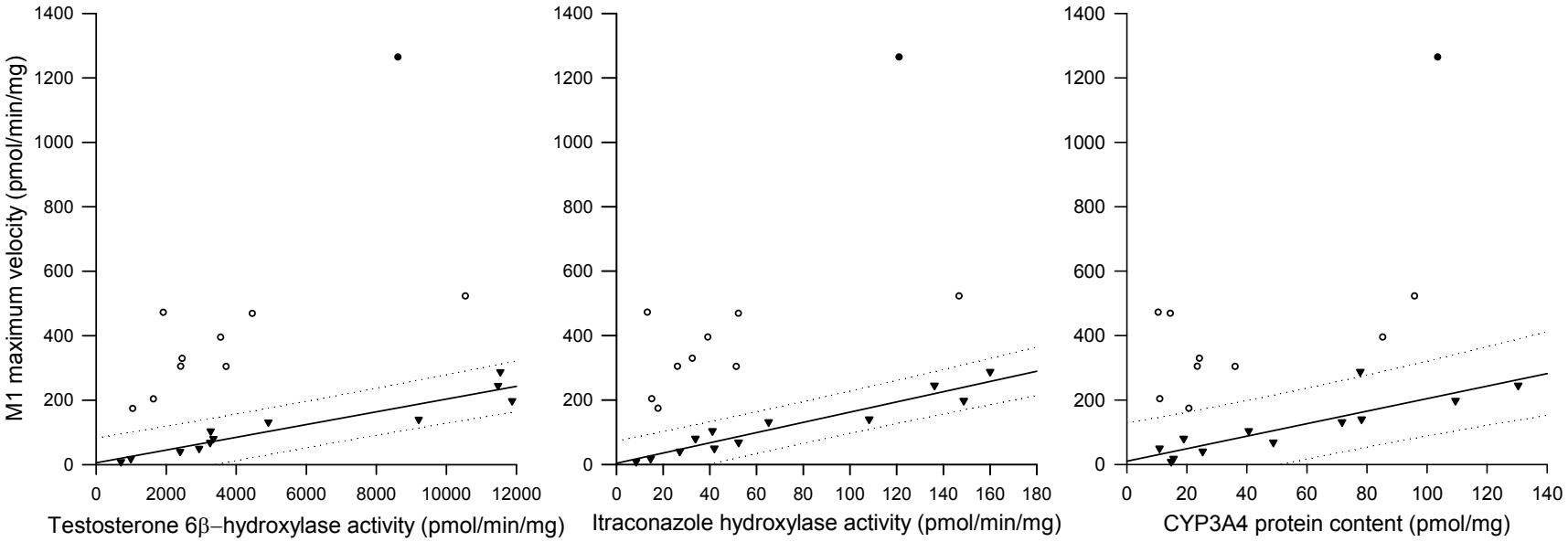

Fig. 29. Correlation of the maximum rates of M1 formation to 6β-OH testosterone hydroxylase activity (a), itraconazole hydroxylase activity (b), and CYP3A4 protein content (c) in human liver microsomes. The livers are separated by CYP3A5 expression: ▼ low expression, ○ heterozygous high expression (*CYP3A5*1/*0*), and ● homozygous high expression (*CYP3A5*1/*1*). Two microsomes (IUL-57 and IUL-71) with a genotype of *CYP3A5*1/*0* are plotted as CYP3A5 low expressers. Data from low CYP3A5 expressers was fit by linear regression (solid lines) with 95% confidence intervals (dotted lines).

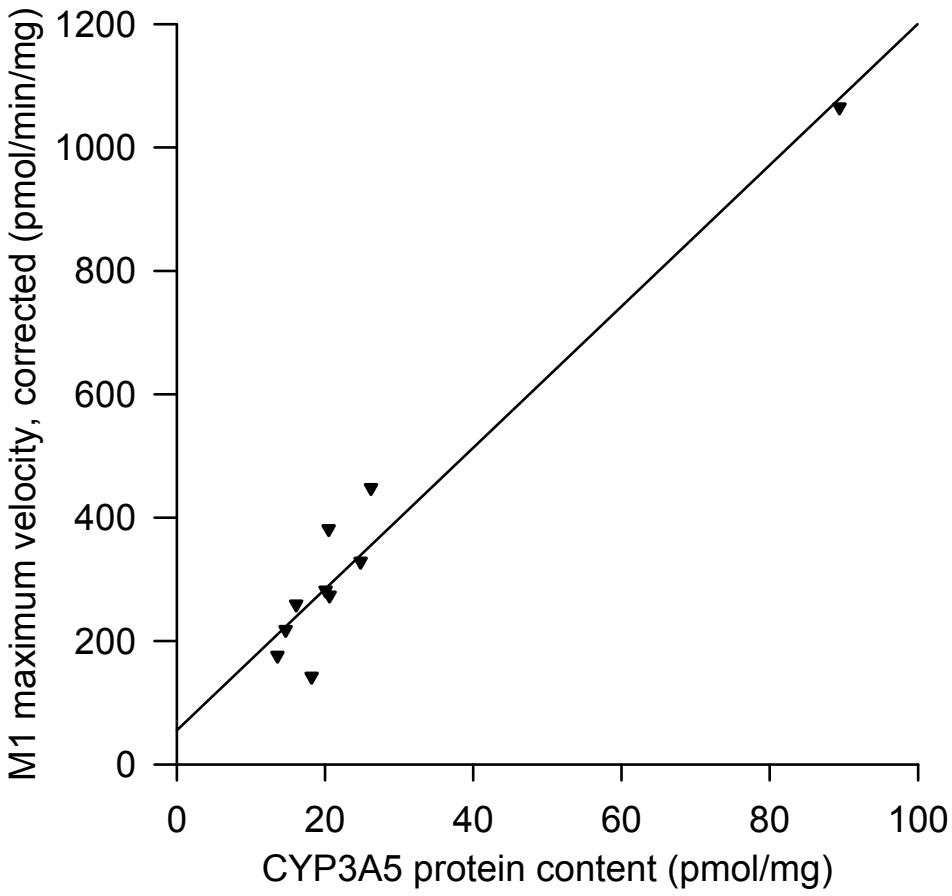

Fig. 30. Correlation of the corrected maximum rate of M1 formation to CYP3A5 content. The M1 formation mediated by CYP3A5 was quantified by subtracting the CYP3A4 contribution as determined by linear regression with the *CYP3A5*3/*3* samples using itraconazole hydroxylase activities.

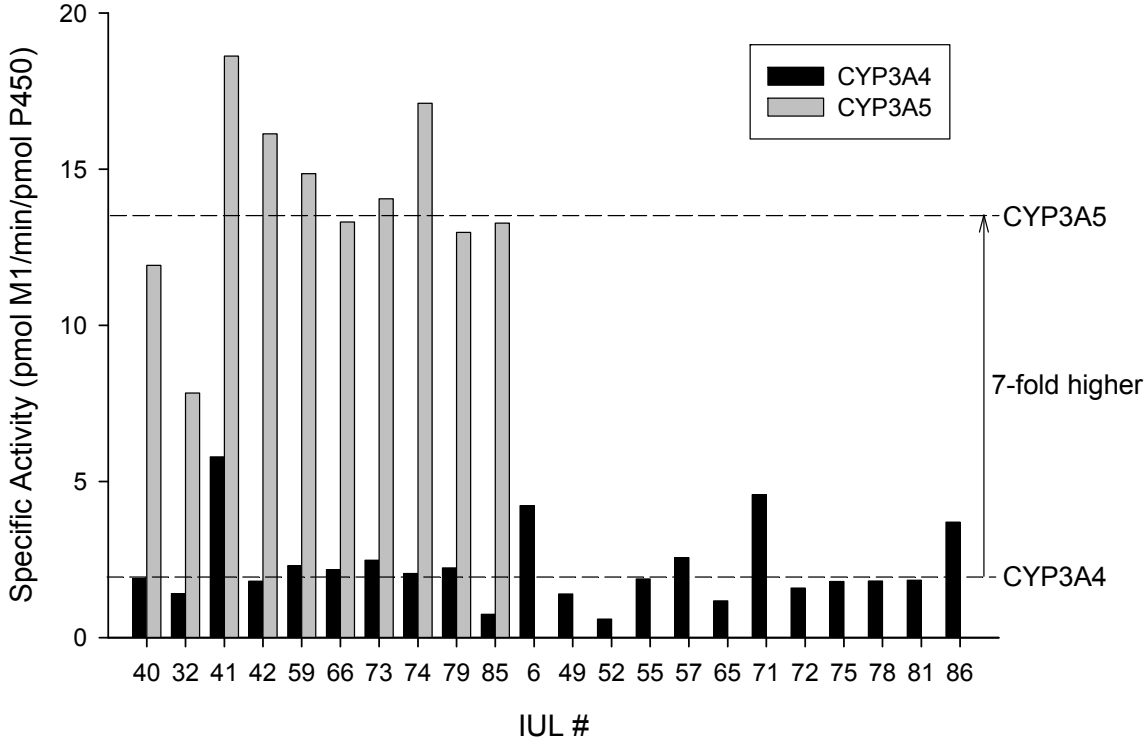

Fig. 31. Specific activities of CYP3A4 and CYP3A5 in the formation of M1 from vincristine at V_{max} for CYP3A5 high expressers. The CYP3A4 and CYP3A5 contributions to M1 activity are estimated by normalization to testosterone 6β-hydroxylase activities of *CYP3A5*3/*3* livers. The specific activities of CYP3A4 and CYP3A5 for each microsome are calculated using the CYP3A4 and CYP3A5 protein concentrations as determined by Western blot. Using the median values of the microsomes (dotted lines), the CYP3A5 activity is 7-fold higher than the CYP3A4 activity.

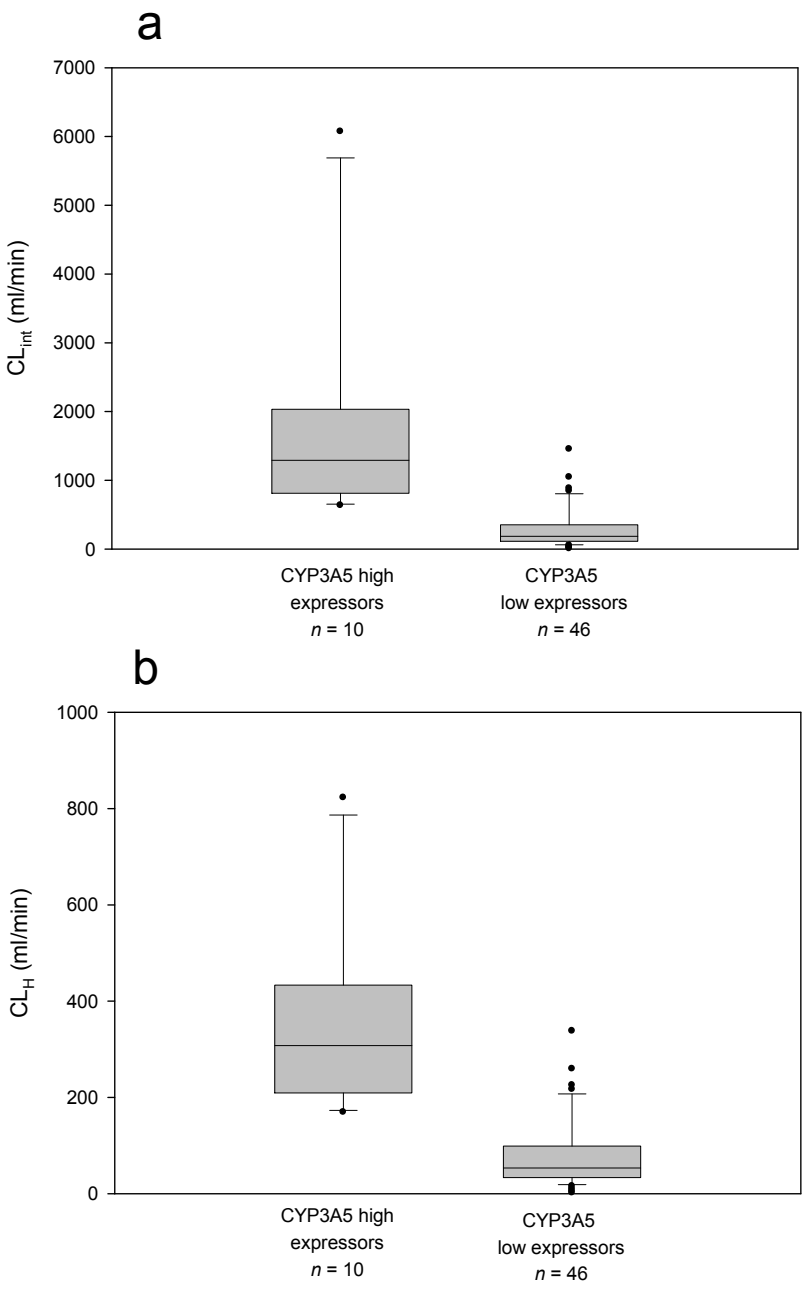

Fig. 32. Estimation of intrinsic (a) and hepatic (b) clearances by in vitro/in vivo scaling with human liver microsomes. The clearances were predicted for CYP3A5 high expressers (n = 10) and low expressers (n = 46). Using the M1 formation velocity from 12 HLMs, the distribution of clearance values for CYP3A5 low expressers was determined by linear regression of the testosterone 6β-hydroxylase activity for the bank of HLMs (n = 46).

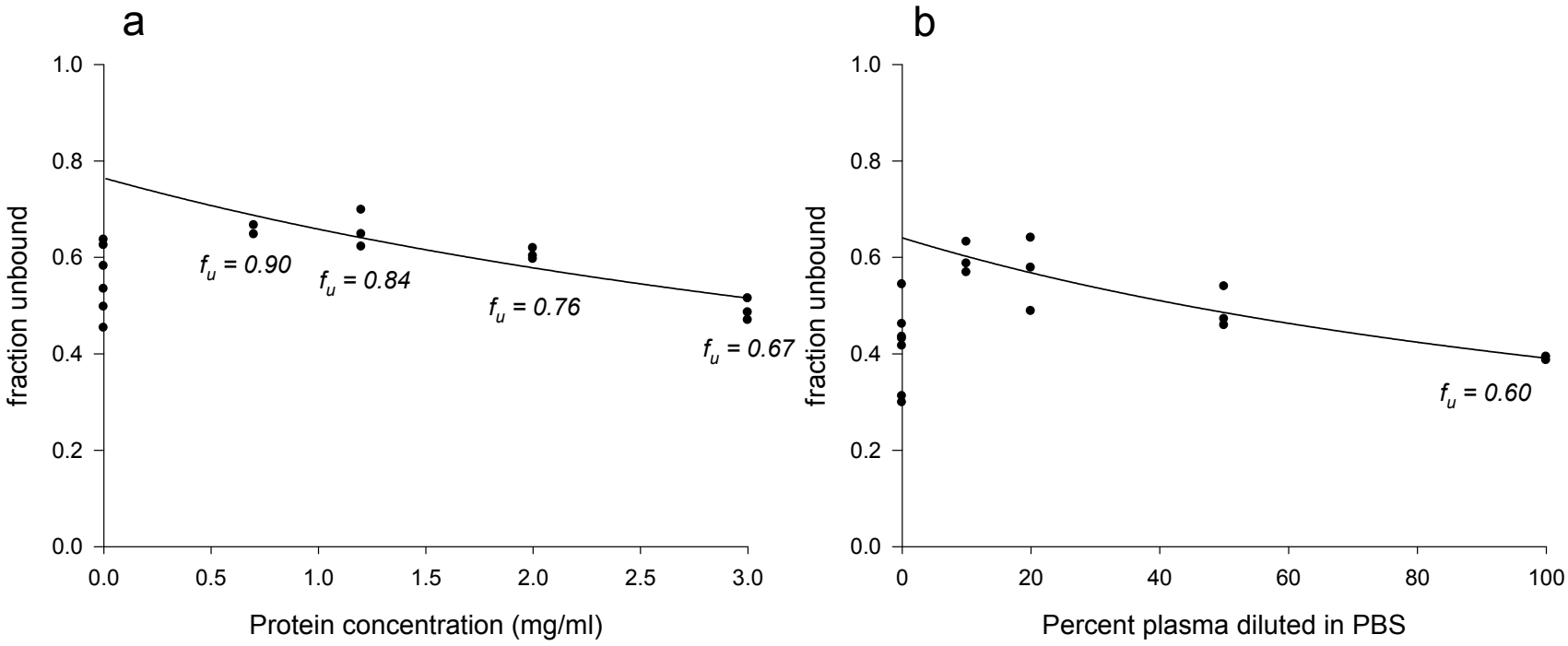

Fig. 33. Protein binding of vincristine to human liver microsomes (a) and plasma (b). VCR (5 μM) was incubated at 37°C with various concentrations of pooled HLMs. The apparent fraction unbound was calculated by dividing the concentration of the ultrafiltrate to the unprocessed VCR concentration in microsomal incubation buffer. The concentrations were quantified by HPLC. VCR (1 μM) was incubated at 37°C with human plasma from one donor diluted with phosphate buffer saline (PBS). The apparent fraction unbound was determined in triplicate for each concentration. The fraction unbound caused by non-specific binding ($f_{u,nsb}$, the y intercept) and the binding parameter (K) for microsomes and plasma were estimated by non-linear regression using Eqn. 2. The fraction unbound (f_u) was calculated for the plasma and each concentration of protein (labeled above).

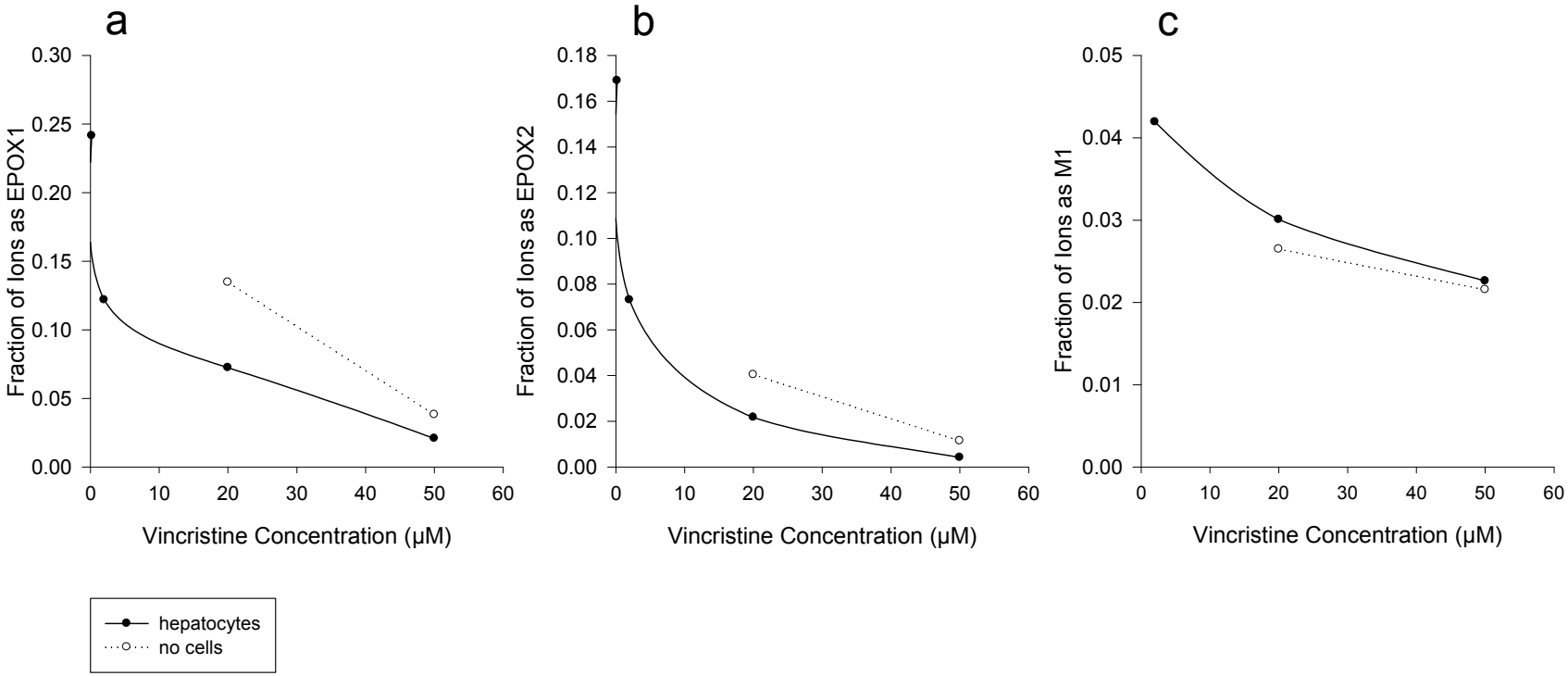

Fig. 34. Metabolite profiling of vincristine with cryopreserved hepatocytes. Cyropreserved hepatocytes (lot SD012, SD017) were incubated in 24-well plates over 4 h at 5 x 105 cells/mL with 0.2, 2, and 20 µM VCR. The cell density at 50 µM VCR was 1 x 10^6 cells/mL. No cell controls were not performed for the two lowest concentrations of vincristine.

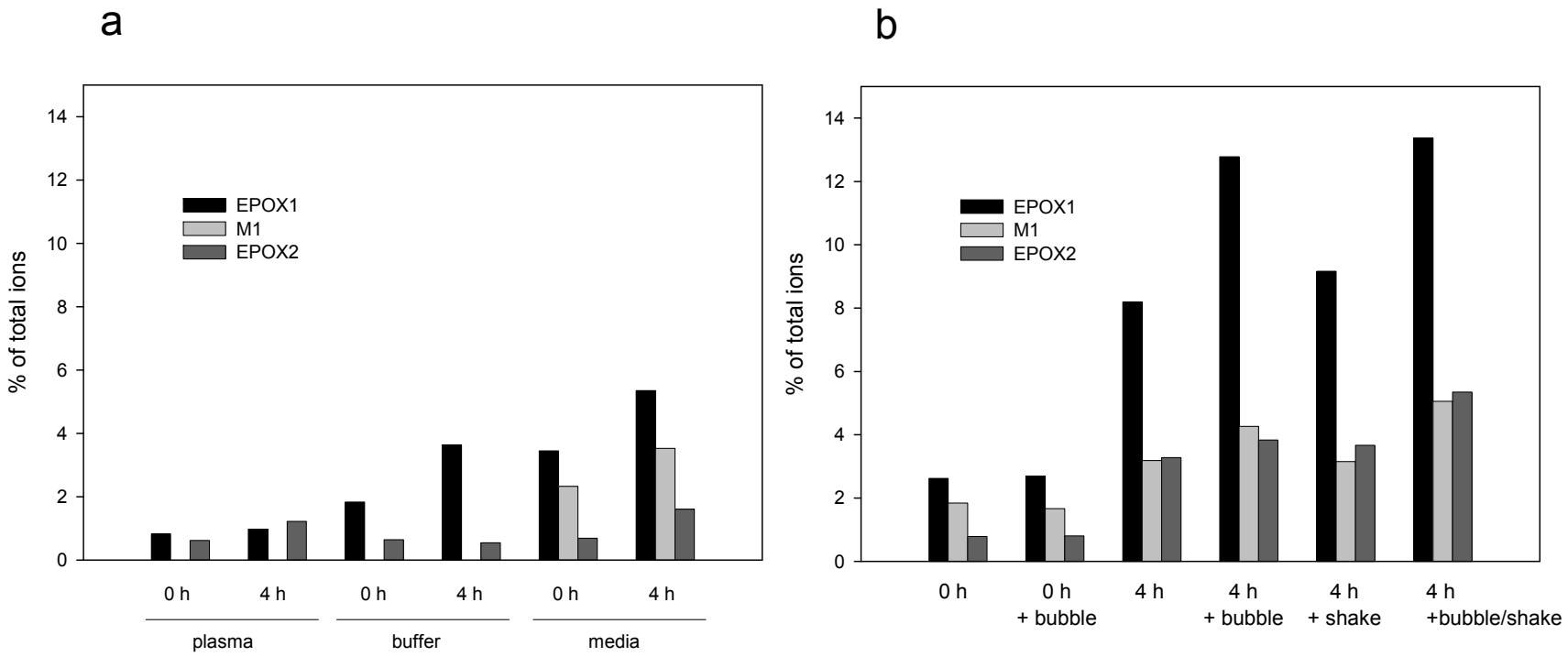

Fig. 35. Vincristine degradation in plasma, buffer, and media. VCR (15 μM) was incubated at 37°C in plasma, buffer, and media for 0 and 4 h (a). VCR (10 μM) was incubated in media for 0 and 4 h with different processing conditions (b). Before certain incubations, the media was bubbled with 95% oxygen. The impact of the shaker on degradation was also evaluated. The samples were assayed by LC/MS.

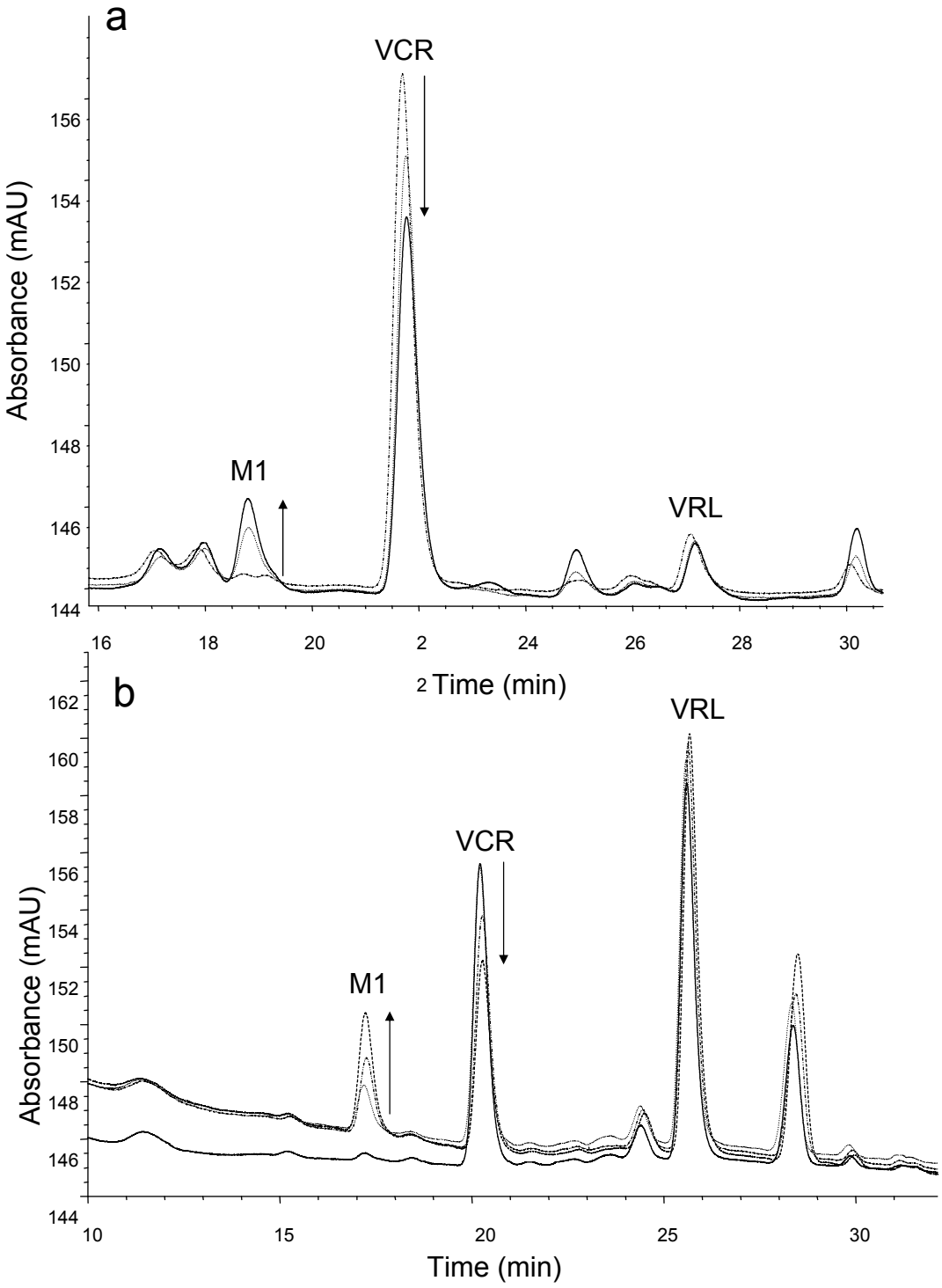

Fig. 36. UV chromatograms of M1 formation and vincristine depletion with intact hepatocytes (a) and hepatocyte cell lysate supplemented with NADPH (b). Vincristine (4 μM) was incubated with intact cells in media and a sonicated cell preparation from cryopreserved hepatocytes (lot EHI, 1.5 x 10^6 cells/mL) with NADPH. The intact cell incubation was quenched after 0, 1.5, and 4 h. The lysate preparation was quenched after 0, 10, 20, and 40 min. Arrows indicate the growth of M1 and the depletion of VCR over time. VRL is the internal standard. The peak at 25 min (a) is not VCR-related.

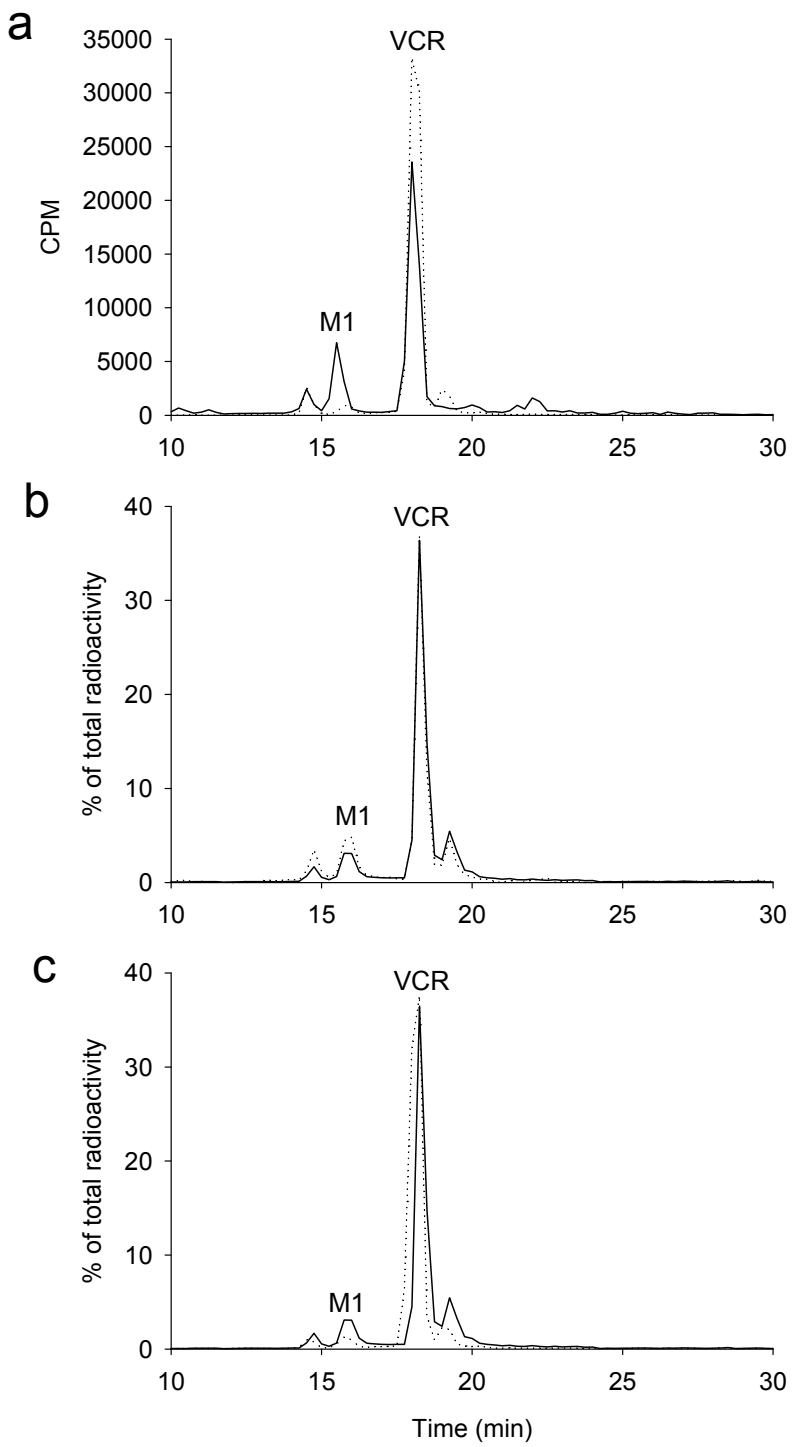

Fig. 37. Radiochromatograms of vincristine incubated with cryopreserved hepatocytes. VCR (8 μM) was incubated with two preparations of cryopreserved hepatocytes: cell lysate (a) and intact cells (b and c). For plot (a), the cell lysate was incubated with (solid line) and without (dotted line) supplemented NADPH. The media and cells were quenched with acetonitrile prior to analysis. For plot (b), the media (solid line) and cells (dotted line) were separated by centrifugation prior to the quench. For plot (c), the VCR was coincubated with (dotted line) and without ketoconazole (10 μM, solid line). The media was separated from the cells for analysis.

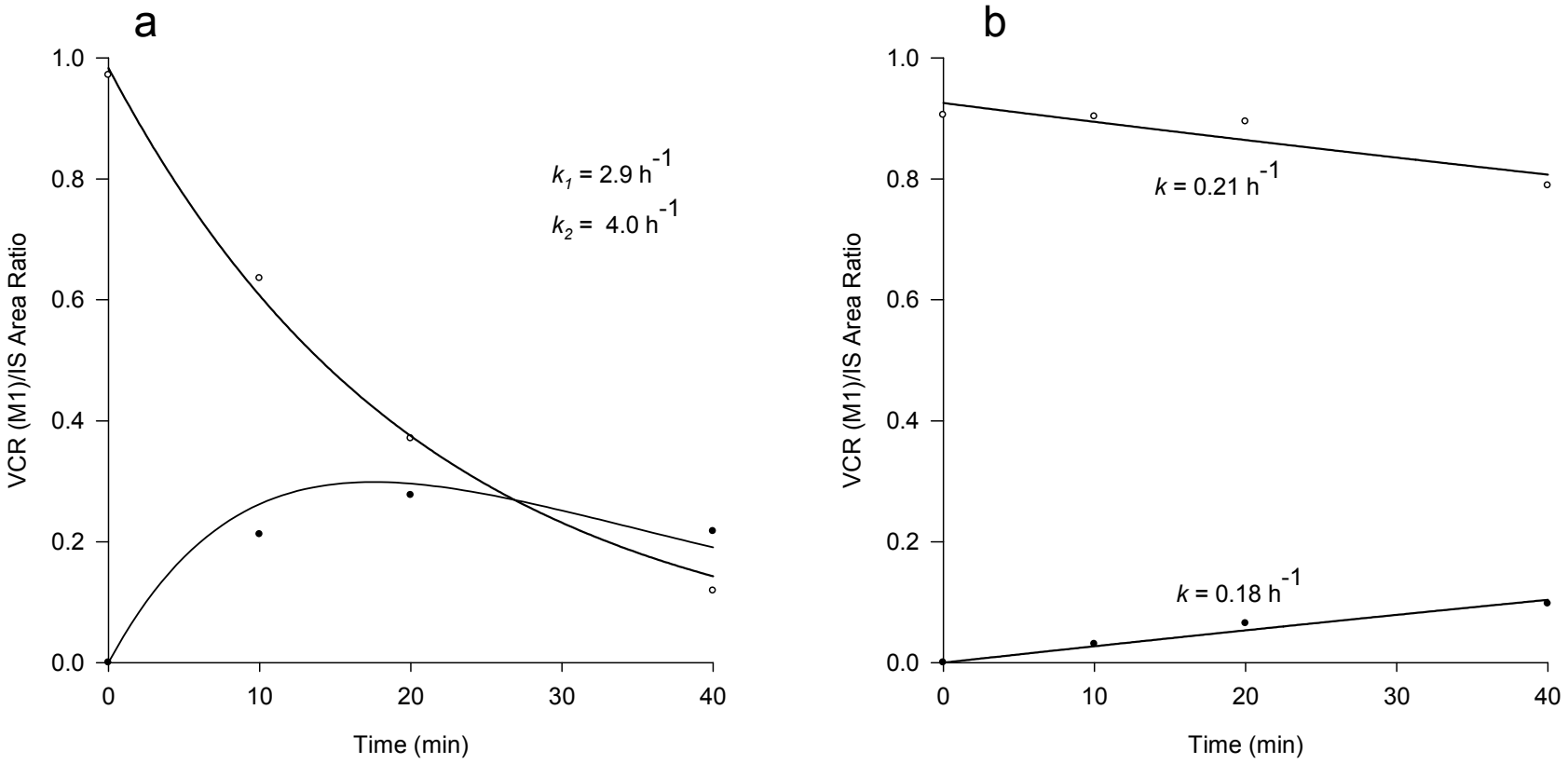

Fig. 38. Vincristine depletion and M1 formation with hepatocyte lysate of microsomal buffer. For VCR depletion and M1 formation, the first-order rate constants (k or k_1) were estimated by non-linear regression for multiple lots of hepatocytes including lot SCA (a) and ZYZ (b). For highly active hepatocytes such as lot SCA, the rate of M1 formation did not fit the model at late time points. An additional first-order rate constant for the degradation of M1 was calculated (k_2) assuming all the VCR was metabolized to M1. For lot FKM, the estimated k_1 was 2.0 h^{-1}, and the k_2 was 2.5 h^{-1}.

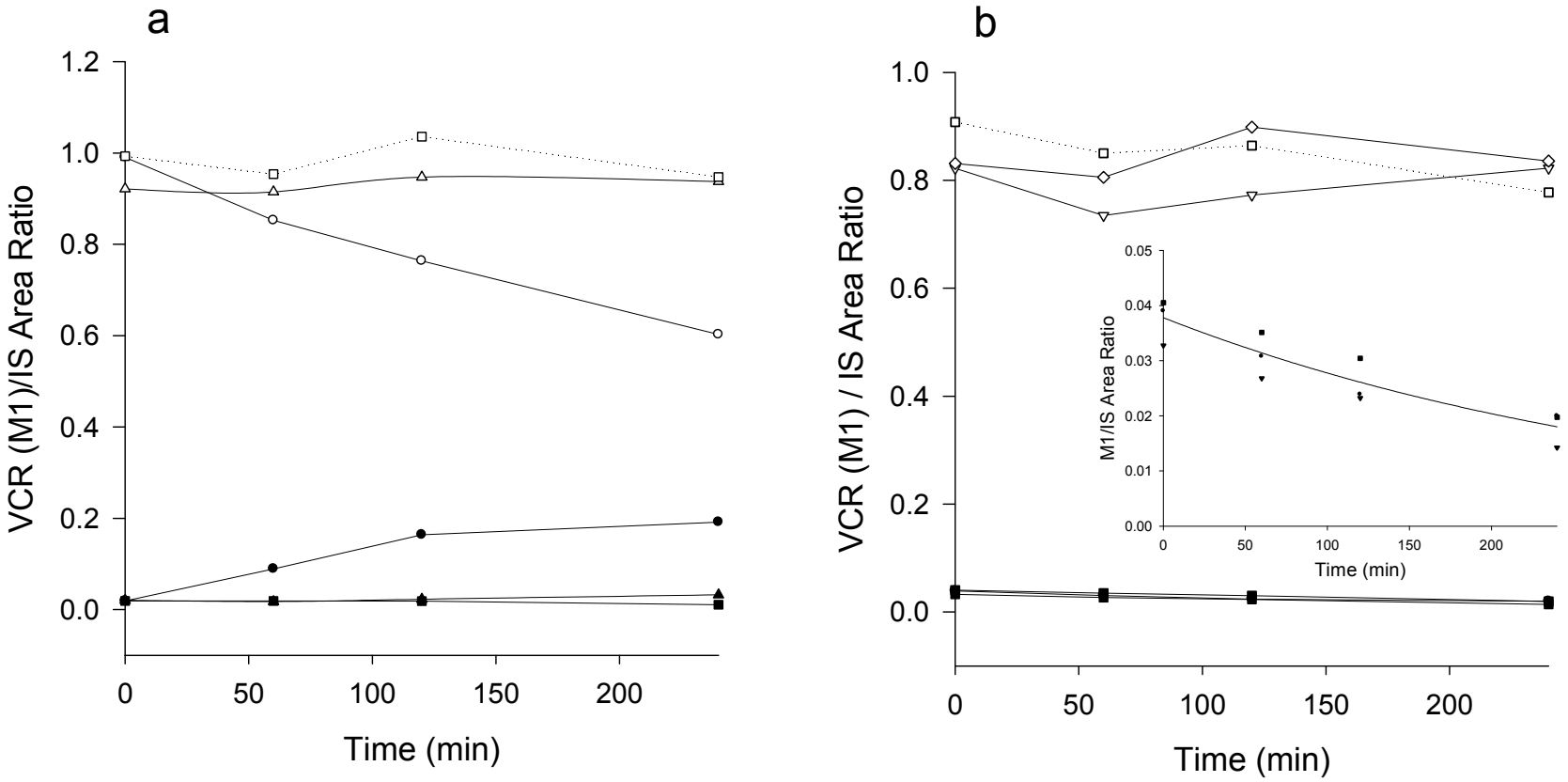

Fig. 39. Vincristine depletion and M1 formation with cryopreserved hepatocytes from one CYP3A5 high expresser (a) and one low expresser (b). Lots EHI (a) and MRS (b) were incubated with VCR (4 μM) alone (circles) and with ketoconazole (10 μM, squares). As an additional control, the hepatocytes were sonicated prior to use (triangles). The solutions were assayed for M1 (solid symbols) and VCR (open symbols) after various incubation times.

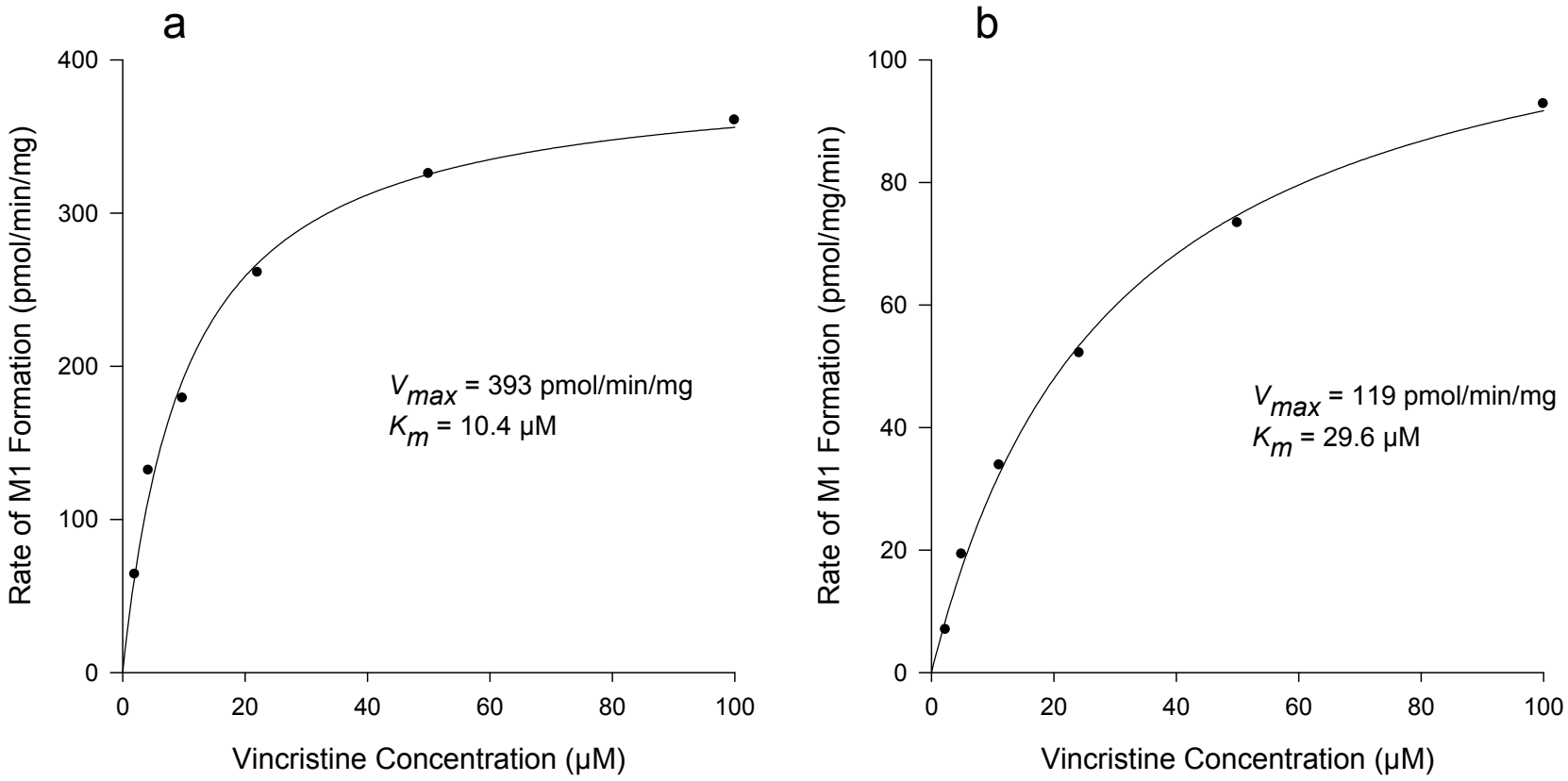

Fig. 40. Michaelis-Menten kinetics of M1 formation with cryopreserved hepatocytes (a) and hepatocyte lysate (b). VCR at various concentrations was incubated with lot EHI (1.5×10^6 cells/mL) for 90 min with intact cells and 13 min with the cell lysate. The rates of M1 formation were quantified by HPLC. The Michaelis-Menten constants were estimated using a one-enzyme model by non-linear regression.

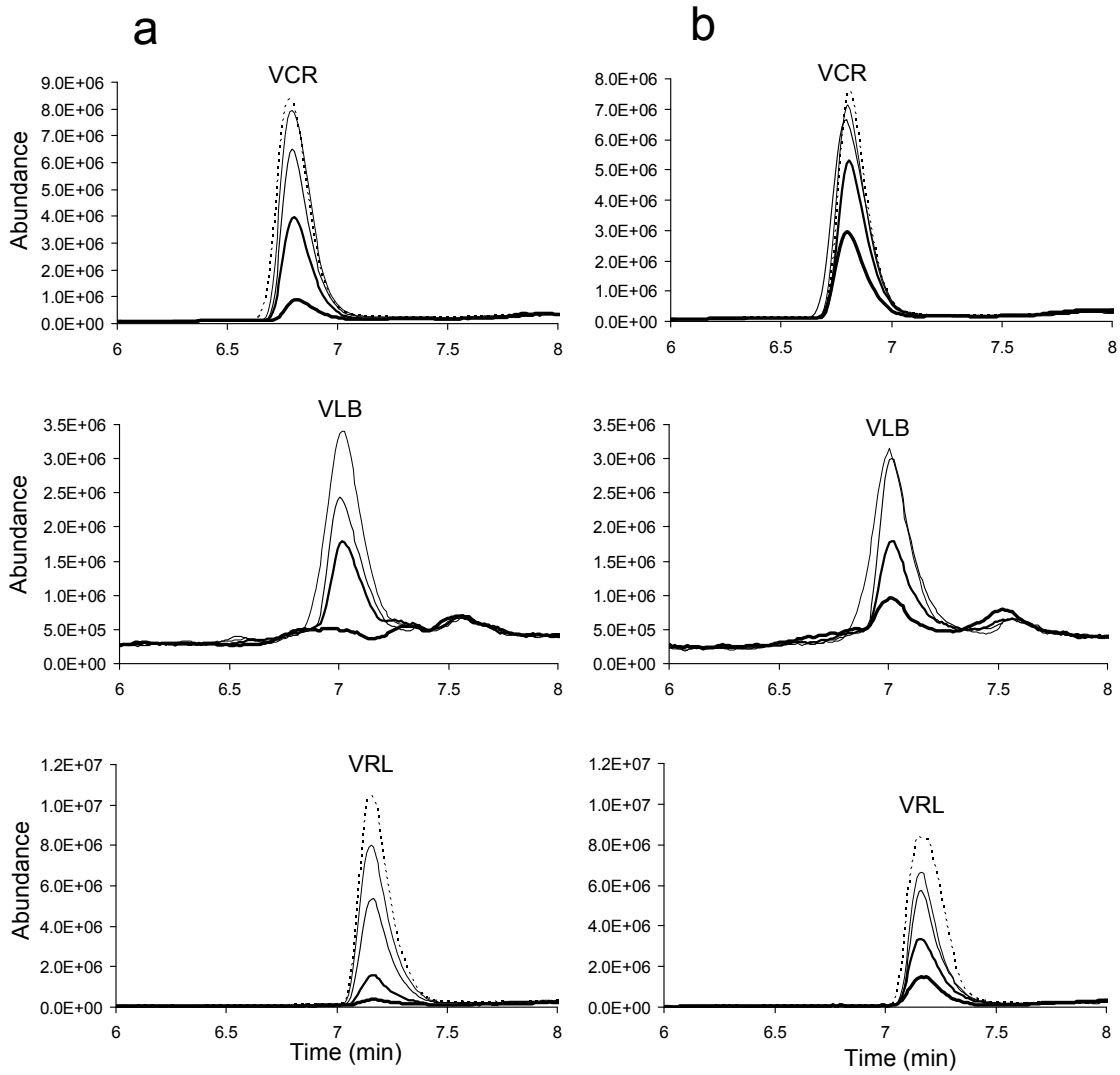

Fig. 41. Adsorption of vincristine, vinblastine, and vinorelbine to glass (a) and polypropylene (b) as a function of methanol concentration. VCR (0.1 μM) and VRL (0.1 μM) in water were formulated in glass or polypropylene tubes with 0, 10, 20, 30, and 40% methanol (dark to light lines). VLB (0.1 μM) was similarly formulated with 0, 20, 37, and 50% methanol (dark to light lines). The relative recoveries were measured by LC/MS.

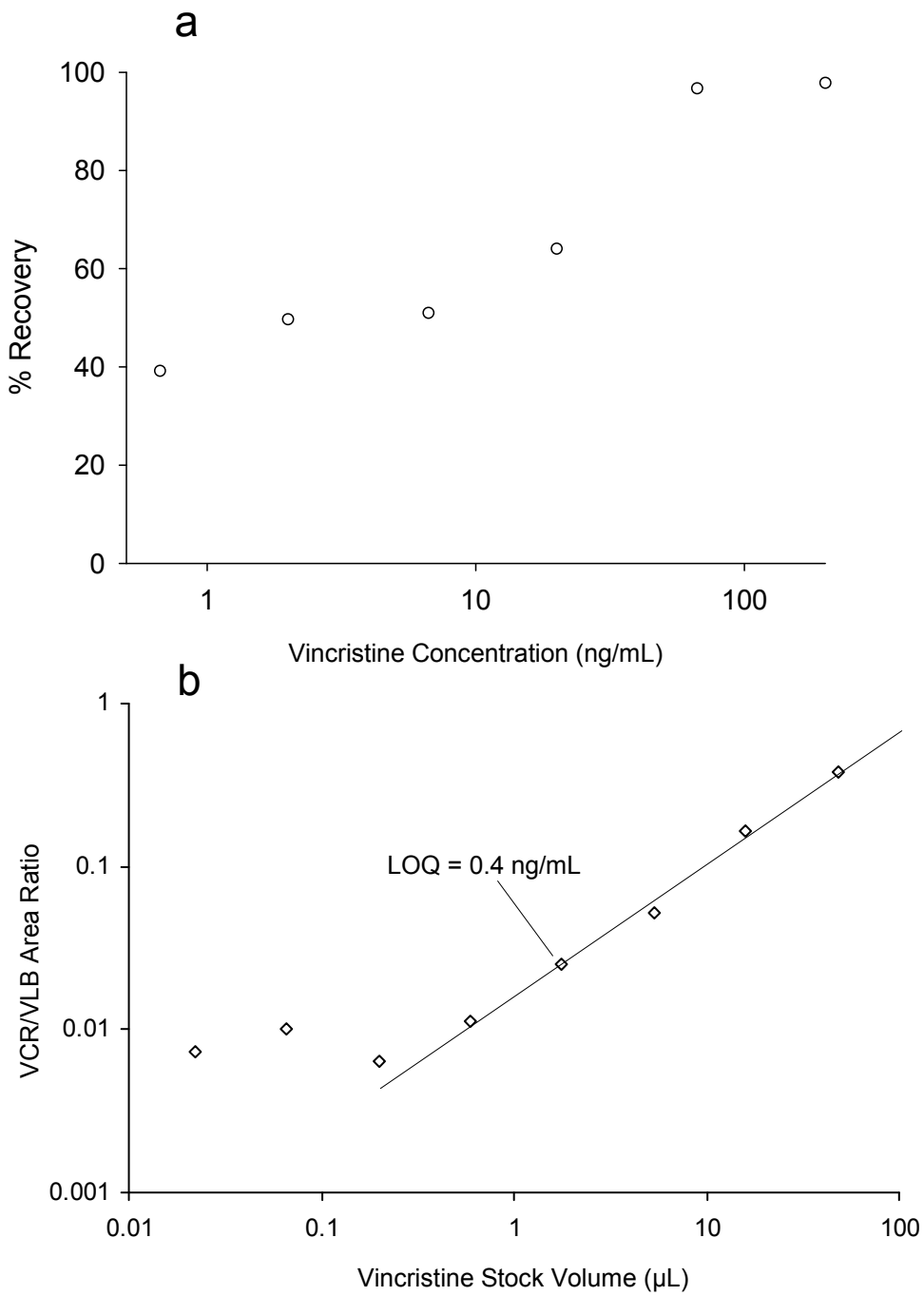

Fig. 42. LC/MS assay development issues – carrier effect of vinblastine with vincristine (a) and baseline interference using initial LC/MS gradient conditions (b). After evaporation, VCR was dissolved in 0.2% formic acid:methanol (20:80) in polypropylene tubes with and without VLB (130 ng/mL). For plot (a), the VCR abundance without VLB was expressed as a percentage of the abundance with VLB. For plot (b), VCR was extracted from plasma using the final extraction procedure. The residue was assayed by LC/MS using fast gradient conditions (see Methods).

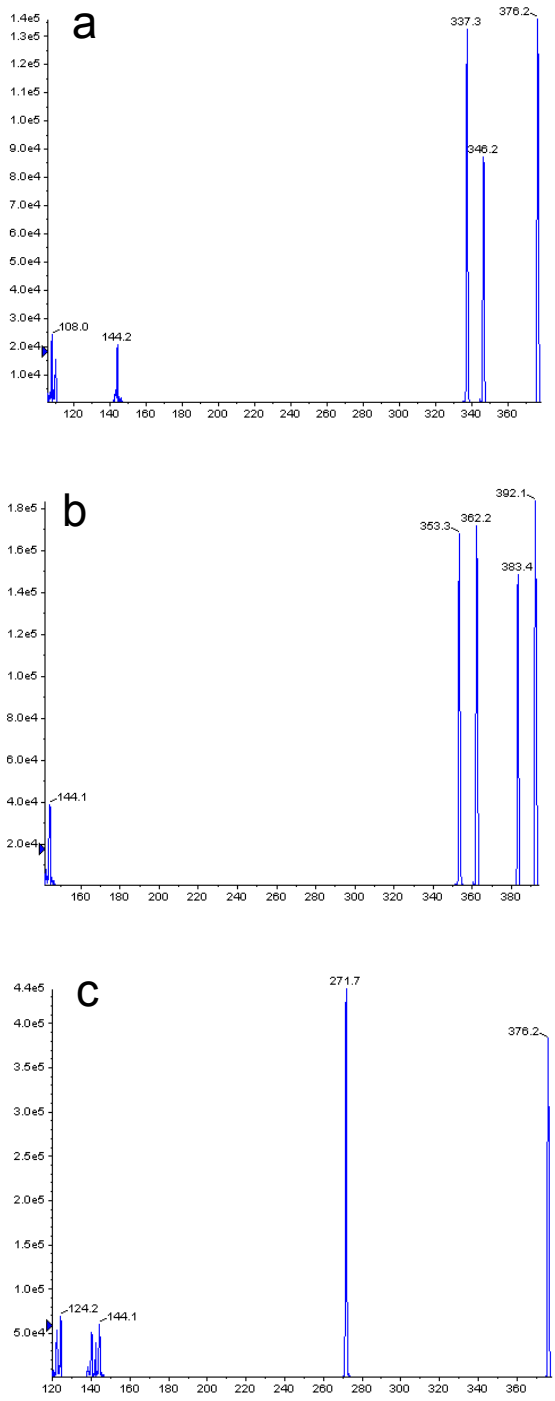

Fig. 43. Product ion spectra of M1 (a), vincristine (b), and the internal standard—vinblastine (c). The precursor ions were $[M+2H]^{2+}$ for all compounds.

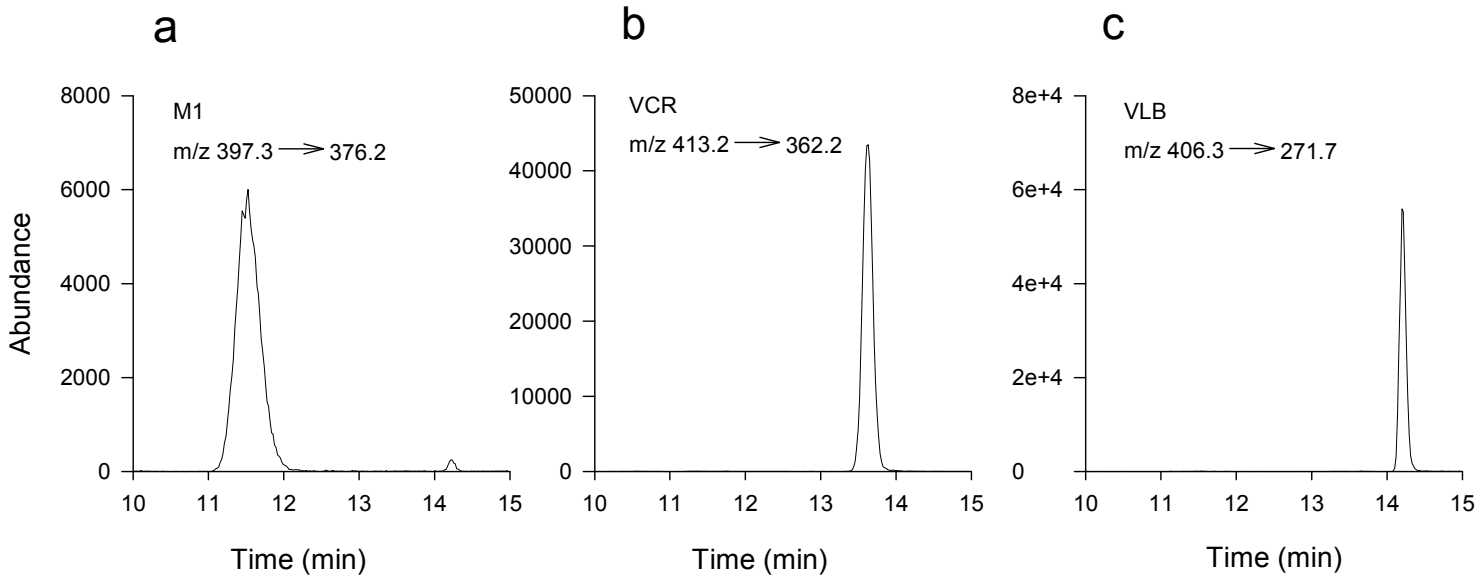

Fig. 44. Representative chromatograms of M1 (a), vincristine (b), and vinblastine (c) extracted from a plasma standard. Blank plasma was spiked with M1 at 4 ng/mL, vincristine at 8 ng/mL, and vinblastine (internal standard). The sample was extracted with methylene chloride and assayed by LC/MS/MS per the validated method. The monitored product ions (and approximate retention times) are as follows: M1 *m/z* 397.3 → 376.2 (11.3 min); vincristine *m/z* 413.2→ 362.2 (13.6 min); and vinblastine *m/z* 406.3→ 271.7 (14.0 min).

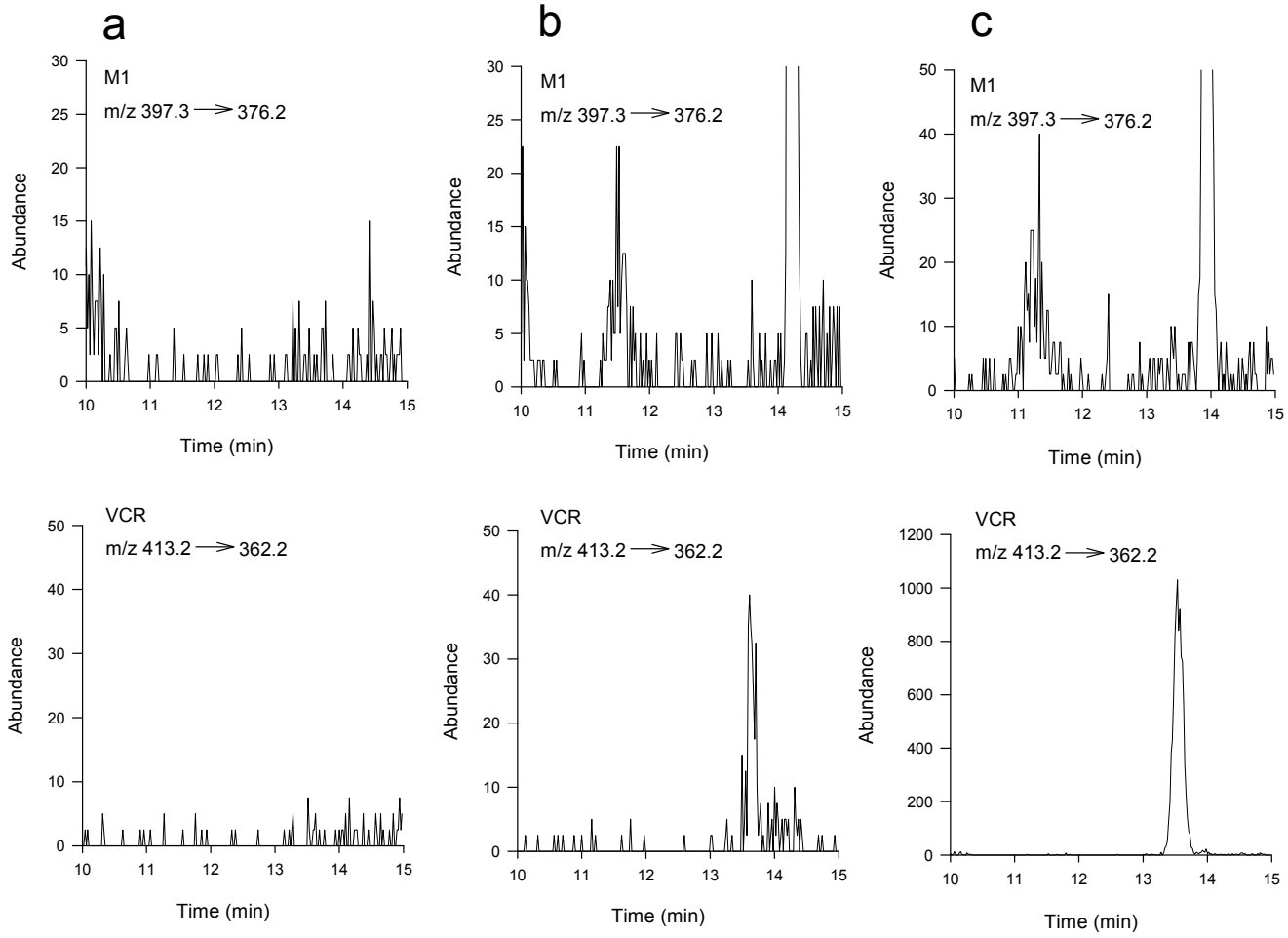

Fig. 45. Representative chromatograms of M1 and vincristine from blank plasma (a), a plasma standard at the LOQ (b), and a patient plasma sample (c). The M1 and VCR LOQ was 12 pg/mL. The patient plasma sample, subject 2, was collected 20 h after vincristine administration. For the patient sample, the estimated concentrations of M1 and vincristine were 31 pg/mL and 430 pg/mL, respectively.

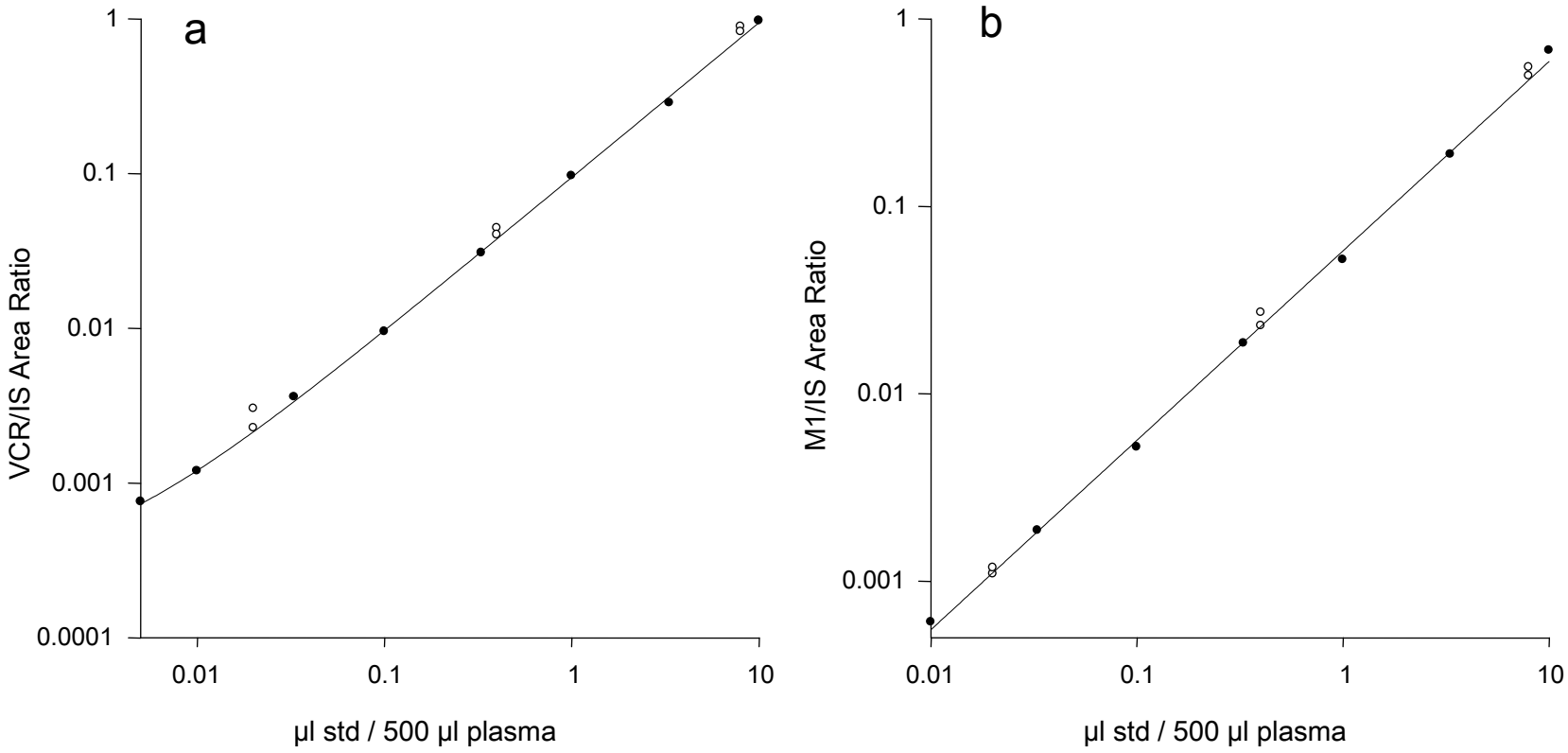

Fig. 46. Typical standard curves for vincristine and M1 quantification in plasma. To generate a standard curve, a stock solution of M1 and VCR was synthesized using cDNA-expressed CYP3A5. The stock solution is diluted with 0.2% formic acid: methanol (80:20, v/v) and spiked into 500 µL plasma at 8 concentrations (0.012 to 24 ng/mL VCR, 0.012 to 12 ng/mL M1, closed circles). Three separate QC concentrations were assayed in dpulicate (open circles).

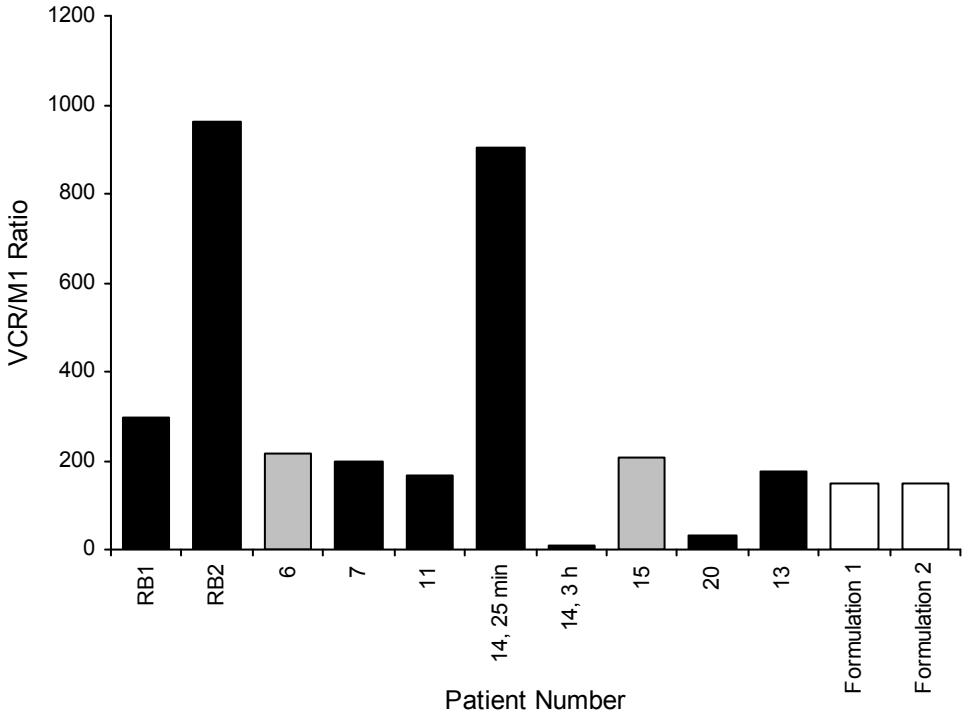

Fig. 47. Metabolite ratios (VCR/M1) in human urine. The M1 and VCR was quantified in urine samples from 2002—2004 clinical studies. Patients with at least one *CYP3A5*1* allele are represented by grey bars. Two samples of the neat IV formulation for VCR were also assayed (white bars).

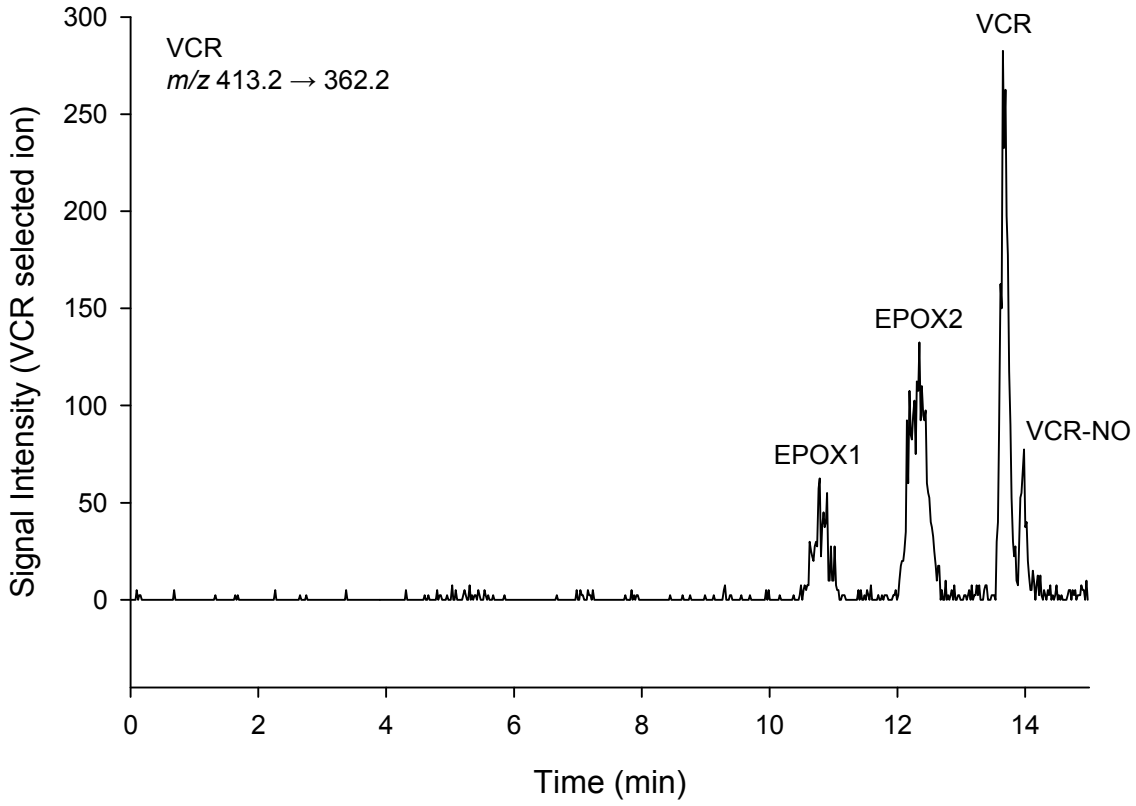

Fig. 48. Representative chromatogram of a plasma sample collected from the 2002—2004 clinical studies. Patient plasma samples were extracted per the validated method in 2007. Four separate peaks were evident by selected ion monitoring of VCR that correspond by retention time to EPOX1, EPOX2, VCR, and VCR-NO.

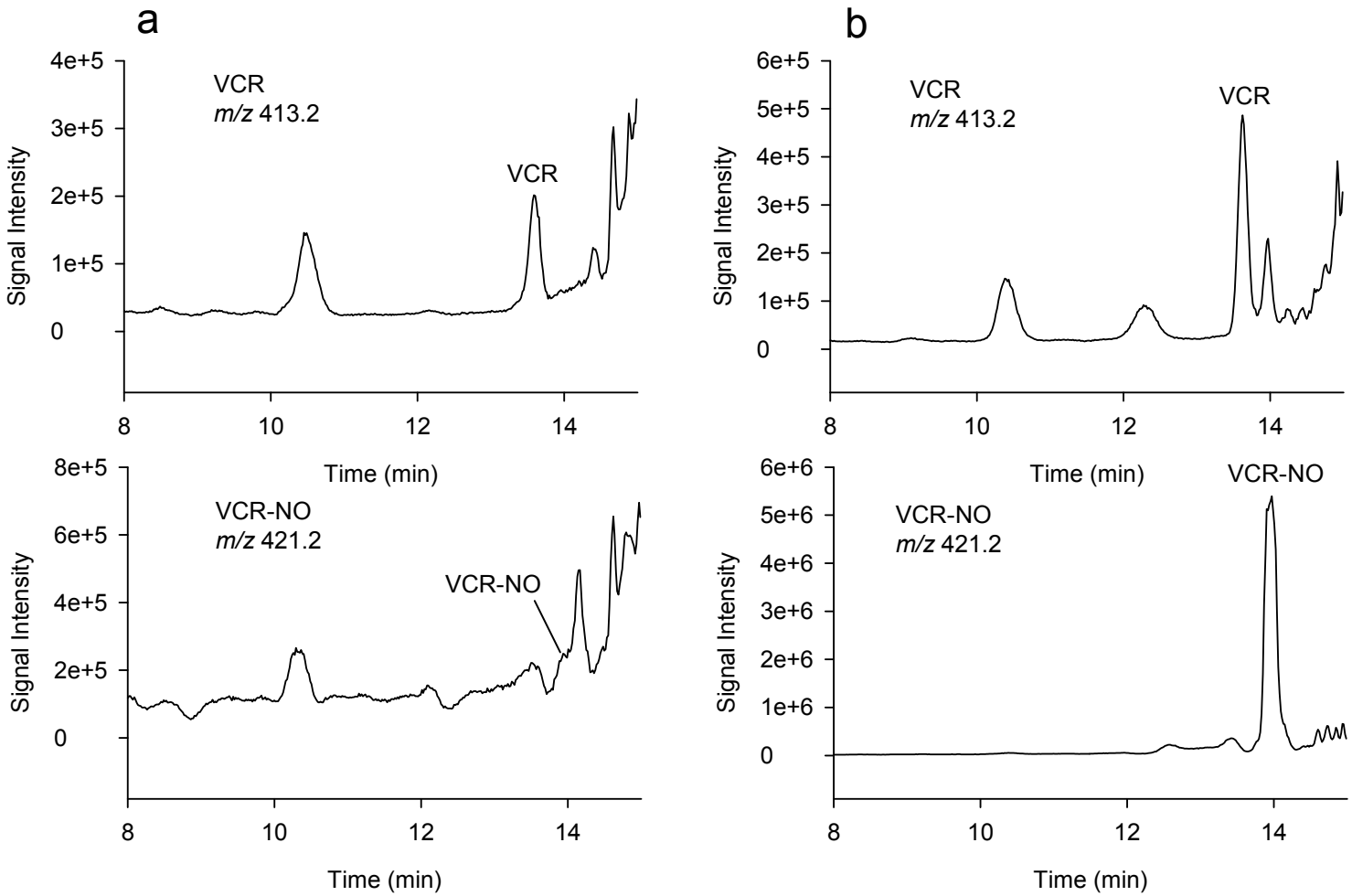

Fig. 49. LC/MS monitoring of vincristine and vincristine N-oxide in plasma samples collected from the 2002—2004 clinical studies. The Q1 signal intensities of VCR and VCR-NO were monitored for a plasma standard spiked with stock solution of VCR and M1 (a) and a patient sample from the 2002—2004 study (b).

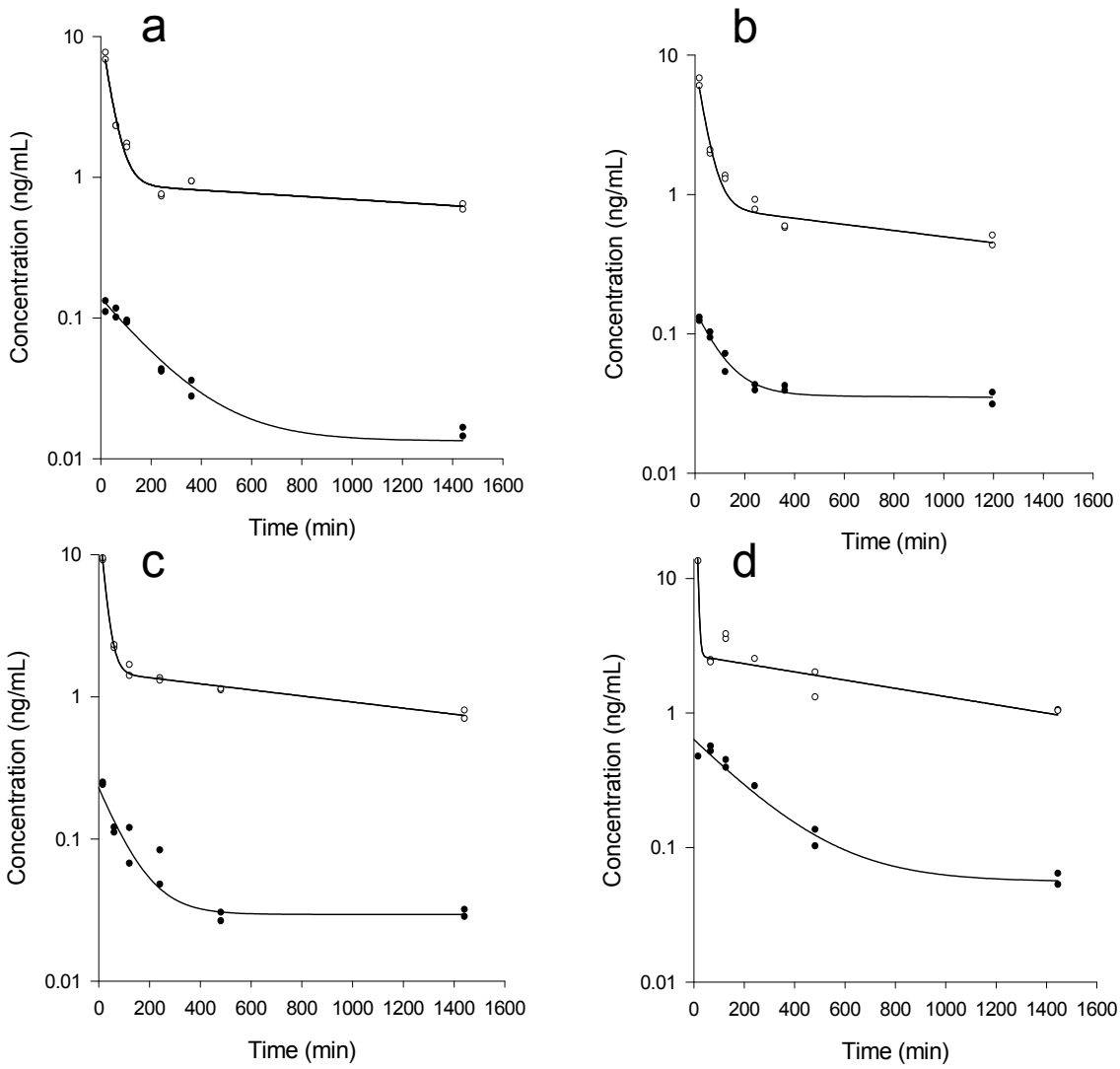

Fig. 50. Semi-logarithmic vincristine and M1 concentrations versus time profiles of four patients. Vincristine (open symbols) and M1 (solid symbols) were fitted data using non-linear regression and a two-compartment model ($1/y^2$ weighting for VCR and no weighting for M1). None of the patients were CYP3A5 high expressers.

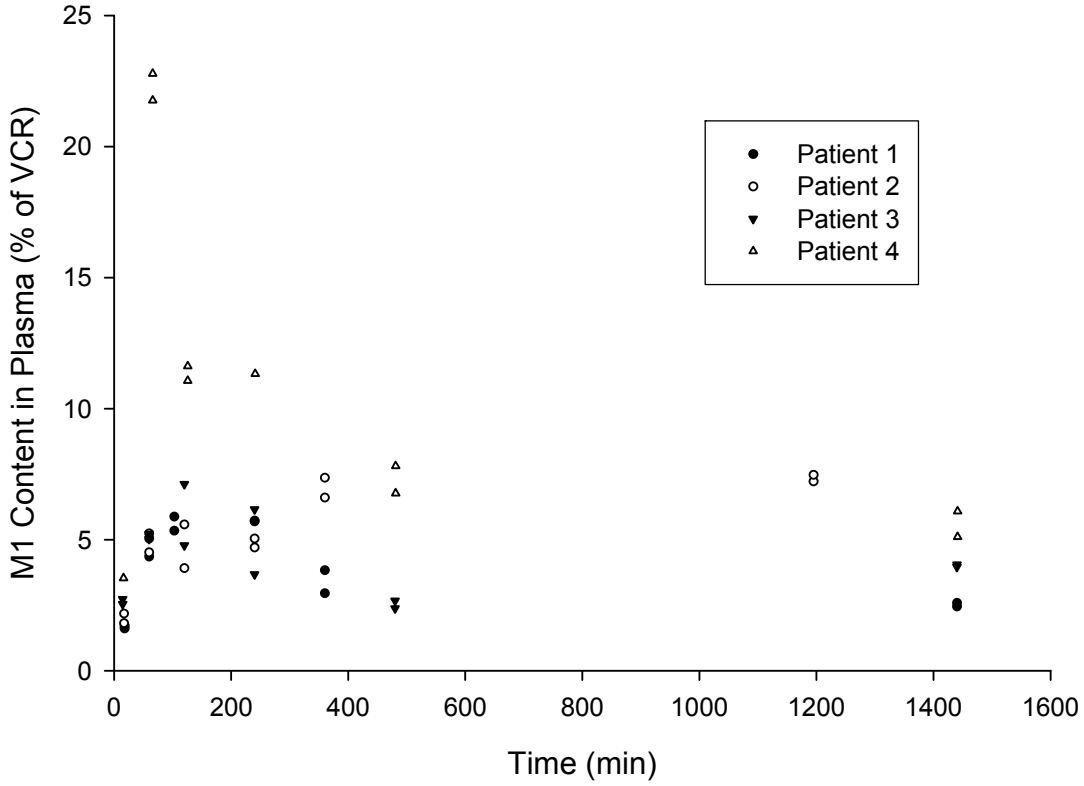

Fig. 51. Relative M1 content in plasma samples from rhabdomyosarcoma patients. The M1 concentration was plotted as a percentage of the vincristine concentration at each time point.

VIII. References

1. Johnson, I.; Armstrong, J.; Gorman, M.; Burnett, J. *Cancer Research* 1963; **23**: 1390-1427.

2. Noble, R. L.; Beer, C. T.; Cutts, J. H. *Ann. N. Y. Acad. Sci.* 1958; **76**: 882-894.

3. Julsing, M. K.; Koulman, A.; Woerdenbag, H. J.; Quax, W. J.; Kayser, O. *Biomol. Eng* 2006; **23**: 265-279.

4. van der, H. R.; Jacobs, D. I.; Snoeijer, W.; Hallard, D.; Verpoorte, R. *Curr. Med. Chem.* 2004; **11**: 607-628.

5. Kuboyama, T.; Yokoshima, S.; Tokuyama, H.; Fukuyama, T. *Proc. Natl. Acad. Sci. U. S. A* 2004; **101**: 11966-11970.

6. *The Merck Index*; Merck & Co., Inc.: 1996.

7. Owellen, R. J.; Donigian, D. W.; Hartke, C. A.; Hains, F. O. *Biochem. Pharmacol.* 1977; **26**: 1213-1219.

8. Sethi, V.; Shimmaiah, K. *Cancer Research* 1985; **45**: 5386-5389.

9. Ahn, S. H.; Duffel, M. W.; Rosazza, J. P. *J. Nat. Prod.* 1997; **60**: 1125-1129.

10. Zhou, X.; Placidi, M.; Rahmani, R. *Anticancer Research* 1994; **14**: 1017-1022.

11. Bender, R. A.; Castle, M. C.; Margileth, D. A.; Oliverio, V. T. *Clin. Pharmacol. Ther.* 1977; **22**: 430-435.

12. Jackson, D. V., Jr.; Castle, M. C.; Bender, R. A. *Clin. Pharmacol. Ther.* 1978; **24**: 101-107.

13. Owellen, R. J.; Hartke, C. A.; Hains, F. O. *Cancer Res.* 1977; **37**: 2597-2602.

14. Jehl, F.; Quoix, E.; Leveque, D.; Pauli, G.; Breillout, F.; Krikorian, A. *Cancer Research* 1991; **51**: 2073-2076.

15. Van Heugen, J. C.; De, G. J.; Zorza, G.; Puozzo, C. *J. Chromatogr. A* 2001; **926**: 11-20.

16. Rahmani, R.; Zhou, X. *Cancer Surveys* 1993; **17**: 269-281.

17. Gigant, B.; Wang, C.; Ravelli, R. B.; Roussi, F.; Steinmetz, M. O.; Curmi, P. A.; Sobel, A.; Knossow, M. *Nature* 2005; **435**: 519-522.

18. Lobert, S.; Fahy, J.; Hill, B. T.; Duflos, A.; Etievant, C.; Correia, J. J. *Biochemistry* 2000; **39**: 12053-12062.

19. Verrills, N. M.; Po'uha, S. T.; Liu, M. L.; Liaw, T. Y.; Larsen, M. R.; Ivery, M. T.; Marshall, G. M.; Gunning, P. W.; Kavallaris, M. *J. Natl. Cancer Inst.* 2006; **98**: 1363-1374.

20. Verrills, N. M.; Liem, N. L.; Liaw, T. Y.; Hood, B. D.; Lock, R. B.; Kavallaris, M. *Proteomics*. 2006; **6**: 1681-1694.

21. Deschesnes, R. G.; Patenaude, A.; Rousseau, J. L.; Fortin, J. S.; Ricard, C.; Cote, M. F.; Huot, J.; Gaudreault, R.; Petitclerc, E. *J. Pharmacol. Exp. Ther.* 2007; **320**: 853-864.

22. Wang, M. S.; Wu, Y.; Culver, D. G.; Glass, J. D. *J. Neuropathol. Exp. Neurol.* 2000; **59**: 599-606.

23. Lobert, S.; Frankfurter, A.; Correia, J. J. *Cell Motil. Cytoskeleton* 1998; **39**: 107-121.

24. Gloeckler Ries LA, Percy CL, Bunin GR. SEER Pediatric Monograph. 2007. National Cancer Institute.

25. www.nci.nih.gov . 2007. National Cancer Institute.

26. Cavaletti, G.; Marmiroli, P. *Expert. Opin. Drug Saf* 2004; **3**: 535-546.

27. McCune, J.; Lindley, C. *American Journal of Health Systems Pharmacy* 1997; **54**: 1755-1758.

28. Bohme, A.; Ganser, A.; Hoelzer, D. *Annals of Hematology* 1995; **71**: 311-312.

29. Kamaluddin, M.; McNally, P.; Breatnach, F.; O'Marcaigh, A.; Webb, D.; O'Dell, E.; Scanlon, P.; Butler, K.; O'Meara, A. *Acta Pediatrica* 2001; **90**: 1204-1207.

30. Murphy, J.; Ross, L.; Gibson, B. *Lancet* 1995; **346**: 443.

31. Sathiapalan, R.; El-Solh, H. *Pediatric Hematology and Oncology* 2001; **18**: 543-546.

32. Picard, N.; Djebli, N.; Sauvage, F. L.; Marquet, P. *Drug Metab Dispos.* 2007; **35**: 350-355.

33. Wang, E. J.; Lew, K.; Casciano, C. N.; Clement, R. P.; Johnson, W. W. *Antimicrob. Agents Chemother.* 2002; **46**: 160-165.

34. Isoherranen, N.; Kunze, K. L.; Allen, K. E.; Nelson, W. L.; Thummel, K. E. *Drug Metab Dispos.* 2004; **32**: 1121-1131.

35. Chan, J. *Pharmacotherapy* 1998; **18**: 1304-1307.

36. Kim, R. B.; Wandel, C.; Leake, B.; Cvetkovic, M.; Fromm, M. F.; Dempsey, P. J.; Roden, M. M.; Belas, F.; Chaudhary, A. K.; Roden, D. M.; Wood, A. J.; Wilkinson, G. R. *Pharm. Res.* 1999; **16**: 408-414.

37. Desta, Z.; Soukhova, N. V.; Flockhart, D. A. *Antimicrob. Agents Chemother.* 2001; **45**: 382-392.

38. Whitelaw, D. M.; Cowan, D. H.; Cassidy, F. R.; Patterson, T. A. *Cancer Chemother. Rep.* 1963; **30**: 13-20.

39. Veerman, A. J.; Hahlen, K.; Kamps, W. A.; Van Leeuwen, E. F.; de Vaan, G. A.; Solbu, G.; Suciu, S.; van Wering, E. R.; Van der Does-Van der Berg *J. Clin. Oncol.* 1996; **14**: 911-918.

40. Pollock, B.; DeBaun, M.; Camitta, B.; Shuster, J.; Ravindranath, Y.; Pullen, D.; Land, V.; Mahoney, D. J.; Lauer, S.; Murphy, S. *Journal of Clinical Oncology* 2000; **18**: 813-823.

41. Lange, B. J.; Bostrom, B. C.; Cherlow, J. M.; Sensel, M. G.; La, M. K.; Rackoff, W.; Heerema, N. A.; Wimmer, R. S.; Trigg, M. E.; Sather, H. N. *Blood* 2002; **99**: 825-833.

42. Bhatia, S.; Sather, H. N.; Heerema, N. A.; Trigg, M. E.; Gaynon, P. S.; Robison, L. L. *Blood* 2002; **100**: 1957-1964.

43. Renbarger JL. 2007. unpublished data.

44. Sethi, V.; Jackson, D.; White, D.; Richards, F.; Stuart, J.; Muss, H.; Cooper, M.; Spurr, C. *Cancer Research* 1981; **41**: 3551-3555.

45. Wierzba, K.; Sugiyama, Y.; Okudaira, K.; Iga, T.; Hanano, M. *J. Pharm. Sci.* 1987; **76**: 872-875.

46. Ahn, Y. S.; Harrington, W. J.; Byrnes, J. J.; Pall, L.; McCrainie, J. *JAMA* 1983; **249**: 2189-2194.

47. Donigian, D. W.; Owellen, R. J. *Biochem. Pharmacol.* 1973; **22**: 2113-2119.

48. Mayer, L. D.; St-Onge, G. *Anal. Biochem.* 1995; **232**: 149-157.

49. Ho, R. H.; Kim, R. B. *Clin. Pharmacol. Ther.* 2005; **78**: 260-277.

50. van, T. O.; Buckle, T.; Jonker, J. W.; van, d., V; Beijnen, J. H. *Br. J. Cancer* 2003; **89**: 1776-1782.

51. Kellie, S.; Barbaric, D.; Koopmans, P.; Earl, J.; Carr, D.; de Graaf, S. *Cancer* 2002; **94**: 1815-1820.

52. Nelson, R. *Medical and Pediatric Oncology* 1982; **10**: 115-127.

53. Van den Berg, H.; Desai, Z.; Wilson, R.; Kennedy, G.; Bridges, J.; Shanks, R. *Cancer Chemotherapy and Pharmacology* 1982; **8**: 215-219.

54. Frost, B. M.; Lonnerholm, G.; Koopmans, P.; Abrahamsson, J.; Behrendtz, M.; Castor, A.; Forestier, E.; Uges, D. R.; de Graaf, S. S. *Acta Paediatr.* 2003; **92**: 551-557.

55. Fedeli, L.; Colozza, M.; Boschetti, E.; Sabalich, I.; Aristei, C.; Guerciolini, R.; Del, F. A.; Rossetti, R.; Tonato, M.; Rambotti, P.; . *Cancer* 1989; **64**: 1805-1811.

56. Crom, W.; de Graaf, S.; Synold, T.; Uges, D.; Bloemhof, H.; Rivera, G.; Christensen, M.; Mahmoud, H.; Evans, W. *Journal of Pediatrics* 1994; **125**: 642-649.

57. de Graaf, S.; Bloemhof, H.; Vendrig, D.; Uges, D. *Medical and Pediatric Oncology* 1995; **24**: 235-240.

58. Gidding, C.; Meeuwsen-de Boer, G.; Koopmans, P.; Uges, D.; Kamps, W.; de Graaf, S. *Cancer Chemotherapy and Pharmacology* 1999; **44**: 203-209.

59. Groninger, E.; Meeuwsen-de Boar, T.; Koopmans, P.; Uges, D.; Sluiter, W.; Veerman, A.; Kamps, W.; de Graaf, S. *Pediatric Research* 2002; **52**: 113-118.

60. Kellie, S. J.; Koopmans, P.; Earl, J.; Nath, C.; Roebuck, D.; Uges, D. R.; de Graaf, S. S. *Cancer* 2004; **100**: 2637-2643.

61. Groninger, E.; Meeuwsen-de, B. T.; Koopmans, P.; Uges, D.; Sluiter, W.; Veerman, A.; Kamps, W.; de, G. S. *Eur. J. Cancer* 2005; **41**: 98-103.

62. Bloemhof, H.; Van Dijk, K. N.; de Graaf, S. S.; Vendrig, D. E.; Uges, D. R. *J. Chromatogr.* 1991; **572**: 171-179.

63. Lewis DF *Guide to Cytochromes P450 Structure and Function*; Taylor and Francis: 2001.

64. Denisov, I. G.; Makris, T. M.; Sligar, S. G.; Schlichting, I. *Chem. Rev.* 2005; **105**: 2253-2277.

65. Schenkman, J. B.; Jansson, I. *Pharmacol. Ther.* 2003; **97**: 139-152.

66. Porter, T. D. *J. Biochem. Mol. Toxicol.* 2002; **16**: 311-316.

67. Yamazaki, H.; Nakano, M.; Imai, Y.; Ueng, Y. F.; Guengerich, F. P.; Shimada, T. *Arch. Biochem. Biophys.* 1996; **325**: 174-182.

68. Loughran, P. A.; Roman, L. J.; Miller, R. T.; Masters, B. S. *Arch. Biochem. Biophys.* 2001; **385**: 311-321.

69. McCune, J. S.; Risler, L. J.; Phillips, B. R.; Thummel, K. E.; Blough, D.; Shen, D. D. *Drug Metab Dispos.* 2005; **33**: 1074-1081.

70. Lin, H. L.; Hollenberg, P. F. *J. Pharmacol. Exp. Ther.* 2007; **321**: 276-287.

71. Huang, W.; Lin, Y. S.; McConn, D. J.; Calamia, J. C.; Totah, R. A.; Isoherranen, N.; Glodowski, M.; Thummel, K. E. *Drug Metab Dispos.* 2004; **32**: 1434-1445.

72. Bosterling, B.; Trudell, J. R. *J. Biol. Chem.* 1982; **257**: 4783-4787.

73. Zhang, H.; Im, S. C.; Waskell, L. *J. Biol. Chem.* 2007.

74. He, P.; Court MH; Greenblatt, D. J.; Von Moltke, L. L. *Clin. Pharmacol. Ther.* 2005; **77**: 373-387.

75. Xie, H. G.; Wood, A. J.; Kim, R. B.; Stein, C. M.; Wilkinson, G. R. *Pharmacogenomics.* 2004; **5**: 243-272.

76. Kuehl, P.; Zhang, J.; Lin, Y.; Lamba, J.; Assem, M.; Schuetz, J.; Watkins, P.; Daly, A.; Wrighton, S.; Hall, S.; Maurel, P.; Relling, M.; Brimer, C.; Yasuda, K.; Venkataramanan, R.; Strom, S.; Thummel, K.; Boguski, M.; Schuetz, E. *Nature Genetics* 2001; **27**: 383-391.

77. Hustert, E.; Haberl, M.; Burk, O.; Wolbold, R.; He, Y.; Klein, K.; Nuessler, A.; Neuhaus, P.; Klattig, J.; Eiselt, R.; Koch, I.; Zibat, A.; Brockmoller, J.; Halpert, J.; Zanger, U.; Wojnowski, L. *Pharmacogenetics* 2001; **11**: 773-779.

78. Shimada, T.; Yamazaki, H.; Mimura, M.; Inui, Y.; Guengerich, F. *Journal of Pharmacology and Experimental Therapeutics* 1994; **270**: 414-432.

79. Thummel, K. E.; Shen, D. D.; Podoll, T. D.; Kunze, K. L.; Trager, W. F.; Bacchi, C. E.; Marsh, C. L.; McVicar, J. P.; Barr, D. M.; Perkins, J. D.; . *J. Pharmacol. Exp. Ther.* 1994; **271**: 557-566.

80. Westlind-Johnsson, A.; Malmebo, S.; Johansson, A.; Otter, C.; Andersson, T. B.; Johansson, I.; Edwards, R. J.; Boobis, A. R.; Ingelman-Sundberg, M. *Drug Metab Dispos.* 2003; **31**: 755-761.

81. Lin, Y. S.; Dowling, A. L.; Quigley, S. D.; Farin, F. M.; Zhang, J.; Lamba, J.; Schuetz, E. G.; Thummel, K. E. *Mol. Pharmacol.* 2002; **62**: 162-172.

82. Floyd, M. D.; Gervasini, G.; Masica, A. L.; Mayo, G.; George, A. L., Jr.; Bhat, K.; Kim, R. B.; Wilkinson, G. R. *Pharmacogenetics* 2003; **13**: 595-606.

83. Pascussi, J. M.; Gerbal-Chaloin, S.; Drocourt, L.; Maurel, P.; Vilarem, M. J. *Biochim. Biophys. Acta* 2003; **1619**: 243-253.

84. Burk, O.; Koch, I.; Raucy, J.; Hustert, E.; Eichelbaum, M.; Brockmoller, J.; Zanger, U. M.; Wojnowski, L. *J. Biol. Chem.* 2004; **279**: 38379-38385.

85. Koch, I.; Weil, R.; Wolbold, R.; Brockmoller, J.; Hustert, E.; Burk, O.; Nuessler, A.; Neuhaus, P.; Eichelbaum, M.; Zanger, U.; Wojnowski, L. *Drug Metab Dispos.* 2002; **30**: 1108-1114.

86. Perrett, H.; Barter, Z.; Jones, B.; Yamazaki, H.; Tucker, G.; Rostami-Hodjegan, A. *Drug Metab Dispos.* 2007.

87. Jones, D. R.; Gorski, J. C.; Hamman, M. A.; Mayhew, B. S.; Rider, S.; Hall, S. D. *J. Pharmacol. Exp. Ther.* 1999; **290**: 1116-1125.

88. McConn, D. J.; Lin, Y. S.; Allen, K.; Kunze, K. L.; Thummel, K. E. *Drug Metab Dispos.* 2004; **32**: 1083-1091.

89. Wang, Y. H.; Jones, D. R.; Hall, S. D. *Drug Metab Dispos.* 2005; **33**: 664-671.

90. Gibbs, M. A.; Thummel, K. E.; Shen, D. D.; Kunze, K. L. *Drug Metab Dispos.* 1999; **27**: 180-187.

91. Soars, M. G.; Grime, K.; Riley, R. J. *Xenobiotica* 2006; **36**: 287-299.

92. Suh, J. W.; Koo, B. K.; Zhang, S. Y.; Park, K. W.; Cho, J. Y.; Jang, I. J.; Lee, D. S.; Sohn, D. W.; Lee, M. M.; Kim, H. S. *CMAJ.* 2006; **174**: 1715-1722.

93. Yu, K. S.; Cho, J. Y.; Jang, I. J.; Hong, K. S.; Chung, J. Y.; Kim, J. R.; Lim, H. S.; Oh, D. S.; Yi, S. Y.; Liu, K. H.; Shin, J. G.; Shin, S. G. *Clin. Pharmacol. Ther.* 2004; **76**: 104-112.

94. Jin, Y.; Wang, Y. H.; Miao, J.; Li, L.; Kovacs, R. J.; Marunde, R.; Hamman, M. A.; Phillips, S.; Hilligoss, J.; Hall, S. D. *Clin. Pharmacol. Ther.* 2007; **82**: 579-585.

95. Williams, J. A.; Ring, B. J.; Cantrell, V. E.; Jones, D. R.; Eckstein, J.; Ruterbories, K.; Hamman, M. A.; Hall, S. D.; Wrighton, S. A. *Drug Metab Dispos.* 2002; **30**: 883-891.

96. Patki, K. C.; Von Moltke, L. L.; Greenblatt, D. J. *Drug Metab Dispos.* 2003; **31**: 938-944.

97. Kamdem, L. K.; Streit, F.; Zanger, U. M.; Brockmoller, J.; Oellerich, M.; Armstrong, V. W.; Wojnowski, L. *Clin. Chem.* 2005; **51**: 1374-1381.

98. Walsky, R. L.; Obach, R. S. *Drug Metab Dispos.* 2004; **32**: 647-660.

99. Dai, Y.; Hebert, M. F.; Isoherranen, N.; Davis, C. L.; Marsh, C.; Shen, D. D.; Thummel, K. E. *Drug Metab Dispos.* 2006; **34**: 836-847.

100. Wong, M.; Balleine, R. L.; Collins, M.; Liddle, C.; Clarke, C. L.; Gurney, H. *Clin. Pharmacol. Ther.* 2004; **75**: 529-538.

101. Shih, P. S.; Huang, J. D. *Drug Metab Dispos.* 2002; **30**: 1491-1496.

102. Utecht, K. N.; Hiles, J. J.; Kolesar, J. *Am. J. Health Syst. Pharm.* 2006; **63**: 2340-2348.

103. Yu, S.; Wu, L.; Jin, J.; Yan, S.; Jiang, G.; Xie, H.; Zheng, S. *Transplantation* 2006; **81**: 46-51.

104. Goto, M.; Masuda, S.; Kiuchi, T.; Ogura, Y.; Oike, F.; Okuda, M.; Tanaka, K.; Inui, K. *Pharmacogenetics* 2004; **14**: 471-478.

105. Villikka, K.; Kivisto, K.; Maenpaa, H.; Joensuu, H.; Neuvonen, P. *Clinical Pharmacology and Therapeutics* 1999; **66**: 589-593.

106. Zhou, X.; Zhou-Pan, X.; Gauthier, T.; Placidi, M.; Maurel, P.; Rahmani, R. *Biochemical Pharmacology* 1993; **45**: 853-861.

107. Zhou-Pan, X.; Seree, E.; Zhou, X.; Placidi, M.; Maurel, P.; Barra, Y.; Rahmani, R. *Cancer Research* 1993; **53**: 5121-5126.

108. Yao, D.; DIng, S.; Burchell, B.; Wolf, R.; Friedberg, T. *Journal of Pharmacology and Experimental Therapeutics* 2000; **294**: 387-395.

109. Kajita, J.; Kuwabara, T.; Kobayashi, H.; Kobayashi, S. *Drug Metabolism and Disposition* 2000; **28**: 1121-1127.

110. Dai, Y.; Iwanaga, K.; Lin, Y. S.; Hebert, M. F.; Davis, C. L.; Huang, W.; Kharasch, E. D.; Thummel, K. E. *Biochem. Pharmacol.* 2004; **68**: 1889-1902.

111. Bradley, S. A.; Krishnamurthy, K.; Hu, H. *J Magn Reson.* 2005; **172**: 110-117.

112. Gorski, J. C.; Jones, D. R.; Wrighton, S. A.; Hall, S. D. *Biochem. Pharmacol.* 1994; **48**: 173-182.

113. Lowry, O. H.; Rosebrough, N. J.; Farr, A. L.; Randall, R. J. *J. Biol. Chem.* 1951; **193**: 265-275.

114. Rodrigues, A. D. *Biochem. Pharmacol.* 1999; **57**: 465-480.

115. Schuhmacher, J.; Buhner, K.; Witt-Laido, A. *J. Pharm. Sci.* 2000; **89**: 1008-1021.

116. Hiratsuka, M.; Takekuma, Y.; Endo, N.; Narahara, K.; Hamdy, S.; Kishikawa, Y.; Matsuura, M.; Agatsuma, Y.; Inoue, T.; Mizugaki, M. *European Journal of Clinical Pharmacology* 2002; **58**: 417-421.

117. Le, C. P.; Parmer, R. J.; Kailasam, M. T.; Kennedy, B. P.; Skaar, T. P.; Ho, H.; Leverge, R.; Smith, D. W.; Ziegler, M. G.; Insel, P. A.; Schork, N. J.; Flockhart, D. A.; O'connor, D. T. *Clin. Pharmacol. Ther.* 2004; **76**: 139-153.

118. Eap, C. B.; Buclin, T.; Hustert, E.; Bleiber, G.; Golay, K. P.; Aubert, A. C.; Baumann, P.; Telenti, A.; Kerb, R. *Eur. J. Clin. Pharmacol.* 2004; **60**: 231-236.

119. Rowland, M.; Benet, L. Z.; Graham, G. G. *J. Pharmacokinet. Biopharm.* 1973; **1**: 123-136.

120. Houston, J. B.; Carlile, D. J. *Drug Metab Rev.* 1997; **29**: 891-922.

121. Dennison, J. B.; Kulanthaivel, P.; Barbuch, R. J.; Renbarger, J. L.; Ehlhardt, W. J.; Hall, S. D. *Drug Metab Dispos.* 2006; **34**: 1317-1327.

122. Goswami, A.; Macdonald, T. L.; Hubbard, C.; Duffel, M. W.; Rosazza, J. P. *Chem. Res. Toxicol.* 1988; **1**: 238-242.

123. Elmarakby, S. A.; Duffel, M. W.; Goswami, A.; Sariaslani, F. S.; Rosazza, J. P. *J. Med. Chem.* 1989; **32**: 674-679.

124. Pang, K. S.; Rowland, M. *J. Pharmacokinet. Biopharm.* 1977; **5**: 625-653.

125. Favretto, D.; Piovan, A.; Filippini, R.; Caniato, R. *Rapid Commun. Mass Spectrom.* 2001; **15**: 364-369.

126. Schmidt, M. S.; Huang, R.; Classon, R. J.; Murry, D. J. *J. Pharm. Biomed. Anal.* 2006; **41**: 540-543.

127. Rosazza, J. P.; Duffel, M. W.; el-Marakby, S.; Ahn, S. H. *J. Nat. Prod.* 1992; **55**: 269-284.

128. Shou, M.; Martinet, M.; Korzekwa, K. R.; Krausz, K. W.; Gonzalez, F. J.; Gelboin, H. V. *Pharmacogenetics* 1998; **8**: 391-401.

129. Lambeth, J. D.; Kitchen, S. E.; Farooqui, A. A.; Tuckey, R.; Kamin, H. *J. Biol. Chem.* 1982; **257**: 1876-1884.

130. Li, X. Q.; Weidolf, L.; Simonsson, R.; Andersson, T. B. *J. Pharmacol. Exp. Ther.* 2005; **315**: 777-787.

131. Chauret, N.; Gauthier, A.; Nicoll-Griffith, D. A. *Drug Metab Dispos.* 1998; **26**: 1-4.

132. Yamaori, S.; Yamazaki, H.; Iwano, S.; Kiyotani, K.; Matsumura, K.; Honda, G.; Nakagawa, K.; Ishizaki, T.; Kamataki, T. *Drug Metab Pharmacokinet.* 2004; **19**: 120-129.

133. Zhou, X. J.; Martin, M.; Placidi, M.; Cano, J. P.; Rahmani, R. *Eur. J. Drug Metab Pharmacokinet.* 1990; **15**: 323-332.

134. Guo, P.; Wang, X.; Zhou, F.; Gallo, J. M. *J. Chromatogr. B Analyt. Technol. Biomed. Life Sci.* 2004; **809**: 273-278.

135. Skolnik, J. M.; Barrett, J. S.; Shi, H.; Adamson, P. C. *Cancer Chemother. Pharmacol.* 2006; **57**: 458-464.

136. Ramirez, J.; Ogan, K.; Ratain, M. *Cancer Chemotherapy and Pharmacology* 1997; **39**: 286-290.

137. Lee, J. I.; Skolnik, J. M.; Barrett, J. S.; Adamson, P. C. *J. Mass Spectrom.* 2007; **42**: 761-770.

138. Ernest, C. S.; Hall, S. D.; Jones, D. R. *J. Pharmacol. Exp. Ther.* 2005; **312**: 583-591.

139. Owellen, R. J.; Blair, M.; Van, T. A.; Hains, F. C. *Cancer Treat. Rep.* 1981; **65**: 469-475.

140. Ito, K.; Houston, J. B. *Pharm. Res.* 2005; **22**: 103-112.

141. Brown, H. S.; Griffin, M.; Houston, J. B. *Drug Metab Dispos.* 2007; **35**: 293-301.

142. Yong, W. P.; Wang, L. Z.; Tham, L. S.; Wong, C. I.; Lee, S. C.; Soo, R.; Sukri, N.; Lee, H. S.; Goh, B. C. *Cancer Chemother. Pharmacol.* 2007.

143. van, Z. L.; Sparreboom, A.; van der, G. A.; Nooter, K.; Eskens, F. A.; Brouwer, E.; Bol, C. J.; de, V. R.; Palmer, P. A.; Verweij, J. *Eur. J. Cancer* 2002; **38**: 1090-1099.

CURRICULUM VITAE

Jennifer Bolin Dennison

EDUCATION:

Texas A&M University, College Station, TX	B.S.	1996
Indiana University, Indianapolis, IN	Ph.D.	2007

HONORS AND AWARDS:

IUPUI Graduate Fellowship	2004–2005
PhRMA Foundation Pre-doctoral Fellowship in Pharmacology	2006–2007

PROFESSIONAL EXPERIENCE:

Albemarle Corporation, Baton Rouge, LA Research and Development Engineer	1996–1999
Eli Lilly and Company, Lafayette, IN Technical Services Representative	1999–2001
GlaxoSmithKline, Philadelphia, PA Sr. Technology Associate	2001–2003

SELECTED PEER-REVIEWED PUBLICATIONS AND ABSTRACTS:

Dennison JB, Kulanthaivel P, Barbuch RJ, Renbarger JL, Ehlhardt WJ, and Hall SD (2006) Selective metabolism of vincristine in vitro by CYP3A5. *Drug Metab Dispos* **34**:1317-1327.

Dennison JB, Jones DR, Renbarger JL, and Hall SD (2006) CYP3A5 phenotyping of human liver microsomes with vincristine. *Drug Metabolism Reviews* **38**:210. (abstract)

Dennison JB, Jones DR, Renbarger JL, and Hall SD (2007) Effect of CYP3A5 expression on vincristine metabolism with human liver microsomes. *J Pharmacol Exp Ther* **321**:553-563.

Dennison JB, Renbarger JL, Jones DR, and Hall SD (2007) Quantification of vincristine and its major metabolite in human plasma by high-performance liquid chromatography/tandem mass spectrometry. *Therapeutic Drug Monitoring*, publication submitted.